EVALUATION OF IN-SITU CHEMICAL FLUSHING AND OXIDATION TECHNOLOGIES FOR THE REMEDIATION OF AQUIFER SYSTEMS CONTAMINATED WITH DNAPLs

by

Zeynep Demiray

B.S. in Geological Engineering, Kocaeli University, 2007

M.S. in Geological Engineering, Çukurova University, 2010

Submitted to the Institute of Environmental Sciences in partial fulfillment of

the requirements for the degree of

Doctor of Philosophy

in

Environmental Technologies

Boğaziçi University

2023

EVALUATION OF IN-SITU CHEMICAL FLUSHING AND OXIDATION TECHNOLOGIES FOR THE REMEDIATION OF AQUIFER SYSTEMS CONTAMINATED WITH DNAPLs

APPROVED BY:

Prof. Dr. Nadim Copty Dissertation Advisor	. . . . .
Assoc. Prof. Dr. Hakan Nihat Akyol Dissertation Co-Advisor	. . . . .
Prof. Dr. Ferhan Çeçen	. . . . .
Prof. Dr. Melek Kazezyılmaz Alhan	. . . . .
Prof. Dr. Geoffrey Tick	. . . . .
Assoc. Prof. Dr. Başak Güven	. . . . .

DATE OF APPROVAL: 09/06/2023

Dedicated to my beloved

father Dr. Erdoğan R. Demiray and uncle Dr. H. Engin Demiray

ACKNOWLEDGEMENTS

I would like to express my deepest gratitude to my advisor, Dr. Nadim K. Copty, for his continuous guidance, patience, all the way support, and belief in me. I have greatly benefitted from his insight, knowledge, and experience. It would not be possible to bring this dissertation out without his feedback throughout the study. I also appreciate the valuable comments and feedback of my committee members Dr. Hakan Nihat Akyol for sharing his knowledge as my Co-Advisor, Dr. Ferhan Çeçen, Dr. Başak Güven, Dr. Melek Kazezyılmaz Alhan and my former committee member Dr. Işıl Balcıoğlu. Special thanks go to Dr. Geoffrey R. Tick for hosting me for the entire year, allowing me to use his laboratory under the difficult circumstances after the pandemic. His support both financial and moral is so valuable. Dr.Tick, apologies for broken glasses and syringes!

I gratefully acknowledge Dr. Qiaoli Liang for her technical help at the mass spectrometry facility in Alabama. I am deeply grateful to Filiz Ayılmaz for her technical, instrumental, and moral help.

I would like to express my sincere gratitude to all the administrative members and friends at Bogazici University Institute of Environmental Sciences. Good times, coffee, and chatting with you will be missed. Also, I am thankful to my friends that I met during my visit to Alabama in and out of the university for the unforgettable moments and memories. Many excuses and appreciation to my friends that I could not contact during this time, your patience and understanding made the stressful times of this journey bearable.

I am thankful to the Turkish Scientific and Technological Research Council of Türkiye (TÜBİTAK) for their financial support through the 2214-A program. This dissertation was also supported by the Research Fund of Boğaziçi University grant (16221) and TÜBİTAK grant (117Y140).

Finally, I would like to thank my family without whom I could not have accomplished what I have. My parents have been an endless source of encouragement and support and I am most grateful to them. Mom and Dad, I always felt your silent support and tremendous sacrifice during these years of my study. I appreciate my sister and her husband also for their warranty on my visit to the USA. I would also like to thank my cousins, aunts, and uncles for their support and for continuing to believe that I would one day finish. Last but not least, I thank my sweetest nephews, Karahan, Mehmet Engin, and my beautiful niece Ada. You bring joy to my life kids, love you all to the moon and back.

ABSTRACT

EVALUATION OF IN-SITU CHEMICAL FLUSHING AND OXIDATION TECHNOLOGIES FOR THE REMEDIATION OF AQUIFER SYSTEMS CONTAMINATED WITH DNAPLs

Organic compounds- such as petroleum hydrocarbons and chlorinated solvents- are widely used in numerous industrial applications. Because of their low solubility many of these compounds are often present in the environment in the form of dense non-aqueous phase liquids (DNAPLs) that act as long-term sources of pollutions. This study focuses on two technologies for the remediation of groundwater resources contaminated with DNAPLs: in-situ enhanced solubilization (ISES) and in-situ chemical oxidation (ISCO). The research aimed to investigate the synergetic benefits of combining these two technologies. Additionally, a numerical multiphase flow model was used to simulate the DNAPL fate and transport to improve our understanding of process mechanisms, and to explore alternative remediation methodologies and strategies. The performed laboratory experiments and modeling work show that the non-ionic surfactant Tween 80 is effective for the recovery of PCE entrapped in both silica sand and natural calcareous soil. For multicomponent DNAPL mixtures, the enhancement factor of each component plays an important role in determining the remediation efficiency. Combining surfactant enhanced dissolution with potassium permanganate produced improved overall mass removal. Pulse injection can yield longer contact times, resulting in more effective DNAPL removal. Heat-activated persulfate oxidation, whereby the system temperature is raised to about 50 ℃, can successfully activate the persulfate, resulting in improved DNAPL mass recovery. Furthermore, this study shows that multiphase modeling is an effective tool that can accurately simulate ISES and ISCO technologies, and potential help in the design and opitimization of field scale remediation of groundwater contaminated with DNAPLs.

ÖZET

DNAPL İLE KİRLENMİŞ AKİFER SİSTEMLERİNİN YERİNDE TEMİZLENMESİNDE KİMYASAL YIKAMA VE OKSİDASYON TEKNOLOJİLERİNİN DEĞERLENDİRİLMESİ

Klorlu solventler ve petrol hidrokarbonları gibi organik bileşikler çok sayıda endüstriyel uygulamada kullanılmaktadır. Düşük çözünürlükleri sebebiyle bu bileşiklerin birçoğu doğada yoğunluğu sudan fazla suyla karışmayan sıvı (DNAPL) şeklinde birikir. Bu çalışma, DNAPL ile kirlenmiş yeraltısuyu kaynaklarının iyileştirilmesinde öne çıkan iki teknolojiye odaklanmıştır: Yerinde arttırılmış çözünürlük (ISES) ve yerinde kimyasal oksidasyon. Bu çalışma, söz konusu iki teknolojinin birlikte kullanılması ile elde edilebilecek faydaların araştırılması üzerine odaklanmıştır. Ayrıca, akıbet ve taşınım işlemlerinin simule edildiği bir nümerik çok fazlı akış modeli kullanılmıştır. Modellemenin amacı, işlem mekanizmalarının daha iyi anlaşılmasına yardımcı olması ve iyileştirmeye alternatif stratejilerin araştırılmasıdır. Laboratuvar deneyleri ve modelleme çalışmaları, silis kumu ve doğal karbonatlı toprakta hapsolan PCE nin geri kazanımında iyonik olmayan bir yüzey aktif madde olan Tween 80 in etkin olduğunu göstermiştir. DNAPL karışımları için ise, her bir bileşenin çözünürlük artış faktörü, iyileştirmenin etkinliğinin belirlenmesinde önemli rol oynamaktadır. Yüzey aktif maddeli arttırılmış çözünürlük ile potasyum permanganatın birleştirilmesi toplam kütle giderimini yükseltmiştir. Kısa-süreli enjeksiyon, daha uzun temas süresini sağlayarak daha efektif DNAPL giderimine neden olmaktadır. Isı ile aktifleştirilmiş persülfat oksidasyonunda, sistemin sıcaklığının 50 ℃ ye çıkarılması persülfatı başarılı bir şekilde aktifleştirebilmiş, DNAPL kütlesi geri kazanımını ilerletmiştir. Ayrıca bu çalışma, çok fazlı modellemenin ISES ve ISCO teknolojilerinin doğru bir şekilde simüle edilebilmesi konusunda etkin bir araç olduğunu göstermekle birlikte DNAPLlı toprağın arazi ölçeğindeki iyileştirmelerinin dizayn ve optimizasyonuna çözümler sağlamıştır.

TABLE OF CONTENTS

ACKNOWLEDGEMENTS....iv
ABSTRACT....v
ÖZET....vi
TABLE OF CONTENTS....vii
LIST OF FIGURES....x
LIST OF TABLES....xix
LIST OF SYMBOLS/ABBREVIATIONS....xxiii
1. INTRODUCTION....1
1.1. DNAPL in the Subsurface....1
1.2. Remedition....1
1.3. Modeling....4
1.4. Objectives....4
2. LITERATURE REVIEW....9
2.1. In-Situ Enhanced Solubilization (ISES)....9
2.2. In-Situ Chemical Oxidation (ISCO)....11
2.2.1. Potassium Permanganate....11
2.2.2. Sodium Persulfate....13
2.2.2.1. Iron Activation....14
2.2.2.2. Heat Activation....16
2.3. In-Situ Chemical Oxidation by Enhancement of Solubilization....20
2.4. Zero-Valent Iron (ZVI)....23
2.5. Modeling Enhanced Dissolution of DNAPL....25
3. MATERIALS AND METHODS....32
3.1. Materials....33
3.2. Experimental Set-up for Batch Miscibility and Solubility....34
3.3. Experimental Set-up for Batch Reactivity....38
3.3.1. Zero-Valent Iron Activation of Persulfate....39
3.3.2. Thermally-Activated Persulfate....41
3.4. Flow-cell Experimental Set-up for In-Situ Enhanced Solubilization and In-Situ Chemical Oxidation....43
3.4.1. Flow-cell #1....43
3.4.2. Flow-cell #2....49

3.5. Tracer Test....53
3.6. Analytical Instruments....54
3.7. Mass Flux Reduction-Mass Removal Relationship....64
3.8. Numerical Modeling....65
3.8.1. Multiphase Flow Model....66
3.8.1.1. Interphase Mass Transfer....66
3.8.1.2. Capillary Pressure and Relative Permeability....67
3.8.1.3. Interfacial Tension....68
3.8.1.4. NAPL Solubility....69
3.8.1.5. Initial DNAPL Distribution....70
3.8.1.6. Dispersivity....70
3.8.1.7. Boundary Conditions, Discretization and Parameter Assignment....70
3.8.1.8. Oxidation Reaction....72
3.8.2. Sensitivity Coefficients....76
3.8.3. NAPL Mass Depletion Model....77
4. RESULTS....80
4.1. Enhanced Solubilization of DNAPL PCE with Different Solubilizing Agents....80
4.1.1. PCE Enhanced Solubilization Batch Experiments....81
4.1.2. Flushing Experiments for Enhanced PCE Dissolution....86
4.1.2.1. Mass Flux Reduction/Mass Removal Relation....92
4.1.3. Multiphase Flow Modeling....95
4.1.3.1. Sensitivity Analysis....96
4.1.3.2. Model Calibration....111
4.1.4. DNAPL Mass-Concentration Relation Modeling....117
4.2. Multiphase Flow Model of DNAPL Mixtures with Different Solubilizing Agents....121
4.2.1. DNAPL Mixture Enhanced Solubilization Batch Experiments....123
4.2.2. DNAPL Mixture Enhanced Solubilization Model Calibration....135
4.3. In-Situ Potassium Permanganate Oxidation Coupled with Enhanced Solubilization of DNAPL PCE....141
4.3.1. Contaminant Elution Behavior....143
4.3.1.1. Mass Flux Reduction-Mass Removal....147
4.3.2. Oxidation Model Calibration....149
4.4. Sodium Persulfate Oxidation Coupled with Enhanced Solubilization of DNAPL PCE....153
4.4.1. Batch Experiments....154
4.4.1.1. PCE Degradation with ZVI-Activated Persulfate....154

4.4.1.2. PCE Degradation with Thermally-Activated Persulfate.....157
4.4.1.2.1. Degradation of PCE in the Pure DNAPL Phase.....158
4.4.1.2.2. Degradation of PCE in the Aqueous Phase.....164
4.4.1.3. Stability and Surfactant (Tween 80) Degradation Capacity of Persulfate at Elevated Temperature.....167
4.4.2. Surfactant Enhanced Thermally-Activated Persulfate Remediation of DNAPL PCE Source Zones.....169
4.4.2.1. Tracer Test in Flow-cell #1.....170
4.4.2.2. Contaminant Elution Behavior in Flow-cell #1.....173
4.4.2.3. Tracer Test in Flow-cell #2.....175
4.4.2.4. Contaminant Elution Behavior in Flow-cell #2.....178
4.5. In-Situ Sodium Persulfate Oxidation and Enhanced Solubilization in Pure Phase TCE....181
4.5.1. Batch TCE Degradation Experiments with Thermally-Activated Persulfate….....181
4.5.2. Tween 80 Enhanced Thermally-Activated Persulfate Oxidation of DNAPL TCE Source Zones.....186
5. CONCLUSIONS AND FUTURE RECOMMENDATIONS.....191
REFERENCES.....197
APPENDIX A: SOIL OXIDANT DEMAND, COMPARISON WITH LITERATURE STUDIES.....222
APPENDIX B: MULTIPHASE FLOW UTCHEM INPUT FILE FOR TWEEN 80 ENHANCED PERMANGANATE FLUSHING IN SILICA SAND.....226
APPENDIX C: MAIN DATA REQUIREMENT OF THE MODEL (silica sand flow zone, PCE enhanced solubilization with 5 % Tween 80).....242

LIST OF FIGURES

Figure 1.1. DNAPL transport and distribution in subsurface.....2

Figure 1.2. Flowchart of the modeling process adopted to the study.....7

Figure 2.1. Ageing process of nanoZVI during time depending on storage conditions.....16

Figure 2.2. Coupling process of surfactant and thermally-activated persulfate on organic contaminant (coal tar) (Wang et al, 2017).....23

Figure 2.3. PCE reductive dechlorination (Ni et al, 2014) 24

Figure 2.4. Thin film model for DNAPL dissolution.....26

Figure 3.1. KSV Sigma 703 digital tensiometer.....35

Figure 3.2. Equipment used in the cloud point titration (40 mL glass vials with minivalve screwed cap, gas tight macro syringes, magnetic stirrer and stirring bar).....36

Figure 3.3. Enhanced solubilization experimental vials placed in horizontal shaker (on the left) and the centrifuge.....37

Figure 3.4. a) Untreated raw iron (on the left), iron surface during acid treatment (on the right), b) Wet vs. dried treated iron (on the left), experimental preparation (on the right), c) 20 mL batch reactors hosting the ZVI rods-PCE- Persulfate.....40

Figure 3.5. a) Reactor preparation for each time interval, b) Heat activation progress in a water bath at 50 °C, c) Ice quenching in styrofoam.....42

Figure 3.6. Flow-cell #1 configuration for experiments a) 1 to 4 and 9 to 12, 17 and 18 (upper flow zone 40-50 mesh silica sand total volume ~730 cm^3), b) 5 to 8 and 13 to 16, 19 and 20 (upper flow zone calcareous soil volume ~500 cm^3).....44

Figure 3.7. Flow-cell #1 configuration for DNAPL TCE experiments from 25 to 27 (upper flow zone 40-50 mesh silica sand total volume ~730cm^3).....48

Figure 3.8. Flow-cell #1 configuration for PCE experiments from 21 to 24 (upper flow zone 40-50 mesh silica sand total volume ~690 cm^3).....49

Figure 3.9. Flow-cell #2 configuration for the experiments from 28 to 31.....50

Figure 3.10. a) DNAPL injection into the plexiglass flow-cell with a syringe pump, b) Experimental setup including the heat source and additional isolated pieces of equipment.....52

Figure 3.11. a) GC/MS with Headspace unit, b) QM-GC/MS, c) Pre-heating procedure for QM-GC/MS.....55

Figure 3.12. GC/MS calibration curves (0.01-0.5 mg/L) for (a) PCE, (b) TCE, (c) 1,1-DCE.....57

Figure 3.13. QM-GC/MS calibration curve for PCE (0.1-2.5 mg/L).....58

Figure 3.14. a) Shimadzu UV-160A vis. spec. (Boğaziçi University), b) Shimadzu UV-1700 vis. spec. (University of Alabama).....59

Figure 3.15. Calibration curve of persulfate a) for UV-160A, b) for UV-1700.....60

Figure 3.16. Calibration curve of PFBA a) for UV-160A, b) for UV-1700.....61

Figure 3.17. HACH DR-1900 spectrophotometer (University of Alabama).....62

Figure 3.18. a) MALDI TOF instrument and sample preparation, b) Tween 80 calibration curve……..…...63

Figure 3.19. Schematic of the flushing experiments. The inset image shows the NAPL distribution prior to flushing in a) Silica sand, b) Natural soil.....71

Figure 3.20. Flowchart of UTCHEM (modified from Korrani et al, 2015; Luo et al, 2016 and Hosseininoosheri et al, 2016).....74

Figure 3.21. Solution scheme for reaction equations in UTCHEM simulator (modified from Korrani et al, 2015; Luo et al, 2016 and Hosseininoosheri et al, 2016).....75

Figure 3.22. Summary of the groundwater remediation technologies, the experiments performed to evaluate these technologies and the modeling studies performed within the scope of the thesis.....79

Figure 4.1. IFT of two-phase systems as a function of Tween 80 concentrations (0-0.0093 %vol or 0-100 mg/L) for DNAPL PCE.....81

Figure 4.2. Ternary phase diagram for Tween 80 – PCE – water (%mass).....82

Figure 4.3. Ternary phase diagram for ethanol – PCE – water (%mass).....83

Figure 4.4. Ternary phase diagram for [ethanol/Tween80] – PCE – water (%mass).....84

Figure 4.5. Ternary phase diagram for ethanol – PCE – Tween 80 (%mass).....85

Figure 4.6. Solubility of PCE with Tween 80.....86

Figure 4.7. Flow-cell configuration composed of 40/50 mesh sand and 70/100 mesh sand bottom used for surfactant-enhanced PCE flushing.....87

Figure 4.8. Flow-cell configuration composed of calcareous soil and <200 mesh soil bottom used for surfactant-enhanced PCE flushing.....87

Figure 4.9. a) PCE effluent concentration as a function of pore volumes in silica sand (1 PV= 2.38 hours), b) PCE effluent concentrations expressed as C/C_{sol} which can be viewed as an enhancement factor, on a log scale in silica sand…….89

Figure 4.10. a) PCE effluent concentration as a function of pore volumes in calcareous soil (1 PV= 2.44 hours), b) PCE effluent concentrations expressed as C/C_{sol} which can be viewed as an enhancement factor on a log scale in calcareous soil…….91

Figure 4.11. PCE mass-flux reduction versus mass removal behavior for the (i) water, (ii) Tween 80, (iii) SDS and (iv) MCD enhanced solubilization flushing experiments for a) silica sand and b) natural soil.....94

Figure 4.12. Effluent concentration for the base case simulation and sensitivity simulations corresponding to the doubling of flushing flow rate (Q) and sensitivity coefficients for a) water, b) Tween 80, c) SDS and d) MCD flushing in silica sand.....98

Figure 4.13. Effluent concentration for the base case simulation and sensitivity simulations corresponding to the doubling of flushing flow rate (Q) and sensitivity coefficients for a) water, b) Tween 80, c) SDS and d) MCD flushing in natural soil.....98

Figure 4.14. Effluent concentration for the base case simulation and sensitivity simulations corresponding to the doubling the NAPL solubility and sensitivity coefficients for a) water, b) Tween 80, c) SDS and d) MCD flushing in silica sand.....99

Figure 4.15. Effluent concentration for the base case simulation and sensitivity simulations corresponding to the doubling the NAPL solubility and sensitivity coefficients for a) water, b) Tween 80, c) SDS and d) MCD flushing in natural soil.....100

Figure 4.16. Effluent concentration for the base case simulation and sensitivity simulations corresponding to the doubling the transversal dispersivity and sensitivity coefficients for a) water, b) Tween 80, c) SDS and d) MCD flushing in silica sand….101

Figure 4.17. Effluent concentration for the base case simulation and sensitivity simulations corresponding to the doubling the transversal dispersivity and sensitivity coefficients for a) water, b) Tween 80, c) SDS and d) MCD flushing in natural soil....101

Figure 4.18. Effluent concentration for the base case simulation and sensitivity simulations corresponding to the doubling the NAPL saturation and sensitivity coefficients for a) water, b) Tween 80, c) SDS and d) MCD flushing in silica sand.....102

Figure 4.19. Effluent concentration for the base case simulation and sensitivity simulations corresponding to the doubling the NAPL saturation and sensitivity coefficients for a) water, b) Tween 80, c) SDS and d) MCD flushing in natural soil.....103

Figure 4.20. Effluent concentration for the base case simulation and sensitivity simulations corresponding to the doubling the mass transfer coefficient and sensitivity coefficients for a) water, b) Tween 80, c) SDS and d) MCD flushing in silica sand.....104

Figure 4.21. Effluent concentration for the base case simulation and sensitivity simulations corresponding to the doubling the mass transfer coefficient and sensitivity coefficients for a) water, b) Tween 80, c) SDS and d) MCD flushing in natural soil....104

Figure 4.22. Effluent concentration for the base case simulation and sensitivity simulations corresponding to the doubling the longitudinal dispersivity and sensitivity coefficients for a) water, b) Tween 80, c) SDS and d) MCD flushing in silica sand.....105

Figure 4.23. Effluent concentration for the base case simulation and sensitivity simulations corresponding to the doubling the longitudinal dispersivity and sensitivity coefficients for a) water, b) Tween 80, c) SDS and d) MCD flushing in natural soil…106

Figure 4.24. Comparison of the best-fit model and experimental results for (a) water, (b) 5% Tween 80, (c) 5% SDS, and (d) 5% MCD in silica sand.....114

Figure 4.25. Comparison of the best-fit model and experimental results for (a) water, (b) 5% Tween 80, (c) 5% SDS, and (d) 5% MCD in natural soil.....116

Figure 4.26. Comparison of simulated and observed dimensionless mass recovered as a function of dimensionless time for the silica sand flushing experiments.....119

Figure 4.27. Comparison of simulated and observed dimensionless mass recovered as a function of dimensionless time for the natural soil flushing experiments.....120

Figure 4.28. Image of DNAPL mixture initial distribution for the a) silica sand, b) calcareous soil. (Experiment 1 with 5% Tween 80).....123

Figure 4.29. IFT of two phase system as a function of (a) Tween 80 (%vol), (b) SDS (%wt), (c) MCD (%wt) for DNAPL mixture (PCE:TCE:1,1-DCE).....125

Figure 4.30. SDS at critical micelle concentration (~0.2%wt).....126

Figure 4.31. Ternary phase diagram for Tween 80 – DNAPL mixture – water (%wt).....128

Figure 4.32. Ternary phase diagrams for DNAPL mixture-water-SDS system (%wt).....129

Figure 4.33. Ternary phase diagrams for DNAPL mixture-water-MCD system (%wt).....130

Figıre 4.34. Variations of TPDs with different solubilizing agent and co-solvent contents for DNAPL mixture.....131

Figure 4.35. Enhanced-solubility of the DNAPL mixture in Tween80-water, SDS-water, and MCD-water system.....132

Figure 4.36. Comparison between the best-fit enhanced solubilization model data and the experimental data obtained in silica sand (1PV=2.38 hours); (a) water flushing; (a1) PCE, (a2) TCE, (a3) DCE, (b) Tween 80 (5%) flushing; (b1) PCE, (b2) TCE, (b3) DCE, (c) SDS (5%) flushing; (c1) PCE, (c2) TCE, (c3) DCE, (d) MCD (5%) flushing; (d1) PCE, (d2) TCE, (d3) DCE.....139

Figure 4.37. Comparison between the best-fit enhanced solubilization model data and the experimental data obtained in calcareous soil (1PV=2.44 hours); (a) water flushing; (a1) PCE, (a2) TCE, (a3) DCE, (b) Tween 80 (5%) flushing; (b1) PCE, (b2) TCE, (b3) DCE, (c) SDS (5%) flushing; (c1) PCE, (c2) TCE, (c3) DCE, (d) MCD (5%) flushing; (d1) PCE, (d2) TCE, (d3) DCE.....140

Figure 4.38. Image of organic-liquid initial distribution in flow-cell prior to flushing. (a) First configuration (sand), (b) Second configuration (calcareous soil).....143

Figure 4.39. Effluent PCE concentration as a function of PV with water flood and with Tween 80 solution in silica sand, with water flood and with Tween 80 solution in natural soil (log-scale).....144

Figure 4.40. Effluent PCE and Chloride ion (Cl^-) concentrations as a function PV for permanganate and Tween 80 enhanced permanganate flushing experiments in silica sand (1PV = 2.38 hours).....145

Figure 4.41. Effluent PCE and Chloride ion (Cl^-) concentrations as a function PV for Permanganate and Tween 80 enhanced permanganate flushing experiments in calcareous soil (1 PV = 2.44 hours).....146

Figure 4.42. PCE mass-flux reduction versus mass removal behavior for the (i) water, (ii) Tween 80-enhanced solubilization, (iii) MnO_4^- oxidation and (iv) Tween 80-enhanced MnO_4^- oxidation flushing experiments for a) silica sand and b) natural soil.....148

Figure 4.43. Comparison of experimental and simulated effluent PCE concentrations including stage 1; chemical flushing, stage 2; interruption, stage 3; water flushing for (a) permanganate flushing in silica sand, (b) permanganate flushing in natural soil, (c) Tween 80 enhanced permanganate flushing in silica sand, (d) Tween 80 enhanced permanganate flushing in natural soil.....152

Figure 4.44. Time-dependent persulfate degradation and product release……..155

Figure 4.45. PCE degradation in the presence of iron filings…….157

Figure 4.46. Quenching of the reaction in case of the removal of activator (pH: 3.47 - 3.72; ORP: 444 - 489 mV).....159

Figure 4.47. Unactivated persulfate DNAPL phase PCE oxidation capability and PCE oxidation in various activated persulfate concentrations.....160

Figure 4.48. Chloride release of DNAPL phase PCE in various persulfate concentration…….160

Figure 4.49 DNAPL phase PCE degradation with various concentrations of Tween 80 enhanced persulfate.....161

Figure 4.50. Chloride release from DNAPL phase PCE in various Tween 80 enhanced persulfate concentration……...162

Figure 4.51. Best-fit DNAPL phase PCE degradation and Chloride production concentration curves of (a) [PCE]/[PS] = 1/10, (b) [PCE]/[PS] = 1/20……...163

Figure 4.52. Aqueous phase PCE degradation with various concentrations of Tween 80 Enhanced persulfate…….....164

Figure 4.53. Chloride release of aqueous phase PCE in various persulfate concentration…….165

Figure 4.54. Best-fit aqueous phase PCE degradation and Chloride production concentration curves of (a) [PCE]/[PS] = 1/170, (b) [PCE]/[PS] = 1/40, (c) [PCE]/[PS] = 1/40 3CMC, (d) [PCE]/[PS] = 1/40 10CMC……...167

Figure 4.55. (a) Time-dependent relative persulfate concentration, (b) Relative persulfate concentrations after 48 hrs.....168

Figure 4.56. Flow-cell #1 configuration for the thermally enhanced persulfate experiments……171

Figure 4.57. Tracer test experimental data and best-fit solution…….172

Figure 4.58. PCE elution behavior under 50 ℃ enhanced flushing.....173

Figure 4.59. PCE elution with Tween 80 enhanced thermally-activated persulfate flushing.....174

Figure 4.60. Flow-cell #2 configuration for the thermally-enhanced persulfate experiments……176

Figure 4.61. Tracer test experimental data and best-fit solution.....177

Figure 4.62. PCE elution behavior of water flooding of in Flow-cell #2……....178

Figure 4.63. Time-dependent change of (a) PCE, (b) Chloride in silica sand (continuous injection).....180

Figure 4.64. a) Aqueous TCE degradation curve. Molar ratioPS/TCE: [10/1]; C_{PS}: 1.14mM, C_{TCE}: 0.114mM, b) Aqueous and DNAPL TCE degradation curve. Molar ratios PS/TCE: [10/1]; C_{PS}: 3.8mM, C_{TCE}: 0.38mM, c) Chloride ion concentration released from aqueous and DNAPL TCE.....183

Figure 4.65. a) Aqueous TCE degradation in the presence of Tween 80. Molar ratios PS/Tween80/TCE: [10/0/1] C_{PS}: 3.8mM, $C_{Tween80}$: 0 mM, C_{TCE}: 0.38mM; [10/0.25/1] C_{PS}: 3.8mM, $C_{Tween80}$: 0.095 mM, C_{TCE}: 0.38mM; [10/0.5/1] C_{PS}: 3.8mM, $C_{Tween80}$: 0.2 mM, C_{TCE}: 0.38mM, b) Chloride ion concentration released from aqueous and DNAPL TCE in the presence of Tween 80.....185

Figure 4.66. Time-dependent change of TCE, Chloride ion, and pH in silica sand (1 PV = 2.4 hrs) a) Continuous persulfate solution through the flow-cell, b) 1PV injection of persulfate solution and flushing with DI water through the flow-cell, c) Continuous persulfate and Tween 80 (1%) mixture solution through the flow-cell.....188

Figure 4.67. Images showed dyed 1 mL of DNAPL mass as a function of time for flushing with 111mM (26.5 g/L) persulfate.....189

LIST OF TABLES

Table 2.1. Mass recoveries with in-situ enhanced solubilization with several solubilizing agents from selected column/flow-cell studies.....10

Table 2.2. Field investigations of ISES to remediate NAPL sites.....11

Table 2.3. Reported rate constants from oxidation reactions between PCE, TCE and permanganate performed in batch kinetic experiments.....12

Table 2.4. 1D, 2D laboratory studies of permanganate oxidation of DNAPLs.....13

Table 2.5. Experimental conditions of thermally activated persulfate for the oxidation of various VOCs (NAPLs) in the literature.....18

Table 3.1. Overview of the performed experimental studies.....32

Table 3.2. General physical properties of DNAPLs used in the study.....34

Table 3.3. Physical and chemical properties of calcareous soil (from Akyol et al., 2011; Akyol and Yolcubal, 2013) 44

Table 3.4. Experiments of in-situ enhanced solubilization (ISES) and coupled with in-situ chemical oxidation (ISCO) with permanganate performed in Flow-cell #1.....46

Table 3.5. In-situ enhanced solubilization (ISES) at 50 ℃ and ISES coupled with in-situ chemical oxidation at 50 ℃ (thermally-activated persulfate -ISCO) experiments performed with Flow-cell #1.....47

Table 3.6. In-situ enhanced solubilization (ISES) coupled with in-situ chemical oxidation experiments at 50 ℃ performed in Flow-cell #2.....51

Table 3.7. Operating conditions of GC/MS with Headspace unit.....56

Table 4.1. Parameters for the PCE enhanced solubilization flow-cell experiments.....88

Table 4.2. List of key parameters used in the model simulations.....96

Table 4.3. Normalized time-averaged of the absolute sensitivity coefficients and correlations between different parameters for WATER flushing experiments in silica sand.....107

Table 4.4. Normalized time-averaged of the absolute sensitivity coefficients and correlations between different parameters for Tween 80 flushing experiments in silica sand.....108

Table 4.5. Normalized time-averaged of the absolute sensitivity coefficients and correlations between different parameters for SDS flushing experiments in silica sand.....108

Table 4.6. Normalized time-averaged of the absolute sensitivity coefficients and correlations between different parameters for MCD flushing experiments in silica sand.....109

Table 4.7. Normalized time-averaged of the absolute sensitivity coefficients and correlations between different parameters for water flushing experiments in natural soil.....109

Table 4.8. Normalized time-averaged of the absolute sensitivity coefficients and correlations between different parameters for Tween 80 flushing experiments in natural soil.....110

Table 4.9. Normalized time-averaged of the absolute sensitivity coefficients and correlations between different parameters for SDS flushing experiments in natural soil.....110

Table 4.10. Normalized time-averaged of the absolute sensitivity coefficients and correlations between different parameters for MCD flushing experiments in natural soil.....111

Table 4.11. Best-fit model parameters for the silica sand flushing experiments.....116

Table 4.12. Best-fit model parameters for the natural soil flushing experiments.....117

Table 4.13. List of flow-cell experiments with DNAPL mixture pool.....122

Table 4.14. Comparison of the solubility values of DNAPL mixture components to data from the literature.....133

Table 4.15. Comparison of the enhancement factors from this study to available literature values.....135

Table 4.16. Key parameters used in DNAPL mixture model.....136

Table 4.17. Best-fit mass transfer coefficients and NRMSE for DNAPL mixture enhanced solubilization models in silica sand.....141

Table 4.18. Best-fit mass transfer coefficients and NRMSE for DNAPL mixture enhanced solubilization models in calcareous soil.....141

Table 4.19. List of Tween 80 enhanced permanganate oxidation of DNAPL PCE flushing experiments.....142

Table 4.20. List of key parameters used in the model simulations.....149

Table 4.21. Best-fit oxidation reaction rate constant (K_o) and corresponding fitting statistics. The percentages of recovered and oxidized DNAPL mass are also given.....153

Table 4.22. Batch experimental conditions for PCE degradation at 50 ^oC.....158

Table 4.23. Best fit DNAPL phase PCE degradation and dechlorination rates for heat-activated persulfate batch kinetic experiments (PCE_0 = 0.3mM (50 mg/L)).....163

Table 4.24. Best fit aqueous phase PCE degradation and dechlorination rates for heat-activated persulfate batch kinetic experiments (PCE_0 = 0.54mM (90 mg/L))……..……..…...165

Table 4.25. List of persulfate experiments performed at 50 ℃.....170

Table 4.26. Dispersion coefficient and dispersivity values determined from tracer test.....172

Table 4.27. Mass recovery values from the experiments in Flow-cell #1.....175

Table 4.28. Dispersion coefficient and dispersivity values determined from tracer test.....177

Table 4.29. Mass recovery values from the experiments in Flow-cell #2.....181

LIST OF SYMBOLS/ABBREVIATIONS

Symbol	Explanation
$KMnO_4$	Potassium permanganate
$NaMnO_4$	Sodium permanganate
$Na_2S_2O_8$	Sodium persulfate
C_2Cl_4	Tetrachloroethene
C_2HCl_3	Trichloroethene
$C_2H_2Cl_2$	Dichloroethene
SO_4^{2-}	Sulfate ion
Cl^-	Chloride ion
$SO_4^{\bullet-}$	Sulfate radical
$OH^\bullet$	Hydroxyl radical
Fe^{2+}	Ferrous iron
Fe^{3+}	Ferric iron
Fe_2O_3	Iron (III) oxide
Fe^0	Zero valent iron
$Fe(OH)_3$	Iron hydroxide
$S_2O_8^{2-}$	Persulfate ion
MnO_4^-	Permanganate ion
CO_2	Carbondioxide
$AgNO_3$	Silver nitrate
K_2CrO_4	Potassium chromate
$NaHCO_3$	Sodium bicarbonate
HCl	Hydrochloric acid
µL	microliter
mV	millivolt
mN	millinewton
J	Diffusive flux
D_{aq}	aqueous phase diffusion coefficient specific to the compound
C	aqueous concentration of the DNAPL (kg/m^3)
z	vertical distance (m)
C_{sat}	aqueous solubility of the DNAPL compound
C_{aq}	DNAPL concentration in the bulk aqueous phase

δ	aqueous phase stagnant film thickness
Jv	rate of mass exchange in a representative volume
K_l	lumped mass transfer coefficient per unit volume of porous medium
Sh	Sherwood number
d_{50}	representative (median) grain size diameter
D_m	molecular diffusion coefficient
k_2	second-order rate constant (m3/[mole s])
C_{ox}	concentration of oxidant within the unit volume (kg/m^3)
k_{ox}	pseudo first-order reaction rate coefficient (1/s)
n	porosity of the subsurface medium [ ]
$x_{i,j}$	cartesian coordinate axis, (m)
D_{ij}	hydrodynamic dispersion coefficient tensor, (m^2/s)
v_i	seepage or linear pore water velocity (m/s)
q_S	volumetric flow rate per unit volume of aquifer (1/s)
C_S	concentration of the source flux for DNAPL, (g/m^3)
X_A	mole fraction
v	velocity [L/T]
Q	flow rate [L^3/T]
n	porosity of the porous media [ ]
A	cross sectional area of the flow zone [L^2]
D_x	longitudinal dispersion coefficient [L^2/T]
D_m	molecular diffusion coefficient [L^2/T]
α_x	longitudinal dispersivity [L]
C_0	influent concentration [M/L^3]
D_x	longitudinal dispersion coefficient [L^2/T]
J	mass-flux [M/T]
MR(t)	fraction of mass removed [ ]
M_i	injected DNAPL mass [M]
β	stoichiometry coefficient [ ]
k	component, DNAPL
$v_{\alpha,i}$	velocity of phase α in the i direction
α	phase
ε_α	volume fraction of phase α which is related to the saturation
ρ_α	mass density of phase α

x_i	cartesian coordinate system
w_k^α	mass fraction of phase α and component k
$J_{k,i}^\alpha$	dispersive flux of phase α for component k in the i direction
I_k^α	mass transfer of phase α
E_k^α	external source of phase α and component k
Sh'	modified Sherwood number
dm	mean grain diameter [L]
D	molecular diffusion coefficient [L^2/T]
P_b	entry pressure
P_c	capillary pressure between the two phases
S_n	normalized aqueous/microemulsion saturation
λ	pore size distribution coefficient
$k_{r,l}$	relative permeability of phase l
$k_{r,l}^o$	endpoint relative permeability of phase l
e_l	exponent of phase l
σ	interfacial tension when a cosolvent is present
σ_0	interfacial tension in the absence of a cosolvent
θ	exponent of the IFT expression assumed to be equal to 1
C_n^w	water concentration in the NAPL phase
C_w^n	NAPL dissolved concentration in the aqueous phase
C_p^c	cosolvent concentration in the cosolvent poor phase
S	aqueous phase DNAPL concentration [M/L^3]
A	oxidant concentration (permanganate) [M/L^3]
Ko	overall oxidation reaction rate constant [L^3/M/T]
Ce	effluent concentration as a function of time and all input parameters
p_i	*i* th input parameter
β	empirical parameter

Abbreviation	**Explanation**
BTEX	Benzene, Toluene, Ethylbenzene, and Xylenes
CMC	Critical micelle concentration
DCE	Dichloroethene
DNAPLs	Dense nonaqueous phase liquids
E	Solubility enhancement factor

E°	Redox potential
EPA	Environmental protection agency
HPCD	Hydroxypropyl beta cyclodextrin
ISES	In-situ enhanced solubilization
ISCO	In-situ chemical oxidation
LNAPLs	Light nonaqueous phase liquids
MCD	Methyl beta cyclodextrin
MCL	Maximum contaminant level
MTBE	Methyl-tertyl-butyl-ether
NAPLs	Nonaqueous phase liquids
PAH	Polyaromatic hydrocarbons
PCE	Tetrachloroethene
PFBA	Pentafluorobenzoic acid
PV	Pore volume
SDS	Sodium dodecyl sulfate
TBA	Tertiary butyl alcohol
TCA	Trichloroethane
TCE	Trichloroethene
TPHs	Total petroleum hydrocarbons
UTCHEM	University of Texas Chemical Simulator
VC	Vinyl chloride
VOCs	Volatile organic compounds
ZVI	Zero valent iron
nZVI	Zero valent iron nanoparticles
eZVI	Zero valent iron emulsified
1-D	one-dimensional
2-D	two-dimensional
3-D	three-dimensional

1. INTRODUCTION

1.1. DNAPL in the Subsurface

Organic compounds -such as petroleum hydrocarbons and chlorinated solvents- are widely used in numerous industrial applications. Because of their low solubility many of these compounds are often present in the environment in the form of non-aqueous phase liquids (NAPLs). When released into the subsurface, small amount of these compounds can potentially contaminate large portion of the groundwater resources for many years due to their high toxicity and persistence and low maximum contaminant levels (MCL).

NAPLs have typically been divided into two categories, dense and light. These terms describe the specific gravity of the NAPL relative to water. The dense non-aqueous phase liquids (DNAPLs) have a specific gravity greater than water, while the light non-aqueous phase liquids (LNAPLs) have a specific gravity less than water (Huling and Weaver, 1991). If spilled into the subsurface through the vadose zone, LNAPLs tend to accumulate at the water table while DNAPLs tend to migrate deeper into the subsurface until they reach a low permeable layer which acts as a capillary barrier that prevents the DNAPLs' further downward migration. Due to their low aqueous solubility, high density and low viscosity, once DNAPLs penetrate below the water table, they can provide a long-term source of contamination. Figure 1.1 shows a schematic of a typical distribution of a DNAPL accidently released in the subsurface.

1.2. Remediation

The persistence of DNAPLs in the subsurface poses a unique challenge for classic "pump & treat" remediation techniques which consists of placing extraction wells downstream of DNAPL zones to pump water from the plume and treating the contaminated water at the ground surface before discharging it (ITRC, 2002). However, field applications have shown that the efficiency of this treatment technology is limited due to several factors; DNAPL mass rate of recovery is limited by the low contaminant solubility, high interfacial tension between the DNAPL and water, contaminant mass entrapped in low permeability zones, the relatively large masses of the DNAPL present in the aquifer and the inability of water flooding to mobilize and displace the DNAPLs from porous media. (Doty and Travis, 1991).

As a result, pump & treat can remove some mobile free phase DNAPL, but most of the contaminant mass would remain entrapped by capillary forces in the aquifer. DNAPL mass is often encountered in the form of pools above confining layers and in areas with low soil permeability. In contrast to residual DNAPL, DNAPL in pool forms are particularly challenging to treat because of the low contact area between the water and the DNAPL phases which leads to high enough concentrations that exceed the maximum allowable limits yet low enough to make the remediation highly inefficient (Johnson and Pankow, 1992).

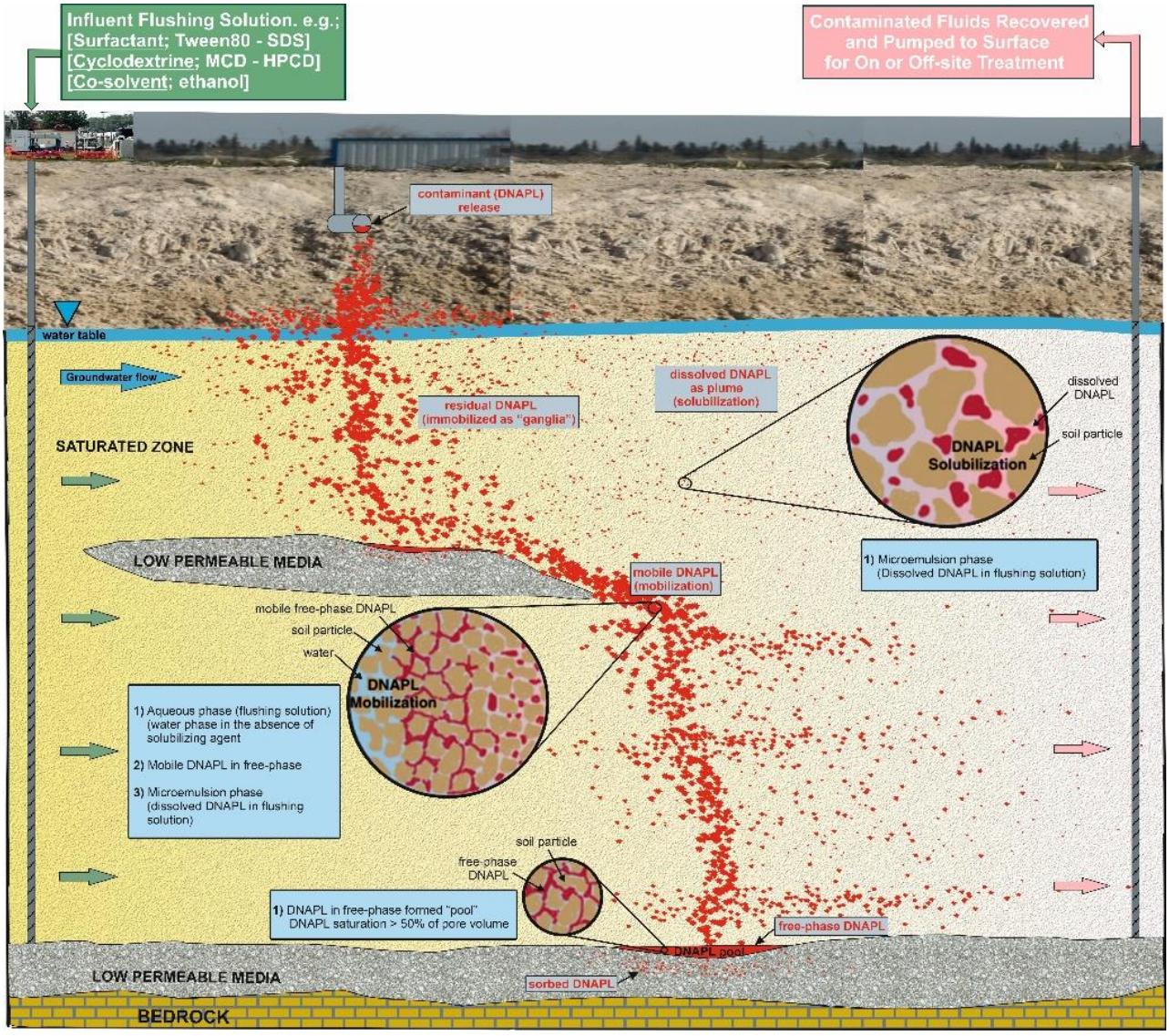

Figure 1.1. DNAPL transport and distribution in subsurface.

Due to the limitations of the classic pump & treat remediation method, various remediation technologies have been developed over the last few decades. Foremost among these techniques are in-situ enhanced solubilization (ISES) and in-situ chemical oxidation (ISCO). Each of these technologies are described below.

In-situ enhanced solubilization (ISES) is a widely used remediation technique which involves the use of chemical agents in the flushing solution to enhance the solubility and mobility of contaminants in the groundwater (Harvell, 2012; Tick et al, 2015). In this technique, dissolution of the immiscible contaminant into the aqueous phase is enhanced by the addition of a solubility-enhancement reagents to the flushing solution. The resulting increase in the mass removal rate speeds up the NAPL recovery from the subsurface relative to classical pump & treat and reduces the remediation time along with the cost of clean-up operations (Boving and Brusseau, 2000). Research over the past decade has shown that the use of co-solvents, surface active agents (surfactants) and complexing agents (such as cyclodextrins) acts to increase the efficiency of DNAPL mass removal from the subsurface by increasing the apparent solubility of the hydrophobic organic contaminants (Akgoze Aydin et al, 2011; Akyol, 2018; Akyol and Turkkan, 2018; Akyol et al, 2013; Aydin-Sarikurt et al, 2016; Boving and Brusseau, 2000; Carroll and Brusseau, 2009; DiFilippo et al, 2010; Harvell, 2012; McCray and Brusseau, 1999; Mohammed et al, 2019; Tick and Rincon, 2009; Tick et al, 2003, 2015; Javanbakht and Goual, 2016; Wu et al, 2016; Demiray et al, 2021).

Surfactants have been widely used because they contain both hydrophobic and hydrophilic moieties. Below the critical micelle concentration (CMC), surfactants exist as monomers and have small effect on the solubility of most organic contaminants. Above the CMC, these monomers aggregate to form micelles. Low polarity contaminants can partition to these micelles. The apparent aqueous solubility can increase, thereby increasing the dissolution and desorption of the contaminants. Another solubilizing agent is methyl-beta-cyclodextrin (MCD), a glucose-based molecule comprising a hydrophobic interior cavity. This is where DNAPL compounds can partition, therefore increasing their apparent solubilities (Badr et al, 2004; Boving and Brusseau, 2000; McCray et al, 2000; Tick and Rincon, 2009; Wang and Brusseau, 1993; Yang et al, 2006).

Another promising technology is in-situ chemical oxidation (ISCO) which involves injecting an oxidizing agent solution into the groundwater that enables direct contact between the oxidant and the organic contaminant source zone/plume leading to the DNAPL chemical degradation in place (Marble, 2005). While a portion of contaminated water that would be treated ex-situ at the surface (pump & treat), ISCO eliminates this step by treating the contaminant at the place of contact with the injected oxidizing agent; thus, large quantities of contaminated water do not need to be treated or disposed of on the surface. ISCO can remediate a wide range of contaminants including: BTEX (benzene, toluene, ethylbenzene, and xylenes), tetrachloroethene (PCE), trichloroethene (TCE), dichloroethene (cis-DCE, trans-DCE, 1,1-DCE), vinyl chloride (VC), MTBE (methyl-tertyl-butyl-ether), and PAH (polyaromatic hydrocarbons) compounds (ITRC, 2002). Studies have shown that

ISCO can effectively reduce the mass of DNAPL in source zones but that its efficiency is mostly limited by the low dissolution rates of DNAPL, particularly when the DNAPL is poorly accessible or is in pool-dominated form (Marble et al, 2010; Akyol and Yolcubal, 2013). Oxidants considered in groundwater remediation studies include permanganate, catalyzed hydrogen peroxide, ozone, and more recently, sodium persulfate. At sites where DNAPL is present as a long-term contaminant source, the persistence of an ISCO oxidant in the subsurface environment is an important factor (Liang and Bruell, 2008).

Among the oxidants that have been considered, potassium or sodium permanganate ($KMnO_4$, $NaMnO_4$) have been used intensively. Sodium persulfate ($Na_2S_2O_8$) is an affective agent because it does not readily react with soil organics, this makes it relatively persistent in soil systems (Brown et al, 2001; Huang et al, 1999). However, sodium persulfate needs to be activated to effectively oxidize many types of DNAPL, unlike permanganate. Sulfate radicals formed in this way are more effective than many oxidants in oxidizing DNAPL. Persulfate can be activated using heat, alkaline, radiation, transition metal ions and metal oxides, carbonaceous based materials, phenol, and quinones (Wang and Wang, 2018).

1.3. Modeling

Mathematical models are often used to understand the fate and transport of contaminants in groundwater systems. Considering the complexity of DNAPL subsurface migration and the evolution of source zone, evaluating the fate and transport often requires the use of a computer-based numerical model. Numerical modeling is able to provide a cost-efficient method to examine the complicated physical and chemical processes such as complex phase behavior and to evaluate the impacts and performance of DNAPL source-zone remediation (Liang and Falta, 2008). Within the context of ISES and ISCO, the objective of the modeling of enhanced solubilization and chemical oxidation of contaminant is to aid in the scale-up and optimization of the design of these types of remediation techniques, to assess the performance of the methods at both the laboratory and field scales with respect to both risk and effectiveness, to improve the understanding of process mechanisms, and to explore alternative strategies and approaches to remediation (Delshad et al, 1996).

1.4. Objectives

While both remediation methods, ISES and ISCO have been studied extensively on their own, studies that combines the two techniques are relatively few. The proposed research aims to investigate

the synergistic benefits of combining these two technologies, in-situ chemical oxidation with enhanced solubilization, whereby the co-solvents, surfactants, or complexing agents transfer the NAPL to the aqueous phase where it then reacts with the oxidizing agents and transform it into harmless products. Additionally, a numerical multiphase flow model is used to simulate the main fate and transport processes.

Therefore, the proposed research consists of two items: (i) laboratory-scale experiments demonstrating the synergistic advantages and potential limitations of the ISES and ISCO technologies and (ii) numerical modeling of multiphase flow and DNAPL transport, dissolution, and oxidation. The experimental component of the study consists primarily of batch tests and 2-D flow-cell flushing experiments. The modeling involves the adaptation of the system of reaction equations and parameters inside the state-of-art computer program UTCHEM (Delshad et al, 1996) to simulate the oxidation and surfactant-enhanced oxidation of DNAPL which were examined experimentally.

The specific tasks of the study include:

1- Bench-scale batch experiments:

(A.1) to determine the miscibility and dissolution potential of a single DNAPL and multi-component DNAPL with different solubilizing agents (Tween 80, SDS, MCD) as a function of solubilizing agent concentrations

(A.2) to investigate whether solubilizing agents interfere with the oxidation processes due to the increased dissolution rate of DNAPL into the aqueous phase

(A.3) to determine the impact of oxidant and surfactant combinations on oxidation reaction rates

(A.4) to investigate different sodium persulfate activation methods

2- Bench-scale flow-cell flushing experiments:

(B.1) to assess the enhanced dissolution potential of different solubilizing agents (Tween 80, SDS, MCD) for single DNAPL and multi-component DNAPL entrapped in water-saturated soil

(B.2) to investigate the oxidation potential of different oxidizing agents (potassium permanganate, sodium persulfate) for DNAPL entrapped in water-saturated soil

(B.3) to assess the combined synergistic effect of enhanced solubilization and chemical oxidation for the in-situ remediation of DNAPL entrapped in water-saturated soil

(B.4) to evaluate the solubilizing agent and oxidant (potassium permanganate) performance of DNAPL remediation both in homogeneous silica sand and natural calcareous soil media

3- Numerical modeling:

(C.1) simulate the above flushing experiments using the computer code UTCHEM, a state-of-art multiphase flow simulator

(C.2) to investigate the impact of solubilizing agents on interphase mass transfer from the DNAPL pool to the aqueous phase, and whether existing models can accurately describe this process

(C.3) to assess the impact of DNAPL entrapment architecture (the initial distribution of the DNAPL mass) on ISCO enhanced ISES for DNAPL mass depletion.

(C.4) to investigate the capability of the code, UTCHEM, for integrating the chemical oxidation processes into the enhanced solubilization multiphase flow model

The procedure for applying a groundwater flow or transport model includes the following steps:

- Define study objectives – Data collection
- Develop a conceptual model
- Select a computer code or algorithm
- Construct a groundwater flow or transport model
- Calibrate the model and perform sensitivity analysis

Generally, these steps are followed in this order, however previous steps are often revisited as new concepts are explored or as new data are obtained (ASTM International, 2004) (Figure 1.2). Modeling steps can be enlarged to fulfil the need of quantitative representation of a system from a small bench to a large field-scale.

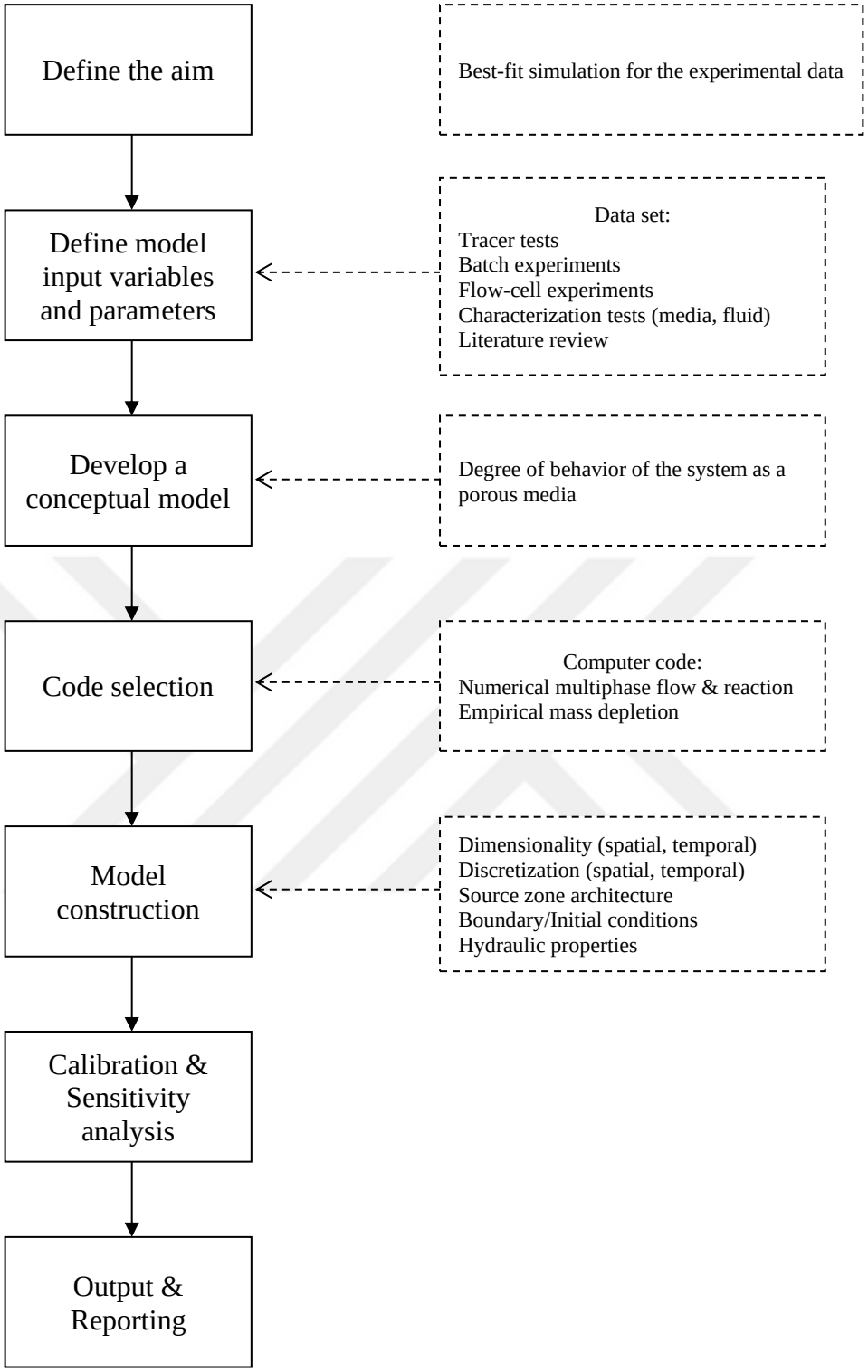

Figure 1.2. Flowchart of the modeling process adopted to the study.

The target DNAPL for the study is the Tetrachloroethene (PCE), (C_2Cl_4), which is considered particularly dangerous to the environment and human health and has been widely encountered at numerous subsurface contamination sites (USEPA, 2016). PCE is a dense non-aqueous phase liquid (DNAPL) because of its relatively high density, 1.6230 g/cm^3 at 20 ℃ (Lide, 2007), with aqueous

solubility of 206 mg/L at 25 ℃ in water (Horvath, 1982). The Agency for Toxic Substances and Disease Registry ranked PCE 33rd in its 2022 listing of hazardous substances (ATSDR, 2022). PCE continues to be one of many volatile organic compounds labeled as a “contaminant of concern”.

Trichloroethene (TCE), (C_2HCl_3) and Dichloroethene (DCE), ($C_2H_2Cl_2$) are found in more than 20% of all sites with groundwater pollution in European countries, with many of these sites being dry cleaning facilities (Honning, 2007) and the combination or one of these three compounds detected in groundwater in more than 50% of Superfund sites in USA (Harvell, 2012). Trichloroethene (TCE), which is mainly used for industrial application, degreasing, and dry cleaning and is released into the environment because of leakage from storage tanks and the use of improper disposal procedures (Peng et al, 2016; Liang et al, 2004). Since TCE is a possible human carcinogen and has acute toxicity to humans, the contamination of groundwater with TCE is of concern (Chang et al, 2018). The US Environmental Protection Agency (EPA) has set a maximum contaminant level (MCL) of 5 µg/L for drinking water to protect public health (USEPA, 2008).

Besides PCE as a single type of DNAPL, enhanced solubilization performances in the presence of multiple component DNAPLs (PCE:TCE:1,1-DCE) were also investigated in the scope of the study.

2. LITERATURE REVIEW

In this chapter, published studies that are most relevant to the thesis are reviewed. In particular, the emphasis is on separate and combined applications of solubilizing agent and oxidant flushing technologies to remediate DNAPL compounds. The studies examined include from batch, column or flow-cell experiments in laboratory as well as few of in-situ field-scale practices. Each subsection will include a general background of the relevant agents used. Most related modeling studies are also reviewed in this section.

2.1. In-Situ Enhanced Solubilization (ISES)

In-situ enhanced solubilization (ISES) involves the use of some agent that enhances the solubility of the DNAPL thereby facilitating its extraction from the groundwater. There are a number of agent groups that have been tested over the years. Co-solvents are water-miscible or partially water-miscible organic compounds, such as methanol, ethanol, and butanol. This group of solvents, when dissolved in water, reduces the polarity of the aqueous phase thus increasing the solubility of hydrophobic organic compounds (Boving and Brusseau, 2000). Co-solvents can greatly reduce interfacial tensions and may begin mobilization of the NAPL phase (Boving and Brusseau, 2000). Surfactants have both hydrophobic and hydrophilic moieties. Above the critical micelle concentration (CMC), the surfactant monomers aggregate to form micelles in aqueous systems which contaminants can partition. This partitioning increases the apparent solubility, thereby increasing the dissolution and desorption of the contaminants (Boving and Brusseau, 2000). Pharmaceutical industry have been using cyclodextrins in their applications such as drug delivery or food industry for a long time.

Cyclodextrin is a polycyclic oligosaccharide, or sugar formed by the degradation of starch by bacteria (Bender and Komiyama, 1978). These cyclo-shaped molecules form complexes with non-polar organic contaminants. The formation of cyclodextrin-organic contaminant complexes greatly enhance the aqueous-phase solubility of organic contaminants (Tick, 2003).

Over the past 2-3 decades, a large amount of research conducted with batch, column and flow-cell experiments has been done to analyze the effectiveness of different flushing agents on DNAPL contaminants. The more directly related studies are highlighted here (Boving and Brusseau, 2000; Tick and Rincon, 2009; Carroll and Brusseau, 2009; Tick et al, 2015; Yang and Yang, 2018).

There are many laboratory studies in the literature regarding the use of in-situ enhanced solubilization technology alone in DNAPL removal. Table 2.1 lists bench scale studies using co-solvent and surfactant/co-solvent flushing.

Table 2.1. Mass recoveries with in-situ enhanced solubilization with several solubilizing agents from selected column/flow-cell studies.

Solubilizing agent	**Media**	**NAPL**	**% saturation**	**PV**	**% Mass Removal**	**Reference**
4 %POE 20[1]	20-30 mesh sand	PCE	15.4	15	90 (S)	Pennel et al, 1994
	40-120 mesh sand		13.5	18	97 (S)	
4 %*DSS*[2]	40-270 mesh sand	PCE	21	<2	80 (M)	Pennel et al, 1994
5 wt% SDS[2]	<2 mm sand (O.C.= 0.29 %)	TCE	19	60-120 Flow interrupted	6.9 (M) 87 (S)	Boving and Brusseau, 2000
5 wt% DOWFAX8390[2]			20		2.7 (M) 90 (S)	
5 wt% MCD[3]			15		12 (M) 81 (S)	
5 wt% HPCD[3]			18		92 (S)	
50 %EtOH			18		11 (M) 84 (S)	
4 %*Tween 80*[1]	Quartz sand	TCE	2.5	2.5	66 (S)	Suchomel et al, 2007
5 %wt HPCD[3]	20-30 mesh sand	DNAPL mix	8-14	113	100 (S)	Tick et al, 2015

[1] nonionic surfactant, [2] anionic surfactants, [3] complex sugar,
S: solubilization, M: mobilization

The use of in-situ enhanced solubilization for the remediation of NAPL zones was also tested under field conditions where soils tend to be more heterogeneous and where the distribution of the NAPL mass is more uncertain. Table 2.2 provides selected examples from field applications. Overall, these studies show the effectiveness of various flushing agents to enhance the solubility of various NAPLs and the possibility of mobilization of the NAPL if the co-solvent content in the flushing solution is high. However, they also point out to some challenges when applying ISES technology in the field. Foremost among these challenges is the lack of exact information on the mass of DNAPL in the subsurface and its saturation distribution and the heterogeneity of the subsurface, especially the presence of low permeability lenses, which tend to limit the contact between the injected enhanced dissolution agent and the entrapped DNAPL where the DNAPL is resided.

Table 2.2. Field investigations of ISES to remediate NAPL sites.

Flushing Solution	Removal Mechanism	NAPL	P.V.	% Mass Removal	Reference
Surfactant *1 %Tween80*[1]	Solubilization	PCE	1.5	>94%	Abriola et al, 2005
Complex sugar *15 %wt HPCD*	Solubilization	PCE	7	48	Tick et al, 2003
Co-solvent *95 %ethanol + 5 %water*	Solubilization, mobilization	PCE	2	62	Jawitz et al, 2000
Co-solvent *80 %tert-butanol, 15 %n-hexanol*	Mobilization	PCE Jet Fuel	4	-	Falta et al, 1999
Surfactant/Co-solvent/Polymer *Hostapur SAS 60*[2] *+ n-butanol*	Solubilization	DNAPL mix	1	~86	Martel et al, 1998
Complex sugar *10 %wt Cyclodextrin*	Solubilization	NAPL mix	8	41	McCray and Brusseau, 1998
Co-solvent *70 %ethanol +12 %pentanol + 28 %water*	Solubilization	PCE Jet Fuel	9	75	Rao et al, 1997; Sillan et al, 1998
Surfactant *2 % solution of nonylphenol ethyoxilate (NPEO)*[3] *and NPEO phosphate*	Solubilization	PCE	14	80	Fountain et al, 1992

[1] Tween80: polyoxyethylene (20) sorbitan monooleate
[2] Hostapur SAS 60: sodium $C_{14/17}$ secondary alkyl sulphonate
[3] NPEO: Nonylphenol Ethoxylates

2.2. In-Situ Chemical Oxidation (ISCO)

ISCO involves the injection of oxidants for the purpose of in-situ oxidation of the DNAPL entrapped in the subsurface. At sites where DNAPL is present as a long-term contaminant source, the persistence of an ISCO oxidant in the subsurface environment is an important factor (Liang and Bruell, 2008). The oxidants considered in groundwater remediation studies include permanganate, catalyzed hydrogen peroxide, ozone, and more recently, sodium persulfate. Studies that considered these oxidants are discussed below.

2.2.1. Potassium Permanganate

Potassium permanganate ($KMnO_4$) is a common form of permanganate (MnO_4^-) used for in-situ treatment of chlorinated solvents (USEPA, 2006). $KMnO_4$ is a crystalline solid which can be used to form aqueous MnO_4^- solutions up to 4 % (40 g/L). The oxidation process strictly involves direct electron transfer, rather than free radical processes that characterize other oxidants such as hydrogen peroxide and persulfate (Siegrist et al, 2001; USEPA, 2006). By-products are innocuous substances including water, carbon dioxide, chloride, and precipitates (manganese oxide - MnO_2). The production of manganese oxide can lead to the clogging of porous media. Permanganate is a strong

oxidant that is capable of attacking chlorinated ethenes through direct electron transfer (redox potential (E°)= 1.68 V (Latimer, 1952)). The overall reactions are given below in reaction (2.1) for TCE (Li and Schwartz, 2004; Akyol and Yolcubal, 2013) and reaction (2.2) for PCE (Zhai et al, 2006),

$$C_2HCl_3 + 2MnO_4^- \rightarrow 2MnO_{2(s)} + 2CO_2 + 3Cl^- + H^+ \quad (2.1)$$

$$3C_2Cl_4 + 4MnO_4^- + 4H_2O \rightarrow 4MnO_{2(s)} + 6CO_2 + 12Cl^- + 8H^+ \quad (2.2)$$

A number of laboratory studies has been performed that investigated the kinetics, mechanisms and pathways for oxidation of TCE and PCE by permanganate (Yan and Schwartz, 1999; Urynowicz, 2000; Hood et al, 2000; Huang et al, 2002) (Table 2.3) as well as the treatment effectivness in porous medium (Table 2.4).

Table 2.3. Reported rate constants from oxidation reactions between PCE, TCE and permanganate performed in batch kinetic experiments.

NAPL	**k ($M^{-1}s^{-1}$)**	**pH range**	**Reference**
TCE	0.67 ± 0.03	4-8	Yan and Schwartz, 1999
TCE	0.88 ± 0.07		Urynowicz, 2000
PCE	0.041 ± 0.001	5.6-7.1	Hood et al, 2000
PCE	0.035 ± 0.004	3-10	Huang et al, 2002
PCE	0.017 ± 0.002 (lower at higher pH)	10.6	Dai and Reitsma, 2002

Table 2.4. 1-D, 2-D laboratory studies of permanganate oxidation of DNAPLs.

NAPL	media	% saturation	Oxidant concentration	Explanation	Reference
PCE	sandy soil (column)	1	10 g/L	250 hours of oxidant flush with 42 cm/day of flow rate	Schnarr et al, 1998
PCE	Sand (batch)	-	2.5 wt%	59 % reduction in PCE after 2hrs of rxn	Gates-Anderson et al, 2001
TCE				90 % reduction in TCE after 2 hours of rxn	
TCE	Sand (Rectangular chamber)	2.5-4.5 (37mL TCE injected)	1 g/L	1/3 PV of oxidant injection followed by 1.2 PV of DI flushing v: 0.2 cm/min	Conrad et al, 2002
TCE	20-30 mesh sand (Rectangular Flow-cell)	0.15	Constant injection of 15 mM oxidant to 4.9 PV	20 % oxidized Pore velocitiy: 3.5 cm/hr	Marble et al, 2010
		0.19	Pulsed injection of 15 mM oxidant to 4.5 PV followed by water flood	14 % oxidized Pore velocitiy: 4.5 cm/hr	
TCE	Caliche soil (Rectangular Flow-cell)	1.5-17 (7.3 mg TCE)	80 mM	98 % oxidized Complete removal after 6 PV Flow interrupted	Akyol and Yolcubal, 2013

2.2.2. Sodium Persulfate

Sodium persulfate is a useful ISCO agent because it does not immediately react with soil organics, making it relatively persistent and available in soil systems (Brown et al, 2001; Huang et al, 1999). Persulfate has a high water solubility which makes it attractive for ISCO applications (saturated solution: 2.5 M $Na_2S_2O_8$ at 20 °C) (Behrman and Dean, 1999), no odor, the effectiveness of oxidation (redox potential (E°)= 2.01 V) over a wide range of pH (Latimer, 1952), and lower affinity for soil organics at typical temperatures encountered in the subsurface (e.g., at 15 °C in the subsurface) (Brown et al, 2001).

Persulfate is typically used in combination with an activator to result in the formation of sulfate-free radicals (Cao et al, 2008; Chen et al, 2009; Killian et al, 2007; Liang et al, 2008; Liang et al, 2009; Tsitonaki et al, 2010; Waldemer et al, 2007). Several researchers have demonstrated that activation of persulfate is not always necessary for some contaminants, including 1,4-Dioxane (Felix-Navarro et al, 2007; Liang et al, 2007, 2008). However, sodium persulfate needs to be activated to effectively oxidize many types of DNAPL compounds. Sulfate radicals formed in this way are more effective than many oxidants in oxidizing DNAPL. This step initiates a chain of radical reactions

involving species (including SO_4•- ,E° = ~ 2.6 V, (Eberson, 1987) and OH• ,E° = 2.7 V, (Buxton et al, 1988) that oxidize contaminants more rapidly than persulfate (E° = 2.01 V, (Latimer, 1952)) does directly (Johnson et al, 2008; Liang and Bruell, 2008). Persulfate can be activated using heat, alkaline, radiation, transition metal ions and metal oxides, carbonaceous-based materials, phenol, and quinones (Wang and Wang, 2018). Elloy et al (2014) was investigated the activation of persulfate by surfactants under acidic and basic conditions resulting the cationic surfactants showed the most potential for persulfate activation.

2.2.2.1. Iron Activation

Iron activation (Fe^{2+}, Fe^{3+}, Fe_2O_3, Fe_3O_4, Fe^0), reported to give effective results in the removal of chlorinated alkenes, is often preferred due to its low cost and environmental friendliness (Chen et al, 2018; Tang et al, 2015; Yen et al, 2011). Since divalent iron (Fe^{2+}) increases the oxidation kinetics of the pollutant, it has been emphasized in the literature, with sulfate radicals forming when it directly reacts with persulfate (Zhou et al, 2019).

Recent findings indicate that persulfate activated with zero-valent iron (Fe^0 or ZVI) has effective activating effect in hydrocarbon-contaminated soil remediation and water treatment processes (Desalegn et al, 2018; Oh et al, 2010). This is because ZVI, the insoluble form of iron, reduces the interaction of excess Fe^{2+} ions with sulfate radicals and forms sulfate radicals by direct reaction with persulfate (Liang and Guo, 2012) (reaction 2.3 and 2.4).

$$Fe^0 + S_2O_8^{2-} \rightarrow Fe^{2+} + 2SO_4^{\bullet-} + 2SO_4^{2-} \quad (2.3)$$

$$S_2O_8^{2-} + Fe^{2+} \rightarrow Fe^{3+} + SO_4^{\bullet-} + 2SO_4^{2-} \quad (2.4)$$

The breakage of Cl–carbon bonds and the release of chloride ions by persulfate oxidation is an index of toxic degradation of chlorinated ethenes (Tsai et al, 2009).

On the other hand, the presence of excess divalent iron (Fe^{2+}) in the aqueous medium can stop the reaction due to the rapid reaction with persulfate and sulfate radicals, which reduces the efficiency of pollutant reclamation from the soil medium (Fordham and Williams, 1951; Liang et al, 2004; Sihyun et al, 2010). In addition, Fe^{3+} ions in the aqueous phase have low solubility at pH>5 and can precipitate as $Fe(OH)_3$. For this reason, it is desirable to adjust the pH of the soil during remediation to ensure the effectiveness of the activation (Pardo et al, 2016). However, in large-scale field

conditions, adjusting the pH is not feasible and may adversely affect the physical and chemical properties of the soil (Usman et al, 2014; Sihyun et al, 2010).

Al Shamsi and Thomson (2013) used persulfate to treat in the presence of a variety of iron activators (i.e., nano-sized ZVI (nZVI), granular ZVI and Fe^{2+}). The study reveals the importance of selecting optimum contaminant/persulfate/nZVI ratio. Prior to investigating the system with contaminant, the authors reported that preliminary or ancillary experiments play a key role to comprehend the behavior of persulfate during the activation. At higher molar ratios of persulfate/nZVI such as 1/0.5, a number of positive effects were reported: (i) less persulfate decomposed, (ii) less production of Fe^{2+}, Fe^{3+} that cause natural corrosion, (iii) higher reaction rate. At lower molar ratios of persulfate/nZVI such as 1/5 a number of adverse effects are observed: (i) more than 99 % of persulfate consumed (decomposed), (ii) Fe^{3+} reached to theoretical end and remaining nZVI did not react with persulfate (deactivated nZVI surface), (iii) drastic reduce in reaction rate, (iiii) transition from oxidizing to reducing. Further this ratio (i.e., 1/7), nZVI attacked TCE directly which is known as reductive dechlorination. They identified the optimal molar ratio for persulfate/nZVI as 1/1.

However, there are several challenges associated with nZVI activation in relation to the degradation of contaminants including aggregation and rapid oxidation of nZVI particles itself (Tan et al, 2017). If the outer part is not coated, there is always a risk that an iron oxide-containing layer will form on the surface of the elemental ZVI, whether in coarse dry powder or nano-sized slurry, as a result of oxidation by air leading to reduced reactivity. This situation reveals that additional precautions should be taken regarding the use of nZVI . Moreover, nZVI in powder form may show irreversible agglomeration and lose its properties when it enters the aqueous environment. The fact that nZVI as slurry is more preferable to its powdered version in both laboratory and field applications is important because of its ease of use and because the particles are emulsified during synthesis under appropriate conditions. However, nZVI slurry has a certain shelf life that is dependent on storage temperature (Figure 2.1).

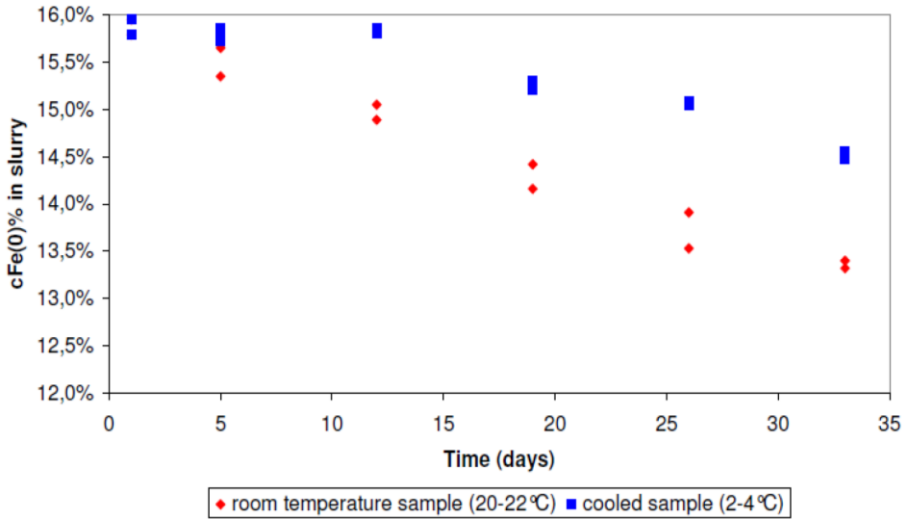

Figure 2.1. Ageing process of nZVI during time depending on storage conditions (https://nanoiron.cz/NanoIron/media/content/Download/nZVI-ageing-short.pdf).

2.2.2.2. Heat Activation

Another persulfate stimulation method leading to release of $SO_4^{\bullet-}$ radicals is heat activation. The thermal decomposition of persulfate follows well-behaved kinetics, which can be readily determined from laboratory feasibility tests (Johnson et al, 2008). However, data show that the lifetime of persulfate (and therefore the availability of sulfate radical) is relatively short at elevated temperatures, which limits the distances over which diffusion of persulfate can be effective and can therefore impose design constraints on the in-situ application of thermally activated persulfate (Johnson et al, 2008). The sulfate-free radical is formed at temperatures of 40-99 °C by the thermal decomposition (also known as "thermal activation") of the persulfate anion in an aqueous phase as shown in the following reaction (2.5) (Liang and Bruell, 2008),

$$S_2O_8^{2-} + \text{Heat} \rightarrow 2SO_4^{\bullet-} \qquad (2.5)$$

From the activation energies calculated, it was found that the rate of the unproductive consumption of persulfate was selectively increased with temperature (Dominguez et al, 2020). On the other hand, various studies reported that ~40 °C is effective for persulfate activation and subsequent contaminant oxidation (Head et al, 2020; Chowdhury et al, 2017; Huang et al, 2005; Liang et al, 2003). The stoichiometry for the oxidation of PCE by persulfate, based on the ratio of products after the complete initial PCE and TCE mass were oxidized, can be described by the following reactions (Costanza et al, 2010) (2.6) and (2.7) or (2.8) (ITRC, 2005; Liang et al, 2007; Chang et al, 2018), respectively.

$$2C_2Cl_4 + Na_2S_2O_8 + 8H_2O \rightarrow 2SO_4^{2-} + 4CO_2 + 8Cl^- + 10H^+ + 3H_2 + 2Na^+ \quad (2.6)$$

$$C_2HCl_3 + 3Na_2S_2O_8 + 4H_2O \rightarrow 6SO_4^{2-} + 2CO_2 + 3Cl^- + 9H^+ + 6Na^+ \quad (2.7)$$

$$C_2HCl_3 + 6SO_4^{\bullet-} + 4H_2O \rightarrow 6SO_4^{2-} + 2CO_2 + 3Cl^- + 9H^+ \quad (2.8)$$

Many studies in the literature agree that there are many complex and reversible reactions between activated persulfate and DNAPL, and this mechanism depends on many parameters such as porous environment, pH, pollutant type, activation type.

ISCO field studies and laboratory tests have been studied extensively. These studies have demonstrated that mass transfer from the DNAPL pool to the reactive aqueous phase is a limiting step to chemical oxidation (Schnarr et al, 1998). Thus, improvements to in-situ oxidation technology may be possible through the understanding and enhancement of DNAPL mass transfer (Petri et al, 2008). Table 2.5 shows batch studies of thermally activated persulfate for the oxidation of various VOCs (NAPLs) in the literature.

To date, documented field applications of thermally activated persulfate are scarce (Head et al, 2020). Thompson et al (2006) used steam-activated persulfate injection in a field-scale demonstration that has been successful for in-situ activation to address the most recalcitrant compounds. During steam injection, soil temperatures up to 45 °C were observed. A final highly targeted injection in a specific area brought the entire suite of chlorinated and petroleum compounds below regulatory standards. Conversely, heat dispersion in the subsurface leads to less efficient and uneven delivery and limited permeability (Li et al, 2020).

Table 2.5. Experimental conditions of thermally activated persulfate for the oxidation of various VOCs (NAPLs) in the literature.

Removal (%)	pH adjust	Rxn rate	Rxn time (h)	Soil/water ratio	Media type	PS/NAPL molar ratio	Solubilizing agent	Activator	Persulfate (PS)	NAPL conc.	Target NAPL	Reference
-	from 6.9 to 6.8	$0.13*10^4$ s^{-1}	24<	-	Aqueous	-	-	20 °C	31.5 mM (8 g/L)	0.06 mM	MTBE	Huang et al 2002
	from 6.9 to 6.7	$0.59*10^4$ s^{-1}	8					30 °C				
	from 6.9 to 6.3	$2.14*10^4$ s^{-1}	2					40 °C				
	from 6.9 to 6.6	$5.8*10^4$ s^{-1}	1					50 °C				
-	PS @pH: 6	0.0018 h^{-1}	ND	-	Aqueous	10:1	-	20 °C	-	0.46 mM (60 mg/L)	TCE	Liang et al 2003
85		0.48 h^{-1}	6					40 °C				
100		1.63 h^{-1}	3					50 °C				
100		4.57 h^{-1}	1					60 °C				
-	from 5 to 3.7 in 6 hrs	0.206 h^{-1}	48	1:5	Soil slurry (foc=1.6%)			50 °C / Fe^{2+} (0.43 mg/L)				
-		0.149 h^{-1}			Soil slurry (foc=1.09%)			50 °C / Fe^{2+} (0.29 mg/L)				
		0.153 h^{-1}			Soil slurry (foc=0.3%)			50 °C / Fe^{2+} (0.01 mg/L)				
-	PS @pH: 6	-	ND		Aqueous	10:1	-	20 °C	-	60 mg/L	TCA	
SD		0.0127	6					40 °C				
40		0.091	6					50 °C				
100		0.555	6					60 °C				
75 (PCE) 79 (TCE) 90 (DCE)	NO from 6.8 to 2.1	0.019 h^{-1} (PCE) 0.0245 h^{-1} (TCE) 0.031 h^{-1} (DCE)	72	-	Aqueous	-	-	40 °C	4.2 mM (1 g/L)	0.1 mg/L for each	PCE TCE DCE	Huang et al 2005
100	NO from 6.8 to 1.7	-							21 mM (5 g/L)			

Table 2.5. *continued*

Removal (%)	pH adjust	Rxn rate	Rxn time (h)	Soil/water ratio	Media type	PS/NAPL molar ratio	Solubilizing agent	Activator	Persulfate (PS)	NAPL conc.	Target NAPL	Reference
100	PS @pH: 7 Rxn adjusted @pH: 2	-	336	-	Aqueous	50:1	-	10 °C	23 mM	0.46 mM (60 mg/L)	TCE	Liang et al 2007
		$1,2*10^2\ h^{-1}$ With EtOH: $0.18*10^2\ h^{-1}$ @pH:4 $0.1\ h^{-1}$ @pH:7 $0.09\ h^{-1}$ @pH:9	168					20 °C				
		-	46					30 °C				
-	NO	-	26	-	Aqueous	10:1	-	30 °C	0.45 mM 20 mM 20 mM	0.045 Mm 2 mM 2 mM	(VOCs): PCE TCE DCE	Waldemer et al 2007
			13					40 °C				
			6					50 °C				
			1.5					60 °C				
			0.4					70 °C				
100	PS @pH: 7	0.43 mM Chloride produced	1.5	-	Aqueous	-	-	50 °C	4.02 mM	0.105 mM	PCE	Costanza et al 2010
-		-	2	1:1 (8g of soil + 8g of GW)	Few types of soil				2.9 g/kg for Great Lakes 0.64 g/kg for others			
76	NO	-	24	-	Aqueous	10:1	EtOH (200 mM)	50 °C	10 mM	1 mM	TCA	Zhu et al 2018
41							TBA (200 mM)					
100	NO	-	6	-	Aqueous	-	-	50 °C	20 mM	0.1 mM for each	BTEX mix	Ma et al 2018
-	NO	-	2.5	-	-	-	-	30 °C	40 g/L	5.54 mg/L	DCB	Dominguez et al 2020
	NO							40 °C				
	NO from 3 to 1.36							50 °C				

2.3. In-Situ Chemical Oxidation by Enhancement of Solubilization

Literature findings from batch experiments showed that the combination of potassium permanganate and surfactant molecules at the critical micelle concentration (CMC) can significantly enhance DNAPL removal (Tsai et al, 2009). The critical micelle concentration is an important surfactant concentration to consider, as micellar transport of DNAPL to the aqueous phase is a key mechanism in DNAPL dissolution (Mayer et al, 1999). Higher pseudo first-order reaction rate constants have been observed with increasing surfactant concentration (Li and Hanlie, 2008). These findings have led in recent years to the testing of various surfactants by soil remediation companies and their pilot-scale applications on contaminated sites, apart from laboratory research. Several studies have been published in the literature relating to the combination of co-solvent, surfactant or complex sugar enhanced aquifer remediation with chemical oxidation in porous media (Gates-Anderson et al, 2001; Conrad et al, 2002; Zhai et al, 2006; O'Hara et al, 2006; Li and Hanlie, 2008; Tsai et al, 2009; Harendra and Vipulanandan, 2011; Zheng et al, 2016).

Gates-Anderson et al (2001) compared $KMnO_4$ and H_2O_2 effectiveness in laboratory-slurry experiments for various VOCs (PCE, TCE, and TCA) in the presence of surfactant (Tween 80). The combined usage of both surfactant and oxidants did not remove TCA (1,1,1-trichloroethane), however higher mass reduction was observed for both TCE and PCE, especially with permanganate.

Shiau (2003) conducted column and pilot-scale (field) studies using surfactant and Fenton's reagent flushing sequentially for NAPL remediation. Results indicate a 99.6 % and 99 % removal of Total Petroleum Hydrocarbons (TPHs) in column and field studies respectively, with a 99.9 % removal of TCE in column tests after coupling surfactant flushing with potassium permanganate.

Zhai et al (2006) performed batch experiments to investigate the use of different co-solvents in the presence of $KMnO_4$. It was found that tertiary butyl alcohol (TBA) and acetone were the most stable with permanganate. The results also indicated that both co-solvents led to increased PCE aqueous solubility significantly. Moreover, the Cl^- production from PCE oxidation with $KMnO_4$ in a 20 % acetone system was significantly more that in the absence of co-solvent, indicating the former system has a higher time-efficiency (amount of PCE destructed per unit time with per unit initial concentration of $KMnO_4$) in utilizing $KMnO_4$.

O'Hara et al (2006) evaluated the performance of emulsified ZVI - eZVI, a surfactant-stabilized, biodegradable emulsion containing nano-zero valent iron- for the field-scale degradation of TCE.

Results of the field demonstration indicated that substantial reductions in TCE soil concentrations (greater than 80 percent) and significant reductions in TCE groundwater concentrations (60 % to 100 %) at all depths targeted with emulsified ZVI (eZVI). Laboratory tests suggest that both nZVI particles and eZVI containing nZVI can provide significant reductions in TCE mass when used to treat TCE in small test reactors.

Li and Hanlie (2008) studied a combination of surfactant solubilization with permanganate oxidation of TCE in batch, flow-through column, and three-dimensional (3-D) tank tests. It was found that the ionic surfactant Sodium Dodecyl Sulfate (SDS) can enhance the reaction rate constant between permanganate and TCE by about three times.

Tsai et al (2009) evaluated the effects of coupled application of Single Green (a commercial nonionic surfactant) with permanganate in batch and column tests. Results showed that the TCE degradation rates increased from 74.1 % – 85.7 % to 83.8 % – 96.3 %.

Harendra and Vipulanandan (2011) investigated the solubilization of PCE in a nonionic (Triton X-100) and a cationic (cetyltrimethylammonium bromide - CTAB) surfactant solution and the degradation of surfactant solubilized PCE using fine to nano size Fe and bi-metallic Fe-Ni particles in continuous stirred batch reactors. The solubility of PCE increased by about ten-fold. The PCE solubilized up to 500 mg/L in both surfactant solutions was totally degraded by 200 g/L of bi-metallic Fe-Ni particles in less than 20 hours, which is higher than the PCE degradation rates reported in the literature.

Iglesias et al (2014) also observed that saponin/Tween 80 mixture had good synergy with electro-Fenton, and the phenanthrene removal rate in soil increased from 19 mg/kg.h to 43 mg/kg.h.

Zhang et al (2019) investigated the surfactant foam combined with oxidant in gaseous form composed of Tween 20 and ozone. The naphthalene contaminated aquifer was remediated, and found that about 96.9 % of naphthalene was removed and 84.9 % of it was oxidized immediately.

Studies on DNAPL remediation from porous media by surfactant-enhanced activated persulfate oxidation have been mostly applied using alkali and/or Fe^{2+} to activate persulfate oxidation (Stroo et al, 2012; Tsai et al, 2009; Zheng et al, 2016).

In a laboratory batch testing system, Tsai et al (2009) found that the presence of Tween 80 can increase the degradation rate of TCE by Fe^{2+} activated persulfate from 31 % to 92 % because of the enhanced solubilization of TCE.

Zheng et al (2016) evaluated the ability of the biodegradable surfactant Tween 80 coupled with an effective oxidant (Fe^{2+} - activation agent, citrate - chelating agent, activated persulfate - oxidant) to remove PCE from porous media with batch and sandbox experiments. While the Tween 80 solution removed about 52 % and 67 % of PCE from the homogeneous and heterogeneous porous media, the combination solution was more effective with removal rates of 80% and 84%, respectively. As a result, PS degraded the PCE from the soluble phase and thus facilitated its dissolution from the source zone, resulting in more efficient use of Tween 80.

On the other hand, Valletti et al (2021) revealed that the kinetics of dissolution is strongly inhibited at high concentrations of surfactants, with a slower rate than in water. They explain the mechanism such as when the surfactants are present at high concentrations, the aggregates they form in solution are larger and can dissolve more TCE molecules, but, as a drawback, move slower into the bulk liquid.

Coupling solubilizing agents with activated persulfate processes at ambient temperature has been investigated in a few laboratory studies and field applications in recent years (Pan et al, 2012; Forsey 2004). Considering that solubilizing agent addition and heating can have synergistic effects on the solubilization of contaminants present as NAPL (Myers, 2005; Rebello et al, 2014), a combination of solubilizing agents and thermally activated persulfate may increase the treatment effectiveness of NAPLs, which remains yet to be systematically investigated.

Wang et al (2017) investigated the most compatible surfactant through various types of solubilizing agents with persulfate at various temperatures. The results of the batch treatability study with coal tar show that an anionic surfactant C_{12}-MADS can significantly enhance not only the oxidation of polyaromatic hydrocarbons contained in coal tar but also enhance the oxidant utilization efficiency, indicating the synergetic promising potential of the proposed coupling process for the treatment of organic contaminants with low aqueous availability. Figure 2.2 visually depicts the general process of the combined methods on molecular basis.

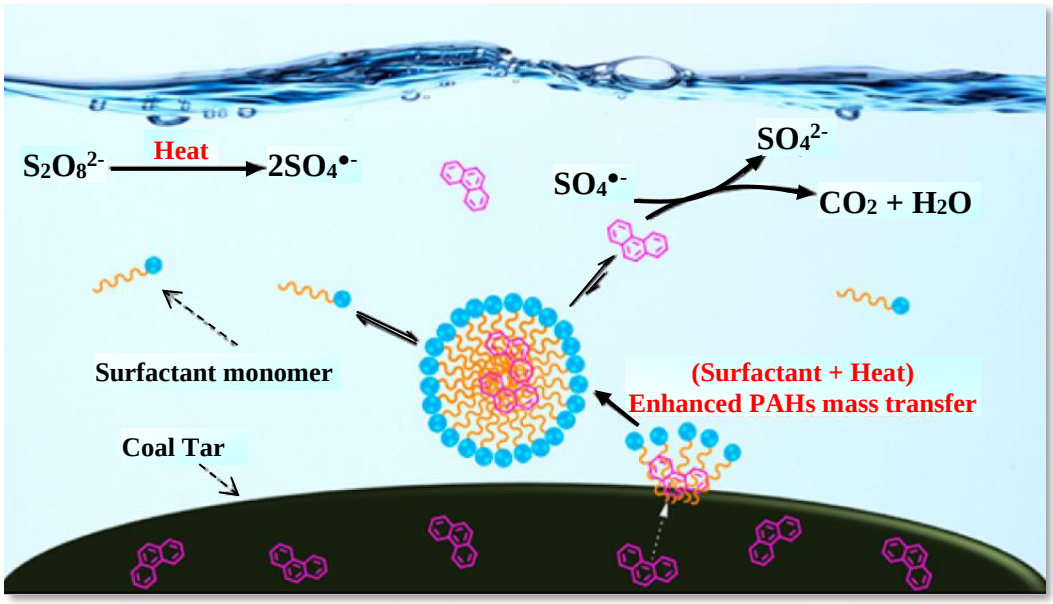

Figure 2.2. Coupling process of surfactant and thermally-activated persulfate on organic contaminant (coal tar) (Wang et al, 2017).

Lominchar et al (2018) applied Verusol-3, a commercial surfactant, with NaOH activated persulfate to remediate fuel oil and PAHs contaminated soil. Results revealed 30 % of contaminants remained in soil without surfactants. On the other hand, in the absence of oxidants, the effluent containing contaminants needed subsequent treatment, suggesting that optimal results are achieved when the surfactant and persulfate are jointly used in the remediation.

Within the scope of this study, I will focus on the surfactant enhanced dissolution coupled with oxidation performance to DNAPL source zones in silica sand using Tween 80 as the solubilizing agent and thermally-activated persulfate at constant temperature (50 °C).

2.4. Zero-Valent Iron (ZVI)

Nano zero-valent iron (nZVI) has been proposed in recent years as a remediation technology for aquifers contaminated with chlorinated organic contaminants (e.g., Al Shamsi and Thomson, 2013; Shan et al, 2020).

Remediation by chemical reduction was investigated using zero-valent iron (Fe^0 or ZVI) at the nano-sized (nZVI) or in granular form (Gillham and O'Hannesin, 1994; Orth and Gillham, 1996; Lien and Zhang, 2001; Cho and Choi, 2010; Kim et al, 2017; Lin et al, 2018). Over the last two decades, many laboratory and field studies have demonstrated that nZVI can effectively transform chlorinated

contaminants at much faster rates than other in-situ technologies (Baker et al, 2016; Fu et al, 2014). nZVI has increasingly gained attention from researchers and practitioners recently due to its high reactivity, cost effectiveness, and potential to treat a wide range of contaminants (Mukherjee et al, 2016). nZVI exhibits greater degradation rates, because it has a greater surface area and potential of reactivity (Goswami et al, 2017; He et al, 2015; Oprckal et al, 2017). On the other hand, a major challenge when using nZVI is that these nano-sized particles can coagulate leading to reduced specific surface area. The delivery of these particles is also difficult as they can get attached to the soil surface. To overcome these delivery difficulties various surface coating is being considered. However, the coating can interfere with their reactivity. Nano-sized particles such as nano-Fe-Pd bimetallic particles have recently been considered in remediation studies at laboratory-scales and field demonstrations but they are still in their infancy.

One important factor that has to be considered in degrading PCE is that it can break down into other hazardous components (Distefano et al, 1992; Jeong et al, 2007). PCE can be transformed by reductive dehalogenation to TCE, DCE (Figure 2.3) and vinyl chloride (Boutonnet et al, 1982; Distefano et al, 1992; Burris et al, 1995; Hwang and Batchelor, 2002; Arvind and Pradeep, 2008),

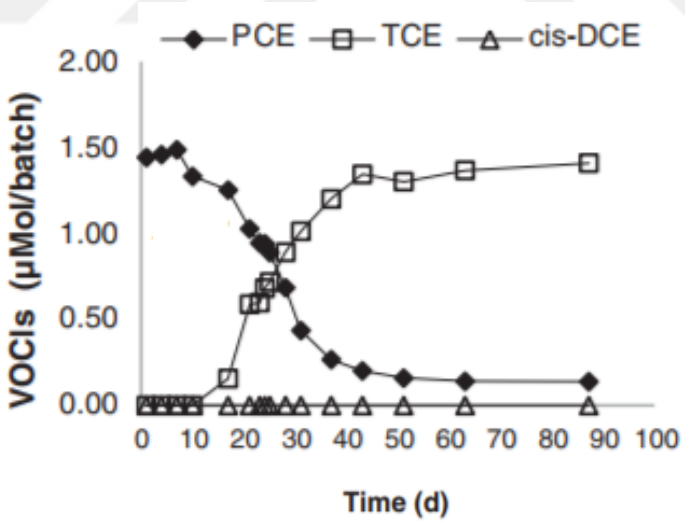

Figure 2.3. PCE reductive dechlorination (Ni et al, 2014).

The complete PCE degradation by ZVI particles can be represented as shown in reaction (2.9) (Harendra and Vipulanandan, 2011),

$$C_2Cl_4 + 4H^+ + Fe^0 \rightarrow C_2H_4 + Fe^{2+} + 4Cl^- \quad (2.9)$$

Similarly, the reductive dechlorination reaction for TCE to DCE by ZVI is shown in reaction (2.10),

$$C_2HCl_3 + 3H_2O + 2Fe^0 \rightarrow C_2H_2Cl_2 + H_2 + 3OH^- + 2Fe^{2+} + Cl^- \quad (2.10)$$

Key reaction products can include daughter chlorocarbons such as dichloroethylene and vinyl chloride (leading to ethene's and ethane's), hydrogen gas, chlorides and iron oxide and hydroxide precipitates (Siegrist et al, 1999).

Granular ZVI applications are predominantly considered as permeable reactive barrier in in-situ remediation studies. Permeable barriers intercept the mass of dissolved contaminants downstream, forcing it to pass through the reactive medium where it reacts with the ZVI which causes the pollutant to oxidize into a form that is not harmful to the environment (Wilkin et al, 2012).

2.5. Modeling Enhanced Dissolution of DNAPL

In comparison to experimental investigations related to in-situ groundwater remediation of DNAPLs, the number of modeling studies is substantially less due the complexity of the equations representing multi-phase flow and the uncertainty in the mathematical representation of the governing processes, especially if chemical oxidation and/or enhanced dissolution are present. The following processes should be represented in mathematical forms to model the application of ISCO: fluid flow, mass transfer and transport, and chemical reaction. The rate of mass transfer to the aqueous phase is a particularly difficult parameter to evaluate because it depends on the interfacial area between the NAPL and aqueous phases and the velocity in the immediate vicinity of the NAPL mass, both of which are very difficult to determine accurately in real life applications (Agaoglu et al, 2015).

Mass transfer from one phase to another is often theorized to occur in a thin stagnant film layer between the two phases, across which solute from one phase diffuses into the other (Cussler, 1997). DNAPL dissolution into water is modeled by Fick's first law of diffusion (Equation 2.11) where the diffusive flux across an area is proportional to the concentration gradient (Siegrist et al, 2001),

$$J = -D_{aq}\frac{dC}{dz} \qquad (2.11)$$

where

J	diffusive flux (kg/[m^2s])
D_{aq}	aqueous phase diffusion coefficient (m^2/s) specific to the compound (DNAPL)
C	aqueous concentration of the DNAPL (kg/m^3)
z	vertical distance (m)

In the stagnant film model which is illustrated in Figure 2.4, the film is assumed to be very thin such that the concentration gradient is linear,

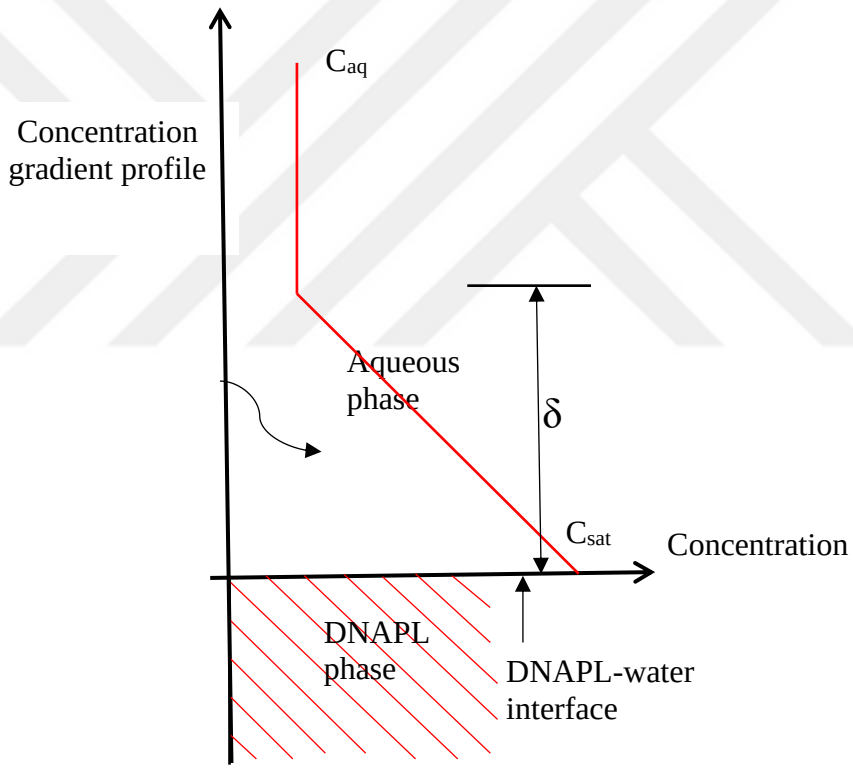

Figure 2.4. Thin film model for DNAPL dissolution.

At the stagnant film boundary, the aqueous concentration of the DNAPL compound is assumed to be at the saturation value for water and the expression in Equation (2.11) simplifies to Equation (2.12) which is a well-known equation described through the stagnant film model developed by Sherwood et al (1975) utilizing a first-order linear driving force,

$$J = \frac{D_{aq}}{\delta}\left(C_{sat} - C_{aq}\right) \quad (2.12)$$

where

C_{sat} aqueous solubility of the DNAPL compound (kg/m^3)

C_{aq} DNAPL concentration in the bulk aqueous phase (kg/m^3)

δ aqueous phase stagnant film thickness (m)

Since the thickness of the stagnant layer is difficult to determine, the thickness of stagnant sublayer δ often is incorporated into the diffusion coefficient, leading to the expression of the mass transfer from the DNAPL to the aqueous phase using Equation (2.13),

$$J_v = K_l\left(C_{sat} - C_{aq}\right) \quad (2.13)$$

where

J_v rate of mass exchange (kg/[m^{3}s]) in a representative volume V (m^3)

K_l lumped mass transfer coefficient per unit volume of porous medium (1/s) (Because the film thickness is unknown, the diffusion coefficient and thickness are lumped together as a single mass transfer coefficient), $\left[K_l = \frac{D_{aq}}{\delta}\right]$

The mass transfer coefficient, K_l, is traditionally defined in terms of the Sherwood number (Sh) (Equation 2.14) which is related to the porous media properties (porosity, mean diameter) and flow conditions (velocity, fluid saturation),

$$Sh = \frac{K_l d_{50}^2}{D_m} \quad (2.14)$$

where

d_{50} representative (median) grain size diameter (m)

D_m molecular diffusion coefficient for a bulk solution of the solute (at an infinitely dilute concentration) (m^2/s)

It has been suggested that chemical oxidation can increase the rate of mass transfer or dissolution from the DNAPL to the aqueous phase and the same general forms of the mass transfer correlation, utilized for surfactant-enhanced dissolution, is used to calculate the modified Sherwood number in

the modeling code. Therefore, solving for K_l is desirable because K_l values are important in modeling for DNAPL dissolution and behaviour during oxidation (Siegrist et al, 2006).

Kinetic studies of DNAPL oxidation by an oxidant suggest that it is a second-order reaction (Yan and Schwartz, 1999) and DNAPL concentrations (resulting from the oxidation reaction) are calculated using Equation (2.15) (Huang et al, 1999; Siegrist et al, 2001)

$$\frac{\partial C_{aq}}{\partial t} = -k_2 C_{ox} C_{aq} \quad (2.15)$$

where

k_2 second-order rate constant (m^3/[mole s])

C_{ox} concentration of oxidant within the unit volume (kg/m^3)

t time (s)

However, because second-order reaction kinetics require an additional mass balance equation for the oxidant, and are mathematically difficult to solve (Siegrist et al, 2006), kinetics of oxidation is sometimes simplified by assuming pseudo first-order reaction as shown in Equation (2.16),

$$k_{ox} = k_2 C_{ox} \quad (2.16)$$

where

k_{ox} pseudo first-order reaction rate coefficient (1/s)

As a result, Equation (2.15) reduces to $\left[\frac{\partial C_{aq}}{\partial t} = -k_{ox} C_{aq}\right]$. The first-order approximation is valid particularly when excess (higher than it is needed) oxidant is injected into the groundwater.

DNAPL dissolution with oxidation can be incorporated into the partial differential equation describing the fate and transport of contaminants in three-dimensional, transient groundwater flow systems as follows in Equation (2.17) (modified by Zheng and Wang, 1999),

$$\frac{\partial C_{aq}}{\partial t} = \underbrace{-\frac{\partial}{\partial x_i}\left(v_i\, C_{aq}\right)}_{\text{Advection}} + \underbrace{\frac{\partial}{\partial x_i}\left(D_{ij}\,\frac{\partial C_{aq}}{\partial x_j}\right)}_{\text{Dispersion}} - \underbrace{K_l\left(C_{sat} - C_{aq}\right)}_{\text{Dissolution}} + \underbrace{\frac{q_s}{n}\,C_S}_{\text{Source}} - \underbrace{k_{ox}\,C_{aq}}_{\text{Reaction}} \qquad (2.17)$$

where

n	porosity of the subsurface medium [ ]
$x_{i,j}$	cartesian coordinate axis (m)
D_{ij}	hydrodynamic dispersion coefficient tensor (m^2/s)
v_i	seepage or linear pore water velocity (m/s), it is related to the specific discharge or Darcy flux through the relationship, $\left[v_i = \frac{q_i}{n}\right]$
q_S	volumetric flow rate per unit volume of aquifer representing fluid sources (positive) (1/s)
C_S	concentration of the source flux for DNAPL (g/m^3)

Although modeling studies simulating the aqueous phase only are numerous, when DNAPLs are present, a multiphase system is present requiring multiphase flow simulator. Existing computer programs that can simulate multiphase flow developed by universities/companies either as open source or commercial include Eclipse, (Schlumberger Eclipse, 2005), UTCHEM (Delshad et al, 1996), T2VOC (Falta et al, 1995) and MUFTE-UG (Hinkelmann, 2005) and the one developed by Reitsma and Kueper (1998a, 1998b). However, among these multiphase programs only UTCHEM has the capability to model surfactant and co-solvent flushing. Therefore, this program was selected for the modeling component of this study.

UTCHEM was originally developed at the University of Texas at Austin for surfactant flooding of an oil reservoir. It is a three-dimensional, multi-component, multiphase, compositional model of chemical flooding processes which accounts for complex phase behavior, chemical and physical transformations and heterogeneous porous media. It has a 3-phase formulation (relative permeability, capillary pressure, NAPL partitioning and ternary phase diagram), and can simulate movement of aqueous and NAPL phases. In addition to the capability of solving multiphase flow problem, UTCHEM includes tracer options where multiple tracers, conservative and partitioning, can be simulated (Jin et al, 1995). The code is also able to simulate the geochemical and biochemical reactions. In this research the primary interest in UTCHEM was its ability to simulate multiphase flow and transport. More detailed information about the equations incorporated into the code and its data needs are discussed in Section 3.8.

The UTCHEM code has been widely validated by the authors (Delshad et al, 1996). For the reaction module used in this study, two types of testing were performed: 1) batch simulations, in which the solutions to the equations provided by the model for simple batch systems were compared to solutions calculated in spreadsheets, and 2) comparison of analytical solutions to UTCHEM simulation results and results of other models published in the literature. The capillary-pressure model was also tested against experimental data indicated that the model is capable of capturing the capillary-pressure behavior in various geological media (Delshad et al, 1996). Additional modeling studies that have tested and utilized UTCHEM as well as other modeling studies relevant to the current study are reviewed below.

Reitsma and Kueper (1998a, 1998b) were one of the first published works that considered modeling co-solvent flushing of NAPLs. The multiphase model using a two-film model for mass transfer calculations was applied to alcohol flooding column experiments.

Roeder and Falta (2001) modified the UTCHEM code, which was originally developed by Pope and Nelson in 1978 to simulate the enhanced recovery of oil using surfactant and polymer processes (Pope and Nelson, 1978), to model unstable conditions which may occur during co-solvent flushing of DNAPLs. Roeder and Falta (2001) reported that adjusting the dispersion coefficients or application of a finer grid may be helpful to model the unstable flushing.

Jawitz et al (2003) developed a model that simulates immobile multi-component NAPL dissolution into a mobile flushing solution by modeling the dissolution process as desorption.

Kaye et al (2008) modeled the over and under ride of co-solvent solution during DNAPL co-solvent flushing.

Liang and Falta (2008) used UTCHEM to model the remediation of a field scale DNAPL contamination using co-solvent flushing with high ethanol content (95%). They also evaluated the influence of initial distribution of NAPL on model simulations.

More recently, Agaoglu et al (2012) performed a series of co-solvent flushing experiments with a bench scale column set-up to evaluate the factors influencing multi-component NAPL (toluene, benzene) recovery mechanisms in a homogeneous sand. The co-solvent flushing experiments modeled with the modified UTCHEM of Liang and Falta (2008). The study highlighted the need to having 2-D or 3-D to more accurately model the DNAPL dissolution process.

Aydın-Sarıkurt et al (2016) performed a series of co-solvent flushing intermediate scale with varying ethanol contents and velocities to evaluate the enhanced remediation of a DNAPL (TCE). The experimental results were also simulated using the modified UTCHEM (Liang and Falta, 2008). The model was used to investigate the impact of cosolvent on the mass transfer coefficient during co-solvent flushing.

Hosseininoosheri et al (2016) developed a 3-D model for the surfactant flooding process using UTCHEM. The model mainly studied the effects of pH, temperature, and salinity on the growth rate of microbial strains.

Recently, Karaoglu et al (2019) used the UTCHEM model to simulate the laboratory-scale experiments involving enhanced dissolution of DNAPL in saturated heterogeneous media. To aid in the calibration of the model, sensitivity coefficients of key parameters- relating to the flow, flushing solution properties, soil parameters, NAPL distribution and mass transfer coefficient- were developed. The DNAPL consisted of both pooled and residual saturation forms. The study highlighted the difficulty and non-uniqueness of model calibration, particularly when incomplete information about the NAPL distribution and soil properties is available.

Since the experiments involve cyclodextrin- and surfactant-enhanced solubilization, A modified version of UTCHEM developed by Liang and Falta (2008) was used. Besides the original surfactant-induced IFT reduction method, the modified version includes the option of an IFT calculation method of (Li and Fu, 1992) which is more suitable for simulating cyclodextrin and cosolvent-induced IFT reduction. The model UTCHEM input files were directly prepared in ASCII following the UTCHEM users' manual without the use of any graphical interface. The primary program output consisted of time dependent phase compositions saved in separate files.

Overall, the literature reviewed in this chapter highlighted the significant efforts that have been directly towards the remediation of DNAPL in the subsurface. Despite the tremendous progress that has been achieved in the last decades, the remediation of aquifers contaminated with DNAPLs remains a very challenging problem. To increase remediation efficiency, researchers are increasingly considering the synergistic effects of different technologies. The focus of this thesis is on investigating the benefits and challenges of combining ISES and ISCO technologies. To gain further insight into the remediation activity, multiphase modeling of the flushing and oxidation processes experiments is also performed.

3. MATERIALS AND METHODS

Within the scope of the thesis, batch and flow-cell expriments were carried out to assess ISCO and ISES technologies and their combination in three separate laboratories. All enhanced solubilization batch tests, the majority of persulfate oxidation batch and flow-cell experiments were performed at the Institute of Environmental Studies of Boğaziçi University, and Department of Geological Sciences of the University of Alabama. My stay at the University of Alabama at the laboratory of Prof. Geoffrey Tick was supported through a TUBITAK scholarship. The enhanced solubility and permanganate oxidation flow-cell experiments were carried out at Kocaeli University at the Department of Geological Engineering.

An overview of the laboratory experiments conducted as part of this study is presented in Table 3.1. All materials used and experimental procedures followed are described in the following sections.

Table 3.1. Overview of the performed experimental studies.

<table>
<tr><th>Number of DNAPL component</th><th>Scale</th><th>Media</th><th>Chemical agent</th><th>Target</th></tr>
<tr><td>3</td><td rowspan="2">Batch</td><td rowspan="2">Aqueous</td><td rowspan="2">Solubilizing agent</td><td rowspan="2">Enhanced solubility and miscibility</td></tr>
<tr><td>1</td></tr>
<tr><td>3</td><td rowspan="2">Flow-cell</td><td>Silica sand</td><td rowspan="2">Solubilizing agent</td><td rowspan="2">Enhanced solubility under steady-state continuous flushing conditions</td></tr>
<tr><td>1</td><td>Calcareous soil</td></tr>
<tr><td rowspan="4">1</td><td rowspan="2">Flow-cell</td><td rowspan="2">Silica sand</td><td>Oxidant 1</td><td rowspan="4">Oxidation under intermittent continuous flushing</td></tr>
<tr><td>Oxidant 1 + Solubilizing agent</td></tr>
<tr><td rowspan="2">Flow-cell</td><td rowspan="2">Calcareous soil</td><td>Oxidant 1</td></tr>
<tr><td>Oxidant 1 + Solubilizing agent</td></tr>
<tr><td rowspan="4">1</td><td rowspan="2">Batch</td><td rowspan="2">Aqueous</td><td>Oxidant 2</td><td rowspan="2">Reaction rate</td></tr>
<tr><td>Oxidant 2 + Solubilizing agent</td></tr>
<tr><td rowspan="2">Flow-cell</td><td rowspan="2">Silica sand</td><td>Oxidant 2</td><td rowspan="2">Oxidation under steady-state continuous flushing conditions</td></tr>
<tr><td>Oxidant 2 + Solubilizing agent</td></tr>
</table>

3.1. Materials

The chemicals used in the study are: Tetrachloroethene (PCE, 99.0 % purity), Trichloroethene (TCE, 99.5 % purity), 1,1-Dichloroethene (1,1-DCE, 99.9 % purity) are ACS grade, Aldrich. Potassium permanganate ($KMnO_4$), Sodium persulfate ($Na_2S_2O_8$), Tween 80 (polysorbate 20) (for synthesis), Sodium sulfate (Na_2SO_4), Sudan IV and Ethanol (reagent grade), Methyl-beta-cyclodextrin (MCD) and Sodium dodecyl sulfate (SDS) were purchased from Sigma-Aldrich. Silver nitrate ($AgNO_3$) and Potassium chromate (K_2CrO_4) were obtained from Merck.

The chemicals that were used at the University of Alabama are: Sodium persulfate ($Na_2S_2O_8$, 98+ % purity) obtained from Acros Organics (Thermo Fisher Scientific, New Jersey). Tetrachloroethene (PCE, 99.9 % purity), Trichloroethene (TCE, 99.9 % purity), and Tween 80 obtained from Sigma-Aldrich (St. Louis, MO). 20 mesh iron rods and sodium bicarbonate ($NaHCO_3$, 99+% purity) were obtained from Ward's Science (lab grade, Rochester, NY). Potassium Iodide (Reagent ACS, 99.98%) was obtained from AZ Laboratories. Ferrover Iron Reagent, Sulfaver 4 Sulfate Reagent, and Ferrous Iron Reagent powder pillows were obtained from Hach Company (Chicago, IL).

DNAPLs were stored at 4 ℃. All chemicals were used without further purification. In some experiments, iron rods were pretreated as described below.

Due to the widespread usage of Tetrachlorethene (PCE) and Trichlorethene (TCE) in the industry, their properties can be generally found in the literature. However, limited characterization experiments have been conducted on 1,1-Dichlorethene/Vinylidine chloride (1,1-DCE). 1,1-DCE, one of the three isomers of dichloroethene, is used in food packaging, textile and as a static intermediate in the production of polymers (latex, resin) used in furniture (Benson, 2003). Table 3.2 summarizes key physicochemical properties of these compounds.

During the study, some difficulties encountered in the preparation and analysis of DNAPL mixtures can be caused by the general physical properties of these pollutants. For example, 1,1-DCE has a high volatility tendency due to its very low boiling point and high vapor pressure (Table 3.2). PCE, on the other hand, can cause water-related problems in chromatographic/spectrometric measurements due to having a higher boiling point than water. These difficulties, required additional precautions in all experimental and analytical procedures from the sample preparation stage and showed the importance of the accuracy of the measurements.

Table 3.2. General physical properties of DNAPLs used in the study.

Type of DNAPL	Chemical formula	Density[1] (g/mL)	Aqueous solubility[2] (mg/L)	Boiling Point (℃)	Viscosity[2] (cP)	Vapor Pressure[2] (mm Hg)	Henry's Constant ($atm.m^3/mol$)
PCE	C_2Cl_4	1.623	206	121.3	0.89	18.5	0.0177
TCE	C_2HCl_3	1.4642	1280	87.2	0.532	69	0.00902
1,1-DCE	$C_2H_2Cl_2$	1.2129	2240	31.7	0.33	600	0.0261

1 at 20 ℃, 2 at 25 ℃

The only surfactant that can be used in pure form is Polysorbate 20 (Tween 80). The titrations for the ternary phase diagrams were performed by adding Tween 80 in pure form. Due to the high viscosity of Tween 80, the solutions were prepared on a volume basis, instead of weight basis which is more difficult for the viscous liquid to determine with sensitive scale. Sodium dodecyl sulfate (SDS) is commercially found as granulated solid, fine-grained sand-sized surfactant which is not suitable for preparing solutions at high concentrations. In case of the presence of a high concentration SDS solution at values lower than the room temperature, it can be deposited as dense crystals and can completely lose its liquid properties. Therefore, the solution prepared at high concentration was allowed to mix in the magnetic stirrer during the whole experiment and analysis. The higher foamability caused more problems in titration and solution preparation, but relatively less in solubility experiments. In addition, a mask was used due to the potential adverse respiratory effects of particles. Methyl-beta-cyclodextrin (MCD) is similar to fine-grained powder, but it is the most suitable surfactant for solution preparation at high concentrations. Foamability is much lower than SDS. The fact that it can remain in solution without crystallizing below or above the room temperature can be seen as an advantage in the analysis.

3.2. Experimental Set-up for Batch Miscibility and Solubility

Prior to the flow-cell flushing tests, batch tests were conducted (i) to characterize the multiphase system, (ii) compare the difference of different solubilizing agents with single and multi-component DNAPL mixtures to identify the most effective agent and (iii) to determine some parameters which will be used later in the modeling. The measured parameters are Interfacial Tension (IFT), Ternary Phase Diagrams (TPD) and Solubility. The methods used to determine these parameters are described below.

All experiments were carried out at an average temperature of 20 ℃ (± 1 ℃). The DNAPL mixture consisted of TCE, PCE, and 1,1-DCE which were prepared to fill 40 mL glass vials according to the 1:1:1 molar ratio. The behavior of single and multi-component DNAPLs in the porous medium is strongly dependent on the interfacial tension between DNAPL and groundwater. The measurement of the interfacial tension is important for the assessment of mobilization mechanisms in groundwater treatment applications. In this study, DNAPL-water-solubilizing agent interfacial tension was measured for different surfactant and cyclodextrin concentrations. The interfacial tension measurements were obtained using the Du Nouy ring method with a manually adjustable KSV Sigma 703 digital tensiometer (Figure 3.1). This method is basically the immersion of a platinum ring, which is suspended on the tensiometer, and the tension generated by the retraction of the ring is expressed in units of mN/m.



Figure 3.1. KSV Sigma 703 digital tensiometer.

Another physico-chemical parameter that influences the removal performance of DNAPL from the porous medium is the ternary phase behavior. The ternary diagram is used to identify the degree of solubility (solubility of the organic phase in the aqueous phase) quantitatively and allows all three components (DNAPL-water-solubilizing agent) to be displayed in the same graph. In this study, the most effective DNAPL solubility values with solubilizing agents were determined by a series of titration processes which form the basis of ternary phase diagrams. Phase diagrams are drawn with the data obtained from titrations made in 40 mL glass vials (Figure 3.2) using the "Cloud point titration" method (St Pierre et al, 2004; Martel et al, 1998; Roeder and Falta, 2001). In this method,

cloud limits are determined by keeping a component constant during the titration of the other components allowing for the “mixing curve between phases” to be drawn.



Figure 3.2. Equipment used in the cloud point titration (40 mL glass vials with minivalve screwed cap, gas tight macro syringes, magnetic stirrer and stirring bar).

Solubility tests were performed to determine the dissolution potential of single and multi-component DNAPLs in aqueous solutions for different solubilizing agent concentrations. Samples with a minimum headspace volume (<1 mL) were prepared by placing 1 mL of DNAPL into the solubilizing agent solutions with different concentrations to determine the enhanced solubility of single and multi-component DNAPLs. 40 mL borosilicate glass screw capped vials with silicone septa were placed in the horizontal shaker and allowed to shake at 360 rpm for 48 hours. The vials were then centrifuged at 4000 rpm for 20 min to provide separation between the DNAPL phase and the aqueous phase (Figure 3.3).

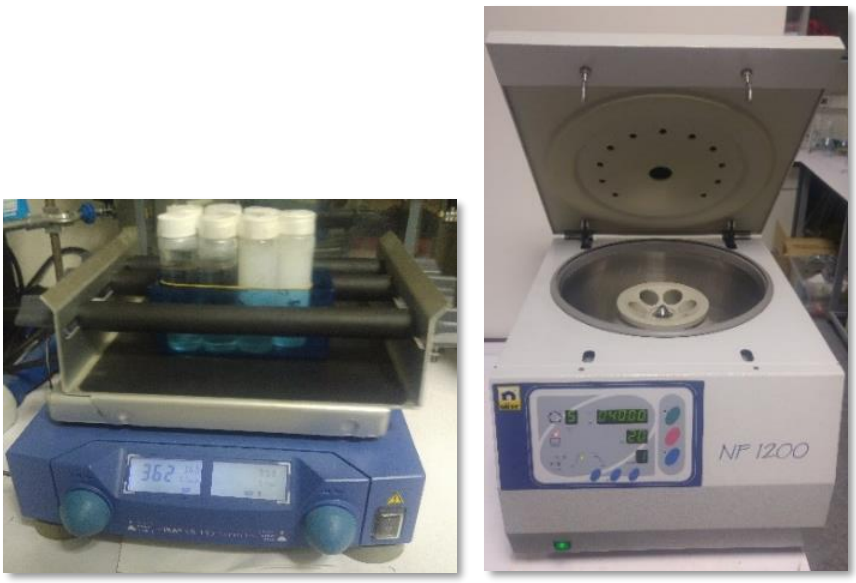

Figure 3.3. Enhanced solubilization experimental vials placed in horizontal shaker (on the left) and the centrifuge.

In ideal mixtures (case where the intermolecular attraction forces between different types of molecules are equal to the intermolecular attraction forces between molecules of the same type) the aqueous solubility of a DNAPL species in the mixture was compared to Raoult's law as shown in the equation (3.1).

$$C_{Amixture} = C_{A_{solubility}} . X_A \quad (3.1)$$

where X_A is the mole fraction and $C_{A_{solubility}}$ is the pure phase solubility.

For example, the effective aqueous solubility value of PCE when present in the form of a DNAPL mixture is obtained by multiplying the solubility value in water by the mole fraction of 0.33.

A stock solution of the surfactant aqueous solutions was also prepared at the highest concentrations that will be used in this study. The stock solutions were then diluted to obtain the required solution that was used in the solubility and interfacial tension experiments.

3.3. Experimental Set-up for Batch Reactivity

Batch reactivity experiments were carried out only with sodium persulfate within the scope of this dissertation. As described in the literature, persulfate needs to be activated prior to oxidation (Chapter 2) For this purpose, before examining the persulfate degradation kinetics of DNAPL, the most suitable activation method for persulfate was examined. In this context, activation of persulfate using 20 mesh (0.84 mm) rod-shaped granular zero valent iron (ZVI) and temperature generated by an external heat source as persulfate activator was investigated.

Batch reactivity experiments were carried out in 20 mL well-sealed crimped capped glass vials with almost no remaining headspace (<0.5 mL). Some experiments were carried out with the addition of the contaminant in its aqueous phase, and some were carried out by adding the contaminant to the reactor in the DNAPL phase. Saturated stock solutions of the chlorinated ethenes were made by allowing the pure nonaqueous phase liquid to equilibrate with deionized (NANOpure water, 18 M-Ohm-cm) water for more than 48 hours with gentle stirring. Sodium persulfate solutions were made within 3 hours of initiating the experiments. All experiments were performed without buffers or ionic strength compensation to avoid potential complications due to the reaction between these additives and SO4•-. Initial molar ratios were determined using stoichiometry. The concentrations were compared to concentrations utilized in similar studies (Zhong et al, 2015). Unactivated persulfate and granular-Fe^0 activated persulfate experiments were carried out at room temperature (20 °C) with no pH adjustment.

Selected experiments were duplicated based on measurement of the concentration of chloride ion, the oxidation product of PCE and TCE. Control experiments for comparison purposes were also performed simultaneously. In addition to the batch reactivity experiments carried out to determine the properties of the activated persulfate-DNAPL-water multiphase system at equilibrium, some enhanced solubility experiments were also performed at 50 °C. The proper persulfate activator for the flushing experiments was decided upon the capability to degrade the DNAPL and sometimes upon the progression of the reaction observing the sulfate ion (SO_4^{2-}), ferrous iron (Fe^{2+}), total iron, chloride ion (Cl^-), pH, ORP produced.

3.3.1. Zero Valent Iron Activation of Persulfate

ZVI activated persulfate experiments were performed with PCE. In the first stage of the experiments; persulfate and PCE stock solutions were mixed at a molar ratio of 10:1 (PS: PCE) in each batch reactor. Then, ZVI rods were added to each 20 mL reactor with a solid/liquid ratio of 1/10 by weight (Zhong et al, 2015). The reactors were crimp-capped and sealed with parafilm. Subsamples (1 mL) were collected throughout the batch experiment and analyzed after necessary dilutions (Figure 3.4.c). According to some researchers, ZVI rods should be used both in the laboratory and in the field without any pretreatment (Zhong et al, 2015). However, some researchers argue that exposing the iron to an acid pretreatment to obtain fresh iron surfaces is necessary before they are introduced to the system (Allen-King et al, 1997; Bautitz et al, 2012; Perini et al, 2014; Matzek and Carter, 2017). Some researchers used both treated iron and untreated iron filings to compare the difference in contaminant degradation performance (Clark et al, 2003).

In the series of experiments performed herein, ZVI rods were categorized as acid pretreated and untreated (raw). Pretreated iron rods were also subdivided into two additional categories; wet and dry. In the dried iron filing process; all iron was pretreated in 100 g batches by washing with 250 mL of 1 N HCl for 15 min then rinsed repeatedly with deionized (NANOpure) water until the supernatant was clear (more than 10 times). After rinsing, the iron was dried overnight at 70 °C. For the wet iron filing process; 100 g of 20 mesh iron rods were pretreated by washing with 250 mL of 1N HCl for 15 min, then rinsed with DI water until the supernatant was almost clear (more than 10 times) (Figure 3.4.a). Finally, the moisture of the fresh iron filing was removed by putting on a filter paper for 20 min at 20 °C (room temperature). Fresh iron filings were then used in the batch experiments (Figure 3.4.b).



(a)



(b)



(c)

Figure 3.4. a) Untreated raw iron (on the left), iron surface during acid treatment (on the right), b) Wet vs. dried treated iron (on the left), experimental preparation (on the right), c) 20 mL batch reactors hosting the ZVI rods-PCE-persulfate.

3.3.2. Thermally-Activated Persulfate

Considering previous studies, 50 °C was selected as the optimum temperature at which persulfate would be activated (see Chapter 2). It has been observed in some studies that above this value, persulfate decomposes (Dominguez et al, 2020). The experiments were individually performed both with pure DNAPL and aqueous phases of TCE and PCE. In the heat-activated persulfate batch experiments, known amounts of DNAPL saturated stock solution were diluted with DI water into the 20 mL vials to reach the desired concentration (Figure 3.5.a). The vials were preheated in the water bath operated at 50 °C for 5 min (Costanza et al, 2010), after which time 1 mL of unbuffered sodium persulfate stock solution was added to the vials under nearly zero headspace conditions to yield an oxidant: contaminant molar ratio of 10:1 (Figure 3.5.b). Subsamples (1 mL) were collected throughout the batch experiment in glass vials and cooled to ~0 °C in an ice-water bath to quench further reaction (Figure 3.5.c). Samples were then immediately analyzed for the concentrations of PCE, TCE, chloride, pH, ORP and persulfate.



(a)



(b)



(c)

Figure 3.5. a) Reactor preparation for each time interval, b) Heat activation progress in a water bath at 50 ℃, c) Ice quenching in styrofoam.

3.4. Flow-cell Experimental Set-up for In-Situ Enhanced Solubilization and In-Situ Chemical Oxidation

2-D-scale flow experiments were performed in two different flow-cells. The characteristics of the flow-cell experimental set-ups called Flow-cell #1 used in Boğaziçi University and Kocaeli University, Flow-cell #2 used in University of Alabama are given below.

3.4.1. Flow-cell #1

The majority of flushing experiments were performed using a rectangular flow-cell 24 cm long by 15 cm high by 3 cm wide constructed of stainless steel frame (Figure 3.6). The front of the flow-cell was made of glass to allow for the visualization of the DNAPL injection and remedial activities. The flow-cell had 3 equally-spaced ports on top for DNAPL injection along with inflow/outflow ports on either end of the flow-cell for injection of the remedial solution and collection of effluent samples, respectively. Water-tight silicon sealant was used to seal the flow-cell. Modeling work was based on the flushing experiments performed with this flow-cell.

The pure PCE and DNAPL mixture enhanced solubilization, and PCE permanganate oxidation flushing experiments were conducted using Flow-cell #1 in two physical configurations. (i) homogeneous packing of 40/50 mesh sand underlain with a layer of 70/100 mesh fine sand which acts as a low permeability barrier (Figure 3.6.a) (ii) natural calcareous soil pack with two lenses of <200 mesh calcareous soil and underlain by <200 mesh calcareous soil to form a low permeability barrier (Figure 3.6.b*).* Silica sand materials were purchased from a private company (Santoz Corp., Gebze/Kocaeli). The organic carbon content of silica sand is quite low (about 0.05 %*)*. The calcareous soil has a texture of poorly sorted sandy loam with a mean grain diameter of 0.12 mm (Table 3.3). The soil has an alkaline character with a pH of 8.4 and is characterized by the presence of abundant amounts of carbonate (96 %) and intermediate amounts of organic carbon (1 %) with minor amounts of quartz (Akyol et al, 2011; Akyol et al, 2015). The oxidant demand of the calcareous soil and silica sand, determined using the standard test method (ASTM D7262-07, 2007), are 19.8 and 4.1 g $KMnO_4$/ kg of soil, respectively (Akyol, 2018).

Table 3.3. Physical and chemical properties of calcareous soil (from Akyol et al, 2011; Akyol and Yolcubal, 2013).

Sand (%)	Silt (%)	Clay (%)	Texture	Specific surface area (m^2/g)	Bulk density (g/cm^3)	TOC (%)	TOM (%)	pH	$CaCO_3$ (%)	SiO_2 (%)
67	30	3	Sandy loam	0.34	1.34	0.97	1.67	8.4	96	2.12

TOC: total organic carbom
TOM: total organic matter

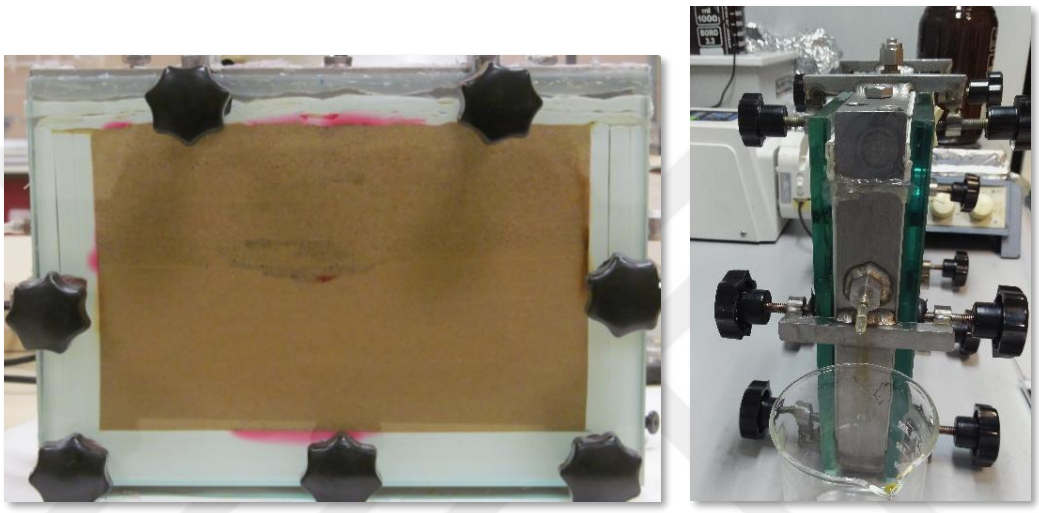

(a)

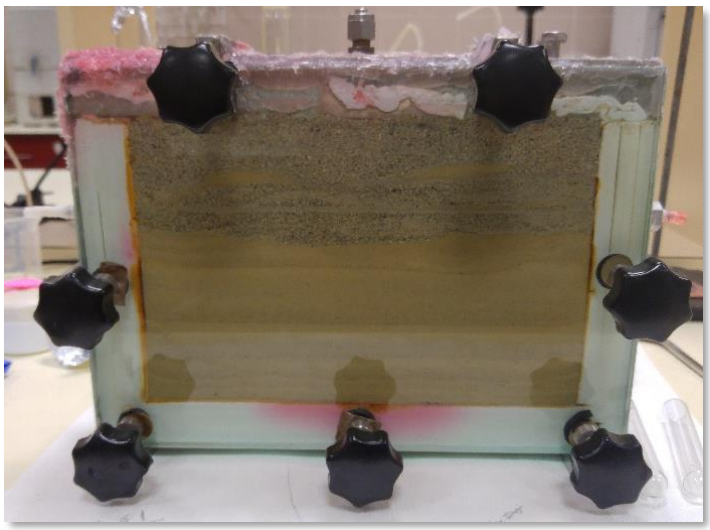

(b)

Figure 3.6. Flow-cell #1 configuration for experiments a) 1 to 4 and 9 to 12, 17 and 18 (upper flow zone 40-50 mesh silica sand total volume ~730 cm^3), b) 5 to 8 and 13 to 16, 19 and 20 (upper flow zone calcareous soil total volume ~500 cm^3).

The flow-cell was first packed with dry porous media and then saturated with DI water through the side inlet ports. After saturation with water, a predetermined amount (0.25 mL) of DNAPL was injected slowly through the middle top port to create a pool dominated zone and allowed to stabilize for 48 hours. ACS grade PCE (Aldrich) was used as the organic liquid. Sudan IV was used to dye the organic liquid. Many studies have shown that Sudan IV has minimal impact on fluid properties (e.g., Schwille, 1988; Kennedy and Lennox, 1997; DiFilippo et al, 2010). The flushing experiments were initiated 48 hours after the injection of the DNAPL.

Prior to DNAPL flushing/oxidation experiments, tracer tests using Pentafluorobenzoic acid (PFBA) were performed to examine the uniformity of the flow-cell packing and estimate the dispersion coefficient needed for the simulation of flushing experiments. The porosity can also be estimated from tracer tests. Like the flushing experiments, the tracer solution was injected through the port on one side of the flow-cell and monitored at the other end. The concentration of the injected PFBA solution was 250 mg/L.

Enhanced solubility flushing experiments with single and multi-component DNAPL (experiments 1 to 16) and permanganate oxidation experiments (experiments 17 to 20) were carried out in Kocaeli University Department of Geological Engineering (Table 3.4). The flushing solution was injected at a constant rate of 2 mL/min, corresponding to an average pore-water velocity of approximately 10 cm/h. This velocity is consistent with the range of velocities commonly considered in flushing activities (e.g., Saba and Illangasekare, 2000; Nambi and Powers, 2003; Yaksi et al, 2021). All enhanced flushing experiments were conducted under continuous flow conditions. Agent flushing terminated when effluent DNAPL concentration reached below 0.5-1 mg/L. In contrast, permanganate oxidation experiments were carried out in intermittent flow whereby the flow was temporary halted to enhance the contact between the oxidant and DNAPL before resuming the flow. Tank effluent samples were collected with glass syringe (0.5 mL) and diluted for analysis.

Table 3.4. Experiments of in-situ enhanced solubilization (ISES) and coupled with in-situ chemical oxidation (ISCO) with permanganate performed in Flow-cell #1.

	DNAPL	Porous media	Flushing type	velocity (cm/h)	Chemical agent
1	PCE/TCE/1,1-DCE	Silica sand	Continuous	10	water (control)
2	PCE/TCE/1,1-DCE	Silica sand	Continuous	10	5 % Tween 80
3	PCE/TCE/1,1-DCE	Silica sand	Continuous	10	5 % SDS
4	PCE/TCE/1,1-DCE	Silica sand	Continuous	10	5 % MCD
5	PCE/TCE/1,1-DCE	Calcareous soil	Continuous	10	water (control)
6	PCE/TCE/1,1-DCE	Calcareous soil	Continuous	10	5 % Tween 80
7	PCE/TCE/1,1-DCE	Calcareous soil	Continuous	10	5 % SDS
8	PCE/TCE/1,1-DCE	Calcareous soil	Continuous	10	5 % MCD
9	PCE	Silica sand	Continuous	10	water (control)
10	PCE	Silica sand	Continuous	10	5 % Tween 80
11	PCE	Silica sand	Continuous	10	5 % SDS
12	PCE	Silica sand	Continuous	10	5 % MCD
13	PCE	Calcareous soil	Continuous	10	water (control)
14	PCE	Calcareous soil	Continuous	10	5 % Tween 80
15	PCE	Calcareous soil	Continuous	10	5 % SDS
16	PCE	Calcareous soil	Continuous	10	5 % MCD
17	PCE	Silica sand	Intermittent	10	45 mM Permanganate
18	PCE	Silica sand	Intermittent	10	45 mM Permanganate + 2.5 % Tween 80
19	PCE	Calcareous soil	Intermittent	10	45 mM Permanganate
20	PCE	Calcareous soil	Intermittent	10	45 mM Permanganate + 2.5 % Tween 80

Persulfate flushing experiments were first performed with TCE as DNAPL. A predetermined amount (0.25 mL) of DNAPL was injected slowly through the middle top port to create a pool dominated zone and allowed to stabilize for 48 hours (Table 3.5, experiments from 25 to 27). Simultaneous injection of the oxidant and surfactant was applied as in the previous set. During the experiments with TCE, the heat source for the solution was provided by a volumetric flusk heater, and the heat source for the flow-cell was provided by a heater infrared lamp (Figure 3.7). The solution flushing terminated when effluent DNAPL concentration reached below 0.5-1 mg/L.

Table 3.5. In-situ enhanced solubilization (ISES) at 50 ℃ and ISES coupled with in-situ chemical oxidation at 50 ℃ (thermally activated persulfate -ISCO) experiments performed with Flow-cell #1.

	DNAPL	**Media**	**Injection type**	**Chemical agent**
21	0.25 mL PCE	Silica sand	Continuous	water control
22	0.25 mL PCE	Silica sand	Continuous	0.00981 % Tween 80*
23	0.25 mL PCE	Silica sand	Continuous	20 mM Persulfate
24	0.25 mL PCE	Silica sand	Continuous	20 mM Persulfate + 0.00981 % Tween 80
ADDITIONAL EXPERIMENTS				
25	0.35 mL TCE	Silica sand	Intermittent	95 mM Persulfate
26	1 mL TCE	Silica sand	Continuous	111 mM Persulfate
27	0.35 mL TCE	Silica sand	Continuous	134 mM Persulfate + 1 % Tween 80

* 0.00981 % Tween 80 corresponds to 3 folds of Tween 80 critical micelle concentration value

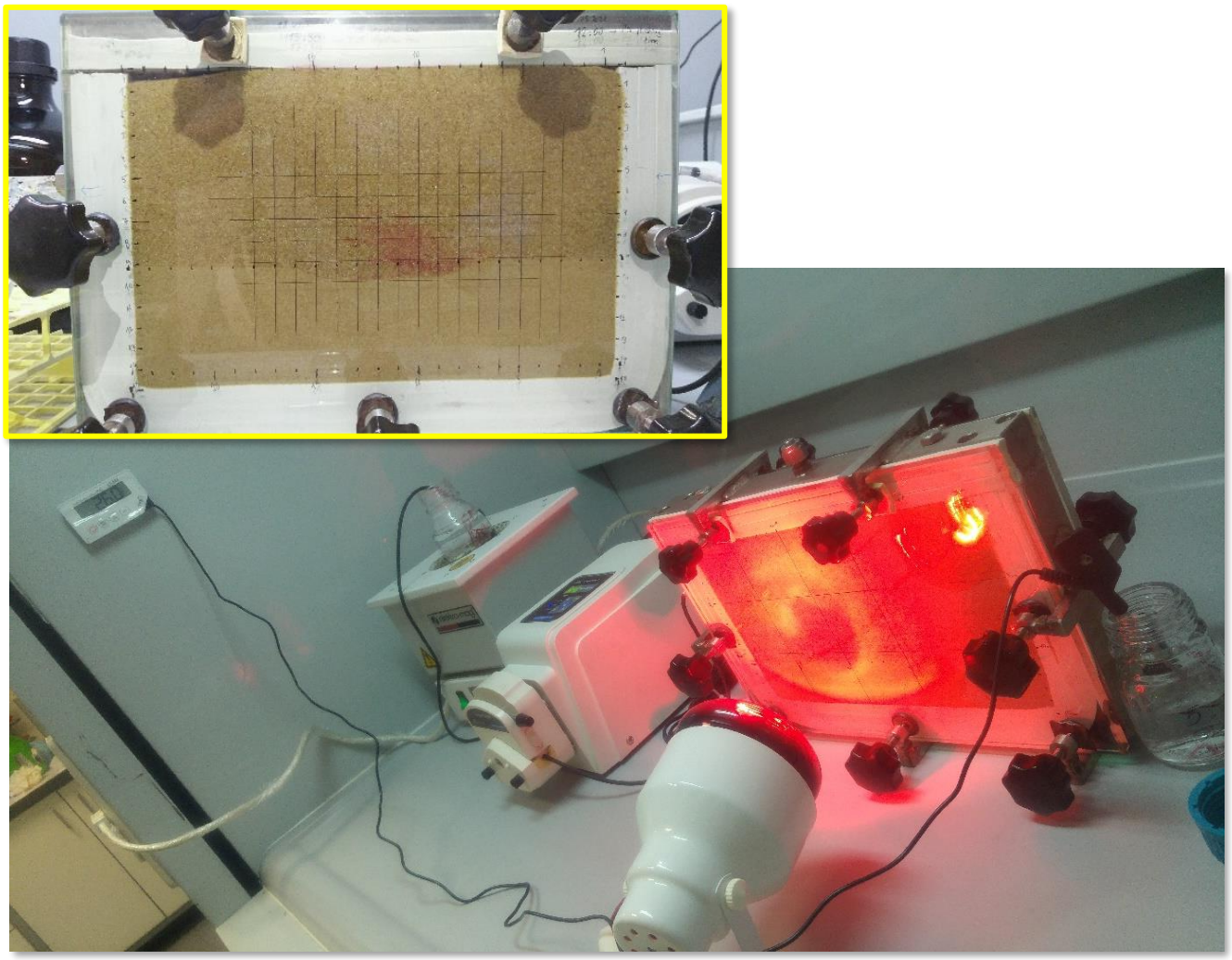

Figure 3.7. Flow-cell #1 configuration for DNAPL TCE experiments from 25 to 27 (upper flow zone 40-50 mesh silica sand total volume ~730 cm^3).

PCE with heat-activated persulfate oxidation experiments with/without surfactant were performed with the same silica sand configuration as the previous sets (Figure 3.6). The main difference of PCE experiments is the need to mantaintain a uniform temperature needed for activation throughout the tank, from the injection solution to the outlet port in the flow-cell. The upper part of the tank, which corresponds mainly of the flow zone, was wrapped with a heating band approximately 2 meters long and covered with aluminum foil (Figure 3.8). The heating band is connected to a heat source with a thermostat and the temperature was kept constant throughout the experiment. A total of 0.25 mL of DNAPL PCE was injected into the tank at a rate of approximately 4 µL/min and left 2 hours to re-distribute as the targeted source zone (experiments from 21 to 24). Differently from TCE experiments, all the persulfate and persulfate-surfactant flushings were applied in a continuous manner in the presence of PCE (Table 3.5).

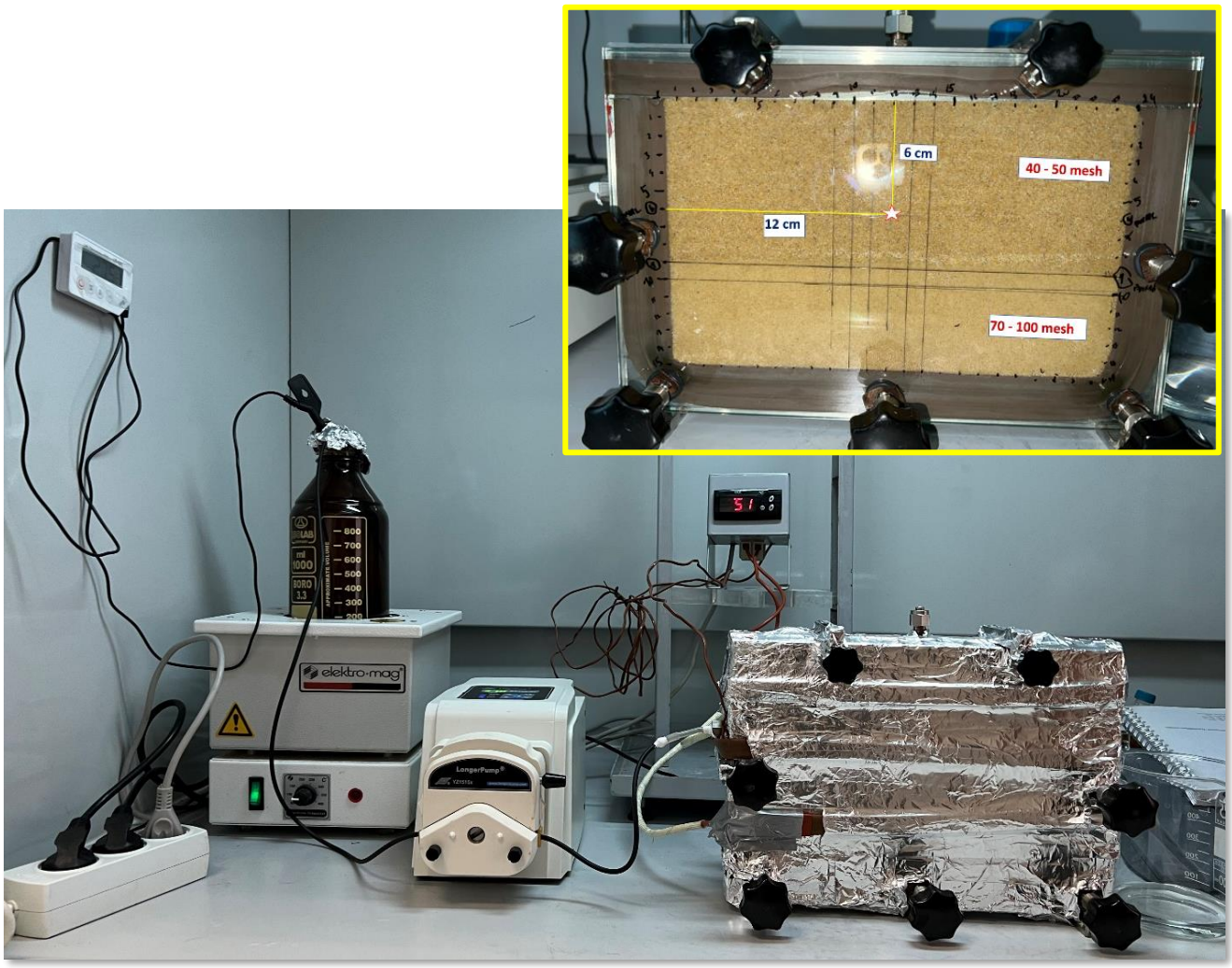

Figure 3.8. Flow-cell #1 configuration for PCE experiments from 21 to 24 (upper flow zone 40-50 mesh silica sand total volume ~690 cm^3).

3.4.2. Flow-cell #2

The persulfate oxidation experiments with Tween 80 were performed with Flow-cell #2 using different oxidant and Tween 80 concentrations. Some previous experiments with this flow-cell were repeated in Flow-cell #1. The flow-cell was made of plexiglass material with dimensions of 20 cm long, 9 cm high and 5 cm wide. The idle top cover of the flow-cell was compressed and siliconized with 6-inch clamps, and thus, saturated zone conditions were created by applying some pressure to the sand via induced pumping. Silica sand was obtained from Accusand Corp., (Ottawa, MN). The 6 cm thick 40-50 mesh zone is bounded by 3 cm from the top and 1 cm from the bottom with <200 mesh sand. The porous media within the flow-cell was then saturated with DI water at a flow rate of 0.2 mL/min. After steady flow conditions were achieved, the flow was interrupted. It was observed

that the part where all the pores were saturated with water was 3 cm thick above the impermeable unit. The porous media configuration in the flow-cell is shown in Figure 3.9.

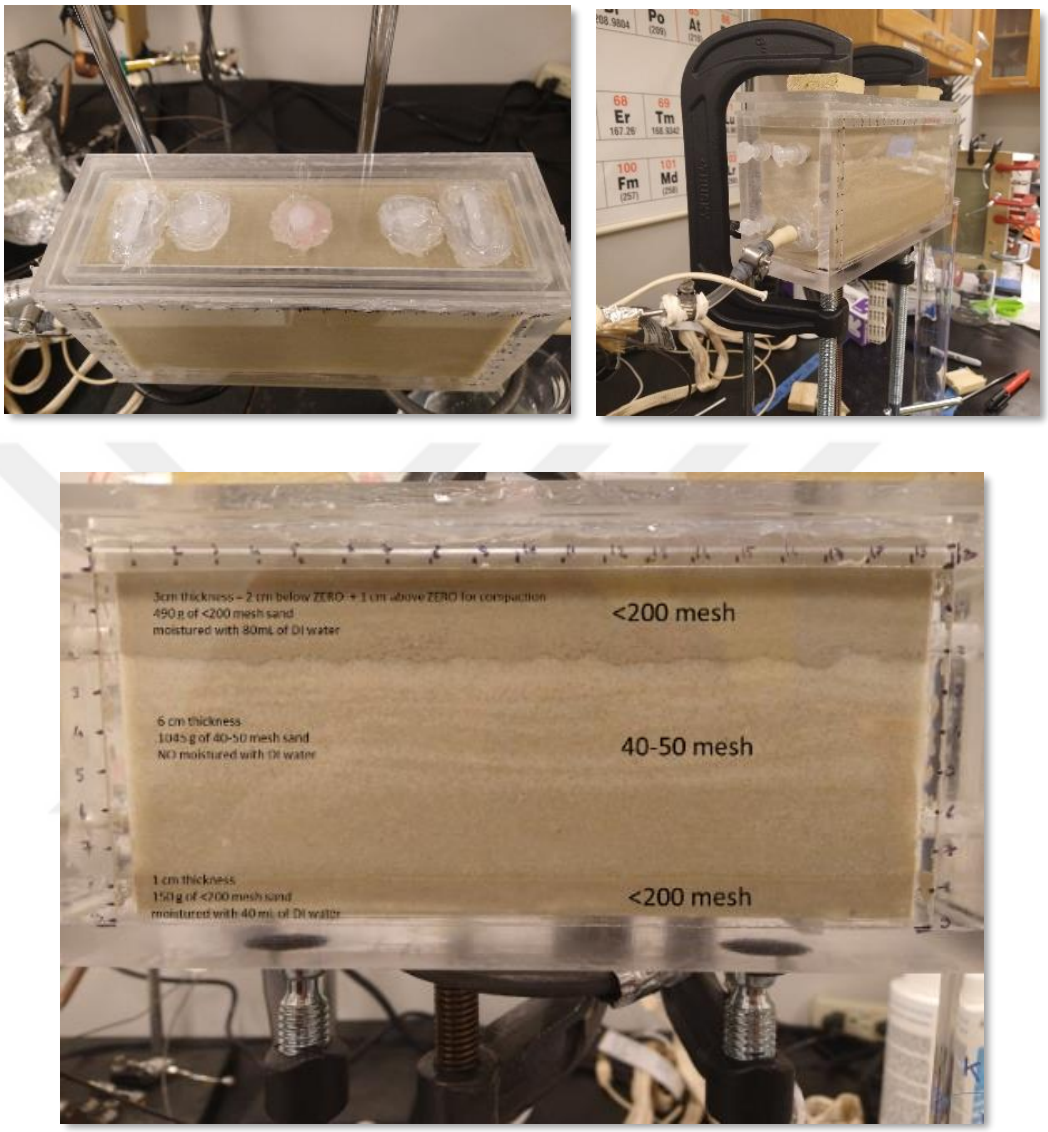

Figure 3.9. Flow-cell #2 configuration for the experiments from 28 to 31.

Following the water saturation process, PFBA tracer test was performed with 240 mg/L into the flow-cell. The experiment was continued until the PFBA concentration at the exit of the tank was equal to the initial concentration, and then the solution was removed from the system by flushing with DI water.

The next step of the experiment involved generating the activation temperature of the persulfate by transferring heat to the system. A temperature controller (BriskHeat Thermal Corporation) and two separate heating bands were used. The longer one was used to wrap the insulated steel tubing

while the shorter one was used to wrap the isolated flow-cell (Figure 3.10.b). The oxidant solution, on the other hand, was isolated with aluminum foil so that the persulfate solution would not be exposed to possible photochemical degradation. The activation temperature was determined to be 50 °C as in the previous sets of experiments. It is reported that temperature below this value will not provide effective activation and above this value may cause degradation (consumption) of persulfate (Dominguez et al, 2020). DNAPL injection were applied using a syringe pump from the mid-top of the flow-cell in the vertical direction, to the part where 40-50 mesh silica sand was observed to be saturated (Figure 3.10.a). A total of 0.25 mL of DNAPL PCE was injected into the tank at a rate of approximately 30 µL/min and left overnight to re-distribute as the targeted source zone. At the beginning of the experiment, the thermostat and the HPLC pump were turned on simultaneously followed by the oxidant solution injection. In addition to PCE and Cl^- measurements during flow, temperature (°C), pH, and ORP (millivolt) values were also measured. All experiments were carried out as continuous injections of the solution.

In total, four oxidation experiments were conducted in silica sand consisting of (i) water control, (ii) low dosage of persulfate, (iii) high dosage of persulfate and (iiii) Tween 80 (2.5 %) containing persulfate (Table 3.6). Tank effluent samples were collected with a glass syringe, diluted, and analyzed. The first of these experiments implemented a 20 mM persulfate oxidation, while the second and third experiments implemented 90 mM persulfate and 2.5% Tween 80 enhanced 20 mM persulfate oxidation experiments, respectively. Finally, water flushing was performed as a control experiment.

Table 3.6. In-situ enhanced solubilization (ISES) coupled with in-situ chemical oxidation experiments at 50 ℃ performed in Flow-cell #2.

	DNAPL	**Media**	**Injection type**	**Chemical agent**
28	PCE	Silica sand	Continuous	water control
29	PCE	Silica sand	Continuous	90 mM Persulfate (at 50℃)
30	PCE	Silica sand	Continuous	20 mM Persulfate (at 50℃)
31	PCE	Silica sand	Continuous	20 mM Persulfate + 2.5 % Tween 80 (at 50℃)



(a)

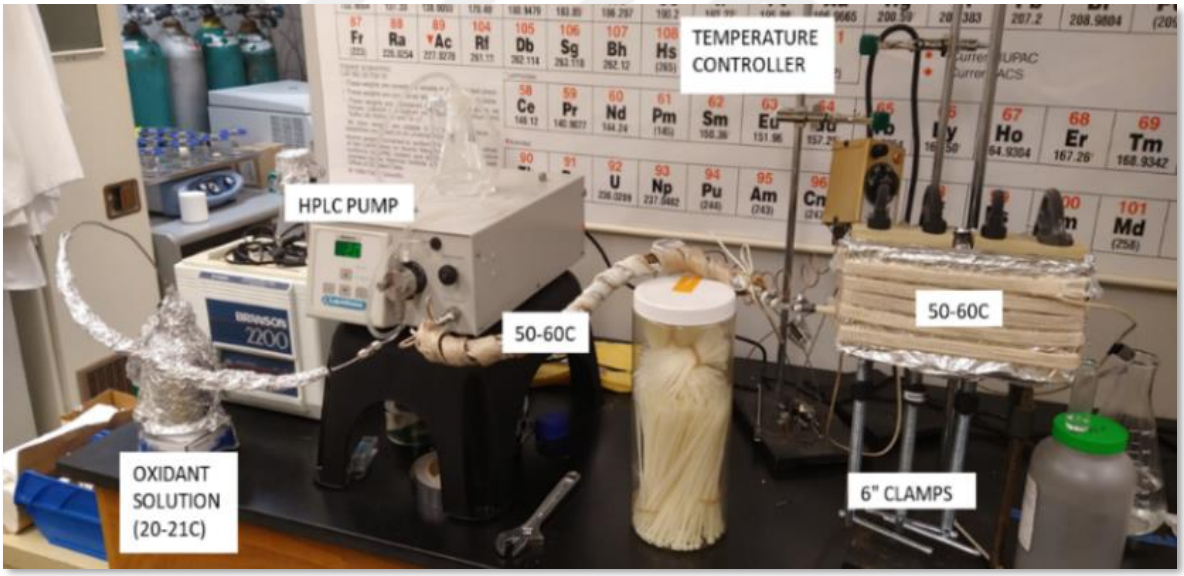

(b)

Figure 3.10. a) DNAPL injection into the plexiglass flow-cell with a syringe pump, b) Experimental setup including the heat source and additional isolated pieces of equipment.

3.5. Tracer Test

In order to evaluate the transport characteristics of the flow-cell system, tracer tests were performed using 250 mg/L pentafluorobenzoic acid (PFBA) at two different temperatures: 20 ℃ and 50 ℃ with a constant pore water velocity of 2.86 m/day. PFBA is generally used as a conservative tracer in groundwater bench scale studies (Helmke et al, 2004). The velocity of the flow was calculated using the following equation (3.2),

$$v = \frac{\mathrm{Q}}{\mathrm{n\,A}} \tag{3.2}$$

where

v	velocity [L/T]
Q	flow rate [L^3/T]
n	porosity of the porous media [ ]
A	cross sectional area of the flow zone [L^2]

Approximately 2.5 and 1.5 pore volumes of tracer solutions were injected for 20 ℃ and 50 ℃, respectively through the influent port and sampled frequently. The experimental data were compared with the solution of the 1-D advection-dispersion (x -coord) description given in equation (3.3),

$$\mathrm{C(x,t)} = \frac{\mathrm{C_0}}{2}\left[\mathrm{erfc}\left(\frac{\mathrm{x}-v\mathrm{t}}{2\sqrt{\mathrm{D_x t}}}\right) + \exp\left(\frac{v\mathrm{x}}{\mathrm{D_x}}\right)\ \mathrm{erfc}\left(\frac{\mathrm{x}+v\mathrm{t}}{2\sqrt{\mathrm{D_x t}}}\right)\right] \tag{3.3}$$

where

$\mathrm{C_0}$	influent concentration [M/L^3]
$\mathrm{D_x}$	longitudinal dispersion coefficient [L^2/T]
x	length in the direction of flow [L]
t	time [T]

The dispersion coefficient in the porous media is defined as the sum of the molecular diffusion and the mechanical mixing (Fetter, 1999). The mechanical mixing is the linear function of the velocity and the dispersivity as shown in equation (3.4),

$$D_x = D_m + \alpha_x v \quad (3.4)$$

where

D_m molecular diffusion coefficient [L^2/T]

α_x longitudinal dispersivity [L]

The dispersion coefficient was determined such that the RMSE (root mean square error) of the sum of the squares difference between the measured and predicted effluent concentrations is minimum.

3.6. Analytical Instruments

To determine the DNAPL aqueous concentration, a Perkin Elmer Clarus 600 Gas Chromatography equipped with Clarus 600T Mass spectrometer (GC/MS) and TurboMatrix 40 Trap Headspace sampling unit was used (Figure 3.11.a). The analytical settings used in GC/MS instrument are given in Table 3.7. From a 20 mL batch reactor, 1 mL aliquot was taken and diluted to a desired concentration range. 5 mL of diluted sample was then injected into a 20 mL crimp-type headspace vial to which priorly 3.5 g sodium sulfate was added. GC/MS calibration curves (0.01-0.5 mg/L) for PCE, TCE and 1,1-DCE are shown in Figure 3.12.

At the University of Alabama; a Quattro micro GC mass spectrometer (QM-GC/MS-MS, Waters Micromass) that was placed in the Department of Chemistry and Biochemistry was used to analyze DNAPL aqueous concentrations (Figure 3.11.b). From a 20 mL batch reactor, a 1 mL aliquot was taken and diluted into 10 mL pre-cooled DI water priorly placed in a crimp-type headspace vial. Samples were kept for no more than 3-4 hours in ice-bath. After heating the vial at 80 °C for 15 min on a heater, a 20 µL gas sample volume was withdrawn from the headspace using Series A-2 with a push-button valved gas syringe and injected manually into the GC/MS-MS for analysis (Figure 3.11.c). A capillary DB-1701 column with a length of 30 m, an inner diameter of 320 µm, and a film thickness of 1 µm were employed for chlorinated ethene analysis. The analysis conditions include the split ratio of 1/30. The oven temperature was increased from 40 to 250 °C at a rate of 20 °C/min. Helium (He, 99.999 %) was used as the carrier gas at a flow rate of 0.8 mL/min. QM-GC/MS calibration curve for PCE (0.1-2.5 mg/L) is shown in Figure 3.13.

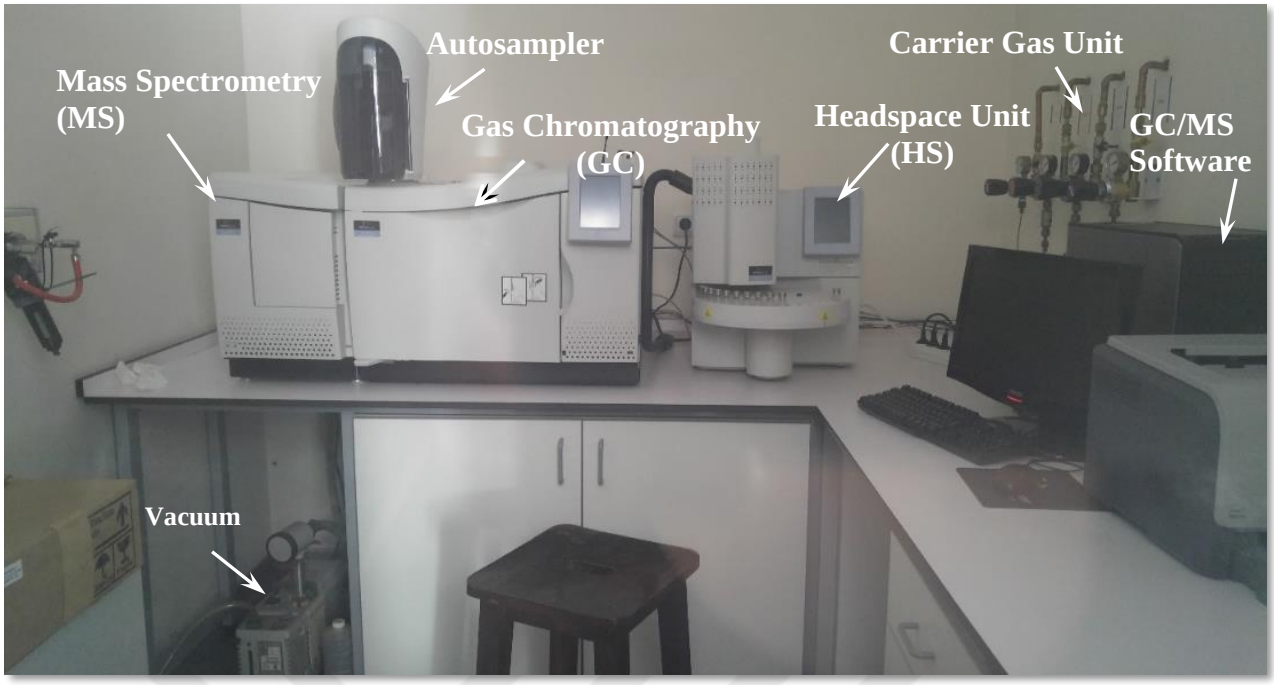

(a)



(b)



(c)

Figure 3.11. a) GC/MS with Headspace unit, b) QM-GC/MS, c) Pre-heating procedure for QM-GC/MS.

Table 3.7. Operating conditions of GC/MS with Headspace unit.

OVEN	COLUMN
Initial temp. : 40 ℃ Holding time : 5 min Rate of increase : 180 ℃ @ 8 ℃/min Final temp. : 220 ℃ Maximum temp. : 240 ℃ Program time : 26.83 min	Model : Elite-624 Equivalent phase : USP G43 Max. Temp. : 240 ℃ Length : 30 m Inner diameter : 0.5 mm Film thickness : 3 µm
HEADSPACE UNIT	METHOD
Oven temp. : 70 ℃ Needle temp. : 80 ℃ Transfer line temp. : 120 ℃ Pressurize time : 0.2 min Withdraw time : 0.2 min Inject time : 1 ml/0.5 min Termo time : 10 min GC cycle : 30 min Column PPC : 20 psi Operating mode : constant Inject mode : volume	Mode : Split Split ratio : 10/1 Carrier gas : Helium Gas flow :1 mL/min

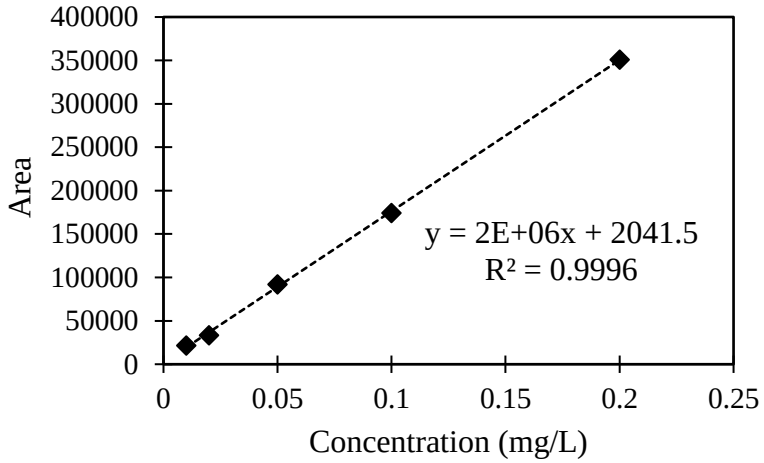

(a)

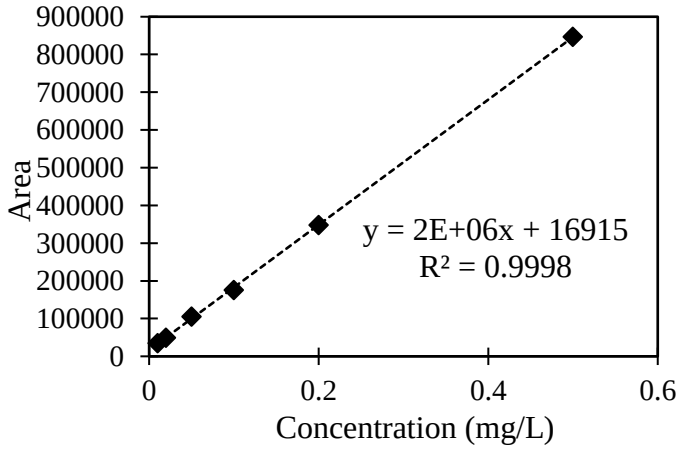

(b)

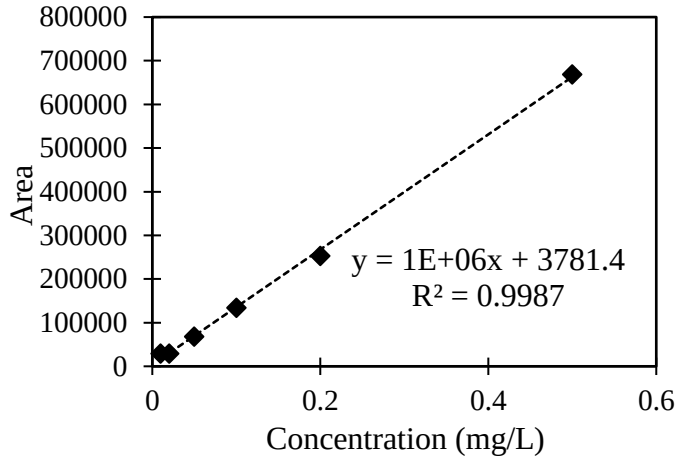

(c)

Figure 3.12. GC/MS calibration curves (0.01-0.5 mg/L) for (a) PCE, (b) TCE, (c) 1,1-DCE.

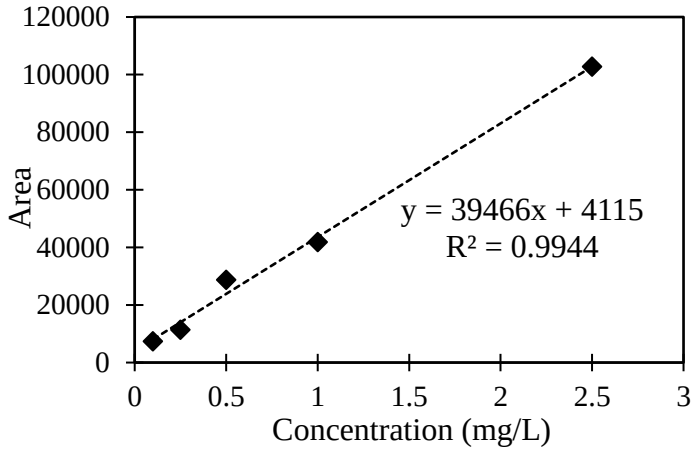

Figure 3.13. QM-GC/MS calibration curve for PCE (0.1-2.5 mg/L).

Permanganate was measured with UV-vis spectrophotometer at 525 nm. Persulfate concentration was determined by the iodometric method (Liang et al, 2008) using UV-visible spectrophotometer (Figure 3.14). The persulfate and potassium iodide (KI) alone solutions show interference in the same spectrum with chlorinated ethenes (PCE, TCE, DCE). To prevent this interference, according to the iodometric method, persulfate calibration was conducted by preparing a series of standard solutions, i.e., by adding various volumes of sodium persulfate stock solution (0.02 M), some $NaHCO_3$ (approximately 0.02 g), and 4 g KI into 40 mL EPA glass vials. The resulting solutions were hand-shaken and allowed to equilibrate for 15 min. The persulfate anion reacts with KI in the presence of $NaHCO_3$ to form an iodine yellow color that absorbs in the UV-vis range with maximum absorption at 387 nm. The persulfate calibration range is 0.1-50 mg/L for UV-160-A (Figure 3.15a.), 0.5-50 mg/L for UV-1700 (Figure 3.15.b).



(a)



(b)

Figure 3.14. a) Shimadzu UV-160A vis. spec. (Boğaziçi University), b) Shimadzu UV-1700 vis. spec. (University of Alabama).

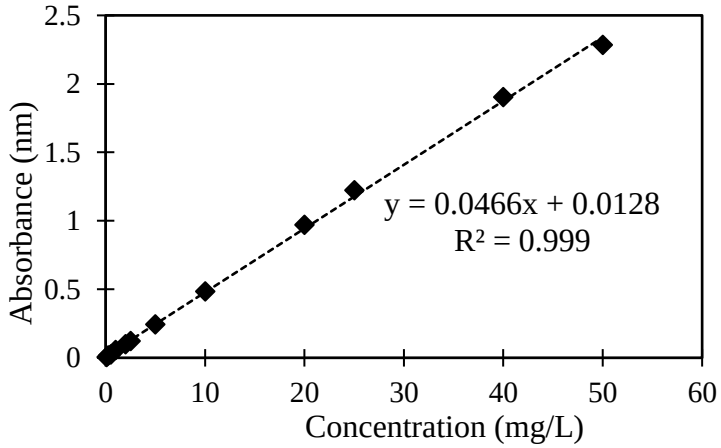

(a)

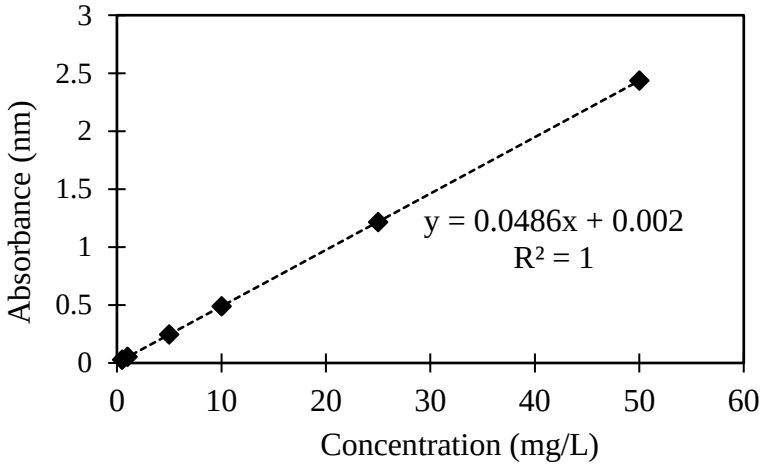

(b)

Figure 3.15. Calibration curve of persulfate a) for UV-160A, b) for UV-1700.

Prior to flushing experiments the conservative tracer Pentafluorobenzoic acid (PFBA) test was performed. PFBA was also measured with UV-visible spectrophotometer at the wavelength of 262 nm for UV-160A, and 234 nm for UV-1700. The PFBA calibration range is 0.5-250 mg/L both for UV-160A and UV-1700 (Figure 3.16).

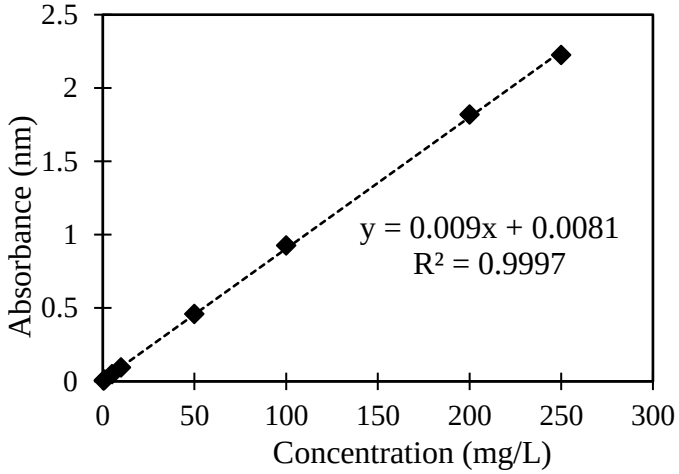

(a)

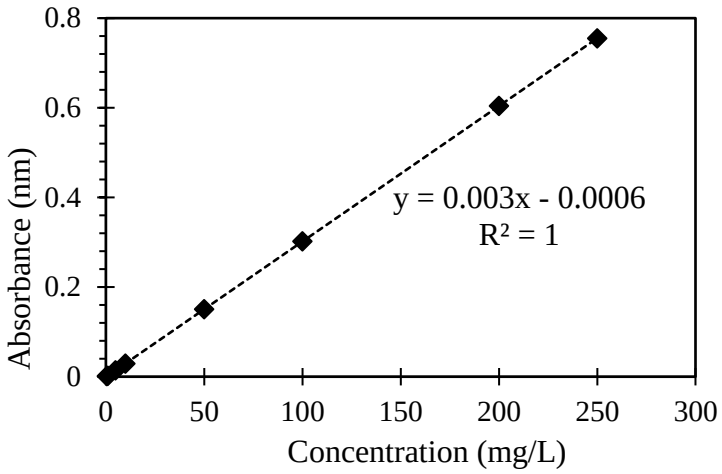

(b)

Figure 3.16. Calibration curve of PFBA a) for UV-160A, b) for UV-1700.

Sulfate, ferrous iron, and total iron were analyzed using DR-1900 HACH spectrophotometry (Figure 3.17) using the USEPA SulfaVer 4 Method 8051, 1,10-Phenantroline Method 8146, and FerroVer Method 10249, respectively. pH and ORP were measured by Sentix-82 pH electrode (pH only) and Beckman 510 pH meters (pH with ORP) and chloride ion concentrations were measured by using WTW Cl-800 and ColePalmer 4Oakton chloride ion-selective electrodes. Silver nitrate titration (Argentometric method) was used to determine chloride ion concentration in further experiments (indicator: potassium chromate).

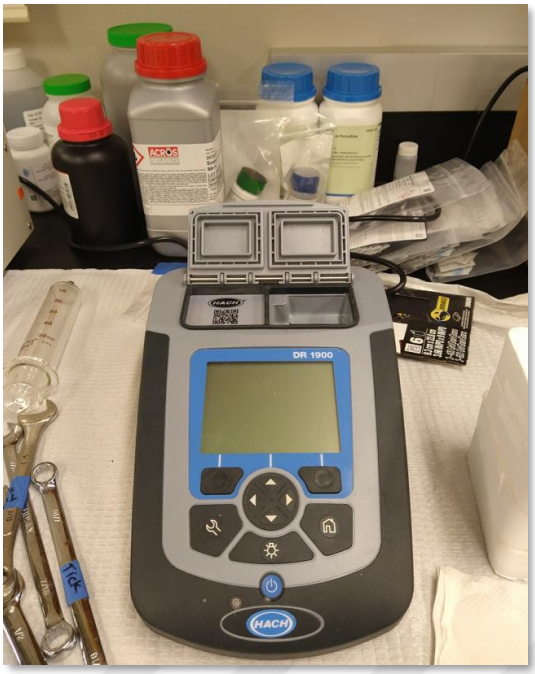

Figure 3.17. HACH DR-1900 spectrophotometer (University of Alabama).

In addition to DNAPL oxidation, nonionic surfactant Tween 80 degradation by heat-activated persulfate was also checked using matrix-assisted laser desorption/ionization time-of-flight mass spectrometry (MALDI-TOF/MS) available within the MS Instrumentation Laboratory of the Chemistry Department at The University of Alabama (Figure 3.18.a). MALDI samples were prepared in 2 mL microcentrifuge tubes, and vortexed for about 15 s before use. A total of 7 mL solution; 1 µL of polyethylene glycol (PEG), 1 µL of 1 µM Angiotensin, 4 µL of 10 µM α-cyano-4-hydroxy-cinnamic acid (CCA), and 1 µL of standard/sample were added in 2 mL tubes (Ayorinde et al, 2000). About 1 mL of each sample solution was deposited on a 100 well sample plate. The deposited samples crystallized within 30 s upon evaporation of the solvent. The sample plate was then loaded into the MALDI ion source. A five-point calibration curve of polysorbate Tween 80 was obtained using the concentrations of 0.0015%, 0.0075%, 0.015%, 0.075%, and 0.15% with peaks over the mass range of interest (Figure 3.18.b).

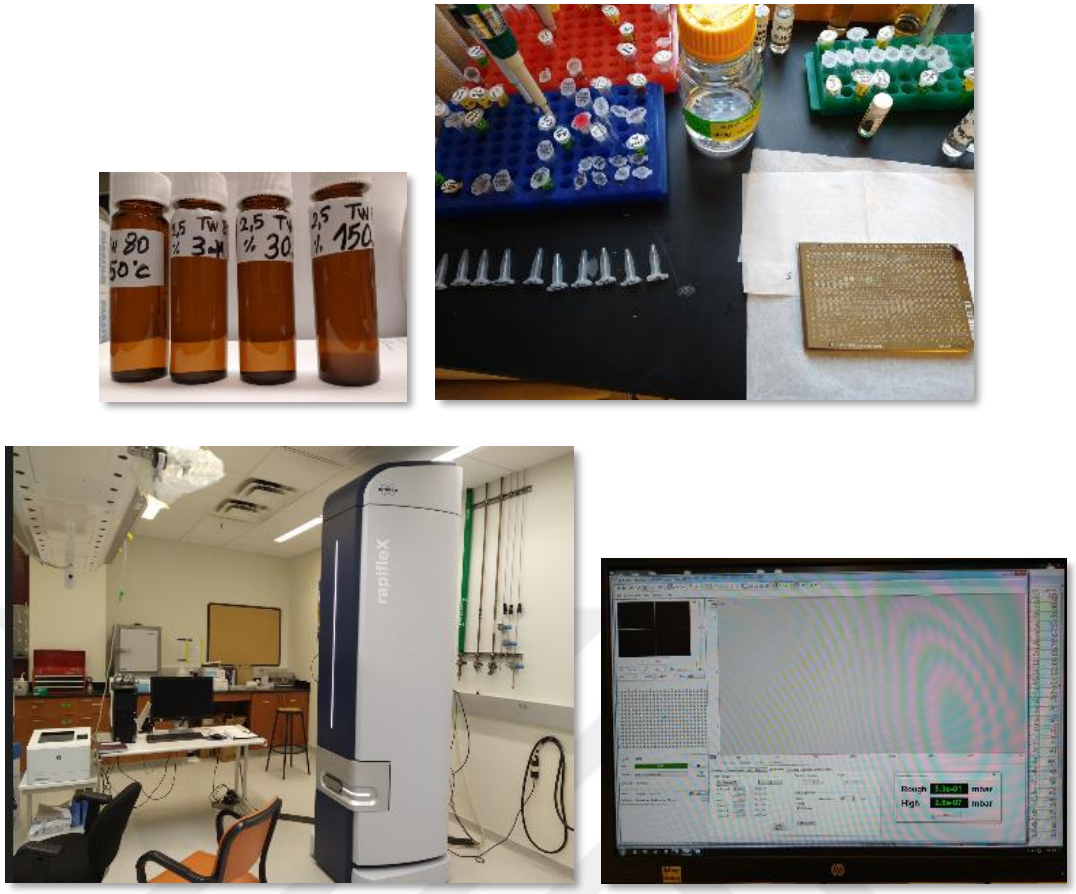

(a)

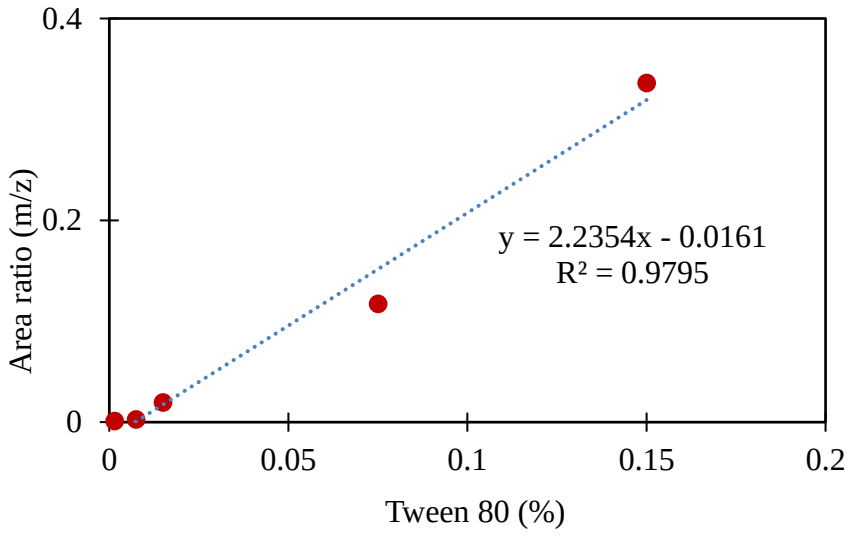

(b)

Figure 3.18. a) MALDI TOF instrument and sample preparation, b) Tween 80 calibration curve.

3.7. Mass Flux Reduction-Mass Removal Relationship

The flushing experiments were also examined in terms of the relation between the mass flux and mass removal (MF/MR) (DiFilippo and Brusseau, 2008). Such relationships are useful to assess the DNAPL removal efficiency of different solubilization agents. A linear relationship would indicate that the mass flux decreases gradually as remaining DNAPL mass diminishes. On the other hand, a nonlinear relationship would indicate that less efficient DNAPL mass recovery or a more efficient mass recovery is achieved depending on whether the mass recovery is delayed or not (Tick and Rincon, 2009). Non-ideal behavior would mean that recovery is likely influenced by other system properties such as non-uniform porous media properties and DNAPL mass distribution.

Mass-flux-reduction (MFR)/mass-removal (MR) behavior was simulated based on treating changes in mass-flux as a direct function of the change in contaminant mass as shown below (DiFilippo and Brusseau, 2008; Difilippo et al, 2010; Akyol et al, 2013; Tick et al, 2015; Akyol and Turkkan, 2018):

$$\mathrm{MFR} = 1 - \frac{\mathrm{J}_f}{\mathrm{J}_i} = 1 - \frac{\mathrm{Q}_f \mathrm{C}_f}{\mathrm{Q}_i \mathrm{C}_i} \tag{3.5}$$

where

J mass-flux [M/T]

C effluent concentration [M/L^3]

Q flow rate [L^3/T]

and the subscripts *i* and *f* represent the initial and final, respectively. The mass flux reduction mass removal relationship was computed from the effluent concentrations for each DNAPL component separately.

The MFR/MR relationship was examined differently for the oxidation experiments considering the effluent PCE and chloride concentrations. The mass flux reduction was calculated from (DiFilippo and Brusseau, 2008; Akyol et al, 2013),

$$\mathrm{MFR(t)} = 1 - \frac{\mathrm{J(t)}}{\mathrm{J}_i} = 1 - \frac{\mathrm{QC(t)}}{\mathrm{Q}_i\mathrm{C}_i} \tag{3.6}$$

where

J mass-flux [M/T]

Q volumetric flow rate, assumed steady [L^3/T]

C concentration [M/L^3]

t time [T]

The subscript *i* represent the initial. The fraction of mass removed from the flow-cell is calculated as the sum of PCE mass recovered from the effluent and the mass oxidized by the permanganate, the latter determined from the effluent chloride concentration is,

$$\mathrm{MR(t)} = \frac{\int \mathrm{QCdt} + \beta \int \mathrm{QC_{Cl}dt}}{\mathrm{M}_i} \tag{3.7}$$

where

MR(t) fraction of mass removed [ ]

M_i injected DNAPL mass [M]

β stoichiometry coefficient relating the mass concentration of chloride to the mass concentration of PCE [ ]

The two integrals in the numerator of equation (3.7) are the time-dependent DNAPL and chloride mass recovered from the effluent, respectively.

3.8. Numerical Modeling

The flushing experiments were modeled using two approaches. The first approach is a physics-based simulation of the governing multiphase, multi-component flow using the finite-difference UTCHEM computer program (Delshad et al, 1996). The second approach relies on an empirically-based function between the NAPL mass and aqueous phase concentration. Each of these two approaches are described in the following sections.

3.8.1. Multiphase Flow Model

The main equation that UTCHEM solves is (Pankow and Cherry, 1996):

$$\frac{\partial(\varepsilon_\alpha \rho_\alpha w_k^\alpha)}{\partial t} + \frac{\partial(\varepsilon_\alpha \rho_\alpha w_k^\alpha v_{\alpha,i})}{\partial x_i} - \frac{\partial}{\partial x_i} J_{k,i}^\alpha = I_k^\alpha + E_k^\alpha \quad (3.8)$$

The above equation is the conservation of mass equation for component k where:

k	in our problem is the DNAPL, or the water/chemical agent phase
$v_{\alpha,i}$	velocity of phase α in the i direction (for two dimensional flow i will be 1 or 2)
α	phase (in our problem there will be two phases: DNAPL phase and aqueous phase)
ε_α	volume fraction of phase α which is related to the saturation
ρ_α	mass density of phase α
x_i	cartesian coordinate system
w_k^α	mass fraction of phase α and component k
$J_{k,i}^\alpha$	dispersive flux of phase α for component k in the i direction
I_k^α	mass transfer of phase α
E_k^α	external source of phase α and component k

The main processes governing the enhanced solubilization experiments and the corresponding input parameters are described below.

3.8.1.1. Interphase Mass Transfer

The interphase mass transfer between the NAPL and aqueous phases is modeled as a product of the concentration difference and the lumped mass transfer coefficient (Powers et al, 1994):

$$\frac{\partial M}{\partial t} = K_l(C_s - C) \quad (3.9)$$

where

C_s	reagent-enhanced contaminant solubility [M/L^3]
C	contaminant concentration in the aqueous phase adjacent to the NAPL [M/L^3]
K_l	lumped mass transfer coefficient per unit volume of porous medium [1/T]

K_l is referred to as the lumped mass transfer coefficient because the interfacial area between the NAPL and aqueous phases (which is generally not known) is lumped into the mass transfer coefficient. The lumped mass transfer coefficient is often expressed in terms of the non-dimensional modified Sherwood number defined as:

$$Sh' = \frac{K_l \, d_m^2}{D} \tag{3.10}$$

where

Sh'	modified Sherwood number
dm	mean grain diameter [L]
D	molecular diffusion coefficient [L^2/T]

The Sh' can be more readily compared across different studies than K_l because it is a non-dimensional quantity that incorporates other relevant parameters, namely the mean grain diameter and diffusion coefficient. Because the mass transfer coefficient, K_l, cannot be directly measured, it was selected to be one of the main calibration parameters.

Sherwood numbers were calculated using equation (3.10) for dm = 0.359 mm for silica sand and 0.150 mm for natural soil. The mean grain diameters were determined from particle size analysis. Molecular diffusion coefficient was assumed to be $Dm=1x10^{-9}$ m^2/s (Gabler et al, 1996).

3.8.1.2. Capillary Pressure and Relative Permeability

The Brooks-Corey method (Brooks and Corey, 1966) was used to compute the capillary pressure between the NAPL phase and aqueous or microemulsion phases and to model the relative permeability of each phase. The capillary pressure is calculated as follows:

$$\left(\frac{P_b}{P_c}\right)^{\lambda} = 1 - S_n \tag{3.11}$$

where

P_b	entry pressure
P_c	capillary pressure between the two phases
S_n	normalized aqueous/microemulsion saturation
λ	pore size distribution coefficient

Both P_b and P_c are scaled with respect to interfacial tension, porosity and permeability (Brooks and Corey, 1966). The entry pressure for PCE is obtained from (Ağaoğlu et al, 2012) computed as 5.032 kPa using the Young–Laplace equation with a contact angle of 20°. This value showed good agreement with the literature (Eichel et al, 2005). The pore size distribution index was taken as 2, a value typical for fine sand (Agaoglu et al, 2012). The relative permeability for each phase was also computed using the Brooks–Corey formulation (Brooks and Corey, 1966):

$$k_{r,l} = k_{r,l}^{o}\left(S_{n,l}\right)^{e_l} \tag{3.12}$$

where

$k_{r,l}$ relative permeability of phase l

$k_{r,l}^{o}$ endpoint relative permeability of phase l

e_l exponent of phase l

3.8.1.3. Interfacial Tension

The UTCHEM was originally developed to simulate surfactant-enhanced solubilization. Since the experiments performed in this study involve cyclodextrin as well as surfactant-enhanced solubilization, a modified version of UTCHEM version 9 was used. The modified version includes the option of an IFT calculation method of Li and Fu (1992) which is more suitable for simulating cyclodextrin and co-solvent-induced IFT reduction, in addition to the original option of surfactant-induced IFT reduction method. The modified IFT method was incorporated into UTCHEM by Liang and Falta (2008).

For the surfactant-enhanced flushing experiments when surfactant contents are greater than the critical micelle concentrations (CMC), the reduction of interfacial tension is calculated using Huh's equation (Huh, 1979) which relates the interfacial tension to the solubilization ratio (Delshad et al, 1996). The interfacial tension for the cyclodextrin flushing experiment was computed according to the correlation of Li and Fu (1992) as suggested by Liang and Falta (2008) for cases when co-solvent flushing is also present:

$$\sigma = \sigma_0 \left(\frac{X}{X_0}\right)^{\theta} \quad (3.13)$$

$$X = log\ (C_n^w + C_w^n + C_p^c) \quad (3.14)$$

where

$X_0 = X$ when $C_p^c = 0$

σ interfacial tension when a co-solvent is present

σ_0 interfacial tension in the absence of a co-solvent

θ exponent of the IFT expression assumed to be equal to 1 (Li and Fu, 1992)

C_n^w water concentration in the NAPL phase

C_w^n NAPL dissolved concentration in the aqueous phase

C_p^c co-solvent concentration in the co-solvent poor phase (in this case the NAPL phase)

3.8.1.4. NAPL Solubility

The UTCHEM model requires the definition of the NAPL solubility in both the pure water and in the microemulsion (flushing solution). The dissolution into the pure water is only present during the first pore volume of the simulation until the flushing solution reaches the DNAPL. The PCE solubility in pure water was taken as 0.206 g/L (Horvath et al, 1999; Yalkowsky et al, 2016). The reagent-enhanced DNAPL solubility was determined using Hand's equation (Hand, 1930). Hand's rule assumes that equilibrium phase concentration ratios are straight lines on a log-log scale. The binodal curve is computed by:

$$\frac{C_{3l}}{C_{2l}} = A\left(\frac{C_{3l}}{C_{1l}}\right)^{B} \quad l = 1,2,3, \qquad A = \left(\frac{2C_{3max}}{1-C_{3max}}\right)^{2} \quad (3.15)$$

where

C refers to the concentration of each component in each phase: $l = 1$ is aqueous phase, $l = 2$ is NAPL phase, and l = 3 is the microemulsion and B= -1

The values of the empirical parameter A was determined such that the solubility in the model is equal to the agent-enhanced solubilities as measured with batch solubility experiments. (Chapter 4, Table 4.14) lists the solubility values for the different reagents used in the flushing experiments.

3.8.1.5. Initial DNAPL Distribution

The initial DNAPL distribution after the injection of the DNAPL is an important parameter that is seldom known with sufficient detail to accurately simulate DNAPL source zone remediation. In the conducted laboratory experiments, the injected DNAPL volume is known. The location of the low permeability barrier is known. However, the exact DNAPL distribution (dimensions and saturation) is not known. Therefore, these two parameters were determined as part of the model calibration.

3.8.1.6. Dispersivity

The porous media dispersivity was determined from the conservative tracer pentafluorobenzoic acid (PFBA) test. Specifically the dispersivity was determined by matching the observed tracer experiment to the model concentrations. Two model solutions were used to estimate the tracer: the UTCHEM solution with no DNAPL and the analytical 1-D advection-dispersion solution (Ogata and Banks, 1961). The best-fit dispersivity value was determined by minimizing the root mean square of the error (RMSE) between the observed and modeled concentration.

3.8.1.7. Boundary Conditions, Discretization and Parameter Assignment

Prescribed flow rates equal to 2 mL/min were defined at the two injection locations shown in Figure 3.19. The remaining cells along the left and right hand side of the model were assumed to be no flow-cells. This corresponds to an average Darcy velocity of 86.4 cm/day for silica sand flow-cell and 137 cm/day for natural soil flow-cell which are consistent with velocities encountered during enhanced dissolution (e.g., Kokkinaki et al, 2013; Aydin-Sarikurt et al, 2016). The model was discretized into 30 by 48 uniform gridblocks. The dimensions of these gridblocks were 0.5 cm by 0.5 cm. The configurations of the experimental set-up are presented in Figure 3.19. All initial aqueous PCE concentration were assumed zero in each cell. Initial saturation conditions were based on the volume of NAPL injected and images of the tank after DNAPL injection.

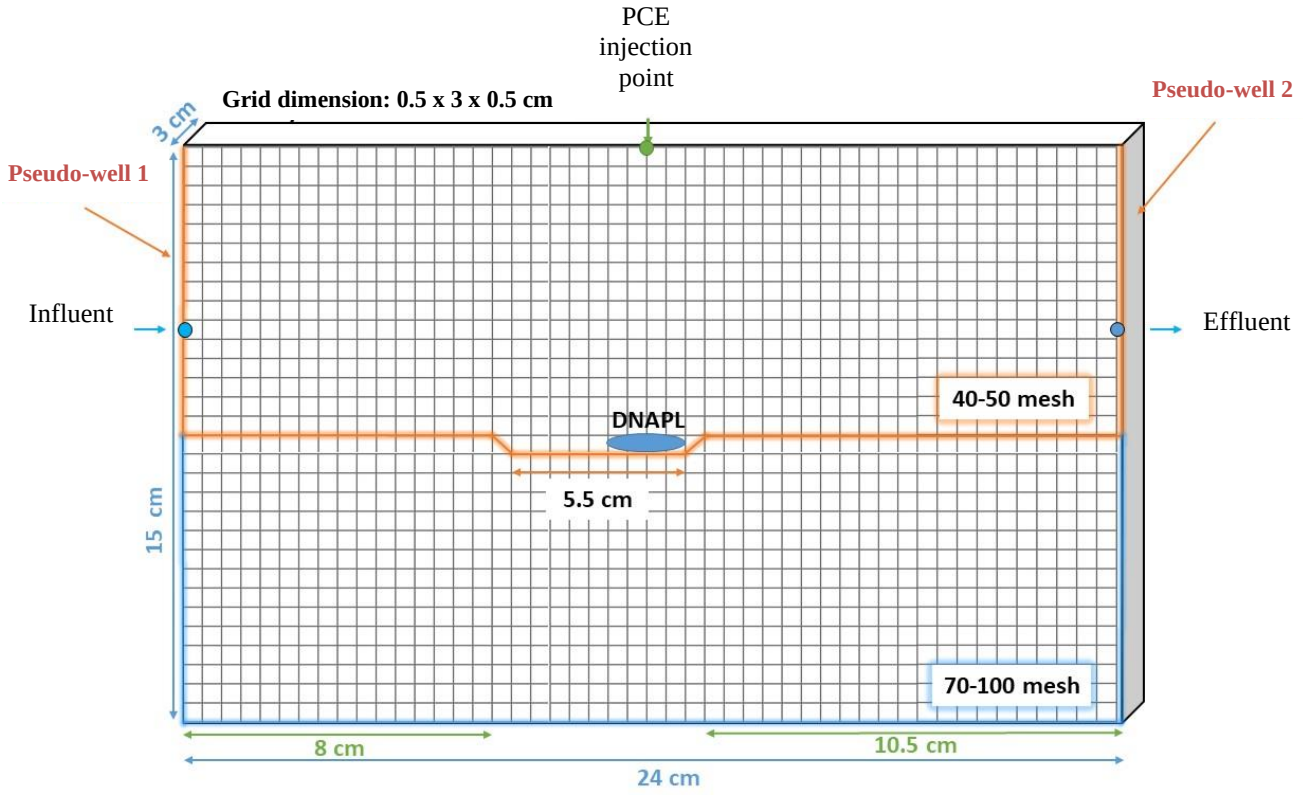

(a)

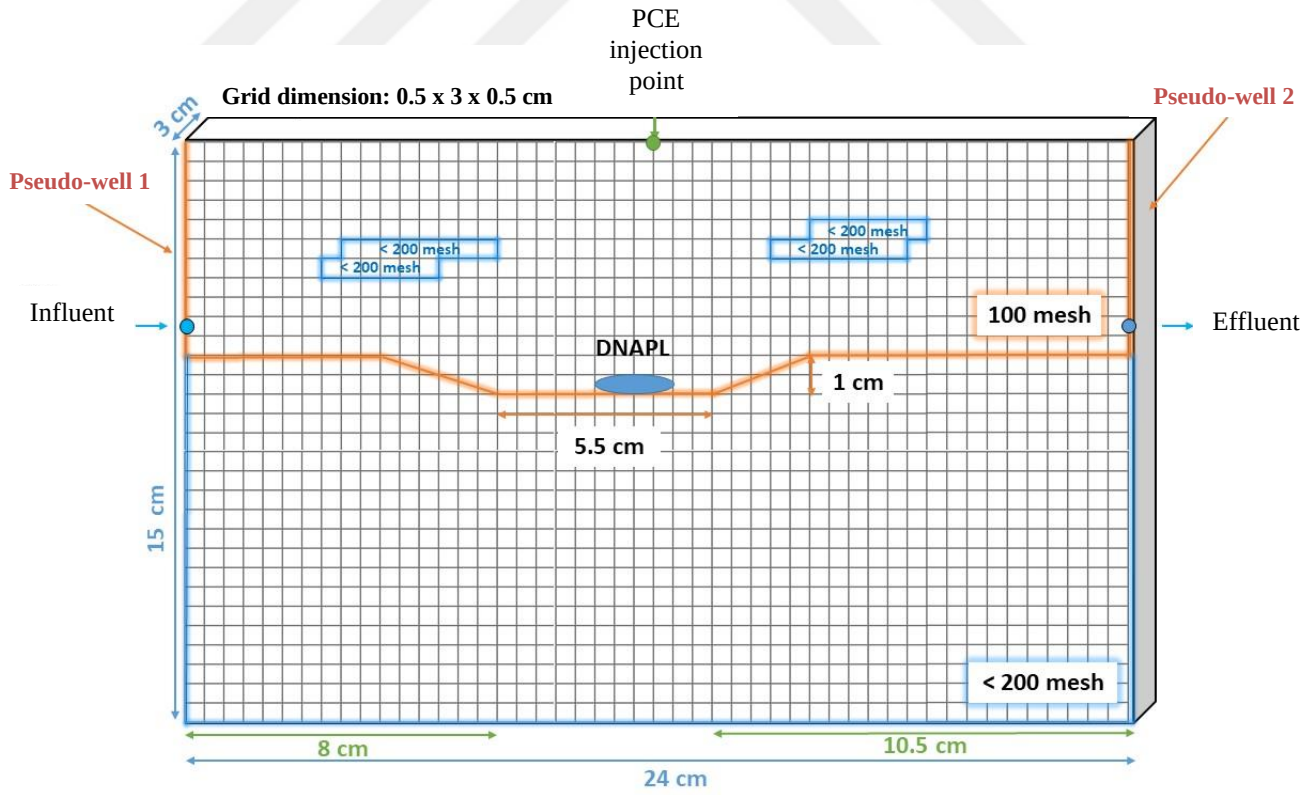

(b)

Figure 3.19. Schematic of the flushing experiments. The inset image shows the NAPL distribution prior to flushing in a) Silica sand, b) Natural soil.

3.8.1.8. Oxidation Reaction

The coupled solubilization and oxidation flow-cell experiments were also simulated using the UTCHEM computer program (Delshad et al, 1996). The primary equations that the program solves is the mass conservation equations for each chemical species and a pressure equation that consists of the generalized Darcy equation (see Equation 3.8). The program also incorporates a series of equations representing the complex multiphase behaviour and the properties associated with these parameters such the interfacial tension (IFT), phase relative permeability, phase capillary pressure and viscosity (all described in the previous sections). For further details can be found User's manual of UTCHEM (Delshad et al, 1996).

The reaction term included in UTCHEM -initially defined for biodegradation problems- was manipulated and rearranged to account for permanganate oxidation rate expressed as a linear function of PCE aqueous concentration and permanganate concentration. The oxidation reaction rate between PCE and permanganate is defined in equation (3.16),

$$\frac{dS}{dt} = -K_O SA \qquad (3.16)$$

where

S aqueous phase DNAPL concentration [M/L^3]

A oxidant concentration (permanganate) [M/L^3]

K_o overall oxidation reaction rate constant [L^3/M/T]

The model domain was divided into 30 by 48 uniformly-sized gridblocks with dimensions 0.5 cm by 0.5 cm. Appendix C provides source and range of main input parameters represented in a data requirement table. The main calibration parameter used to match the oxidation experimental data was the oxidation rate constant (K_o). The reaction constant was systematically adjusted until the difference between the experiments and model results is minimized. Specifically, the target was to reduce the normalized root mean square of the error (NRMSE) defined as equation (3.17),

$$\text{NRMSE} = \frac{1}{w}\{\sum[C_m(t) - C_e(t)]^2\}^{0.5} \quad (3.17)$$

is minimum where

$C_m(t)$ effluent PCE concentration as a function of time calculated from the model [M/L^3]

$C_e(t)$ effluent PCE concentration as a function of time determined from the experiments [M/L^3]

w normalizing parameter taken as the difference between the peak concentration from each experiment and minimum concentration (equal to zero) [M/L^3]

Smaller values of NRMSE indicate better agreement between experiments and model results.

The UTCHEM calculation flowchart and solution scheme for reaction equations in the UTCHEM simulator are shown in Figure 3.20 and 3.21. After defining the initial value of all input parameters, the pressure distribution within the model domain is calculated. This includes the effect of boundary conditions and wells. The groundwater velocity is calculated as well. Knowing the flow field for time t, the phase saturations and concentrations of all species and are calculated using the conservation of mass principle. Parameters which depend on the saturations and concentrations such as the hydraulic conductivity updated next. Reaction, if present, are accounted for next. Parameters dependent on concentrations such as fluid properties (Density, viscosity) are updated. The calculations are then repeated for the next time step until the end of the simulation time.

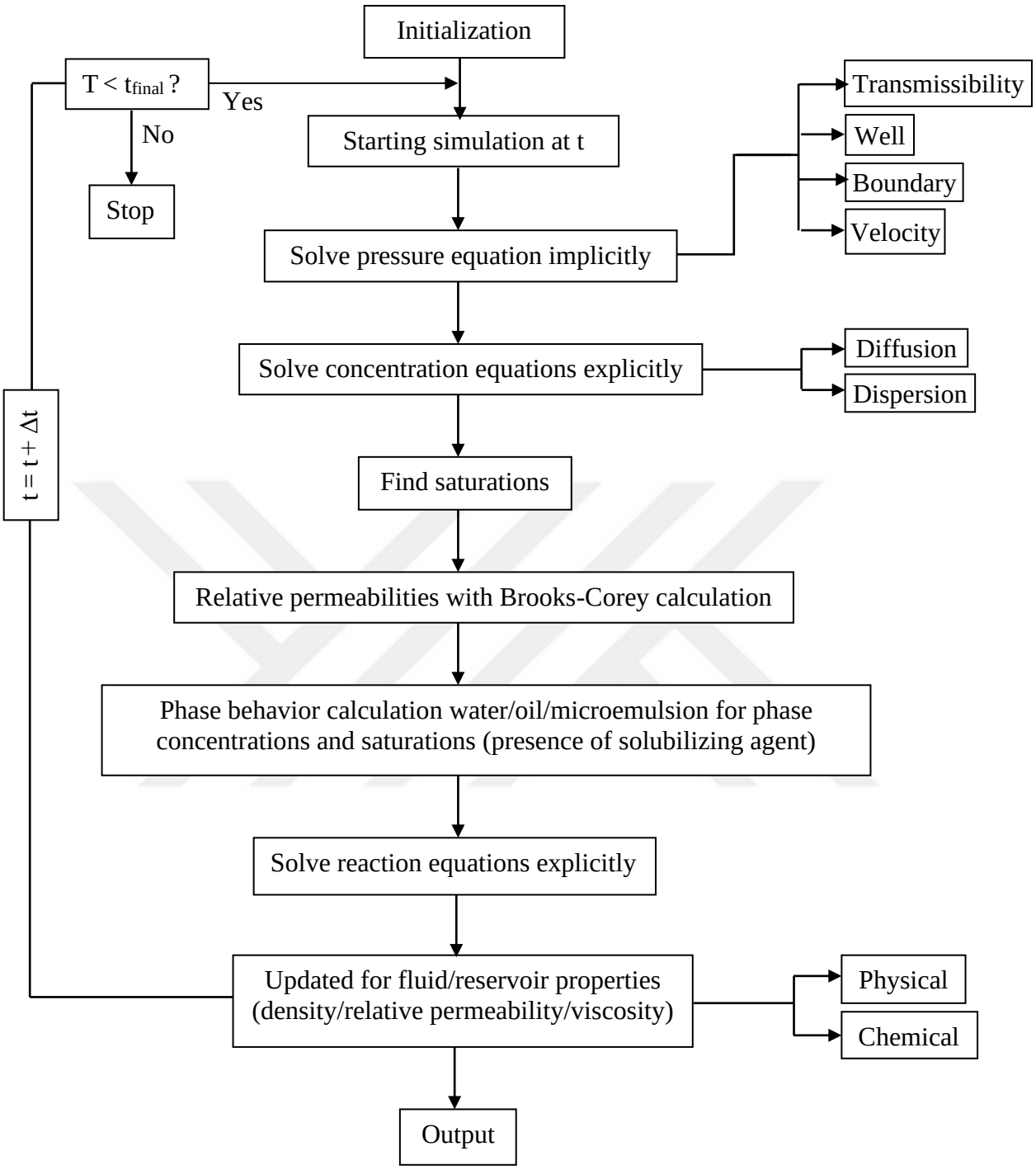

Figure 3.20. The flowchart of UTCHEM (modified from Korrani et al, 2015; Luo et al, 2016 and Hosseininoosheri et al, 2016).

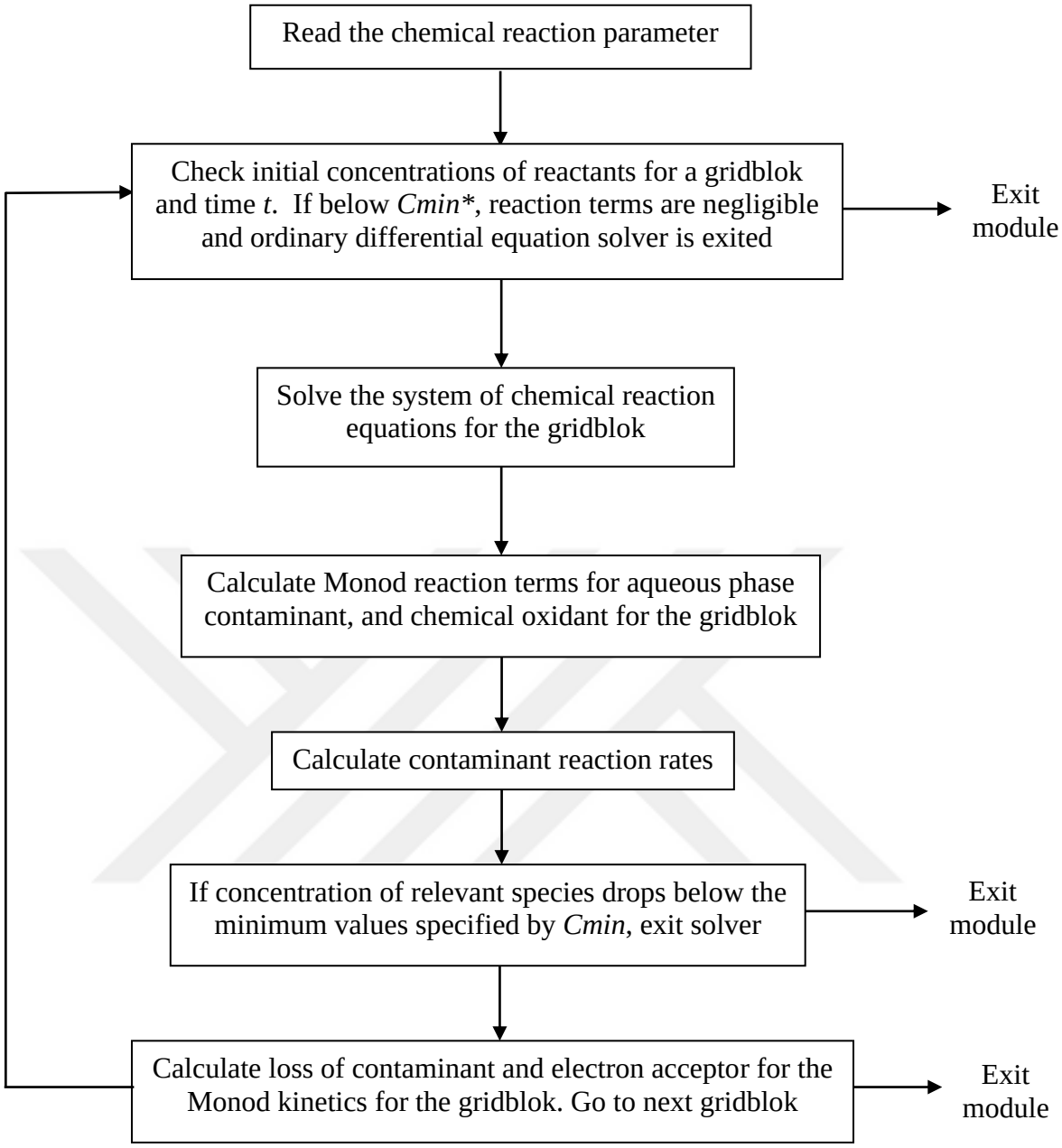

Cmin :* Minimum concentration of the contaminant (aqueous phase PCE) and electron acceptor (permanganate) that is of interest

Figure 3.21. The solution scheme for reaction equations in UTCHEM simulator (modified from Korrani et al, 2015; Luo et al, 2016 and Hosseininoosheri et al, 2016).

3.8.2. Sensitivity Coefficients

To numerically evaluate the impact of the various input parameters on the DNAPL dissolution and the corresponding time-dependent effluent concentration, the multiphase flow model was used to calculate sensitivity coefficients. Sensitivity coefficients are measures of the change of a dependent variable, in this case the effluent concentration, due to changes in the input parameters (see e.g., Saltelli et al, 2004):

$$SC = \frac{\partial C_e}{\partial p_i}(t, p_1, p_2 \dots p_n) \tag{3.18}$$

where

SC Sensitivity coefficient

Ce effluent concentration as a function of time and all input parameters

p_i i th input parameter

To better compare the sensitivity coefficients for the different parameters considered, a non-dimensional form is computed which normalizes the dependent and independent variables:

$$SC = \frac{\partial C_e}{\partial p_i}(t, p_1, p_2 \dots p_n)\frac{p_i}{C_e} \tag{3.19}$$

The correlation between the sensitivity coefficients is an indicator of the uniqueness of the calibration process. If the correlation of the sensitivity coefficients of two parameters are close to ± 1, then this indicates that these two parameters can not be uniquely determined (Geza et al, 2010).

Specifically, the sensitivity coefficients are computed by changing the input parameters and observing the corresponding impact on the time-dependent effluent concentration. The sensitivity coefficients are calculated for selected input parameters relating to the flow, NAPL properties and distribution, and porous media properties: (i) flushing flow rate, (ii) NAPL solubility, (iii) transversal (lateral) dispersivity, (iv) NAPL saturation, (v) interphase mass transfer coefficient, (vi) longitudinal dispersivity.

3.8.3. NAPL Mass Depletion Model

To avoid some of the difficulty of defining detailed soil parameters and DNAPL source zone architecture, the DNAPL mass depletion was also modeled in terms of a simplified dissolution model proposed by Cheng and Zhu (2021). From conservation of mass, the rate of DNAPL dissolution can be expressed as:

$$\frac{dM}{dt} = -QC \tag{3.20}$$

where

M dimensionless DNAPL mass, equal to the DNAPL mass remaining M^* normalized by the initial mass M_0^*

Q dimensionless flow rate, equal to the flow rate Q^* normalized by the initial flow rate, Q_0^* Q =1 for constant flow conditions

C dimensionless aqueous concentration, equal to the concentration C^* normalized by the peak concentration C_0^*

t dimensionless time defined as $t = \frac{t^*}{\tau}$ where $t^*$is time and t is the characteristic time for the dissolution of the DNAPL mass defined as: $\tau = \frac{M_0^*}{Q_0^* C_0^*}$

In the above definitions, the superscript * refers to dimensional quantities.

The recovered dimensionless mass, MR, can be expressed as,

$$MR = 1 - M \tag{3.21}$$

Cheng and Zhu (2021) proposed different functional forms relating C to the remaining DNAPL mass: $M = g(C)$ such as a power function or a bilinear model or a sinusoidal function. All these functions have the following properties: $g(0) = 0$ and $g(1) = 1$. In the current analysis, a power function will be used to model the DNAPL mass-concentration relation (Equation 3.22),

$$g(C) = C^{\beta} \tag{3.22}$$

where

β is an empirical parameter which was determined from the experimental data such that the normalized mean square of the error (NRMSE) between the simulated and observed recovered mass (MR) is minimum.

The governing ordinary differential equations were solved using the Runge Kutta order four method (Burden and Faires, 1997).

Overall summary of the experimental and modeling studies carried out within the scope of the dissertation are presented in the following flow chart (Figure 3.22).

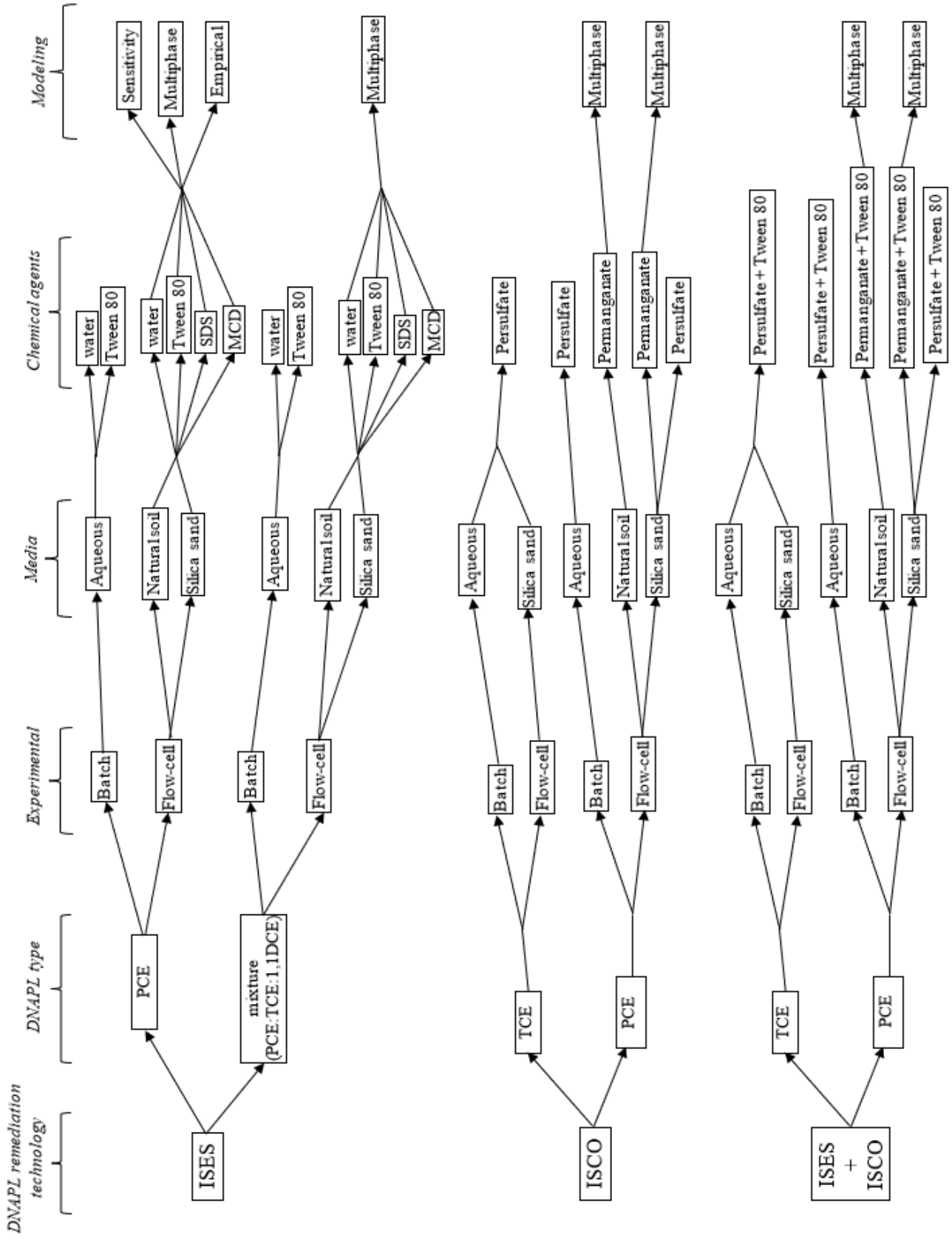

Figure 3.22. Summary of the groundwater remediation technologies, the experiments performed to evaluate these technologies and the modeling studies performed within the scope of the thesis.

4. RESULTS

This chapter describes all the laboratory experiments and modeling work performed to assess the use of different technologies to recover the DNAPL from subsurface. Section 4.1 compares enhanced solubilization of PCE using different remedial agents. Section 4.2 presents the enhanced dissolution results for DNAPL mixtures (consisting of PCE, TCE and DCE). Section 4.3 discusses the benefits of combining the surfactant-enhanced dissolution with oxidation through potassium permanaganate. Finally, Section 4.4 presents the results of surfactant-enhanced dissolution with oxidation using activated sodium persulfate.

In all sections the results of batch and flushing experiments are presented followed the conducted modeling work. A flowchart summarizing the different technologies investigated experimentally and the accompanying modeling work was presented in Chapter 3 (see Figure 3.22).

4.1. Enhanced Solubilization of DNAPL PCE with Different Solubilizing Agents

The results presented in this section were published in the journal *Water, Air, & Soil Pollution* entitled "Experimental Assessment and Modeling of Enhanced Solubilization of Pool-dominated Tetrachloroethene Source Zone in Heterogeneous Porous Media" (Demiray et al, 2021).

The main purpose of the study reported herein was to investigate the contaminant elution behavior of pool-dominated DNAPL from heterogeneous (calcareous soil) porous media. The DNAPL selected in the current work is tetrachloroethene (PCE), which is considered particularly dangerous to human health and the environment and has been widely encountered at numerous subsurface contamination sites (Volpe et al, 2007; Soga et al, 2004; Zheng et al, 2016). The specific objectives of this study are two-fold. First, the study compares the effect of different solubilization agents (SDS, Tween 80 and MCD) on effluent aqueous phase concentration and DNAPL source zone depletion. The goal here is to compare the DNAPL-zone depletion for different solubilization agents (Surfactants, cyclodextrins) as well as water flushing in heterogeneous porous media. The second objective is to model the elution behavior of the multiphase system using two approaches: a fully multiphase flow model based on the UTCHEM computer program (Delshad et al, 1996) and a simplified model based on the empirical DNAPL mass-concentration function proposed by Cheng and Zhu (2021). Through analysis of the flushing experiments, we examine what information can be retrieved from these two modeling approaches as well as the advantages and limitations of each.

DNAPL PCE enhanced solubilization flow-cell flushing experiments were performed at Kocaeli University Geological Engineering Department (TÜBİTAK project: 117Y140)

4.1.1. PCE Enhanced Solubilization Batch Experiments

The interfacial tension measurement procedure is discussed in chapter 3, section 3.2. In this section, the interfacial tension (IFT) and ternary phase diagram (TPD) experiments were performed for PCE-Tween 80 system. The data obtained from the batch tests are used for the development of surfactant enhanced solubilization modeling described in Section 4.1.3.

The measured IFT between the DNAPL PCE and the aqueous phase as a function of Tween 80 content is shown in Figure 4.1. The IFT between DNAPL PCE and water is 45 mN/m. Then it gradually decreases with increase in Tween 80 content. The critical micelle concentration (CMC) value of Tween 80 (~0.00327 %vol or ~35 mg/L) corresponds to ~7 mN/m. This value is quite compatible with the literature which is reported as about 10 mN/m at 35 mg/L Tween 80 concentration (Cheng et al, 2016; Bak and Podgorska, 2016). Small changes may be due to different analytical instruments. For Tween 80 concentrations exceeding the CMC, where the surfactant molecules start to aggregate to form micelles, the IFT remains approximately constant at around 3.4 mN/m regardless of surfactant concentration.

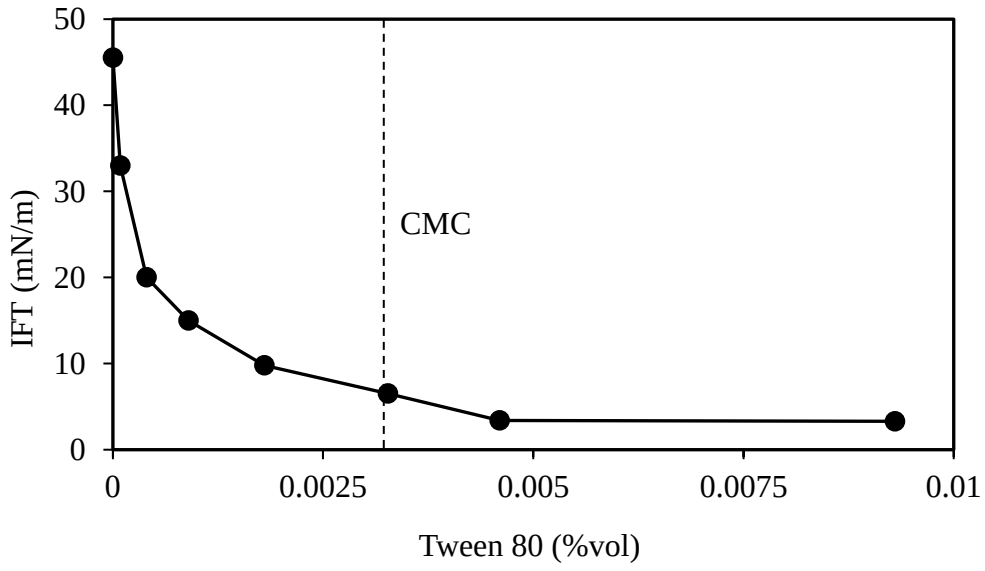

Figure 4.1. IFT of two-phase systems as a function of Tween 80 concentrations (0-0.0093 %vol or 0-100 mg/L) for DNAPL PCE.

In the multiphase system, miscibility curves were obtained with the “cloud point titration” and represented in a ternary phase diagram (TPD). The TPD between Tween 80 - PCE - water system is presented in Figure 4.2. The titration of Tween 80 with PCE was performed in more than one step because of the high viscosity of pure Tween 80, as gels were formed when the aqueous solution exceeded about 30 % in the system. The formation of gels caused the solutions to be highly viscous which prevented the titration performance. The first stage is the part that constitutes the left side of the Tween 80; PCE; water curve starting the ratio from 0; 0; 100 to 29.2; 18.9; 51.9 % by mass. The second stage is the part that constitutes the right side of the Tween 80; PCE; water curve starting the ratio from 0; 100; 0 reached to 32.3; 55.6; 12.0) % by mass. The titration process was not physically possible after reaching these ratios. The third and last step was to reach the maximum Tween 80 concentration that the Tween 80 - PCE - water system was able to mix. Starting from 50; 50; 0 and 55; 45; 0 reached up to 39.7; 39.7; 20.6 and 42.3; 34.6; 23.1, respectively.

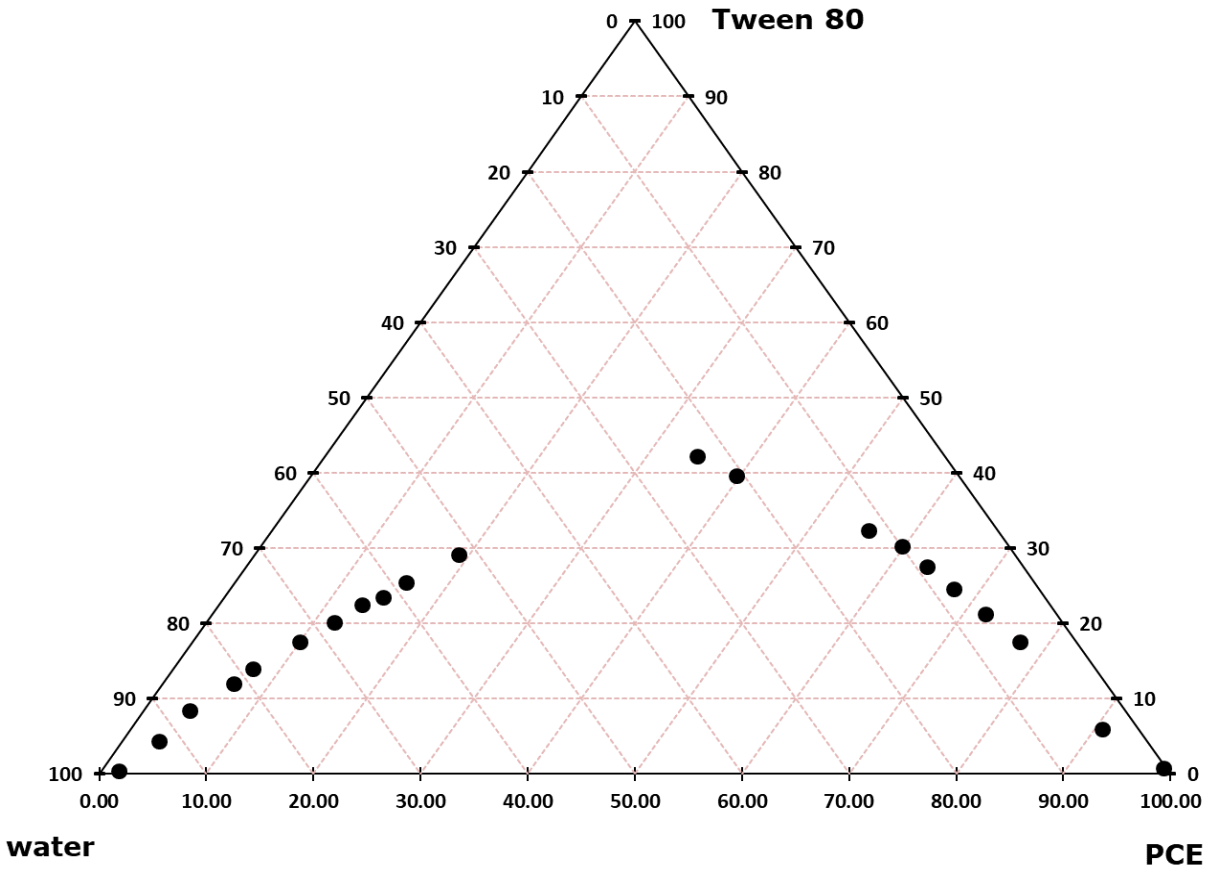

Figure 4.2. Ternary phase diagram for Tween 80 - PCE - water (% mass).

The Tween 80 - PCE - water miscibility diagram was compared to miscibility representations of other DNAPLs with Tween 80 from the literature. Poteshnova and Zadymova (2006) examined the ternary diagram of Tween 80 - Toluene - water system. They performed a detailed study on water-

rich corner of the phase diagram where they divided into 5 subregions. Mostly based on visual definitions, they named (I) single phase region: a molecular solution of Toluene and Tween 80, (II) single-phase region: a transparent micellar Tween 80 solution containing solubilized Toluene, (III) single-phase region: opalescent microemulsions, (IV) two-phase region: an aqueous molecular solution of Tween 80 and Toluene/Toluene, and (V) two-phase region: oil-in-water microemulsion/Toluene. As a result, it is argued that multi-phase systems with surfactants show a different and more complicated behavior compared to systems with co-solvents.

In addition to examining the surfactant - PCE - water phase behavior, the presence of co-solvent in the system was also investigated in a co-solvent - PCE - water ternary plot. Pure ethanol was added to the system as a co-solvent. Figure 4.3 gives the miscibility of the co-solvent - PCE - water system for different co-solvent contents. Specifically, for the compositions above the imaginary curve following the dots, the system is fully miscible, and only one phase is present. For compositions below the miscibility curve, two phases would be present which are the aqueous phase and NAPL-rich phase. The multiphase system is fully miscible at ethanol contents higher than 60 %.

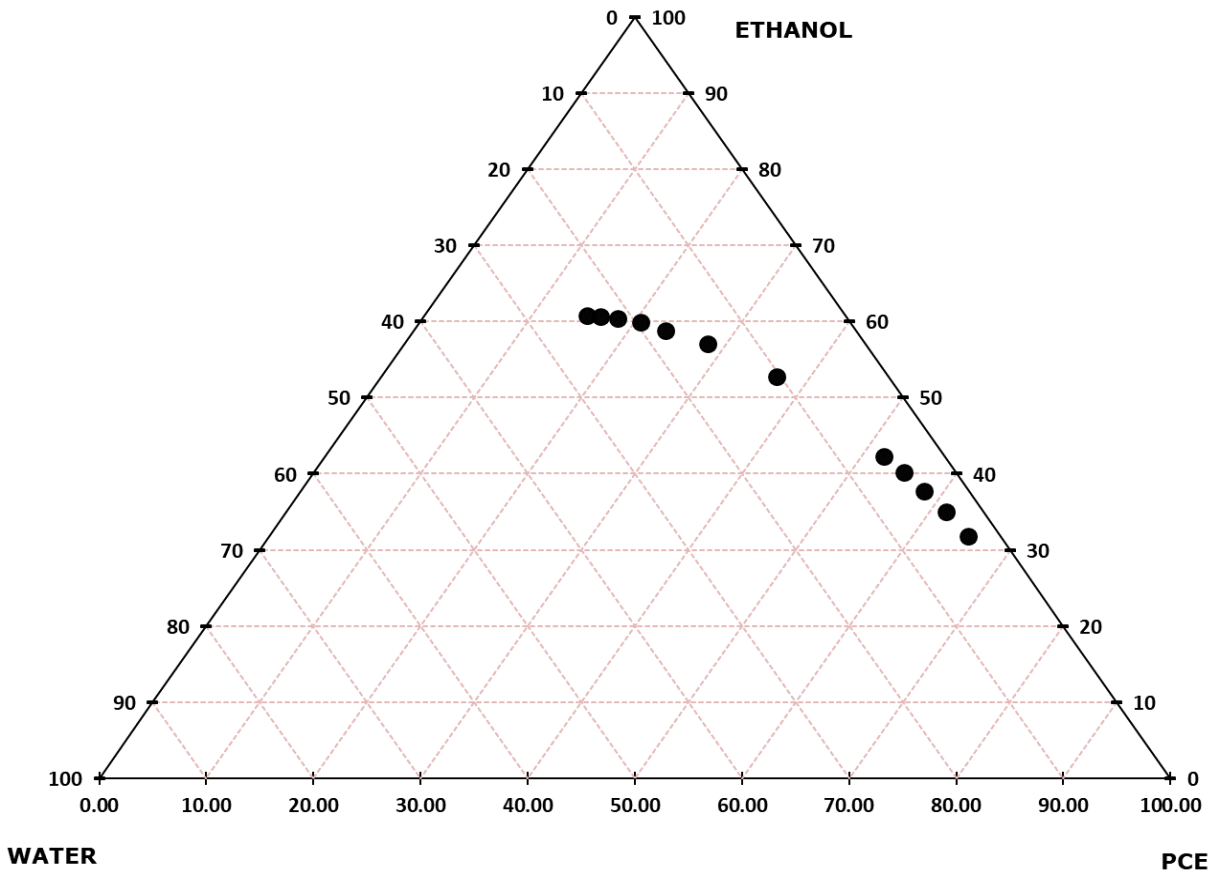

Figure 4.3. Ternary phase diagram for ethanol - PCE - water (% mass).

In addition to the presence of Tween 80 and ethanol in the system separately, the impact of their mixture on the ternary phase system was also examined. As the first mixing trial, the curve obtained from the PCE-rich region with two solubilizing agents introduced into the system at the same ratio (Ethanol:Tween 80 = 1 (vol/vol)) is shown in Figure 4.4. When Tween 80 is added to ethanol in the system, the miscibility decreases to 40 %. That is, the area above the curve where the complete miscibility is represented is increasing.

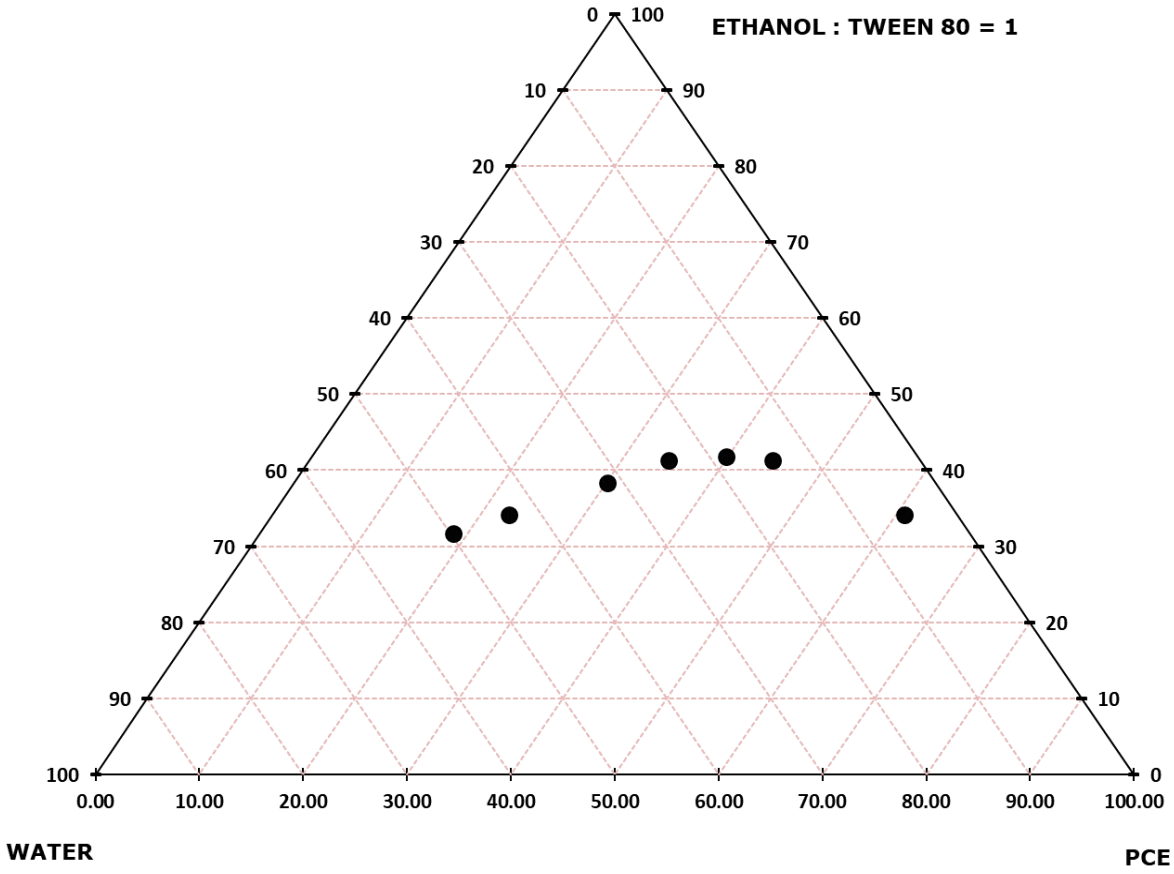

Figure 4.4. Ternary phase diagram for [ethanol/Tween 80] - PCE - water (%mass).

The final mixed solubilizing agent titration experiment was carried out, in which 10 % Tween 80 was used instead of the third component, water (Figure 4.5). Although the system behaves similarly to that of Figure 4.3, the curve increased up to 60 % in a more unstable way, but decreased after this value. It should be noted that maximum solubility of Tween 80 in water is 10 %vol.

The phase behavior of the mixture of alcohol and surfactant with DNAPL was also investigated by Martel et al (1998). A similar curve was obtained, and they concluded the best solvent to use with a given alcohol-surfactant solution must have a lower curve close to the water-solvent axis, and a single-phase zone wide enough to allow a high surfactant-alcohol concentration.

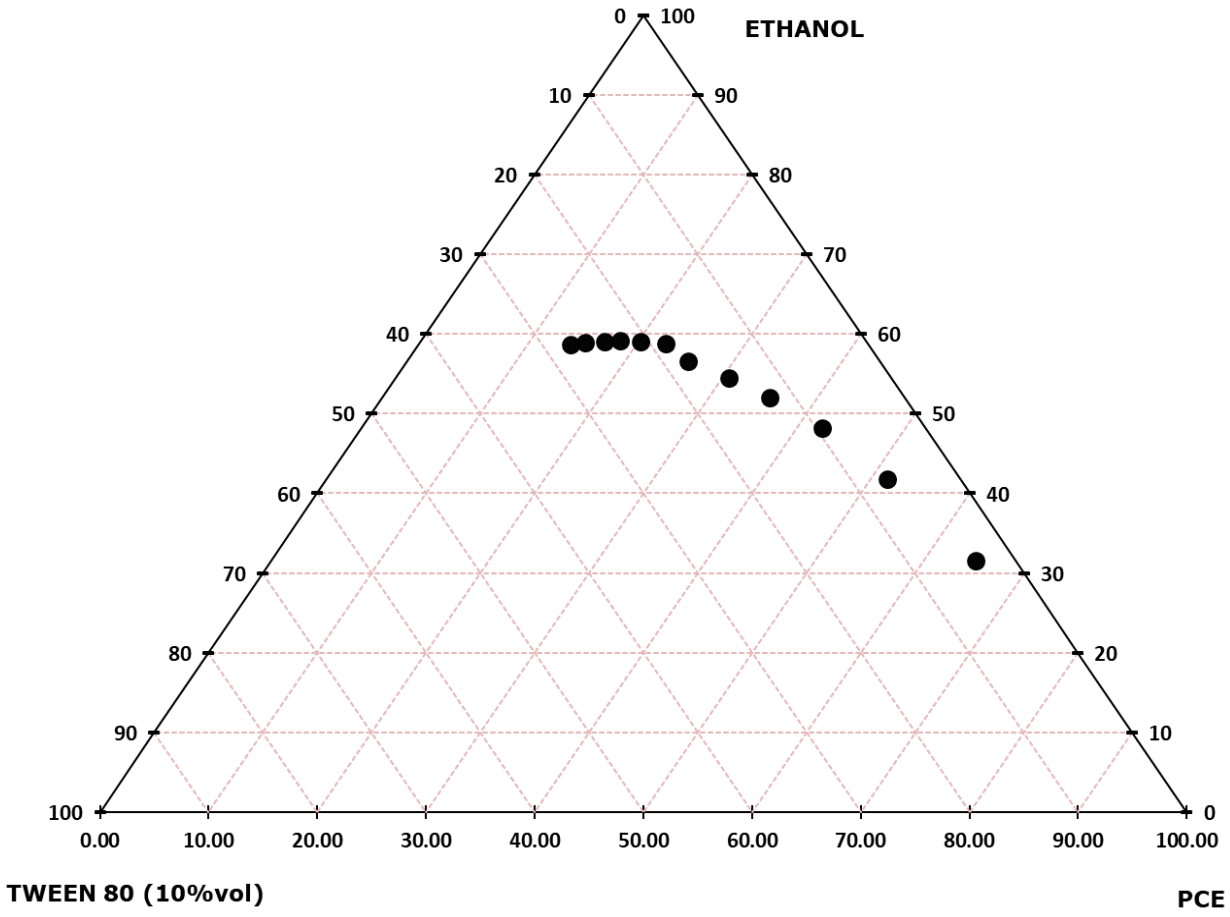

Figure 4.5. Ternary phase diagram for ethanol - PCE - Tween 80 (%mass).

The measured solubility of PCE for Tween 80 solution contents at 0 % (water solubility), 2.5 % and 5 % by volume is presented in Figure 4.6. At 2.5 % Tween 80, the solubility of PCE increased to about 50 folds of the solubility in pure water, from 216 mg/L to 10520 mg/L. The highest PCE solubility is obtained for 5 % Tween 80 with 23065 mg/L which is more than 100 folds of water solubility. These results are consistent with enhanced solubility values of PCE with Tween 80 obtained by Taylor et al (2004) which are included in the graph for comparison purposes.

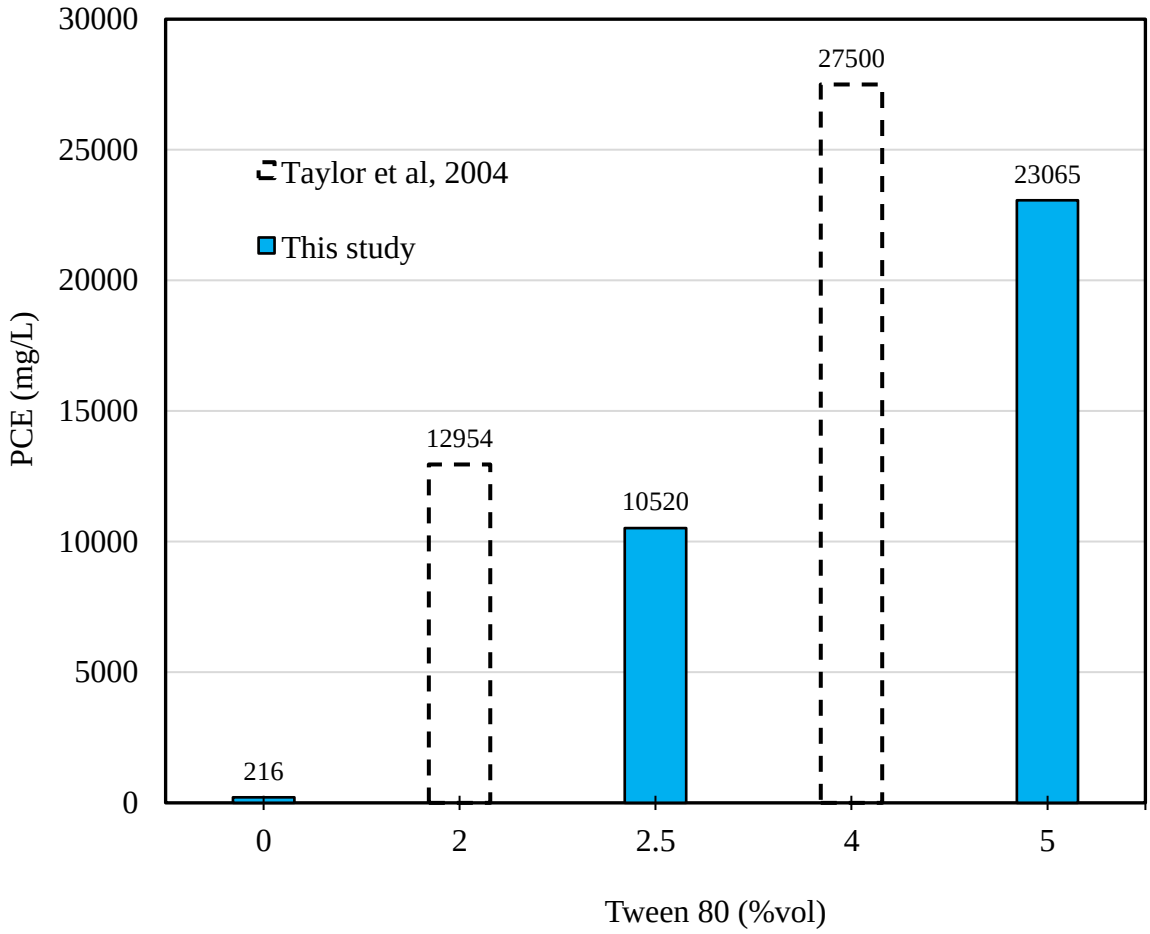

Figure 4.6. Solubility of PCE with Tween 80.

4.1.2. Flushing Experiments for Enhanced PCE Dissolution

PCE enhanced dissolution experiments were performed using Flow-cell #1. The properties of the flow-cell and porous media in which the experiments are carried out are given in chapter 3, section 3.4.1 and briefly summarized here. A total of 8 experiments were performed, 4 of which were in silica sand and 4 in calcareous soil. DNAPL PCE (0.25 mL) was injected through the top injection port. The injection needle was driven into the flow-cell down to the top of lower-K zone, creating a point injection source (Figure 4.7 and 4.8). The DNAPL was injected at a rate of 1 mL/min and allowed to naturally distribute within the porous media for a period of 48 h prior to the initiation of reagent or water flushing. The experimental conditions and agents used are listed in Table 4.1.

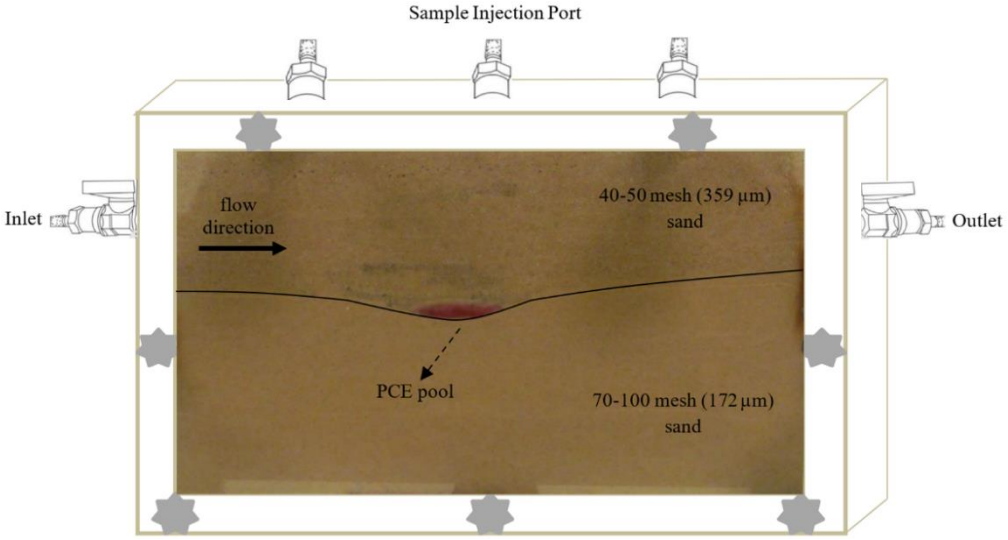

Figure 4.7. Flow-cell configuration composed of 40/50 mesh sand and 70/100 mesh sand bottom used for surfactant-enhanced PCE flushing.

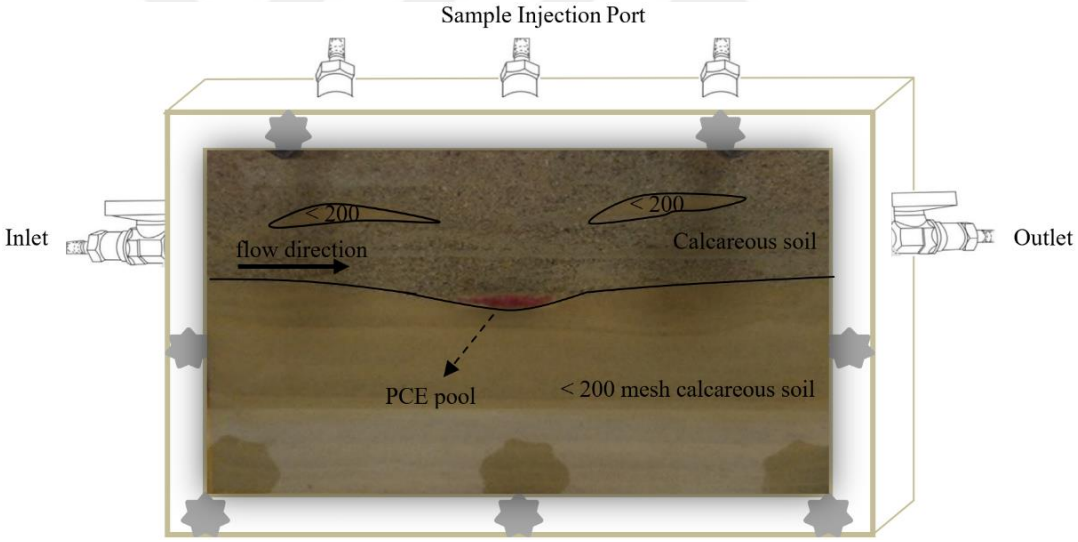

Figure 4.8. Flow-cell configuration composed of calcareous soil and <200 mesh soil bottom used for surfactant-enhanced PCE flushing.

Table 4.1. Parameters for the PCE enhanced solubilization flow-cell experiments.

Silica sand flow-cell experiments	Velocity (cm/h)	Flushing solution	PCE initial saturation * (%)	PCE Recovery (%)
1	10.1	5 % Tween 80	0.04	97.1
2	10.1	5 % SDS	0.04	99.5
3	10.1	5 % MCD	0.04	98.7
4	10.1	water	0.04	73.8
Calcareous soil flow-cell experiments	Velocity (cm/h)	Flushing solution	PCE initial saturation * (%)	PCE Recovery (%)
1	9.9	5 % Tween 80	0.04	97.5
2	9.9	5 % SDS	0.04	98.2
3	9.9	5 % MCD	0.04	98.9
4	9.9	water	0.04	62.7

* defined as the volume of organic liquid divided by the pore volume of the entire system

The PCE elution curves obtained from the first set of flushing experiments in silica sand is presented in Figure 4.9. As expected, the effluent concentrations are higher than the water solubility of PCE (~206 mg/L) in the presence of enhanced solubilization agents for both configurations. The highest effluent concentration (271 mg/L) was observed with Tween 80, dropping below 1 mg/L after about 14 pore volumes (PV). PCE peak concentration with SDS and MCD reached 239 mg/L and 223 mg/L, respectively. In addition, Tween 80 reached the highest value at 2 PVs, followed by SDS with 2.5 PVs and MCD with 2.6 PVs. MCD and SDS have longer flushing times than Tween 80. The control water flushing reached a value lower than the PCE aqueous solubility (~206 mg/L) due to rate-limited mass transfer from the DNAPL to the aqueous phase and dilution effects resulting from some of the injected water bypassing the DNAPL (Nambi and Powers, 2000; Brusseau et al, 2002; Agaoglu et al, 2015).

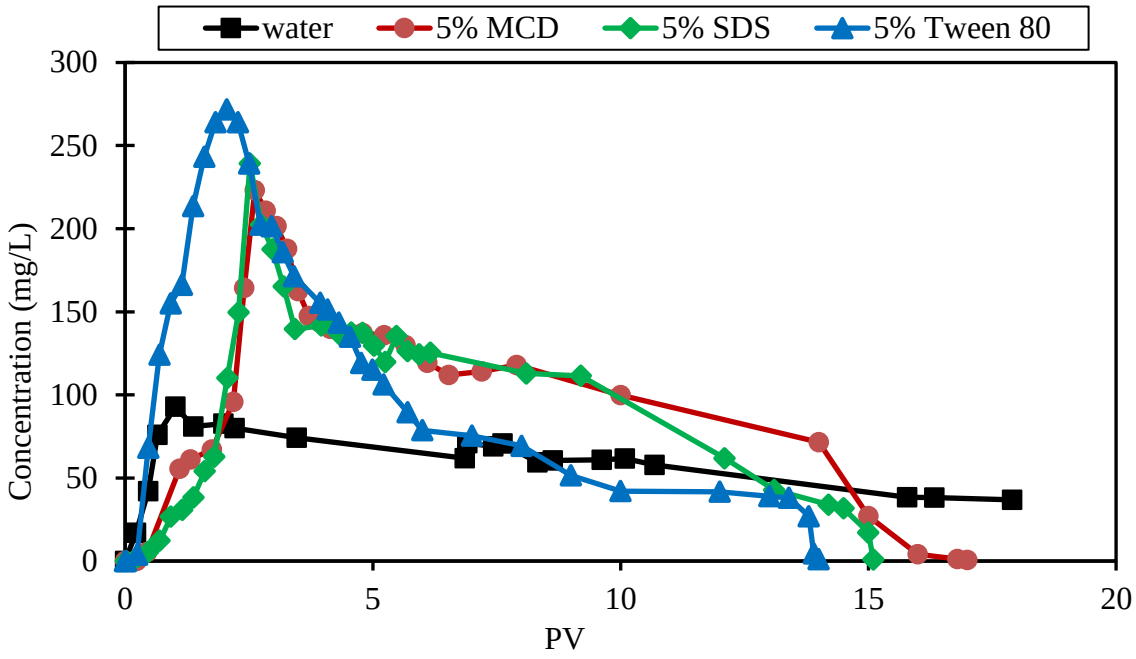

(a)

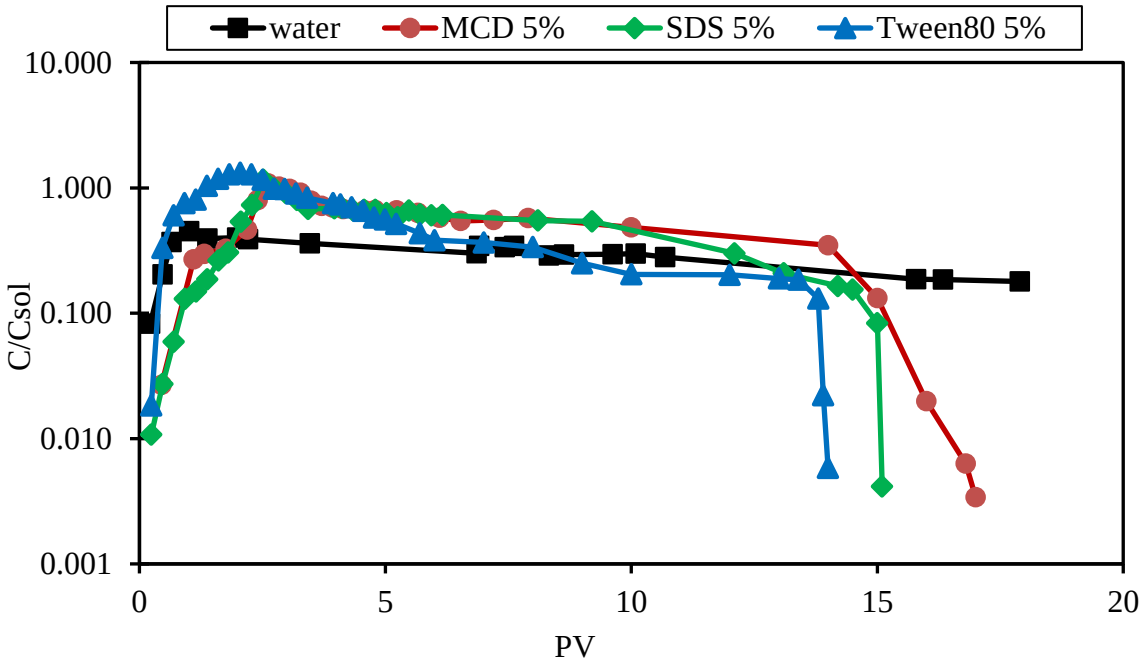

(b)

Figure 4.9. a) PCE effluent concentration as a function of pore volumes in silica sand (1 PV= 2.38 hours), b) PCE effluent concentrations expressed as C/C_{sol} which can be viewed as an enhancement factor, on a log scale in silica sand.

Figure 4.10 shows the results of the second set of experiments conducted with calcareous soil. The highest PCE effluent concentration (233 mg/L) were obtained with Tween 80, dropping below 1 mg/L after about 16 PVs. PCE peak concentration with SDS and MCD reached 182 mg/L and 187 mg/L, respectively. In addition, Tween 80 reached the highest value at 2.2 PVs, followed by SDS with 2.52 PVs and MCD with 2.9 PVs. MCD and SDS have longer flushing times than Tween 80 in natural soil. Finally with water flushing, the PCE value reached a maximum 76 mg/L and decreased to 40-50 mg/L followed by a near steady concentration for almost 25 PVs.

In both set of experiments, flushing with 5 % Tween 80 solutions resulted in the shortest flushing time followed by 5 % SDS and then 5 % MCD. The flushing times with pure water were substantially longer than all other flushing agents (43 PVs). Overall, the performance of agents on PCE source zone remediation was found to be in the following order: Tween 80> SDS> MCD>>Water. Remediation performance order of such agents was also observed for TCE as noted by other researchers (Boving and Brusseau, 2000; Tick and Rincon, 2009; Kilavuz and Akyol, 2018).

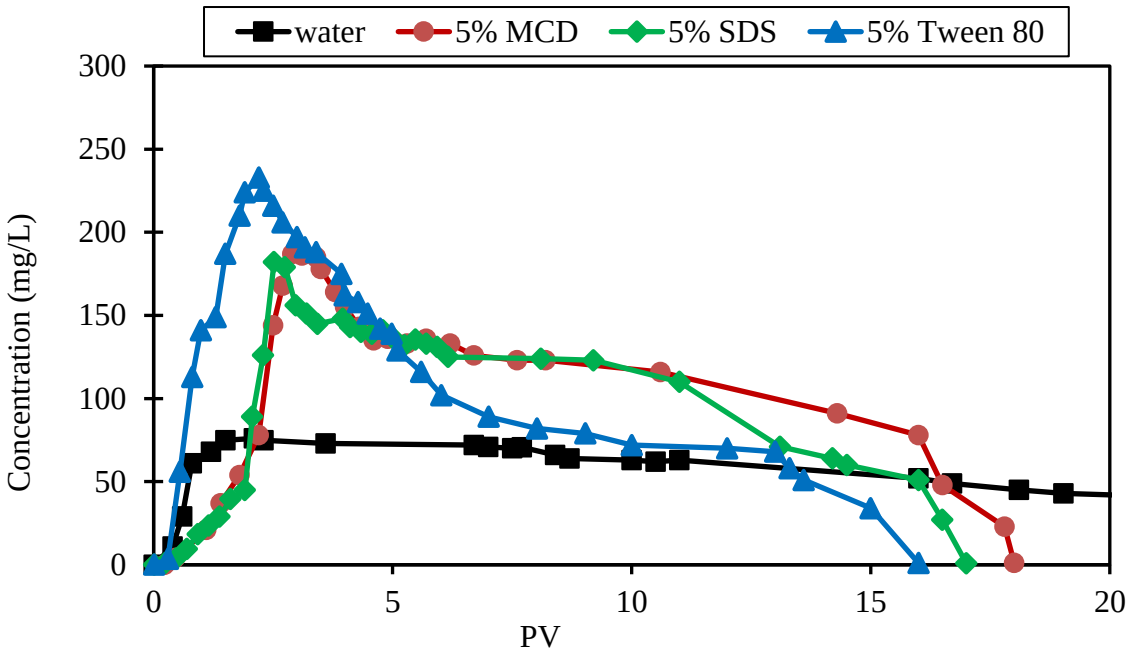

(a)

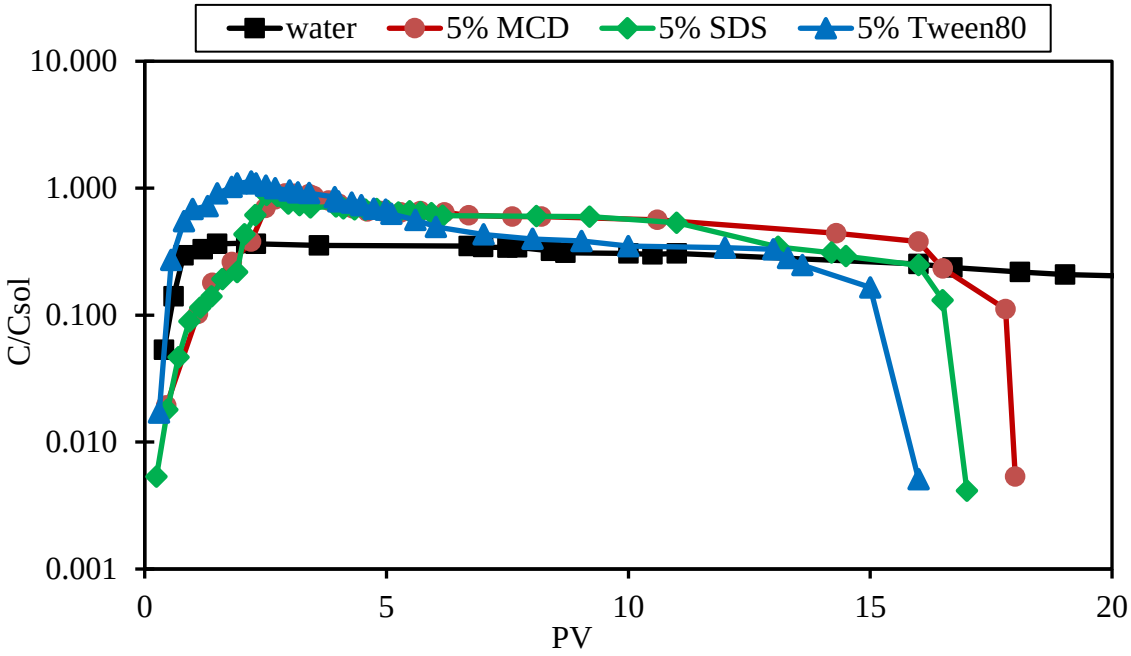

(b)

Figure 4.10. a) PCE effluent concentration as a function of pore volumes in calcareous soil (1 PV= 2.44 hours), b) PCE effluent concentrations expressed as C/C_{sol} which can be viewed as an enhancement factor on a log scale in calcareous soil.

All experiments for both porous media showed that the elution curves were characterized by an extended multi-step behavior. The elution curves of the enhanced-dissolution experiments exhibited relatively extensive periods wherein the concentrations increased to highest value and decreased gradually before reaching long steady-state effluent concentrations. This was followed by rapid decrease in concentration towards the end of the experiment. The duration of the steady-state stages after peak concentrations varied with type of porous media and the flushing solution content. The multi-step elution behavior is attributed to the presence of less-hydraulically accessible pool-dominated source zones where PCE can be trapped.

The experiments also showed the predominant effect of pool dominated PCE source zones for both physical configurations, which suggests that the injected contaminant mass remaining in the system is associated with the pool regions (Figures 4.7 and 4.8). This behavior is also consistent with that observed in previous dissolution studies using homogeneous as well as heterogeneous porous media (Russo et al, 2009; Mahal et al, 2010; DiFilippo et al, 2010; Akyol et al, 2013; Akyol, 2018; Akyol and Turkkan, 2018). It is hypothesized that the pore-scale spatial distribution of the organic liquid, type of enhanced-solubilization agent and the flow profile configuration are quite complex for the silica sand and natural soil which leads to the observed non-ideal dissolution behavior. As a consequence, the performance of technology depends on the site-specific properties which are critical to characterize effective DNAPL remediation strategies for contaminated sites.

4.1.2.1. Mass Flux Reduction/Mass Removal Relation

Figure 4.11 shows the experimental data expressed in terms of PCE mass flux removal versus the fraction of DNAPL remaining (MFR-MR). We note that the endpoints of the water flushing experiments are further away from the upper right corner of the graph because of the early termination of the experiment before complete recovery of the DNAPL is achieved (DiFilippo and Brusseau, 2008).

The results indicate that the MFR-MR relationship for all solubilizing agents and water flushing experiments exhibited partial multi-step behavior. In the first stage, significant reductions in PCE mass flux occurred (Figure 4.11). Subsequently, the MFR-MR curve was linear until the end of the experiment when a sharp decrease in the flux is observed. The initial stage of each solubilizing agent or water flooding for both physical media configuration is attributed to the removal of PCE mass from the more hydraulically accessible zones, while the latter stages of the MFR-MR curve is associated with the removal of poorly-accessible PCE mass from pool-dominated zones and/or

entrapped within low hydraulic conductivity lens and at the top of impermeable zone along the bottom of the flow-cell. This non-ideal behavior is directly related to the contaminant elution curves (Figure 4.9, 4.10), wherein concentrations increased to a maximum level before decreasing gradually until reaching steady-state concentration for the majority of SDS and Tween 80 flooding, ending finally with a sharp decrease in effluent flux. The MFR-MR exhibited greater non-ideality for the natural calcareous soil compared to the silica sand configuration for both water and solubilizing agent flushing.

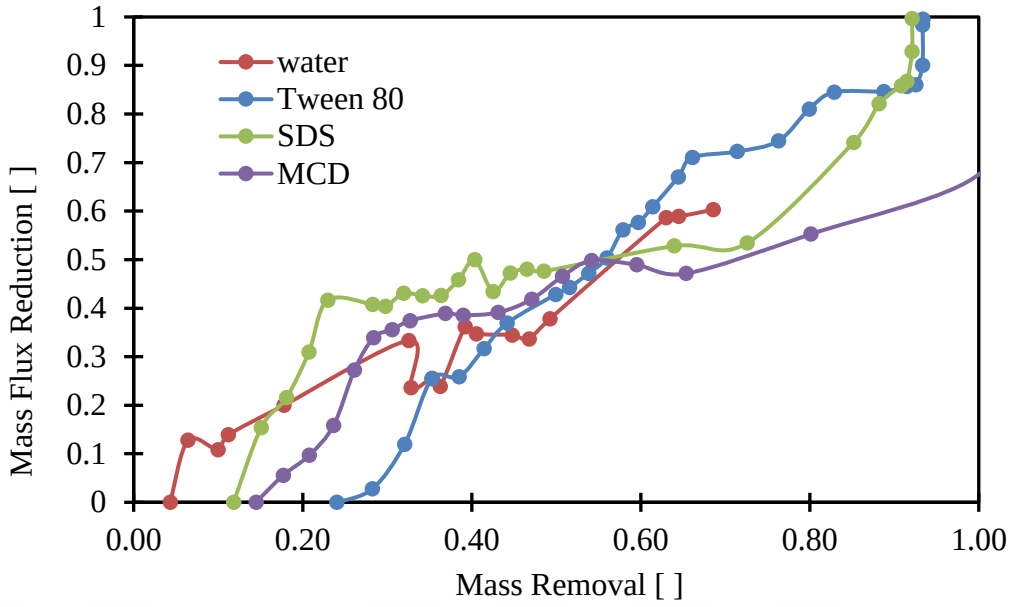

(a)

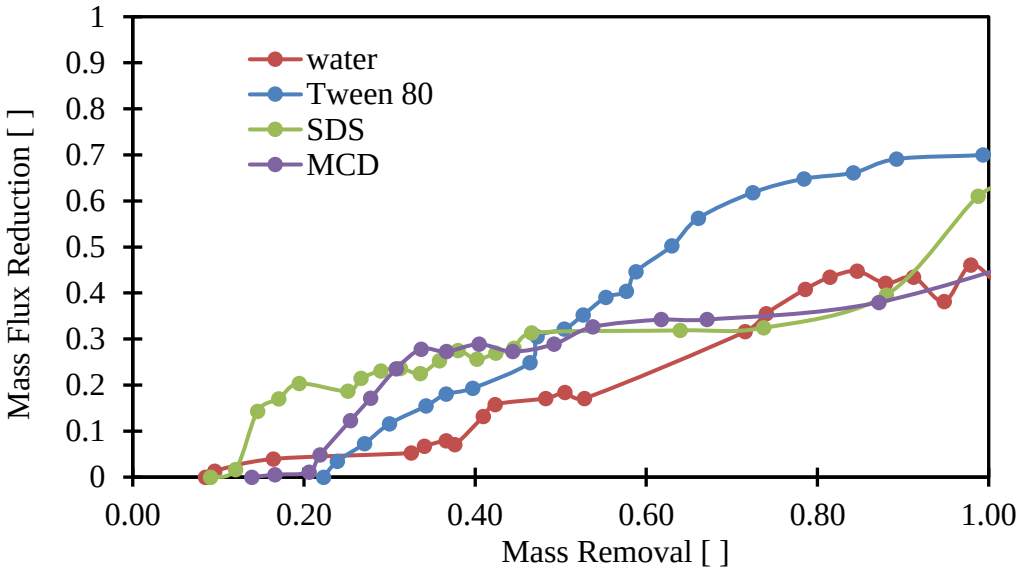

(b)

Figure 4.11. PCE mass-flux reduction versus mass removal behavior for the (i) water, (ii) Tween 80, (iii) SDS and (iv) MCD enhanced solubilization flushing experiments for a) silica sand and b) natural soil.

4.1.3. Multiphase Flow Modeling

To further assess enhanced-dissolution of DNAPL with different agents, the experiments were also simulated using the multiphase flow model, UTCHEM. The model was specifically used to evaluate the sensitivity of different input parameters (sensitivity analysis) and simulate the enhanced dissolution of PCE with different agents. The multiphase model results were also compared to a simplified emprically based model described in section 4.1.4.

The model domain covering the entire flow-cell area was discretisized into 30 by 48 uniform gridblocks. The dimensions of these gridblocks were 0.5 cm by 0.5 cm. The PCE solubility in water was taken as 0.206 g/L (Horvath et al, 1999; Yalkowsky et al, 2016). The agent-enhanced DNAPL solubility was determined using Hand's equation (Hand, 1930). Hand's rule assumes that equilibrium phase concentration ratios are straight lines on a log-log scale. The values of the Hand rule parameters were determined such that the solubility in the model is equal to the agent-enhanced solubilities. CMC values used in the model are based on batch experiments and literature values. For the water flushing equation, the NAPL-water interfacial tension was assumed to be 45 mN/m. The initial DNAPL distribution was defined based on the images taken prior to flushing and the known injected DNAPL volume. The spatial distribution was slightly adjusted as part of the model calibration. The porous media dispersivity was determined from the breakthrough curve of conservative tracer test. The key input parameters are given in Table 4.2.

Table 4.2. List of key parameters used in the model simulations.

Porosity		
	Silica sand	flow zone: 0.36 (d_{50} = 359 μm) impermeable zone: 0.38 (d_{50} = 172 μm)
	Natural soil	flow zone: 0.58 (d_{50} = 150 μm) impermeable zone: 0.38 (d_{50} < 76 μm)
Intrinsic permeability		
	Silica sand	flow zone: 20 darcy impermeable zone: 0.02 darcy
	Natural soil	flow zone: 20 darcy impermeable zone: 0.02 darcy
Longitudinal dispersivity		
	Silica sand	0.02 m[a]
	Natural soil	0.04 m[a]
PCE solubility		
	Pure water	0.206[b] g/L
	Tween 80 (5 %)	23[c] g/L
	SDS (5%)	32.88[c] g/L
	MCD (5%)	3.73[c] g/L
PCE aqueous phase interfacial tension		
		45 mN/m
Critical Micelle Concentration (CMC)		
	Tween 80	0.035[d] g/L
	SDS	2.1[e] g/L

a Longitudinal dispersivity determined from tracer test; b Horvath et al, 1999; c Enhanced solubility values determined from batch experiments; d Zhong et al, 2003; e Boving and Brusseau, 2000

4.1.3.1. Sensitivity Analysis

To numerically evaluate the impact of the various input parameters on DNAPL dissolution and the corresponding time-dependent effluent concentration, the multiphase flow model was used to calculate sensitivity coefficients. Sensitivity coefficients were computed by varying the input parameters one at a time and assessing the impact on effluent concentration. Sensitivity coefficients can aid in the calibration of the numerical model based on the conducted flushing experiments. It is important to note that sensitivity coefficients are dependent upon the base case simulation (e.g., Ambas and Baltas, 2012). As such, the base case problem is constructed to resemble the flushing experiments conducted in this study. The key input parameters used for the base case simulation were all mentioned in the previous chapter, section 3.8.2. The correlation between the sensitivity coefficients is an indicator of the uniqueness of the calibration process. If the correlation of the sensitivity coefficients of two parameters are close to ± 1, then this indicates that these two parameters can not be uniquely determined (Geza et al, 2010). The sensitivity coefficients are calculated for selected input parameters relating to the flow, DNAPL properties and distribution, and porous media properties: (i) flushing flow rate, (ii) DNAPL solubility, (iii) transversal dispersivity, (iv) saturation, (v) interphase mass transfer coefficient, (vi) longitudinal dispersivity. Sensitivity analysis was conducted for the two porous media; silica sand and calcareous soil. The partial sensitivity analysis

was applied to the base case by changing values in one direction. An increase in flow rate provides us to assess the potential mobilization risk. An increase in solubility or mass transfer coefficient is directly related to the surfactant or cyclodextrin concentrations. Further analysis could consider decrease and increase in parameter values as well as different magnitudes of parameter change.

Figures from 4.12 to 4.23 compare the effluent concentration for each sensitivity simulations to the base case simulation. For each sensitivity simulation, an input parameter was doubled from the base case values. As obtained from the best-fit model, the peak concentrations for all these simulations correspond to about 1-2 PV when both the high and less saturated zones of DNAPL are dissolving into the Tween 80, SDS, MCD flushing and water flood. For water flood, this is followed by concentration tailing period, corresponding to the slower kinetic dissolution from the DNAPL rich core zone. The corresponding sensitivity coefficients for these simulations are shown in Figure from 4.12 to 4.23. The impact of each input parameter is discussed below.

Increasing the Flow Rate (Q)

For all types of flushing agent simulations, increasing the flow rate decreases the contact time between the DNAPL and the flushing solution. This leads to a decrease in the mass transfer into the aqueous phase, reduced effluent concentration and a negative sensitivity coefficient. For water flooding (Figure 4.12.a, 4.13.a); the impact is greater for the first 10 PVs when the whole DNAPL mass is dissolving; for PVs greater than 10, only the highly saturated core DNAPL zone remains. However, for the surfactants and cyclodextrin flushings; the impact is greater usually for the first 3-4 PVs followed by a multistep dissolution of remaining DNAPL

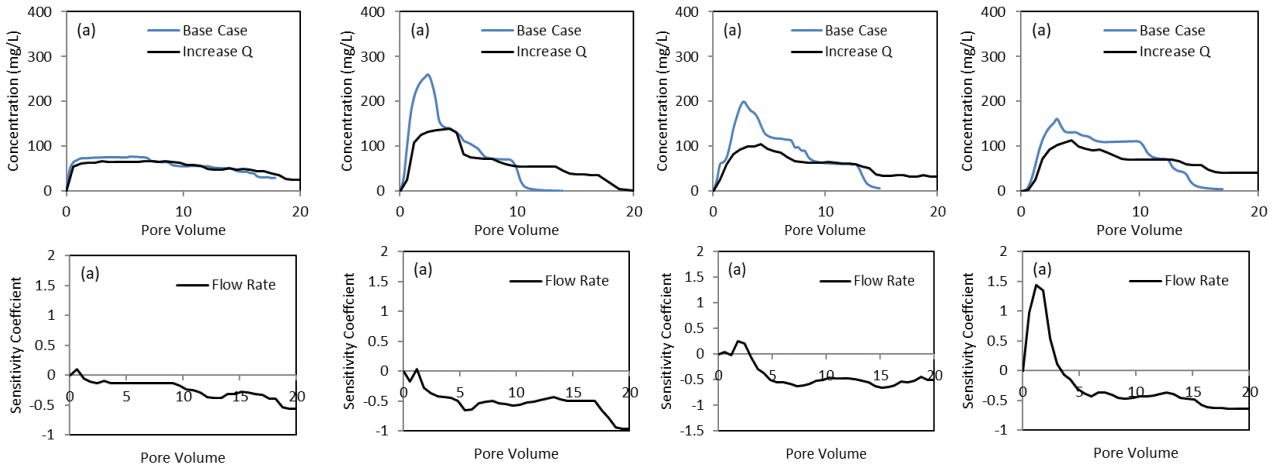

(a) (b) (c) (d)

Figure 4.12. Effluent concentration for the base case simulation and sensitivity simulations corresponding to the doubling of flushing flow rate (Q) and sensitivity coefficients for a) water, b) Tween 80, c) SDS and d) MCD flushing in silica sand.

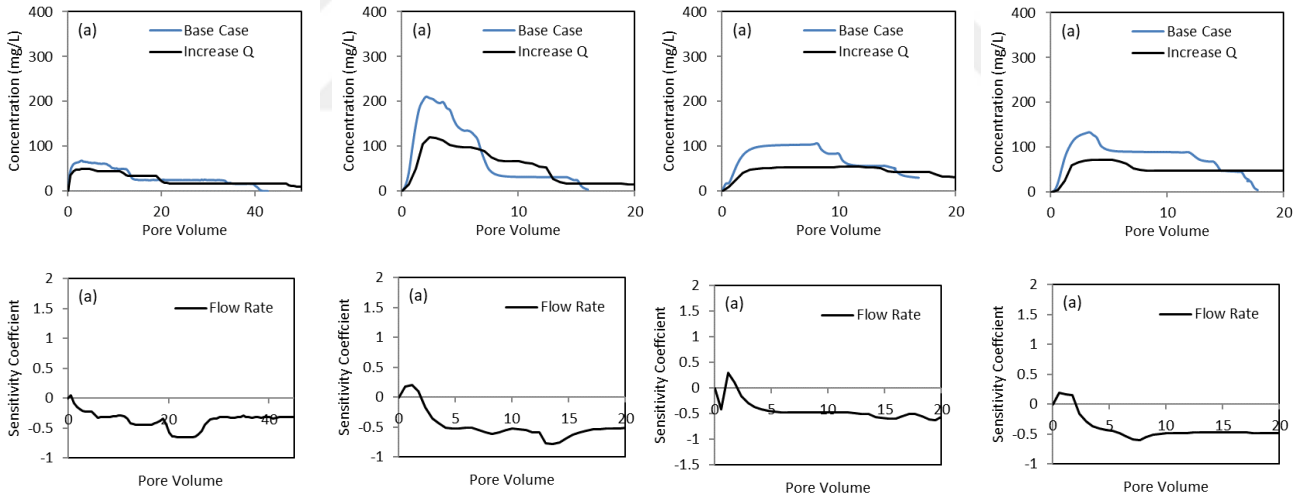

(a) (b) (c) (d)

Figure 4.13. Effluent concentration for the base case simulation and sensitivity simulations corresponding to the doubling of flushing flow rate (Q) and sensitivity coefficients for a) water, b) Tween 80, c) SDS and d) MCD flushing in natural soil.

Increasing the Solubility

When the DNAPL aqueous phase solubility is increased, the effluent concentration increases due to the larger concentration difference in the mass transfer expression (Eq. (3.9)). This is seen through the first 8-9 PVs of the water flooding simulation. The increase in effluent concentration when the solubility is increased corresponds to a positive sensitivity coefficient. Through the end of simulation that corresponds to negative sensitivity coefficient, the effluent concentrations decreased and reached zero which means that nearly all DNAPL mass was transferred to aqueous phase.

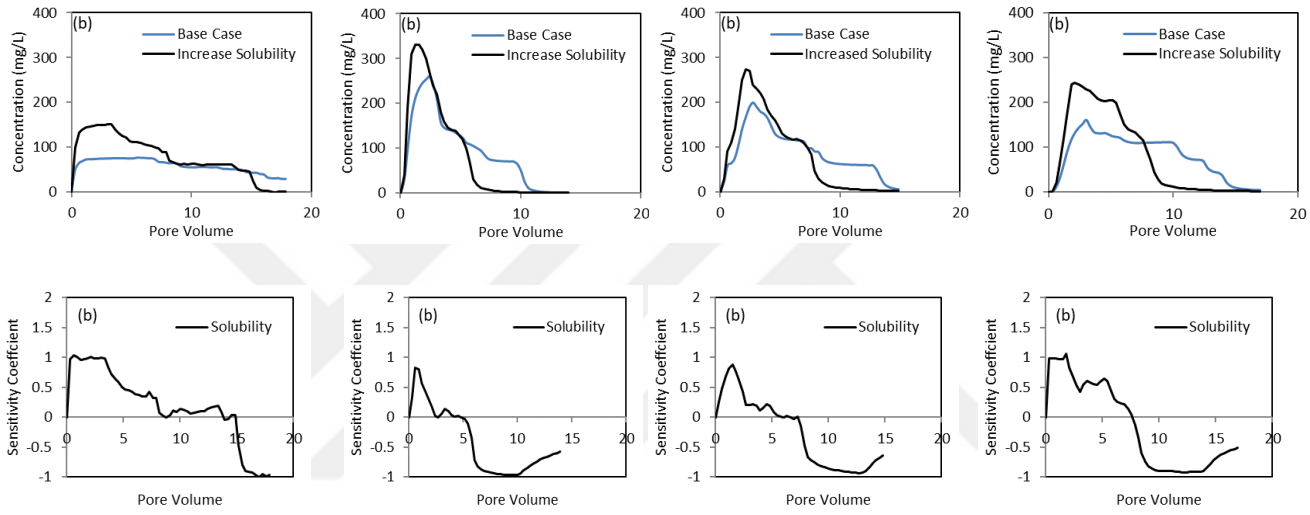

(a) (b) (c) (d)

Figure 4.14. Effluent concentration for the base case simulation and sensitivity simulations corresponding to the doubling the NAPL solubility and sensitivity coefficients for a) water, b) Tween 80, c) SDS and d) MCD flushing in silica sand.

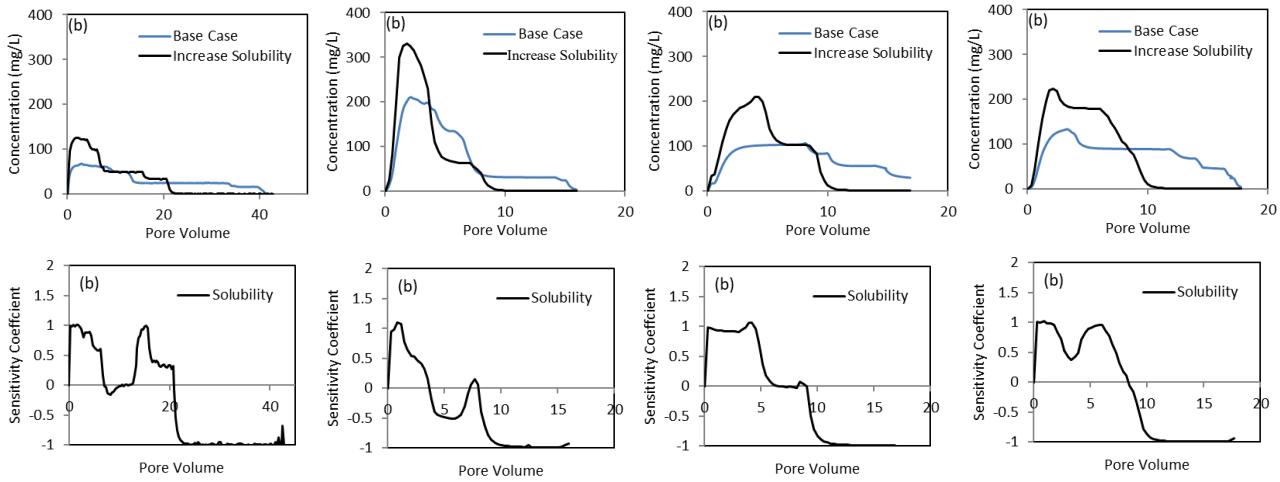

(a) (b) (c) (d)

Figure 4.15. Effluent concentration for the base case simulation and sensitivity simulations corresponding to the doubling the NAPL solubility and sensitivity coefficients for a) water, b) Tween 80, c) SDS and d) MCD flushing in natural soil.

Increasing the Transversal Dispersivity

The transversal dispersion is an important parameter that can enhance DNAPL dissolution because it provides a mechanism for transporting the dissolved DNAPL away from the DNAPL surface. This leads to greater concentration gradients at the DNAPL-flushing solution interface which induces more dissolution (Eq. (3.9)). The corresponding sensitivity coefficients are near zero and negative at later times.

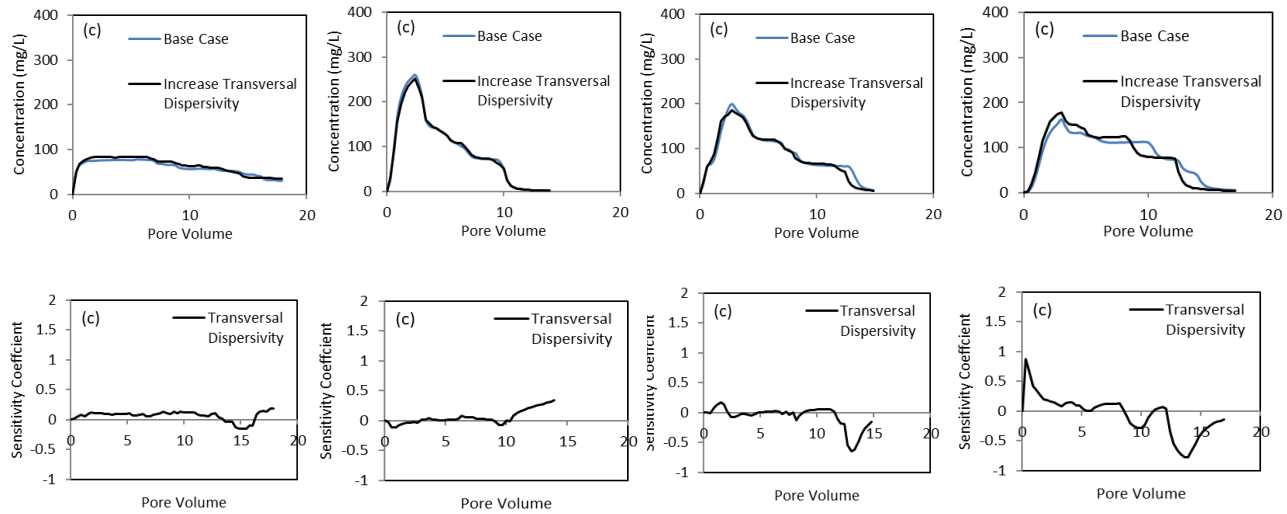

(a) (b) (c) (d)

Figure 4.16. Effluent concentration for the base case simulation and sensitivity simulations corresponding to the doubling the transversal dispersivity and sensitivity coefficients for a) water, b) Tween 80, c) SDS and d) MCD flushing in silica sand.

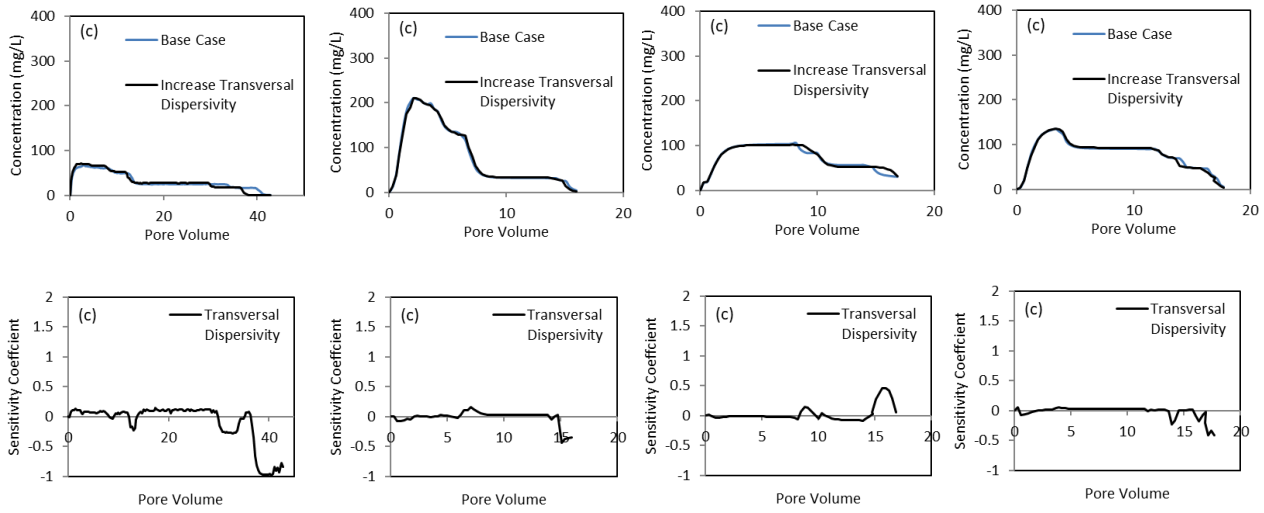

(a) (b) (c) (d)

Figure 4.17. Effluent concentration for the base case simulation and sensitivity simulations corresponding to the doubling the transversal dispersivity and sensitivity coefficients for a) water, b) Tween 80, c) SDS and d) MCD flushing in natural soil.

Increasing the NAPL Saturation

For all sets of experiments, increasing the saturation increases both the amount of NAPL per unit volume (especially of the NAPL-rich core) and the contact between the DNAPL and flushing solution which prevents the ready solubilization of NAPL at early times and results in concentration increase at later times. As a result, the saturation sensitivity coefficient is negative at early times and becomes positive at later times.

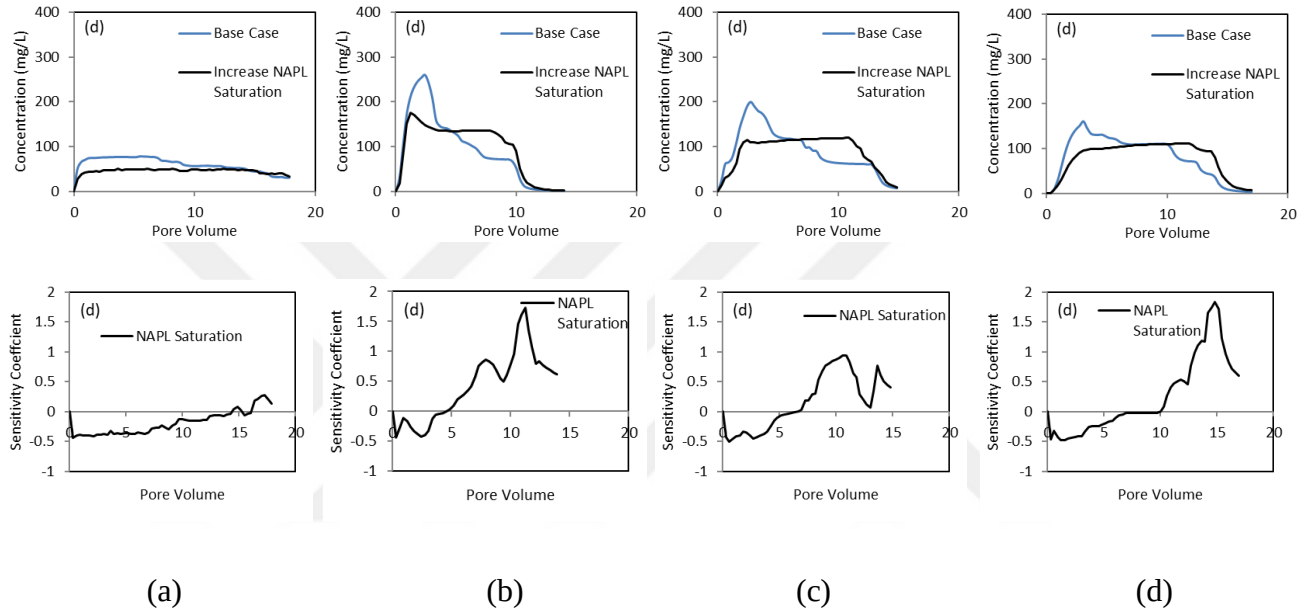

(a) (b) (c) (d)

Figure 4.18. Effluent concentration for the base case simulation and sensitivity simulations corresponding to the doubling the NAPL saturation and sensitivity coefficients for a) water, b) Tween 80, c) SDS and d) MCD flushing in silica sand.

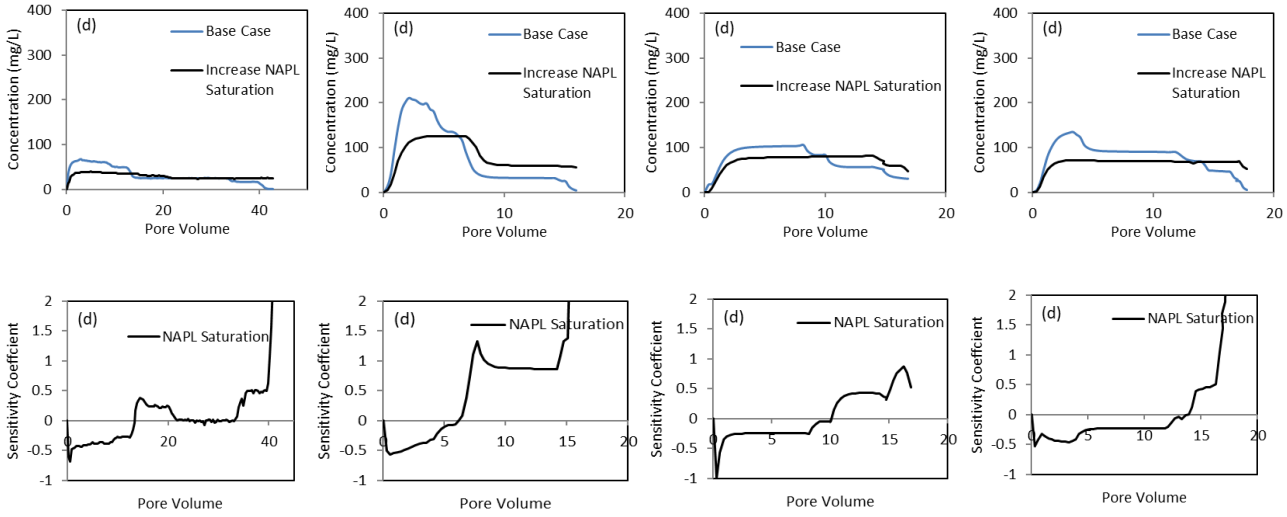

(a) (b) (c) (d)

Figure 4.19. Effluent concentration for the base case simulation and sensitivity simulations corresponding to the doubling the NAPL saturation and sensitivity coefficients for a) water, b) Tween 80, c) SDS and d) MCD flushing in natural soil.

Mass Transfer Coefficient (CNEM)

Increasing the mass transfer coefficient, K_l, leads to an increase in the effluent concentration at early times. The higher dissolution rate of the DNAPL means that the readily transferred DNAPL is completely dissolved at an earlier time, and that in turn leads to decreased effluent concentrations. At later times (especially after 5 PV), the effluent concentrations corresponding to the sensitivity simulation is lower. The corresponding sensitivity coefficient are positive at early times and negative through the later times.

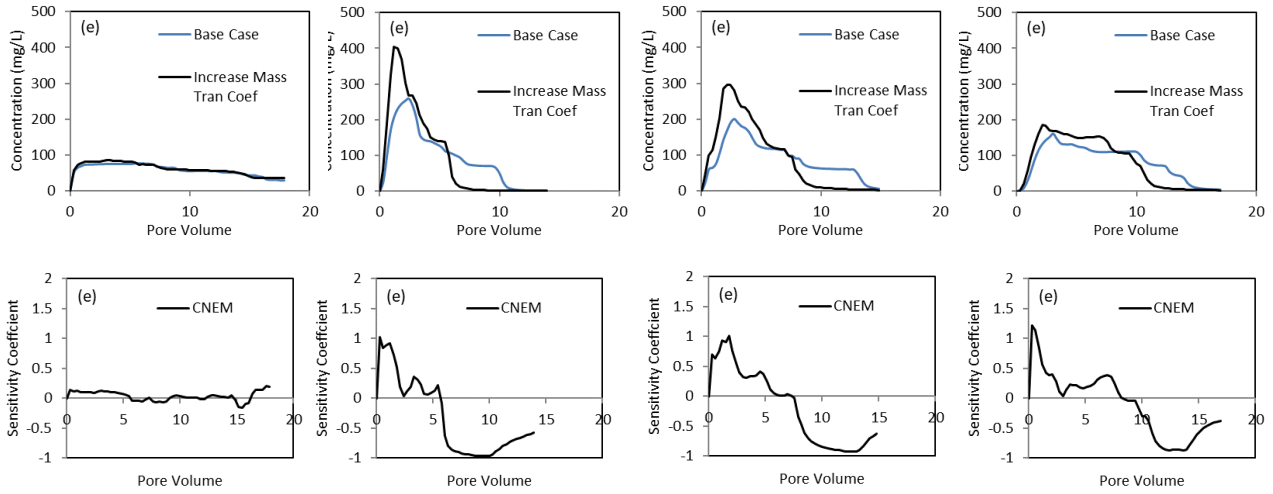

(a) (b) (c) (d)

Figure 4.20. Effluent concentration for the base case simulation and sensitivity simulations corresponding to the doubling the mass transfer coefficient and sensitivity coefficients for a) water, b) Tween 80, c) SDS and d) MCD flushing in silica sand.

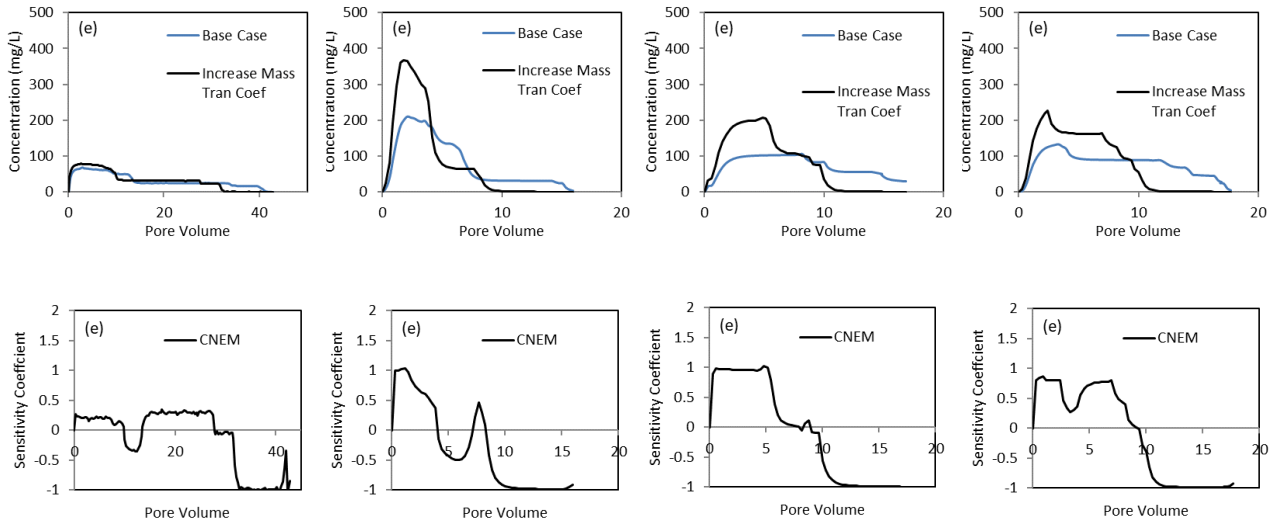

(a) (b) (c) (d)

Figure 4.21. Effluent concentration for the base case simulation and sensitivity simulations corresponding to the doubling the mass transfer coefficient and sensitivity coefficients for a) water, b) Tween 80, c) SDS and d) MCD flushing in natural soil.

Increasing the Longitudinal Dispersivity

Increasing the longitudinal dispersivity does not have a significant impact on concentration change. The longitudinal dispersivity has the most effect at early times at the leading edge of the plume and at late times at the tale of the plume. However, for most of the time, the longitudinal dispersivity has a small effect.

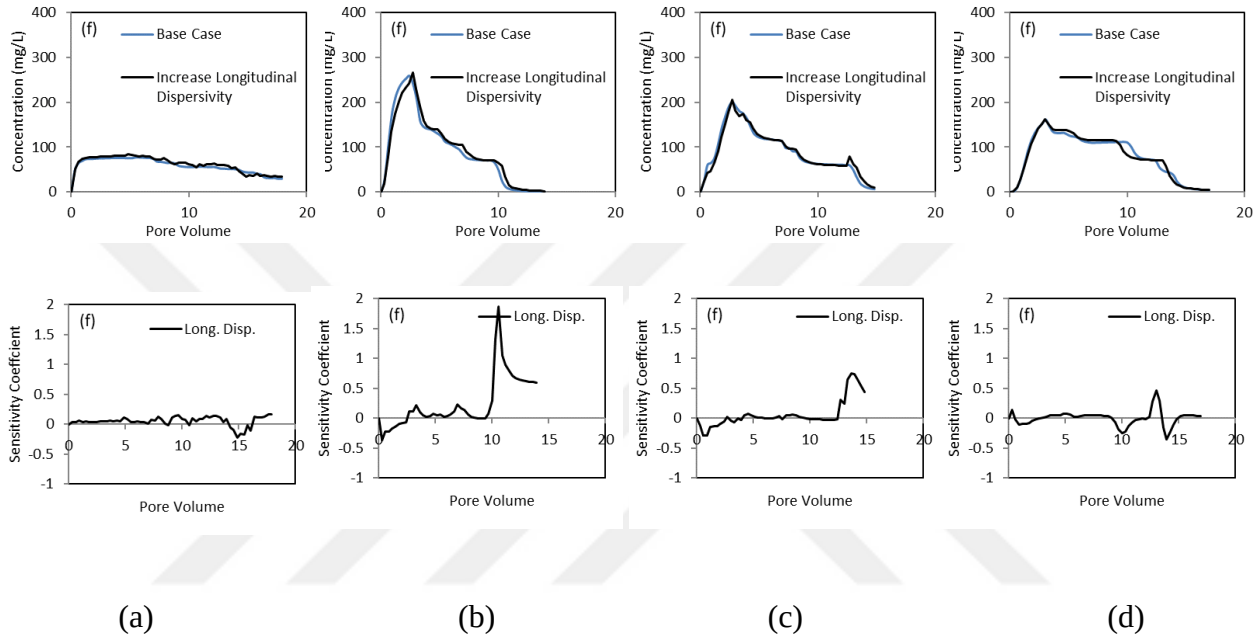

(a) (b) (c) (d)

Figure 4.22. Effluent concentration for the base case simulation and sensitivity simulations corresponding to the doubling the longitudinal dispersivity and sensitivity coefficients for a) water, b) Tween 80, c) SDS and d) MCD flushing in silica sand.

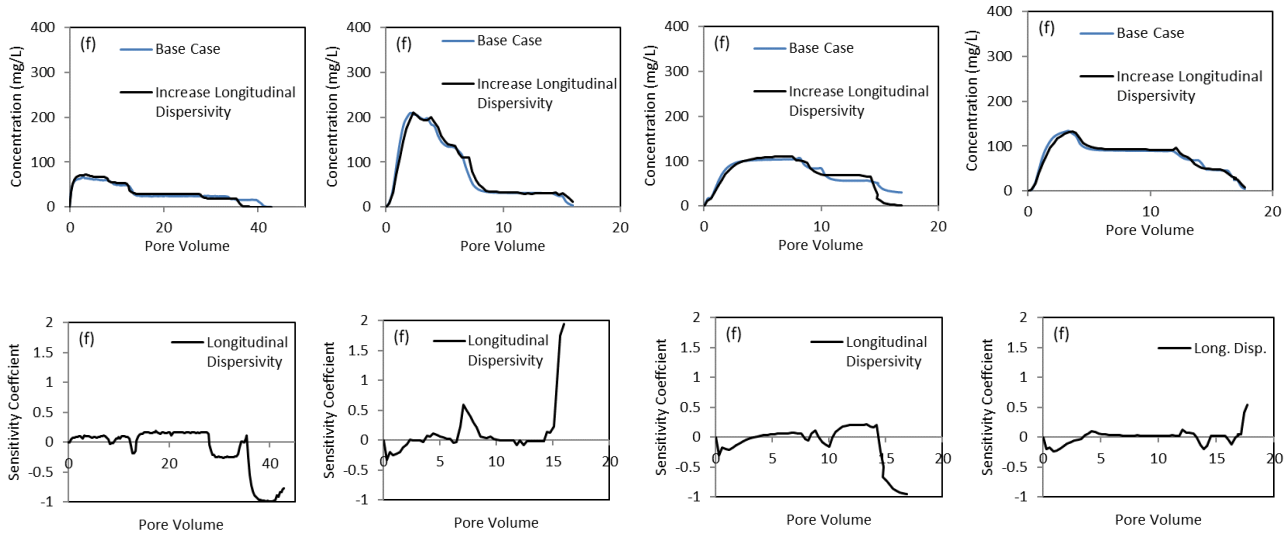

(a) (b) (c) (d)

Figure 4.23. Effluent concentration for the base case simulation and sensitivity simulations corresponding to the doubling the longitudinal dispersivity and sensitivity coefficients for a) water, b) Tween 80, c) SDS and d) MCD flushing in natural soil.

Table 4.3 to 4.10 show the time-averaged of the absolute value of the sensitivity coefficients normalized by the time-averaged sensitivity coefficient of the highest sensitivity value in these simulations. The effluent concentrations are most sensitive to DNAPL solubility and saturation for water flushing. On the other hand, the effluent concentrations with surfactant simulations are most sensitive to the interphase mass transfer coefficient and flow rate for the silica sand. For the heterogeneous case, the sensitivity of effluent concentrations with surfactants is highest for mass transfer coefficient and saturation. This is mostly followed by solubility and flow rate especially for the surfactant flushing. In general sensitivities corresponding to heterogeneous media exhibits more complexity.

Although the flushing solution flow rate and DNAPL solubility have relatively high sensitivity coefficients, they were not defined as calibration parameters because they are known with relatively high levels of confidence. The dispersivity values have less impact. The longitudinal value was determined from previous tracer tests. Estimate of the longitudinal dispersivity derived from the tracer test serves as an upper limit to the transverse dispersivity. The transverse value is reported in the literature to be a factor of about 2-10 less than the longitudinal dispersivity (Gelhar, 1993).

Table 4.3 to 4.10 also gives the correlations between the different parameters. Correlations close to one indicate that the parameters cannot be determined uniquely (for example the mass transfer coefficient through the NAPL zone and the solubility which both have similar positive sensitivity coefficients at early PVs and negative sensitivity coefficients at late PVs). The correlations between three calibration parameters (1. The mass transfer coefficient (CNEM), 2. Initial DNAPL saturation, 3. Transversal dispersivity) ranged from 0.33 to 0.97 for simulations in silica sand which indicates that non-uniqueness of the calibration is moderate (Geza et al, 2010) and 0.17 to 0.95 for simulations in natural soil which indicates that non-uniqueness of the calibration is poor to moderate.

Table 4.3. Normalized time-averaged of the absolute sensitivity coefficients and correlations between different parameters for water flushing experiments in silica sand.

	Q	Solubility	Transversal Dispersivity	Saturation	CNEM	Longitudinal Dispersivity
Normalized time-averaged *SC*	**0.77**	**1.00**	**0.20**	**0.48**	**0.14**	**0.17**
Correlations						
Flushing flow rate	1.00	0.94	0.87	0.34	0.92	0.85
DNAPL solubility		1.00	0.89	0.38	0.95	0.88
Transversal dispersivity			1.00	0.63	0.97	0.99
Saturation				1.00	0.59	0.66
Interphase mass transfer coefficient					1.00	0.96
Longitudinal dispersivity						1.00

Table 4.4. Normalized time-averaged of the absolute sensitivity coefficients and correlations between different parameters for Tween 80 flushing experiments in silica sand.

	Q	Solubility	Transversal Dispersivity	Saturation	CNEM	Longitudinal Dispersivity
Normalized time-averaged *SC*	**0.99**	**0.91**	**0.14**	**0.89**	**1.00**	**0.50**
Correlations						
Flushing flow rate	1.00	0.93	0.92	0.77	0.92	0.87
DNAPL solubility		1.00	0.88	0.61	1.00	0.84
Transversal dispersivity			1.00	0.86	0.88	0.99
Saturation				1.00	0.62	0.85
Interphase mass transfer coefficient					1.00	0.84
Longitudinal dispersivity						1.00

Table 4.5. Normalized time-averaged of the absolute sensitivity coefficients and correlations between different parameters for SDS flushing experiments in silica sand.

	Q	Solubility	Transversal Dispersivity	Saturation	CNEM	Longitudinal Dispersivity
Normalized time-averaged *SC*	**1.00**	**0.92**	**0.19**	**0.70**	**0.99**	**0.23**
Correlations						
Flushing flow rate	1.00	0.91	0.88	0.42	0.91	0.75
DNAPL solubility		1.00	0.91	0.32	1.00	0.85
Transversal dispersivity			1.00	0.66	0.92	0.95
Saturation				1.00	0.33	0.67
Interphase mass transfer coefficient					1.00	0.86
Longitudinal dispersivity						1.00

Table 4.6. Normalized time-averaged of the absolute sensitivity coefficients and correlations between different parameters for MCD flushing experiments in silica sand.

	Q	Solubility	Transversal Dispersivity	Saturation	CNEM	Longitudinal Dispersivity
Normalized time-averaged *SC*	**0.99**	**1.00**	**0.36**	**0.71**	**0.65**	**0.12**
Correlations						
Flushing flow rate	1.00	0.92	0.87	0.32	0.94	0.78
DNAPL solubility		1.00	0.86	0.30	0.91	0.79
Transversal dispersivity			1.00	0.64	0.95	0.96
Saturation				1.00	0.51	0.78
Interphase mass transfer coefficient					1.00	0.90
Longitudinal dispersivity						1.00

Table 4.7. Normalized time-averaged of the absolute sensitivity coefficients and correlations between different parameters for water flushing experiments in natural soil.

	Q	Solubility	Transversal Dispersivity	Saturation	CNEM	Longitudinal Dispersivity
Normalized time-averaged *SC*	**0.37**	**0.45**	**0.13**	**1.00**	**0.25**	**0.16**
Correlations						
Flushing flow rate	1.00	0.93	0.92	0.70	0.96	0.92
DNAPL solubility		1.00	0.87	0.75	0.87	0.87
Transversal dispersivity			1.00	0.77	0.95	0.99
Saturation				1.00	0.72	0.78
Interphase mass transfer coefficient					1.00	0.95
Longitudinal dispersivity						1.00

Table 4.8. Normalized time-averaged of the absolute sensitivity coefficients and correlations between different parameters for Tween 80 flushing experiments in natural soil.

	Q	Solubility	Transversal Dispersivity	Saturation	CNEM	Longitudinal Dispersivity
Normalized time-averaged *SC*	**0.52**	**0.66**	**0.06**	**1.00**	**0.68**	**0.17**
Correlations						
Flushing flow rate	1.00	0.94	0.90	0.56	0.93	0.85
DNAPL solubility		1.00	0.86	0.50	0.99	0.81
Transversal dispersivity			1.00	0.81	0.88	0.99
Saturation				1.00	0.53	0.86
Interphase mass transfer coefficient					1.00	0.84
Longitudinal dispersivity						1.00

Table 4.9. Normalized time-averaged of the absolute sensitivity coefficients and correlations between different parameters for SDS flushing experiments in natural soil.

	Q	Solubility	Transversal Dispersivity	Saturation	CNEM	Longitudinal Dispersivity
Normalized time-averaged *SC*	**0.76**	**0.98**	**0.10**	**0.47**	**1.00**	**0.30**
Correlations						
Flushing flow rate	1.00	0.83	0.82	0.39	0.85	0.89
DNAPL solubility		1.00	0.75	0.14	0.98	0.67
Transversal dispersivity			1.00	0.65	0.79	0.89
Saturation				1.00	0.17	0.66
Interphase mass transfer coefficient					1.00	0.70
Longitudinal dispersivity						1.00

Table 4.10. Normalized time-averaged of the absolute sensitivity coefficients and correlations between different parameters for MCD flushing experiments in natural soil.

	Q	Solubility	Transversal Dispersivity	Saturation	CNEM	Longitudinal Dispersivity
Normalized time-averaged *SC*	**0.66**	**1.00**	**0.07**	**0.72**	**0.91**	**0.10**
Correlations						
Flushing flow rate	1.00	0.77	0.90	0.31	0.81	0.84
DNAPL solubility		1.00	0.70	0.19	0.98	0.66
Transversal dispersivity			1.00	0.56	0.74	0.99
Saturation				1.00	0.22	0.61
Interphase mass transfer coefficient					1.00	0.70
Longitudinal dispersivity						1.00

4.1.3.2. Model Calibration

The enhanced DNAPL solubilization experiments were used to calibrate the UTCHEM-based multiphase flow model. The primary calibration parameter was the interphase mass transfer coefficient. Because the tracer tests provided estimates of the longitudinal dispersivity values, the transverse dispersivity was also treated as a calibration parameter. Moreover, small changes in the initial DNAPL spatial distribution were also considered to improve the calibration.

Figures 4.24 and 4.25 compare the best fit and experimental breakthrough curves as a function of pore volume for different experiments. These results correspond to a transversal dispersivity of 0.002 for silica sand and 0.004 for natural soil corresponding to dispersivity anisotropy ratio of 0.1 which is consistent with literature data (Gelhar, 1993). Aqueous phase concentrations were much lower than the effective solubilities, which justified the need for a rate-limited mass transfer process. The best-fit mass transfer coefficients, along with the corresponding modified Sh′ number, the normalized root mean square error (NRMSE) and the correlation coefficient, R^2, between the simulated and observed curves are shown in Table 4.11 and 4.12. In the calculation of the NRMSE, the square root of the mean square of the error was normalized by the maximum observed concentration of each experiment. The smaller the NRMSE, the better is the agreement between the model and experimental results. The R^2 is another measure of the agreement between the observed and simulated data, with a value of 1 meaning that the two data sets are perfectly correlated. For all

simulated silica sand experiments the NRMSE were low, ranging from 0.08 and 0.1 with R^2 values ranging from 0.81 to 0.93 indicating good agreement between the observed experimental concentrations and the best-fit model results. For simulated natural soil experiments, the NRMSE were ranging from 0.12 and 0.19 with R^2 values ranging from 0.66 to 0.91. Better agreement in silica sand experiments is attributed to the heterogeneity of the calcareous soil relative to the silica sand.

The results shown in Tables 4.11 and 4.12 indicate that the Sherwood numbers are about an order of magnitude higher for the calcareous soil compared to the silica sand (Sh′=0.0059-1.5 for sand compared to ((Sh′=0.0008-0.13 for calcareous soil). These results suggest that the mean grain diameter (dm=0.359 mm for the sand and dm=0.15 mm for the calcareous soil) and the heterogeneity of the soil, which are the main differences between the two sets of experiments can have a significant effect on the interphase mass transfer.

For the simulations with surfactants which are capable to form micelles, the best-fit mass transfer coefficients range from 3.2 to 6 day^{-1} which correspond to Sh′=0.0008-0.0089. The best-fit mass transfer coefficients for MCD ranged from 27 to 50 day^{-1} (Sh′=0.007-0.075) and 500-1000 day^{-1} (Sh′=0.13-1.5) for the water flushing experiments. This suggests that the mass transfer may be influenced by the agent used and the ensuing flushing solution properties. In particular, the mass transfer coefficient corresponding to the surfactant flushing solutions are substantially lower than that of the MCD solution or pure water flushing, partially offsetting the significantly higher effective solubilities when surfactants are present (see Table 4.2). Most mass transfer studies and corresponding Sherwood correlations are based on NAPL dissolution into pure water (for example, Saba and Illangasekare, 2000; Nambi and Powers, 2003). The results of the multiphase flow model suggest that further research is needed to evaluate the effect of agent type and fraction on the interphase mass transfer.

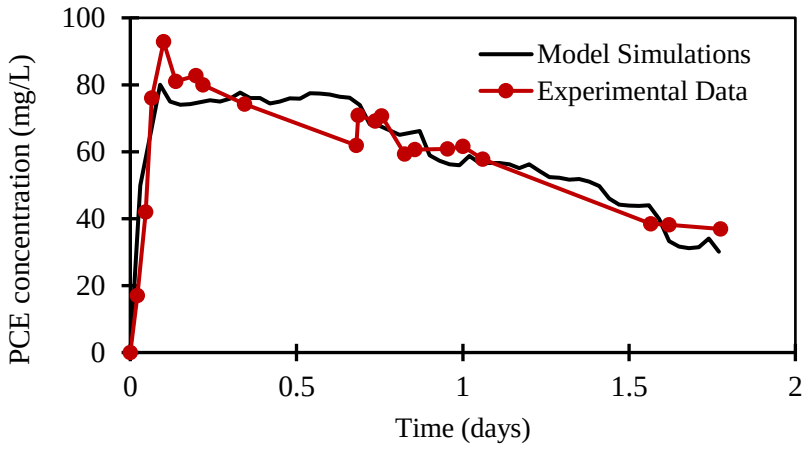
100
80
60
40
20
0
PCE concentration (mg/L)
0
0.5
1
1.5
2
Time (days)
Model Simulations
Experimental Data

(a)

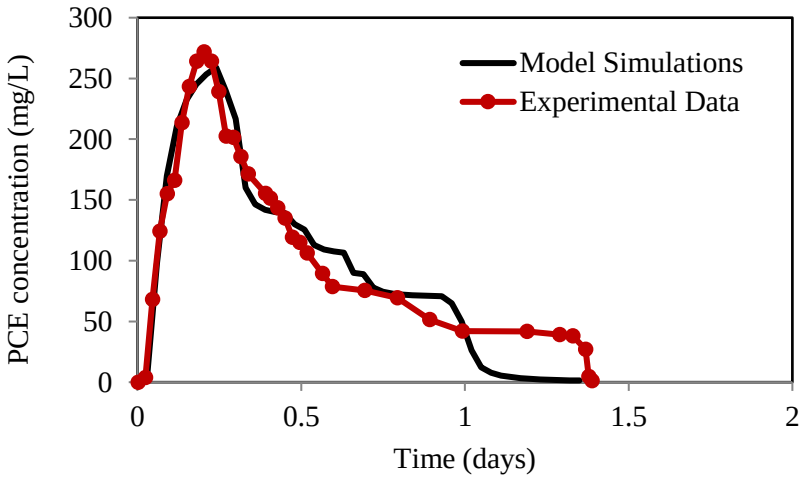
300
250
200
150
100
50
0
PCE concentration (mg/L)
0
0.5
1
1.5
2
Time (days)
Model Simulations
Experimental Data

(b)

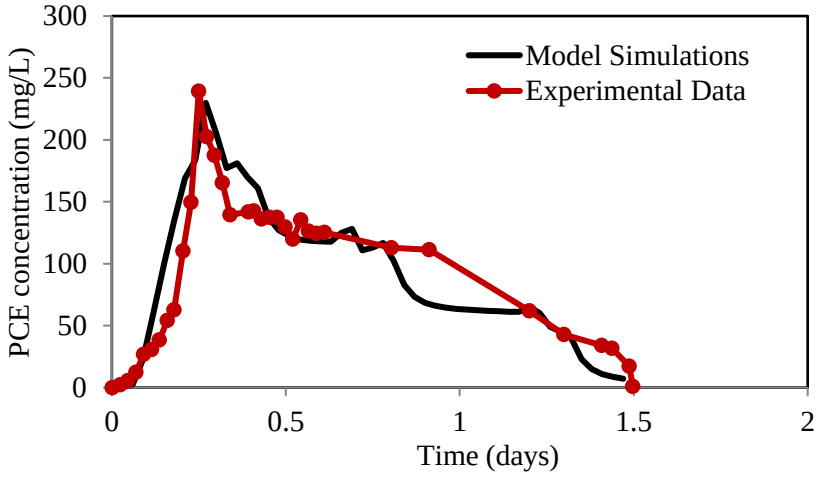
300
250
200
150
100
50
0
PCE concentration (mg/L)
0
0.5
1
1.5
2
Time (days)
Model Simulations
Experimental Data

(c)

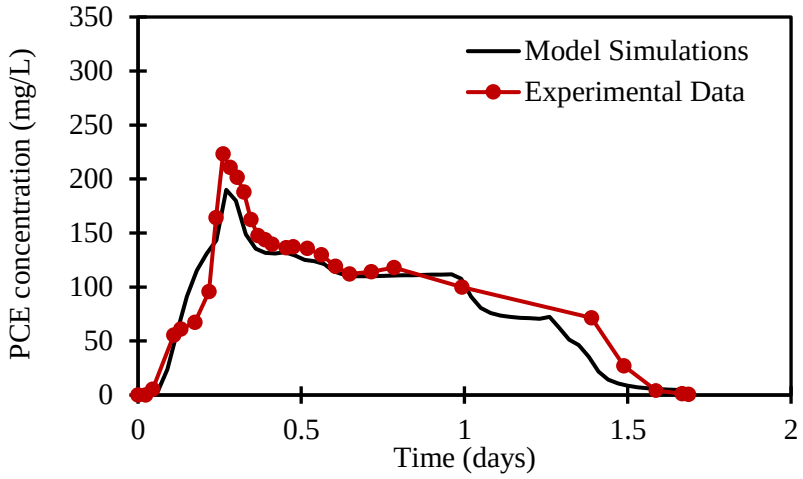

(d)

Figure 4.24. Comparison of the best-fit model and experimental results for (a) water, (b) 5 % Tween 80, (c) 5 % SDS, and (d) 5 % MCD in silica sand.

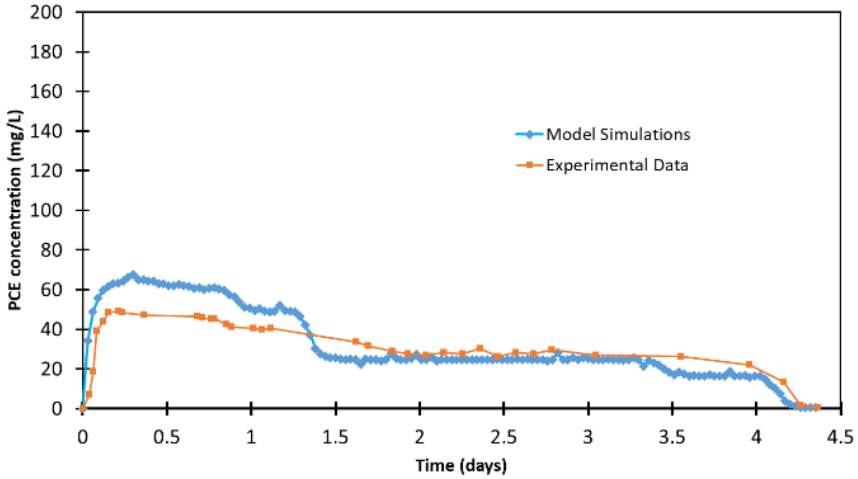
PCE concentration (mg/L)
Time (days)
Model Simulations
Experimental Data

(a)

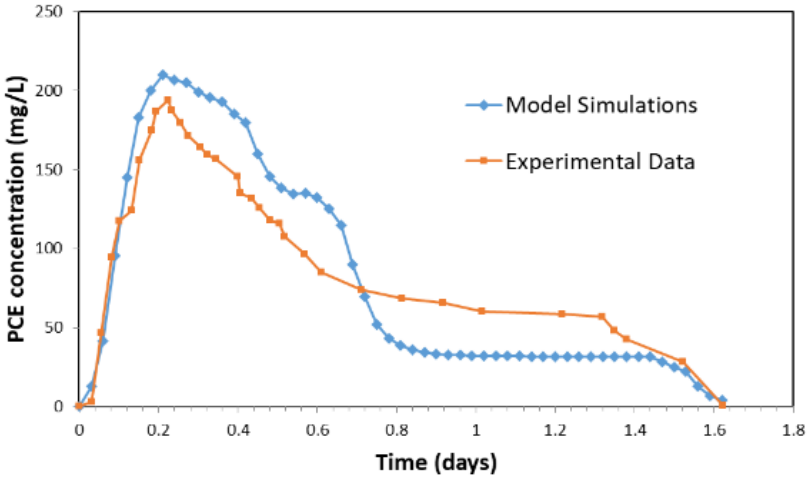
PCE concentration (mg/L)
Time (days)
Model Simulations
Experimental Data

(b)

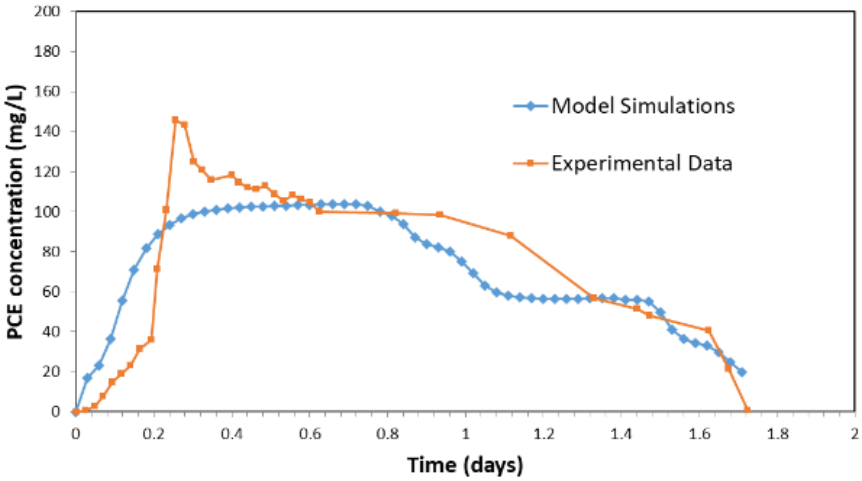
PCE concentration (mg/L)
Time (days)
Model Simulations
Experimental Data

(c)

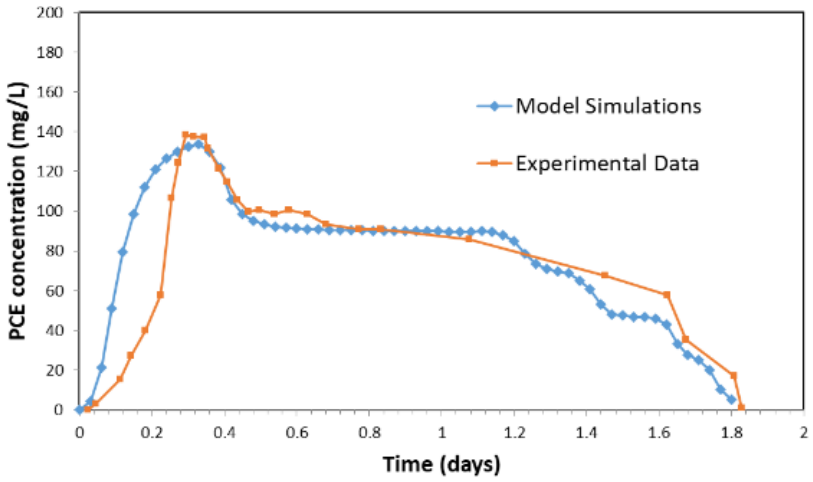

(d)

Figure 4.25. Comparison of the best-fit model and experimental results for (a) water, (b) 5 % Tween 80, (c) 5 % SDS, and (d) 5 % MCD in natural soil.

Table 4.11. Best-fit model parameters for silica sand flushing experiments.

	Multiphase Flow Modeling				Mass-Concentration Relation Modeling		
Flushing Agent	Mass Transfer Coefficient (day^{-1})	Sh'^{a}	NRMSE	R^2	β	NRMSE	R^2
water	1000	1.5	0.099	0.81	1.23	0.015	0.999
Tween 80 (5 %)	6	0.0089	0.085	0.93	1.16	0.033	0.998
SDS (5 %)	4	0.0059	0.12	0.82	1.28	0.043	0.990
MCD (5 %)	50	0.075	0.080	0.91	1.21	0.046	0.988

[a] calculated using Equation 3.10 for dm=0.359 mm and $D=10^{-9}$ $m^2.s^{-1}$

Table 4.12. Best-fit model parameters for the natural soil flushing experiments.

	Multiphase Flow Modeling				Mass-Concentration Relation Modeling		
Flushing Agent	Mass Transfer Coefficient (day^{-1})	Sh′[a]	NRMSE	R^2	β	NRMSE	R^2
water	500	0.130	0.193	0.81	2.27	0.013	0.998
Tween 80 (5 %)	5.5	0.0014	0.14	0.91	1.33	0.040	0.998
SDS (5 %)	3.2	0.0008	0.12	0.80	1.88	0.013	0.999
MCD (5 %)	27	0.0070	0.14	0.66	1.33	0.027	0.996

[a] calculated using Equation 3.10 for dm=0.150 mm and $D=10^{-9}$ $m^2.s^{-1}$

4.1.4. DNAPL Mass-Concentration Relation Modeling

The conducted flushing experiments were also modeled using a simplified mass conservation model that incorporates an empirical DNAPL mass-concentration model. Figures 4.26 and 4.27 show plots of the dimensionless recovered mass MR (Equation 3.21) as a function of dimensionless time for each of the flushing experiments. It is remarkable that a simple empirical model with a single parameter (β) was able to reproduce the experimental data with very small NRMSE values and near 1 correlations R^2 values. Although several complex factors influence the DNAPL concentration including the soil heterogeneity and the pore scale DNAPL architecture, the power function $M = g(C) = C^{\beta}$ with a single fitting parameter (β) was able to capture well the overall dissolution mechanism both for the water flood as well as the enhanced-agent flood.

A summary of the best fit β values for each of the sand and natural soil experiments along with the NRMSE and R^2 values are summarized in Tables 4.11 and 4.12. The β value for both the sand and natural soil experimental sets were greater than one. The β value of the power function $M = g(C) = C^{\beta}$ reveals the dependence of the flux on remaining DNAPL mass. At early times the DNAPL, both M=1 and C=1 and consequently, the discharge from the DNAPL zone is also highest. At early times, as M starts to decrease, the discharge concentration decreases according to the relation: $C = M^{1/\beta}$. A β =1 means the discharge concentration C would decrease linearly with a decrease in M. On the other hand, if β>1, a decrease in the remaining mass M causes a smaller decrease in the discharge concentration. This is likely to occur when the DNAPL is present in pooled form such as in the current experiments in this study. For pool-dominated DNAPL, the contact area between the

DNAPL and the flushing solution is only minimally changed due to the initial decrease in M ($t<1$ in Figures 4.26 and 4.27). With time, the more accessible DNAPL mass is gradually dissolved. At late times only the less accessible DNAPL remains, resulting in a significant decrease in the discharge concentration and a flattening of the MR curve.

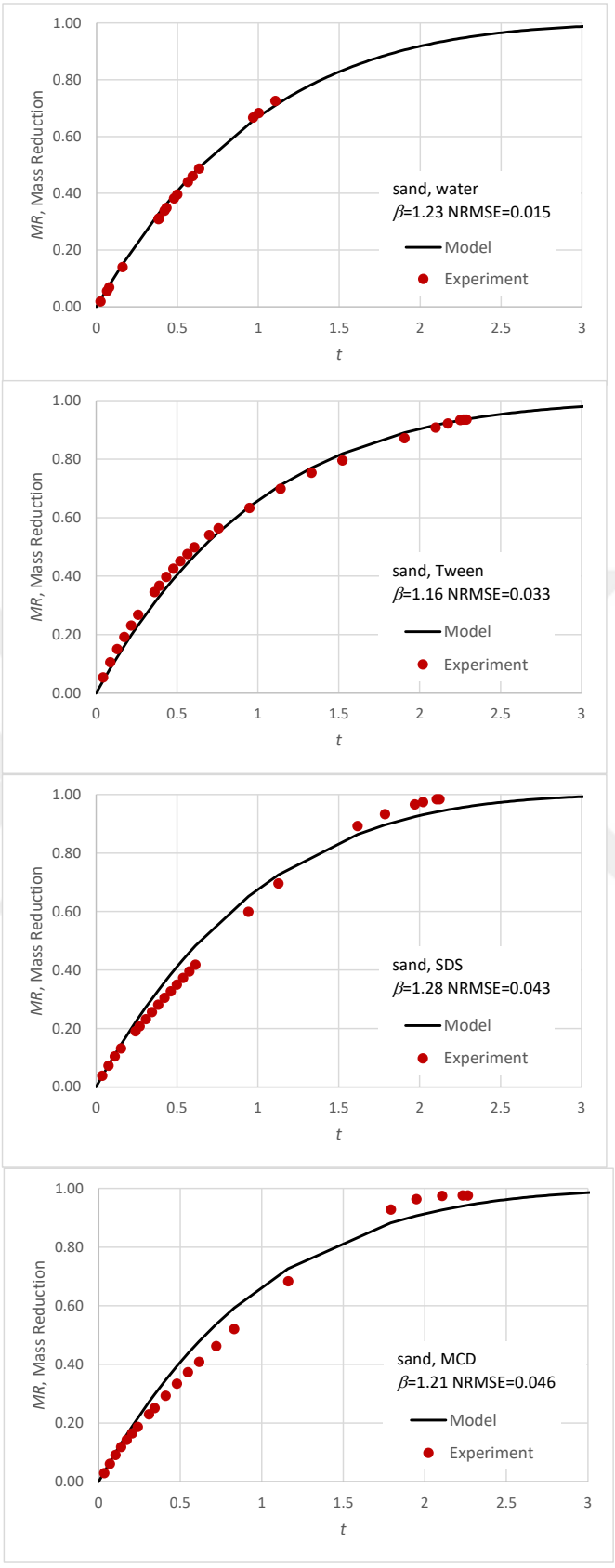

Figure 4.26. Comparison of simulated and observed dimensionless mass recovered as a function of dimensionless time for the silica sand flushing experiments.

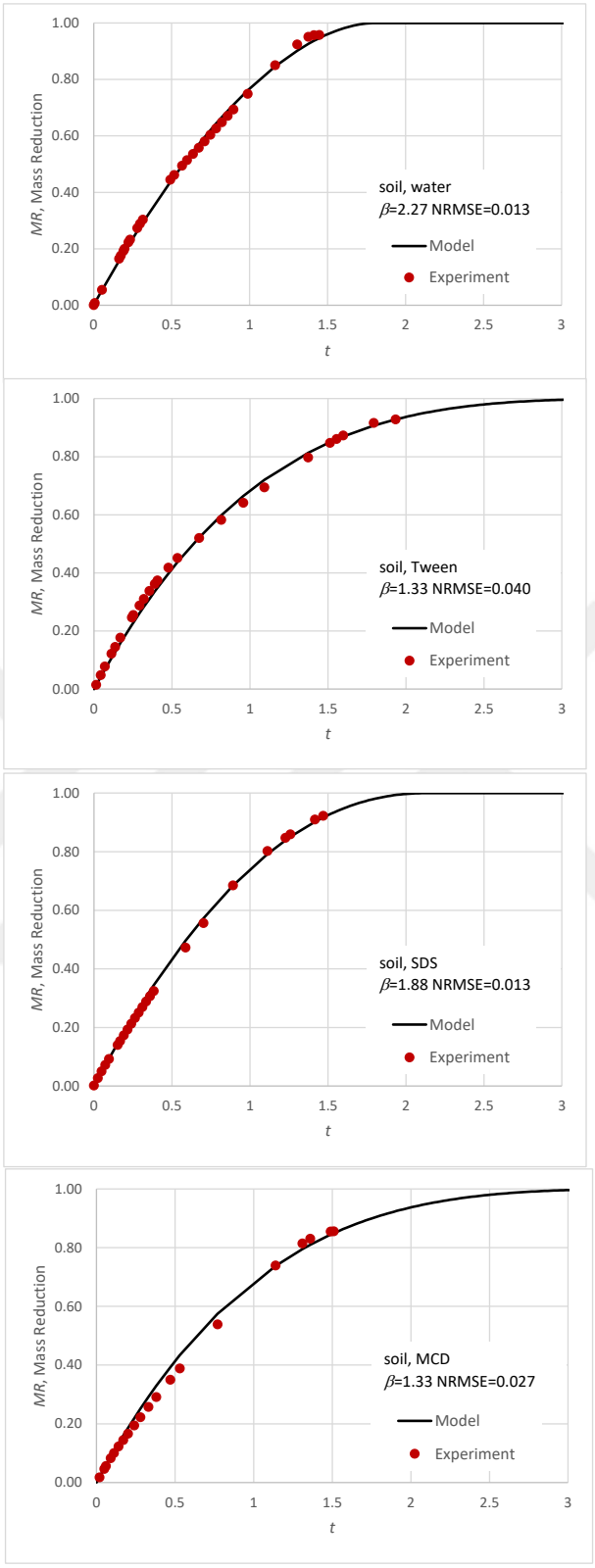

Figure 4.27. Comparison of simulated and observed dimensionless mass recovered as a function of dimensionless time for the natural soil flushing experiments.

Multi-step mass removal/mass-flux-reduction behavior indicating non-ideal dissolution behavior due to the soil heterogeneity and NAPL zone architecture distribution was also reported earlier (Brusseau et al, 2007; DiFilippo and Brusseau, 2008; Brusseau et al, 2008; DiFilippo et al, 2010; Akyol et al, 2013; Brusseau et al, 2013; Akyol and Turkkan, 2018; Akyol, 2018). The DNAPL mass-discharge modeling performed here aid to quantify the temporal change of the contaminant discharge concentration from DNAPL source zones. It is important to note that in laboratory-scale experiments, the level of heterogeneity is likely to be much lower than what would be encountered in the field. Moreover, in laboratory-scale experiments, the time between the release of the DNAPL into the porous media and the initiation of flushing is by orders of magnitude smaller than in real field problems (order of 100 days compared to 102-103 days). This means that the DNAPL would likely be less accessible in field settings. For such complex field configurations, more flexible $M = g(C)$ relations involving multiple parameters such as the sinusoidal or bilinear models may be required to represent the mass-concentration relation.

It is evident that the two modeling approaches considered in this study can reveal important aspects of the DNAPL dissolution dynamics. The multiphase flow model provides a physics-based representation of the governing processes. For the current set of experiments, it allowed for the estimation of the interphase mass transfer coefficient and the impact of agent type and soil properties (sand vs natural soil) on the estimation of the interphase mass transfer coefficient. The challenge however is in the definition of the input parameters of the multiphase system, particularly the initial DNAPL mass distribution and the multiphase soil parameters. The empirically based mass-concentration model bypasses the need to fully characterize the multiphase system. The good match between the simulated and observed concentrations is quite encouraging, suggesting that this model may also be able to explain DNAPL mass dissolution dynamics. Further work would be needed to test different functional relations, particularly at the field-scale for different DNAPL zone configurations (residual vs pooled), as well as with and in the absence of agent-based enhanced dissolution.

4.2. Multiphase Flow Model of DNAPL Mixtures with Different Solubilizing Agents

In this chapter, I present the batch and modeling results of DNAPL mixture enhanced solubilization flushing. The flushing data are published in (Akyol et al, 2023). The multiphase code UTCHEM was used to model the experiments.

The relative behavior of DNAPL compounds in the presence of different solubilizing agents were compared through a series of batch experiments. The experimental procedure was described in chapter 3, section 3.2. The properties of the flow-cell and porous media in which the experiments are carried out are given in chapter 3, section 3.4.1. A total of eight sets of experiments were conducted to evaluate the effect of solubilizing agents on remediation of pool-dominated multi-component DNAPL (comprising of TCE, PCE, 1,1-DCE) distributed within two physical heterogeneous configurations comprising of the silica sand and natural calcareous soil (Figure 4.28). The experimental conditions and agents used are listed in Table 4.13. The porous media configuration within the flow-cell are similar as described in the previous section.

Table 4.13. List of flow-cell experiments with DNAPL mixture pool.

Silica sand flow-cell experiments	Flushing solution	Velocity (cm/h)	PCE initial saturation * (%)
1	5 % Tween 80	10.1	0.04
2	5 % SDS	10.1	0.04
3	5 % MCD	10.1	0.04
4	water	10.1	0.04
Calcareous soil flow-cell experiments	Flushing solution	Velocity (cm/h)	PCE initial saturation * (%)
1	5 % Tween 80	9.9	0.04
2	5 % SDS	9.9	0.04
3	5 % MCD	9.9	0.04
4	water	9.9	0.04

*Sn is defined as the injected volume of the organic liquid divided by the pore volume of the entire system



(a)



(b)

Figure 4.28. Image of DNAPL mixture initial distribution for the a) silica sand, b) calcareous soil. (Experiment 1 with 5 % Tween 80).

4.2.1. DNAPL Mixture Enhanced Solubilization Batch Experiments

This section presents the batch test results consisting of IFT data, ternary phase diagrams (TPD) and solubility data for DNAPL mixtures with various surfactants. These data are useful for modeling studies which require the definition of various parameters describing the DNAPL-water-solubilizing agent system. The batch test results are also useful for the selection of agents and their optimal contents.

The IFT between multi-component DNAPL (PCE:TCE:1,1-DCE) and the aqueous phase as a function of surfactant (Tween 80, MCD and SDS) content is shown in Figure 4.29. The DNAPL consisted of PCE, TCE, and 1,1-DCE at equal mole fraction (0.33:0.33:0.33) The IFT between DNAPL mixture and water is ~40 mN/m. As observed for single component PCE measurements (see section 4.1.1, Figure 4.1), the IFT of the DNAPL mixture and aqueous solution gradually decreases with increase in solubilizing agent content.

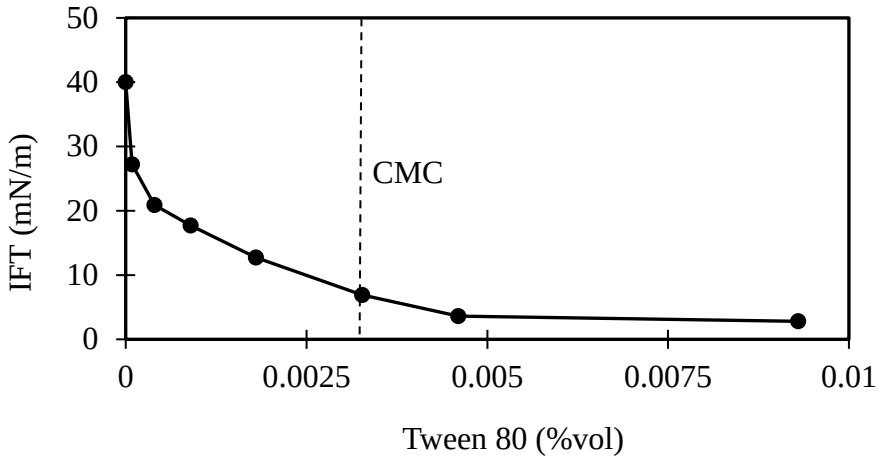

(a)

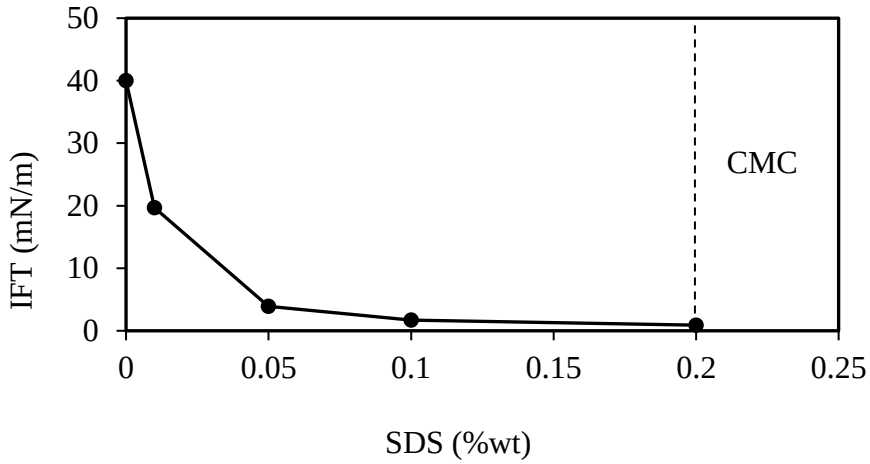

(b)

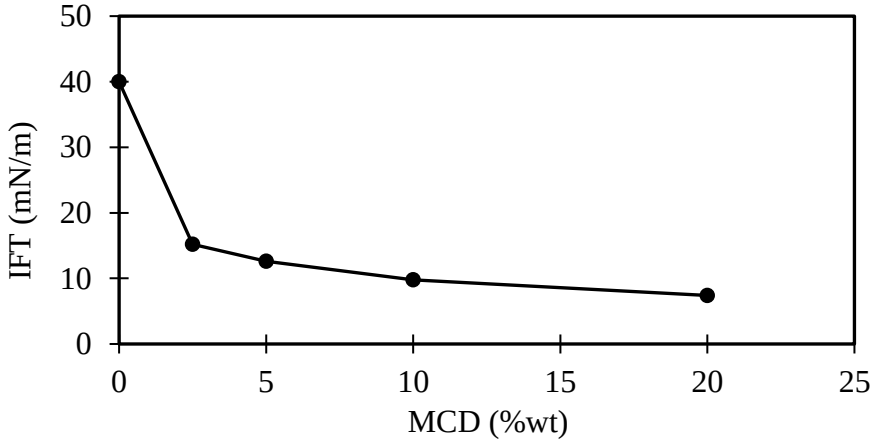

(c)

Figure 4.29. IFT of two phase system as a function of (a) Tween 80 (%vol), (b) SDS (%wt), (c) MCD (%wt) for DNAPL mixture (PCE:TCE:1,1-DCE).

Figure 4.29 shows that at high surfactant concentrations, the IFT reaches very low values. For Tween 80, the degree of decrease in DNAPL mixture-solubilizing agent IFT is not much different from single PCE. The CMC value of Tween 80 (~0.00327 %vol or ~35mg/L) corresponds to 7 mN/m (Figure 4.29.a). For surfactant contents above CMC, the IFT remains approximately constant at around 3.6 mN/m regardless of surfactant concentration.

Very low IFT values were observed with the increasing content of SDS. The CMC value of SDS, where the surfactant molecules start to aggregate to form micelles (Figure 4.30) is 0.21 %wt or ~2100 mg/L. The corresponding IFT was measured as 1 mN/m for DNAPL mixture (Figure 4.29.b). This value is quite lower than the individual IFT values of PCE and TCE found in the literature which were 5 mN/m for TCE and 6.7 mN/m for PCE at CMC value of SDS (Cai and Mohanty, 1997).

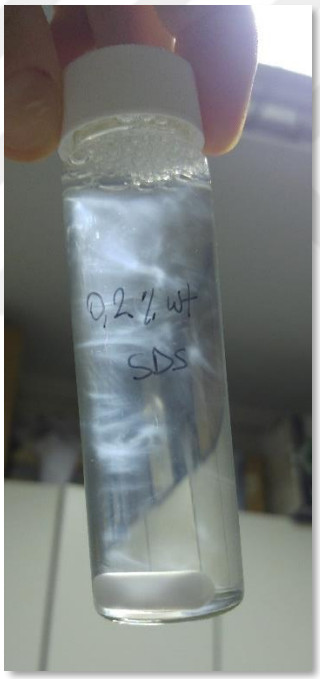

Figure 4.30. SDS at critical micelle concentration (~0.2 %wt).

Interfacial tension measurements between DNAPL mixture-MCD show much slower decrease than the other 2 surfactants. The IFT noticeably decreased to a value of 15.2 mN/m for 2.5 % wt MCD solution. After this concentration, the IFT decrease showed a very slight trend slightly up to 20 %wt (Figure 4.29.c). The IFT measurements with all three solubilizing agent did not reach zero which corresponds to fully miscible solutions.

The IFT rapidly decreases with low Tween 80 contents but exhibits practically no decrease for Tween 80 concentrations greater than 0.005 %wt. This indicates that Tween 80, even at very low contents, is an effective surfactant for enhanced dissolution of chlorinated solvent DNAPL mixtures. However, at higher Tween 80 levels, the IFT is likely not to be sufficiently depressed to cause DNAPL phase mobility. SDS exhibited similar behavior, however much higher agent contents are needed before the IFT approaches zero. On the other hand, the IFT with MCD did not reach zero. These findings, particularly with Tween 80, are consistent with some studies that have examined the effect of solubilizing agents on single component DNAPLs (Cai and Mohanty, 1997; Boving and Brusseau, 2000; Conrad et al, 2002; Suchomel et al, 2007; Cheng et al, 2016).

The miscibility of the multiphase solubilizing agent-DNAPL mixture-water system in the presence of Tween 80, SDS and MCD are presented as ternary phase diagrams (TPDs). This graph, which shows at which contents the system is present as a single phase or multiphase was determined using the cloud point titration experiments (see section 3.2). While most TPDs in the literature consider single component DNAPL, in this study the TPD for the DNAPL mixture and various surfactants was developed. Figure 4.31 shows the TPD, expressed on mass basis, of the Tween 80-DNAPL mixture-water system.

Due to the difficulties associated with Tween 80, the phase behavior curve in the DNAPL mixture titration was similarly formed in more than one stage as in the previous titrations with single PCE (Section 4.1.1). Due to the high viscosity of Tween 80, gels were formed when the aqueous solution exceeded about 26.8; 10.6; 62.6 % by mass. With an increase in DNAPL mixture content, the formation of a highly viscous opaque white microemulsion was observed which interfered with the titration procedure. The Tween 80-DNAPL mixture-water ratio started from 0; 100; 0 to 60; 39; 1 without any physical change. Beyond this ratio, temporary cloudiness was observed with further addition of water. There was a continuous cloudiness and clearness transition with increasing amount of water. At the upper right section of the curve, cloudiness became stable which corresponded to the two-phase region (Figure 4.31).

DNAPL mixture titration experiments with Tween 80 showed that in the single-phase region which constitutes the upper part of the curve and where the amount of the Tween 80 and DNAPL mixture is relatively high, the system misleadingly appeared to behave as a two-phase (transition zone). Repeated experiments have shown that the actual two phase region is reached by further increasing the amount of water by mass. Another observation is that the DNAPL mixture is miscible

with a higher amount of Tween 80 compared to PCE alone. The multiphase system is fully miscible at Tween 80 contents higher than 54 %wt (Figure 4.31) with no formation of bilayer vesicles.

The fact that Tween 80 is used in low concentrations (5 %, 2.5 % etc.) in the flow-cell flushing experiments, thus the mixture curve is on the water-rich side, shows that the problems experienced in titration with Tween80 will not occur in flushing experiments.

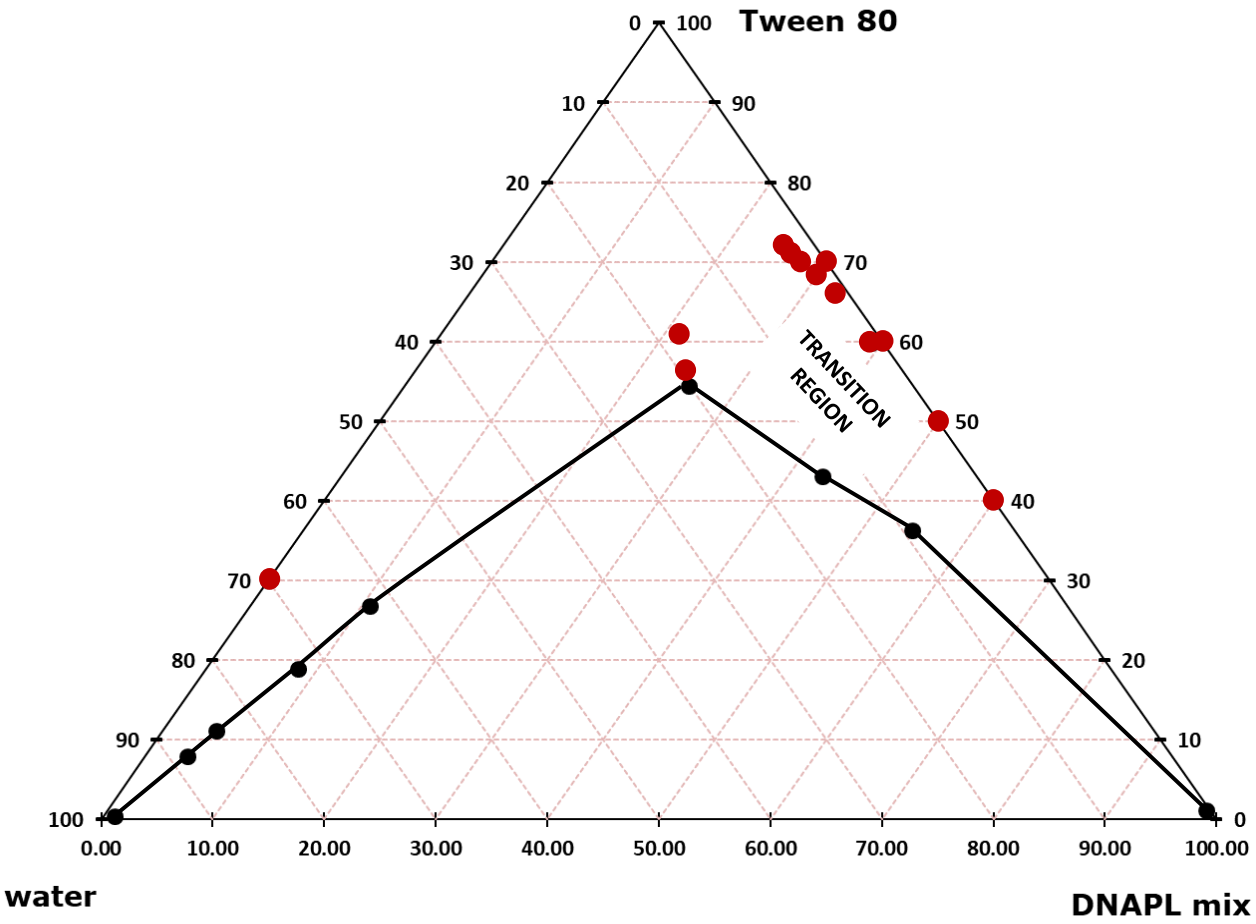

Figure 4.31. Ternary phase diagram for Tween 80-DNAPL mixture-water (%wt).

The ternary phase diagrams obtained from the titrations with SDS and MCD are given in Figure 4.32 and 4.33. Aqueous solutions of MCD and SDS, which are powders and cannot be added in pure form, were prepared (SDS: 19.44 %wt, MCD: 25 %wt) and used in titration.

Unlike Tween 80, clouding and foaming were not observed in the titration for constructing the TPDs of SDS and MCD. As the percent mass increased during the titration, it was difficult to distinguish between clouding and foaming and the experiments were repeated for confirmation. As might be expected, the increase in stirring bar speed on the magnetic stirrer increased the rate of

foaming. Decrease in speed has often led to misleading results about the surfactant solution and DNAPL get into the system. After repeated titrations, a curve formed very close to the water-rich zone. The total amount of water, as one of three component and as a part of solubilizing agent solution, caused the points to concentrate on one side of the graph (Figure 4.32, 4.33). The experiment was started from the ratio of 0; 0; 100 % mass as the first step in titration with both solubilizing agents. The highest point found in the resulting mixture curve coincided with the value obtained by the titration starting from 0; 100; 0, thus the course of the curve is confirmed. These results suggest that the removal mechanism of the DNAPL mixture is likely to be solubilization since the solubilizing agent concentrations used in flow-cell experiments were substantially below the miscibility curve.

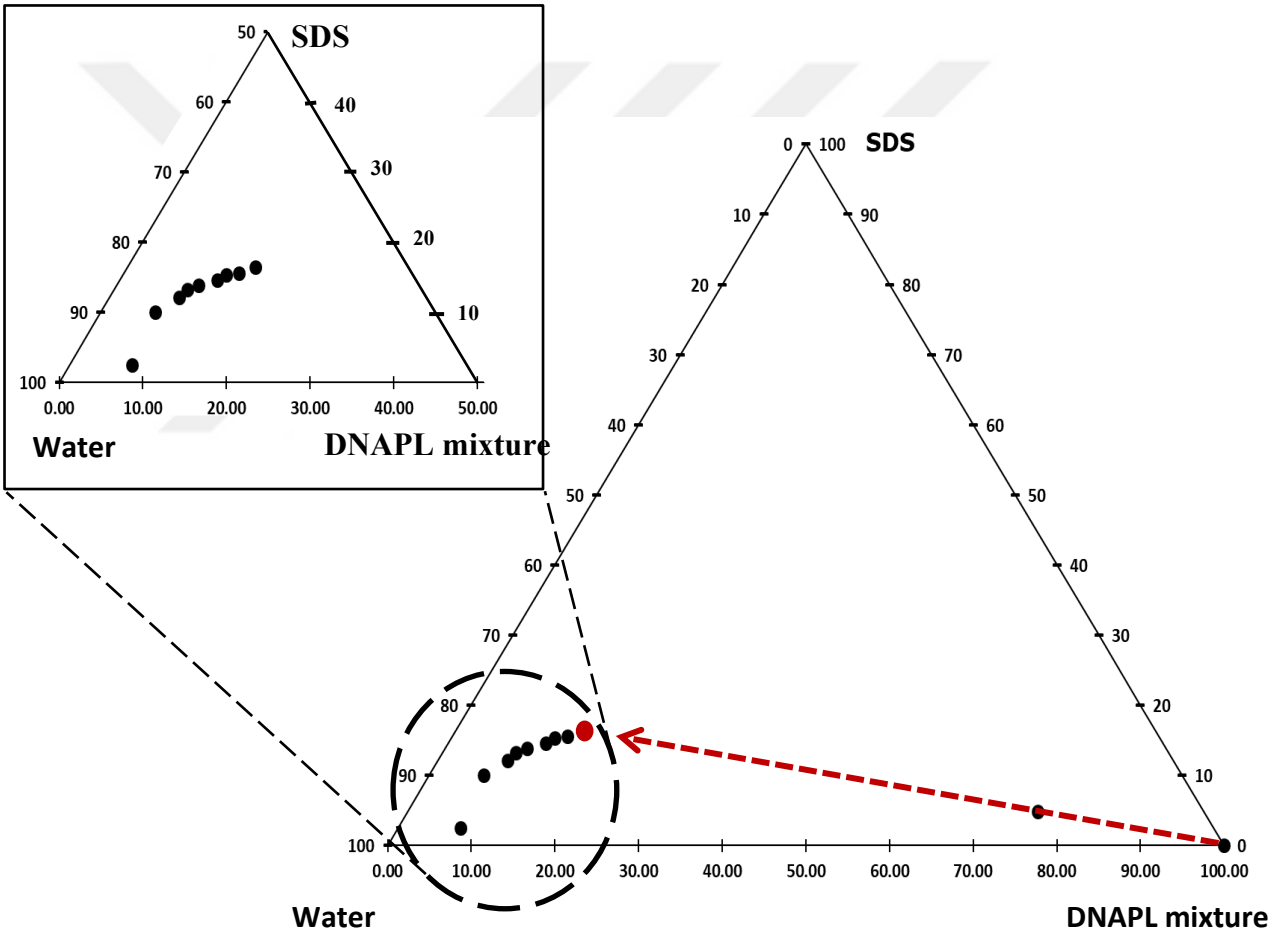

Figure 4.32. Ternary phase diagrams for SDS-DNAPL mixture-water system (%wt).

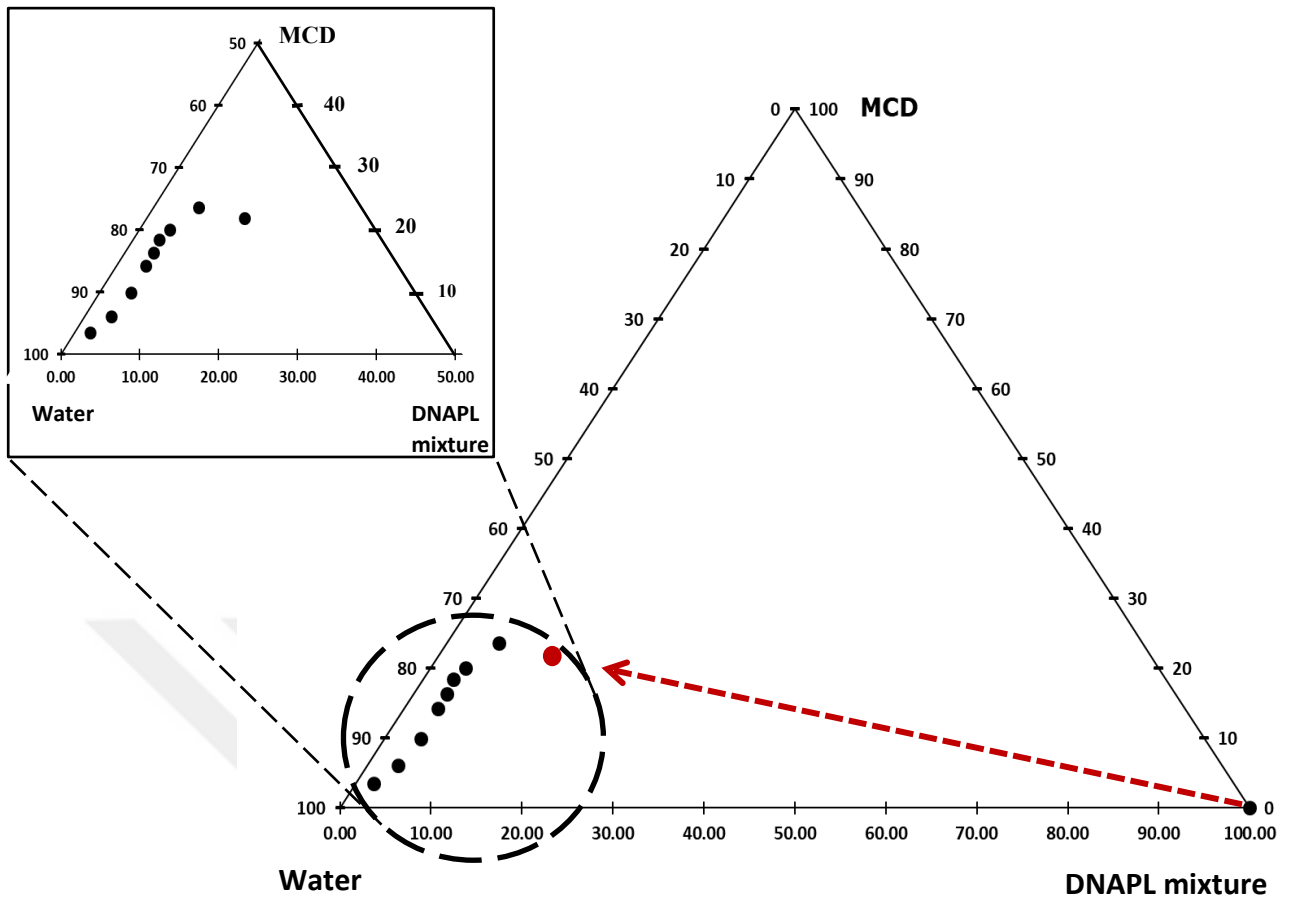

Figure 4.33. Ternary phase diagrams for MCD-DNAPL mixture-water system (%wt).

In addition, the ternary phase diagram of DNAPL mixture with ethanol and ethanol/Tween 80 was also investigated (Figure 4.34). Accordingly, in the system where only PCE is present, the amount of ethanol that can be miscible with PCE (60 %wt) (see Figure 4.3) is higher than the amount for the mixture (52 %wt). When DNAPL mixture is present, the use of ethanol and Tween 80 together can become miscible at a lower value than where they are used alone (40 %wt). When ethanol is used with MCD and SDS, although MCD can reduce the miscibility limit to a value slightly lower than the value when ethanol is alone (50 %wt), this situation is not very valid for SDS (40 %wt).

Overall, TPD of the various solubilizing agent-DNAPL-water system, can shed some light on the multiphase behavior of the system. Depending on the content of solubilizing agent, they can point to the presence of a single miscible liquid vs a multiphase system prior to performing of costly flushing experiments. Moreover, they can provide some guidance on the optimal flushing solution contents.

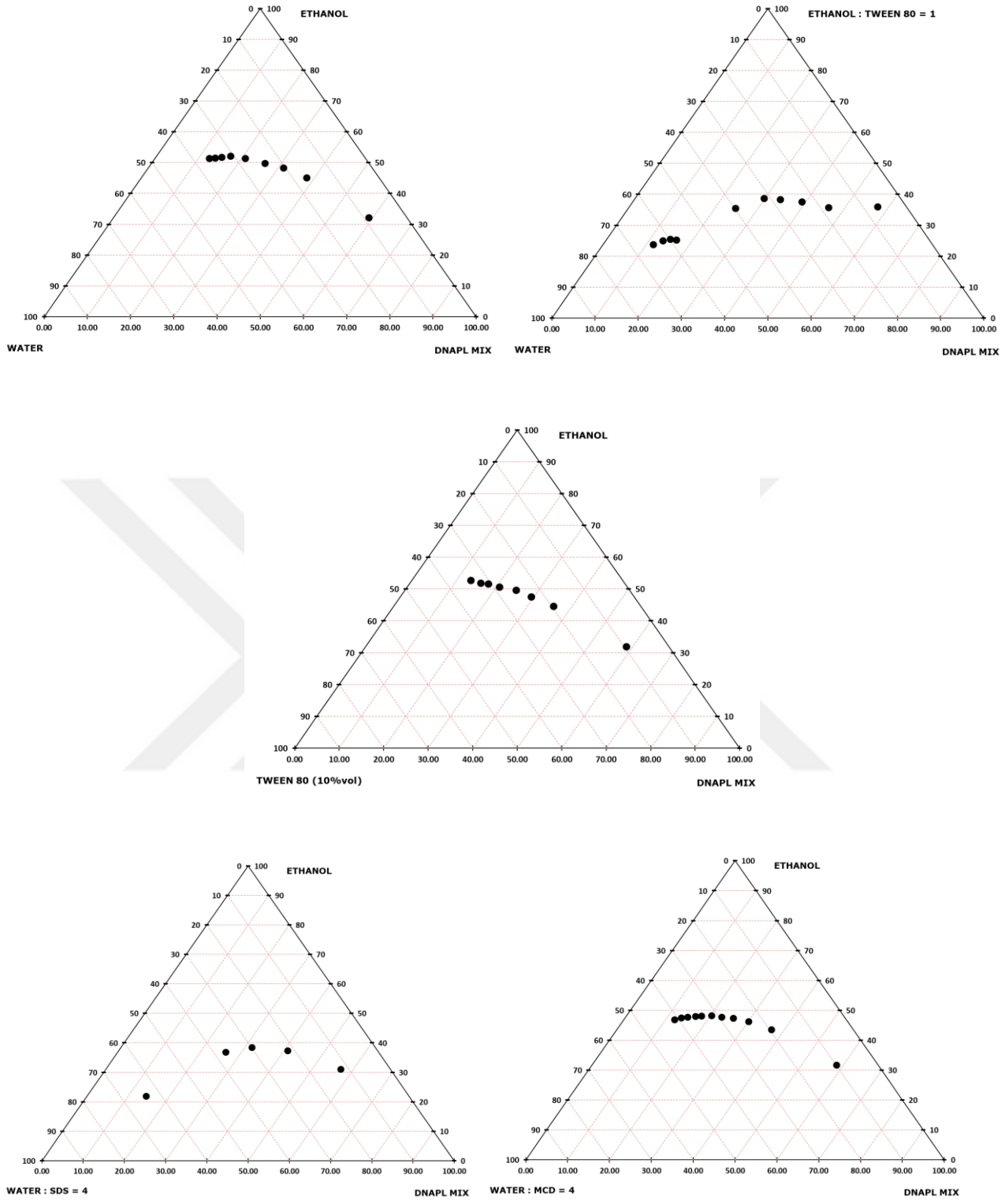

Figıre 4.34. Variations of TPDs with different solubilizing agent and co-solvent contents for DNAPL mixture.

The measured solubilities of the DNAPL mixture (molar ratio of 1:1:1, mole fraction of (0.33:0.33:0.33) for solubilizing agent contents of 2.5 % and 5 % by mass are presented in Figure 4.35. Tween 80 increases the DNAPL component solubilities the most, followed by SDS and finally

MCD. The data are further summarized in Table 4.14. The ratio of the solubility of each DNAPL in 5 % Tween 80 solution to the solubility in pure water is 300 were: 300 times more soluble for PCE, 45 for TCE and 15 for 1,1-DCE. For SDS, the solubility enhancement of PCE relative to that in water was highest (190 times more soluble from its water solubility) while TCE was about 30 times and 1,1-DCE was 10 times higher. MCD lead to lowest increase in solubility: for PCE the solubility enhancement relative to solubility in water was about 20 times , followed by TCE with 5 times and 3 times for 1,1-DCE.

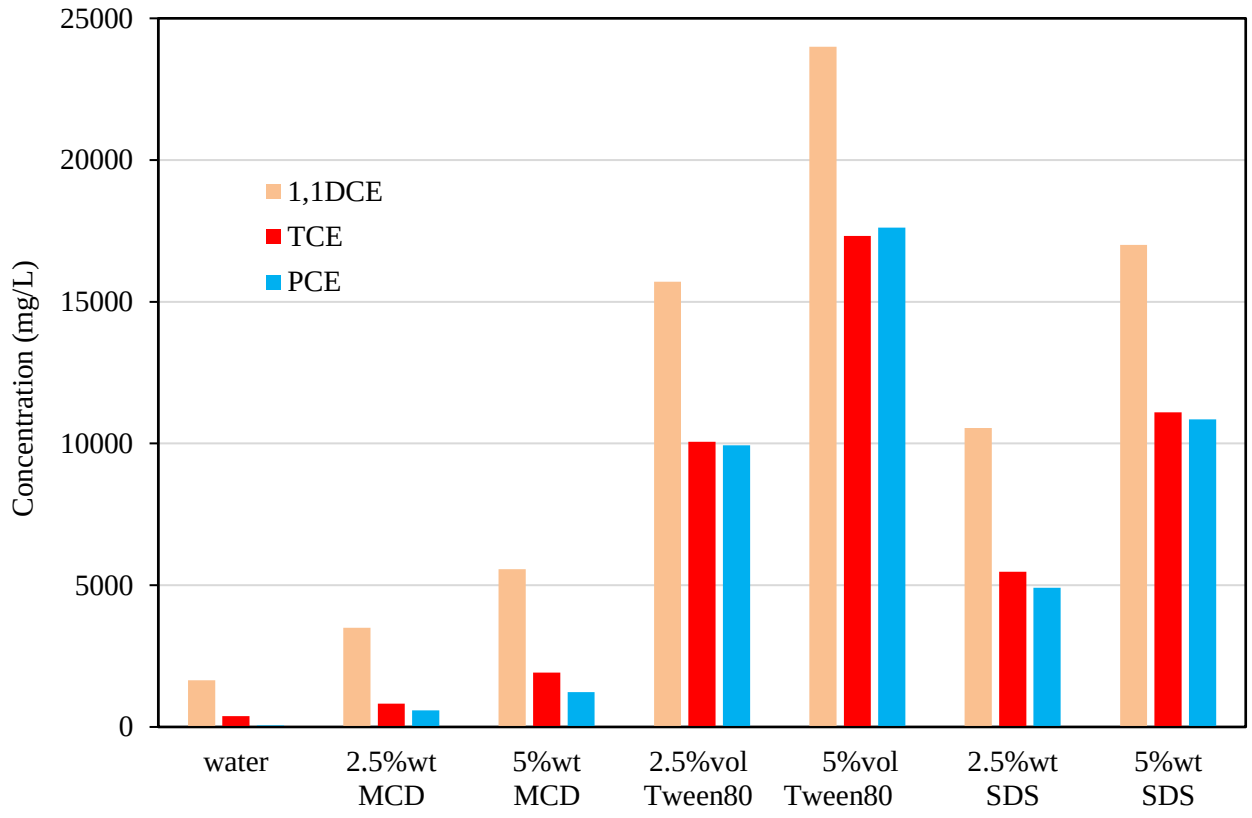

Figure 4.35. Enhanced-solubility of the DNAPL mixture in Tween 80-water, SDS-water, and MCD-water system.

The solubility data measured in this study for different agents are compared in Table 4.14 with values from the literature. Compared to the solubility values obtained by flushing tests, the solubility values determined from batch experiments are much less common in the literature (Table 4.14). No experimental solubility data for 1,1-DCE in various surfactant contents were found in the literature from either batch or flushing experiments. Similarly, no solubility data for PCE could be found with MCD and SDS. The solubility values of TCE were consistent with literature data. As a general interpretation, the percent error between literature data and the results of this study is within

acceptable limits considering the volatility of the DNAPL components and the difficulty of measurements.

Table 4.14. Comparison of the solubility values of DNAPL mixture components to data from the literature.

				Literature			
DNAPL mixture	**Solubilizing agent (%)**		**This study**	**Pure phase DNAPL***	**0.33 mol fraction**	**% Error**	**Reference**
1,1-DCE	water	-	1650	3000	990	66.5	Dill et al, 1980
	MCD	2.5	3500	-	-	-	No data available
		5	5570				
	Tween 80	2.5	15700				
		5	24000				
	SDS	2.5	10600				
		5	17000				
TCE	water	-	390	1200	400	2.2	Horvath et al, 1999
	MCD	2.5	820	-	-	-	No data available
		5	1920	5500	1800	5.3	Boving and Brusseau, 2000
	Tween 80	2.5	10100	34300	11300	11.0	Huh, 1979
		5	17300	49500	16300	6.0	Zhong et al, 2003
				85800	28300	38.8	Suchomel et al, 2007
	SDS	2.5	5480	10000	3300	66.0	Zhong et al, 2003
		5	11100	23600	7800	43	Zhong et al, 2003
				30700	10100	9.5	Boving and Brusseau, 2000
PCE	water	-	58	200	66	12	Horvath, 1982
	MCD	2.5	580	-	-	-	No data available
		5	1230				
	Tween 80	2.5	9940	16500	5440	82.5	Taylor et al, 2004**
		5	17600	33500	11100	59.4	
	SDS	2.5	4900	-	-	-	No data available
		5	10900				

(*) : The values (pure phase DNAPL solubility, $C_{solubility}$, and the solubility enhancement factor, E) obtained from batch experiments were taken into consideration.
(**) : Experimental study (Taylor et al, 2004), up to 4 % concentration. The solubility corresponding to the 5 % concentration was obtained from the regression equation ($R^2 = 0.999$).

An alternative to the solubility values that helps to understand the effective solubility is the solubility enhancement factor (E), defined as the solubility of DNAPL with surfactant divided by the solubility of DNAPL in pure water equation (4.1),

$$Solubility\ Enhancement\ Factor\ (E) = \frac{C_{enhanced\ solubility}}{C_{water\ solubility}} \quad (4.1)$$

In the literature, the E values have been determined from flow-cell and column experiments rather than batch experiments. Solubility enhancement factors determined according to different test methods and sampling locations are summarized in Table 4.15. Although batch experiments are accepted as the method which yields more accurate results as it generally allows for longer contact between the DNAPL and solubilizing agent solution, studies reporting solubilities derived from batch experiments are limited in literature. For the solubilities obtained with similar test methods solubility enhancement factors obtained in this study were found to be compatible with the data available from similar studies.

The solubility enhancement factors of each DNAPL mixture component in 5 %wt of each solubilizing agent solution are discussed here. For 5 % Tween 80, enhancement factors are 303.1 for PCE, 44.8 for TCE, and 14.6 for 1,1-DCE. 5 % SDS content increased the solubility of PCE, TCE and 1,1-DCE by factors of 186.7, 28.7 and 10.3, respectively. Finally, for 5 % MCD, the solubilities of PCE, TCE and 1,1-DCE increases by factors of 21.2, 5 and 3.4 respectively.

Overall, the batch solubility experiments reveal that for the selected solubilizing agent contents and DNAPL composition, the performance of the agents followed the corresponding order: Tween80>SDS>MCD>>water. However, greater difficulty was encountered in the preparation and titration of the Tween 80 solution due to its high viscosity.

Table 4.15. Comparison of the enhancement factors from this study to available literature values.

Study	Experimental Conditions		Surfactant (%)	Compound	Solubility Enhancement Factor (E)
Slavic, 2014		Flow-cell/multiple-component	5% SDS	PCE	60
			5% SDS	TCE	16.5
			5% MCD	PCE	15
			5% MCD	TCE	7.7
Boving and Brusseau, 2000		Column/single-component	5% MCD	TCE	4.6
			5% SDS	TCE	25.6
Tick and Rincon, 2009		Column/single-component	5% SDS	TCE	20
Akyol et al, 2013		Column/single-component	5% SDS	TCE	37
		Flow-cell/single-component	5% SDS	TCE	~5-9
Tick et al, 2015	Extraction port	Flow-cell/multiple-component	5% SDS	cis-DCE	5.5
	Extraction port		5% SDS	TCE	18.6
	Extraction port		5% SDS	PCE	58.5
	Source-zone port		5% SDS	cis-DCE	3.4
	Source-zone port		5% SDS	TCE	5.3
	Source-zone port		5% SDS	PCE	12.7
Zhong et al, 2003		Batch/single-component	5% SDS	TCE	19.6
			5% Tween80	TCE	41.25
Suchomel et al, 2007		Batch/single-component	5% Tween80	TCE	71.5
			4% Tween80	TCE	52.9
Taylor et al, 2004		Batch/single-component	4% Tween80	PCE	137.5
This study		Batch/single-component	5% Tween80	PCE	106.6
		Batch/multiple-component	5% SDS	PCE	186.7
		Batch/multiple-component	5% MCD	PCE	21.2
		Batch/multiple-component	5% Tween80	PCE	303.1
		Batch/multiple-component	5% SDS	TCE	28.7
		Batch/multiple-component	5% MCD	TCE	5.0
		Batch/multiple-component	5% Tween80	TCE	44.8
		Batch/multiple-component	5% SDS	1,1-DCE	10.3
		Batch/multiple-component	5% MCD	1,1-DCE	3.4
		Batch/multiple-component	5% Tween80	1,1-DCE	14.6

4.2.2. DNAPL Mixture Enhanced Solubilization Model Calibration

This section describes the modeling of DNAPL flushing experiments. Modeling was performed using the UTCHEM model which was described in Section 4.1.3. The goal here is to evaluate whether the multiphase flow model UTCHEM can also simulate the surfactant-enhanced dissolution of DNAPL mixtures.

The key input parameters that were used in the DNAPL mixture enhanced flushing model development are given in Table 4.16.

Table 4.16. Key parameters used in DNAPL mixture model.

Porosity	
Silica sand	Flow zone: 0.36 (d_{50} = 359 μm) Impermeable zone: 0.38 (d_{50} = 172 μm)
Natural soil	Flow zone: 0.58 (d_{50} = 150 μm) Impermeable zone: 0.38 (< 76 μm)
Bulk density (ρ_b)	
Silica sand	1.74 g/cm^3
Natural soil	1.35 g/cm^3
Intrinsic permeability	
Silica sand	Flow zone: 20 darcy Impermeable zone: 2 darcy
Natural soil	Flow zone: 20 darcy Impermeable zone: 0.02 darcy
Longitudinal dispersivity	
Silica sand	0.02 m[a]
Natural soil	0.04 m[a]
DNAPL solubility	
PCE	
Pure water	0.206[b] g/L
Tween 80 (5 %)	25[c] g/L
SDS (5%)	24.3[c] g/L
MCD (5%)	3.73[c] g/L
TCE	
Pure water	1.280 [b] g/L
Tween 80 (5 %)	49.5 [c] g/L
SDS (5%)	36.5 [c] g/L
MCD (5%)	10.3 [c] g/L
DCE	
Pure water	2.500 [b] g/L
Tween 80 (5 %)	90.0 [c] g/L
SDS (5%)	66.6 [c] g/L
MCD (5%)	30.3 [c] g/L
DNAPL aqueous phase interfacial tension	
PCE	45 mN/m
DNAPL mixture	40 mN/m
MCD	θ =3[d], X_0=−3,8239
Critical micelle contentration (CMC)	
Tween 80	0.035[e] g/L
SDS	2.1[f] g/L
Capillary pressure parameter	
	λ=2[g], P_{bl}= 5.032 kPa

Residual saturation	
low capillary number	S_r = 0.13[h] for all phases
high capillary number	S_r = 0.05[h] for all phases
Relative permeability (Brooks-Corey formulation)	
End-point relative permeability ( )	
NAPL phase	$k_{r,l}^{o} = 0{,}46$[i]
Flushing solution	$k_{r,l}^{o} = 0{,}46$[i]
exponent (e_l)	
NAPL phase	$e_l = 4$ [i]
Flıshing solution	$e_l = 4$ [i]

[a] Longitudinal dispersivity determined from tracer **test**; b Horvath et al, 1999: [c] c Enhanced solubility values determined from batch experiments and literature review; [d] Li and Fu (1992); [e] Zhong et al (2003); [f] Boving and Brusseau (2000); [g] Brooks and Corey (1966); [h] Shah et al (1995); [i] Corey (1994)

The multiphase flow model of the DNAPL mixture, prepared assuming equimolar fraction of PCE, TCE, 1,1-DCE, was demonstrated by comparing the simulated effluent concentrations to the effluent concentrations obtained from flow-cell experiments. The dissolution of the DNAPL mixture was assumed to be controlled by rate-limited (non-equilibrium) mass transfer behavior. Best-fit mass transfer coefficients, expressed in terms of the dimensionless modified Sh', the root mean squared normalized errors (NRMSE), and correlation coefficients (R^2) between simulated and observed curves are presented in Tables 4.17 and 4.18 for the DNAPL mixture model. The best-fit and experimental curves over time for different flushing agents are shown in Figures 4.36 and 4.37. It was found that the NRMSE values of Tween 80 (5 %) in the flushings performed in both environments varied between 0.079 and 0.227; R^2 values were found to vary between 0.63 and 0.92. Among other DNAPL components, the highest mean error in flushing with Tween 80 and the lowest correlation between experimental data and model results is seen in the case of PCE, but the best correlation is with TCE. Again, in both environments, the NRMSE values in the flushings with SDS (5 %) varied between 0.092 and 0.216; R^2 values were found to vary between 0.65 and 0.90. In flushing with SDS, the relationship between experimental data and model results was found to be most inconsistent in the case of PCE, and the component with the best correlation was TCE. NRMSE values ranged between 0.083 and 0.335; while R^2 values were found to vary between 0.73 and 0.87. TCE with 5 % MCD while the worse correlation was obtained with PCE.

It was observed that the NRMSE values obtained in flushing with water in both porous media varied between 0.147 and 0.239, and the correlation coefficients were observed to be quite low for PCE (R^2= 0.27) and DCE (R^2= 0.38) in water flushing in silica sand (Figure 4.36). A low correlation between experimental data and model results was observed only for PCE (R^2= 0.31) in water flushing in natural soil (Figure 4.37). These results suggest that the DNAPL mixture behavior model is more

affected by the properties of DNAPL components than the heterogeneity of natural soil. Moreover, they point to the challenges of simulating the remediation when DNAPL mixtures are present. Such models require significantly more data to characterize the multiphase system. Moreover, the experimental data needed to calibrate the model are more difficult to find.

The most suitable mass transfer coefficients are 8 day^{-1} in the simulations with Tween 80 and SDS, 45 and 400 day^{-1} in the simulations with MCD and water, respectively. Sherwood values vary between 0.012 and 0.596 for silica sand, and between 0.002 and 0.104 for natural soil. These values remained within the range of Sherwood values obtained from DNAPL PCE experiments (Table 4.11).

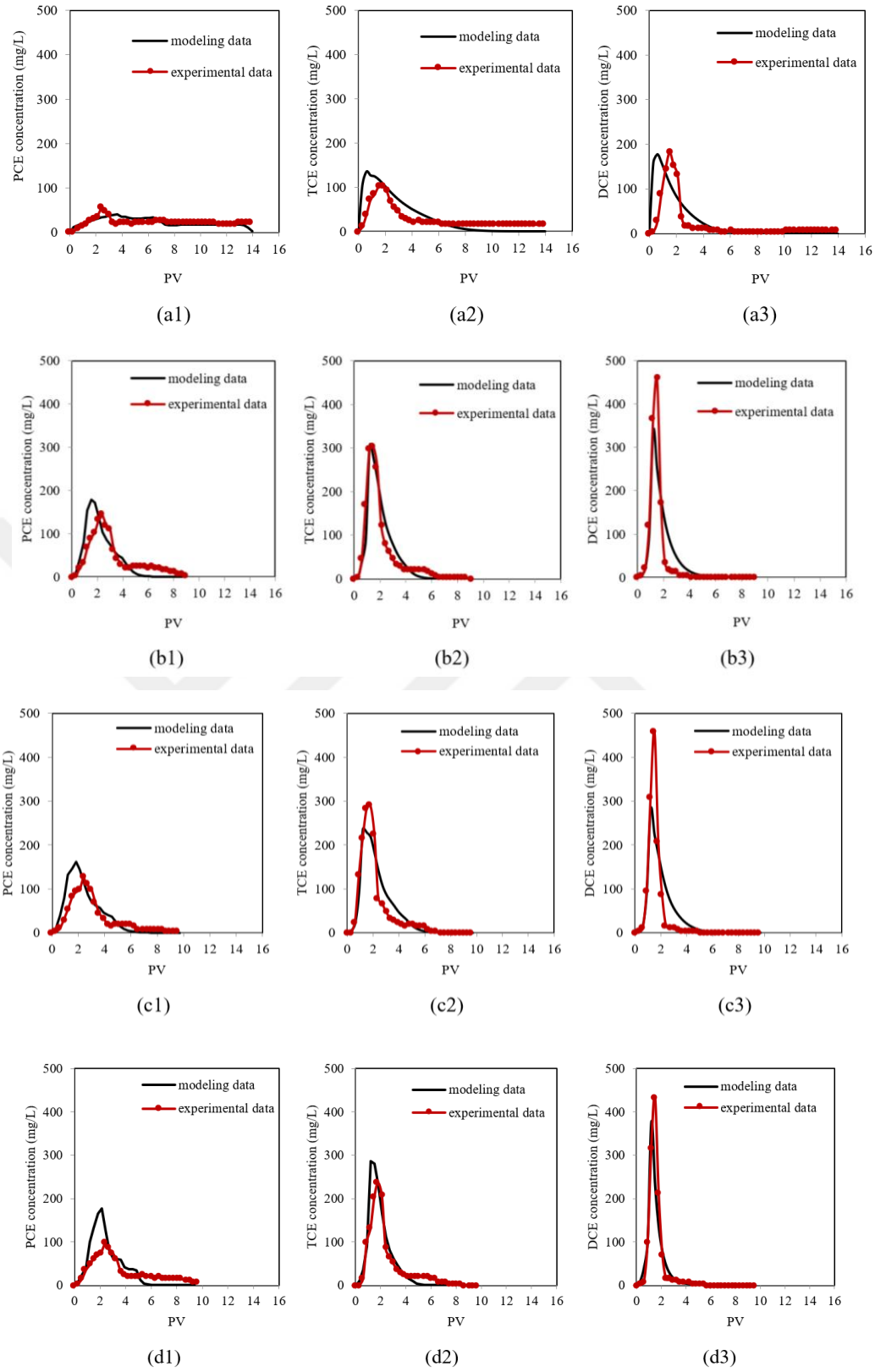

Figure 4.36. Comparison between the best-fit enhanced solubilization model data and the experimental data obtained in silica sand (1PV=2.38 hours); (a) water flushing; (a1) PCE, (a2) TCE, (a3) DCE, (b) Tween 80 (5 %) flushing; (b1) PCE, (b2) TCE, (b3) DCE, (c) SDS (5%) flushing; (c1) PCE, (c2) TCE, (c3) DCE, (d) MCD (5 %) flushing; (d1) PCE, (d2) TCE, (d3) DCE.

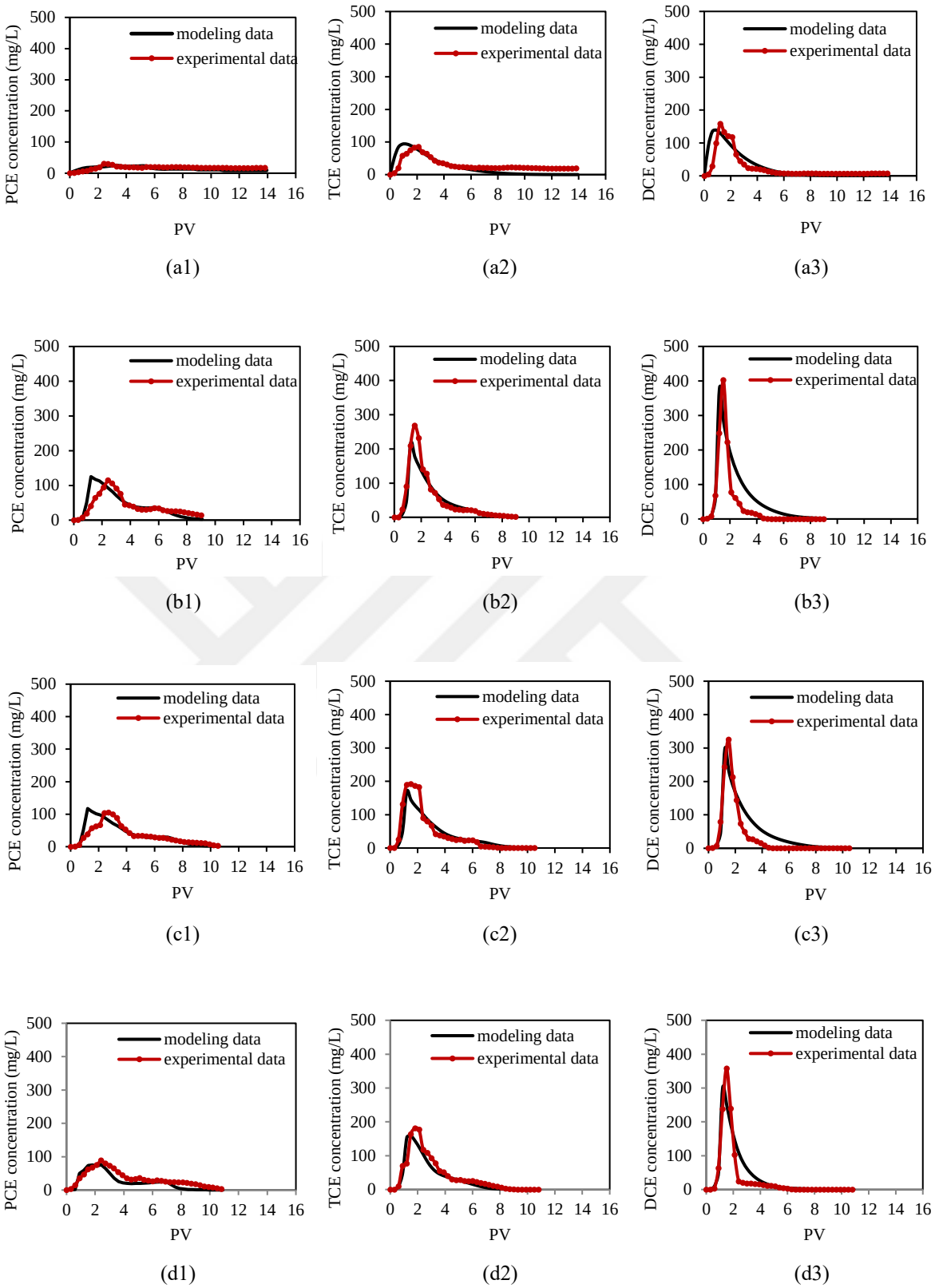

Figure 4.37. Comparison between the best-fit enhanced solubilization model data and the experimental data obtained in calcareous soil (1PV=2.44 hours); (a) water flushing; (a1) PCE, (a2) TCE, (a3) DCE, (b) Tween 80 (5 %) flushing; (b1) PCE, (b2) TCE, (b3) DCE, (c) SDS (5 %) flushing; (c1) PCE, (c2) TCE, (c3) DCE, (d) MCD (5 %) flushing; (d1) PCE, (d2) TCE, (d3) DCE.

Table 4.17. Best-fit mass transfer coefficients and NRMSE for DNAPL mixture enhanced solubilization models in silica sand.

Flushing agent	Mass transfer coefficient (day^{-1})	Sh′ [a]	NRMSE			R^2		
			PCE	TCE	DCE	PCE	TCE	DCE
water	400	0.596	0.159	0.239	0.185	0.27	0.60	0.38
Tween 80 (5 %)	8	0.012	0.227	0.079	0.101	0.66	0.92	0.84
SDS (5 %)	8	0.012	0.216	0.092	0.104	0.73	0.90	0.80
MCD (5 %)	45	0.067	0.335	0.139	0.094	0.73	0.85	0.84

[a] calculated using Equation 3.10 for dm=0.359 mm and $D=10^{-9}$ m^2/s

Table 4.18. Best-fit mass transfer coefficients and NRMSE for DNAPL mixture enhanced solubilization models in calcareous soil.

Flushing agent	Mass transfer coefficient (day^{-1})	Sh′ [b]	NRMSE			R^2		
			PCE	TCE	DCE	PCE	TCE	DCE
water	400	0.104	0.196	0.222	0.147	0.31	0.67	0.69
Tween 80 (5 %)	8	0.002	0.196	0.09	0.118	0.63	0.92	0.79
SDS (5 %)	8	0.002	0.191	0.120	0.098	0.65	0.89	0.85
MCD (5 %)	45	0.011	0.158	0.108	0.083	0.82	0.87	0.86

[b] calculated using Equation 3.10 for dm=0.150 mm and $D=10^{-9}$ m^2/s

4.3. In-Situ Potassium Permanganate Oxidation Coupled with Enhanced Solubilization of DNAPL PCE

In this section, flow-cell flushing experiments were conducted to examine the effectiveness of combining enhanced solubilization with ISCO for the treatment of DNAPL in pooled form. The DNAPL used in these experiments is PCE. The chemical oxidant is potassium permanganate while the enhanced dissolution agent is the surfactant Tween 80. The flushing experiments were also used to examine the impact of MnO_4^- oxidation, both in the presence and absence of Tween 80, on the mass-flux reduction/mass-removal behavior relationship. The experiments were also modeled by

modifying the UTCHEM program which has not been used previously to model the synergy of these two technologies- enhanced solubilization and ISCO.

Flow-cell experiments were conducted to determine the performance of permanganate and Tween 80-enhanced permanganate oxidation for pool-dominated PCE sources zones entrapped in porous media (Figure 4.38). The flow-cell experimental procedure, properties of the flow-cell and porous media used in the experiments are given in chapter 3, Section 3.4.1. A total of four flushing experiments were performed which are shown in Table 4.19. For comparison purposes, the results of 2 additional experiments (PCE dissolution in water and in 2.5 % Tween 80) that were presented in the previous section are also included in this section.

Table 4.19. List of Tween 80 enhanced permanganate oxidation of DNAPL PCE flushing experiments.

	Media	Flushing type	v (cm/h)	Flushing reagent
1	Silica sand	Intermittent	10	MnO_4^-
2	Silica sand	Intermittent	10	Tween 80/ MnO_4^-
3	Calcareous soil	Intermittent	10	MnO_4^-
4	Calcareous soil	Intermittent	10	Tween 80/ MnO_4^-



(a)



(b)

Figure 4.38. Image of organic-liquid initial distribution in flow-cell prior to flushing. (a) First configuration (sand), (b) Second configuration (calcareous soil).

4.3.1. Contaminant Elution Behavior

Figure 4.39 shows the effluent aqueous phase PCE concentrations for the water and Tween 80 flushing experiments obtained from the previous section. The effluent PCE and chloride concentrations from the permanganate experiments with silica sand (Experiment 1 and 2) and natural soil (Experiments 3 and 4) are presented in Figure 4.40 and 4.41, respectively. For water flushing, PCE effluent concentrations peak after about 1-2 PV, followed by a gradual decrease in the concentrations extending to the end of the experiments. It is observed that the effluent PCE concentrations were lower than its aqueous solubility (206 mg/L) since only a fraction of the injection water comes in contact with the DNAPL. For the natural soil, the effluent concentrations were slightly

lower than those from the silica sand configuration with peak concentration of 76 mg/L for the natural soil compared to 94 mg/L for the silica sand.

For the Tween 80 flushing experiments, the peak effluent PCE concentrations for the silica sand and natural soil, were 270 mg/L and 233 mg/L, respectively, both exceeding the water solubility. The effluent PCE exhibited a multi-step concentration elution behavior. Following the peak concentration, the effluent decreased to about 60-80 mg/L at about 5 PV. A near steady-state period is observed until PV=14-16 when the concentrations dropped sharply to below 1 mg/L. Similar multi-step behavior was observed in other DNAPL flushing experiments for both water and enhanced dissolution conditions (Russo et al, 2009; DiFilippo et al, 2010; Mahal et al, 2010; Akyol and Turkkan, 2018; Demiray et al, 2021). This non-ideal behavior is attributed to the entrapment of DNAPL mass in less-hydraulically accessible zones and the complex pore-scale flow field surrounding the DNAPL zone.

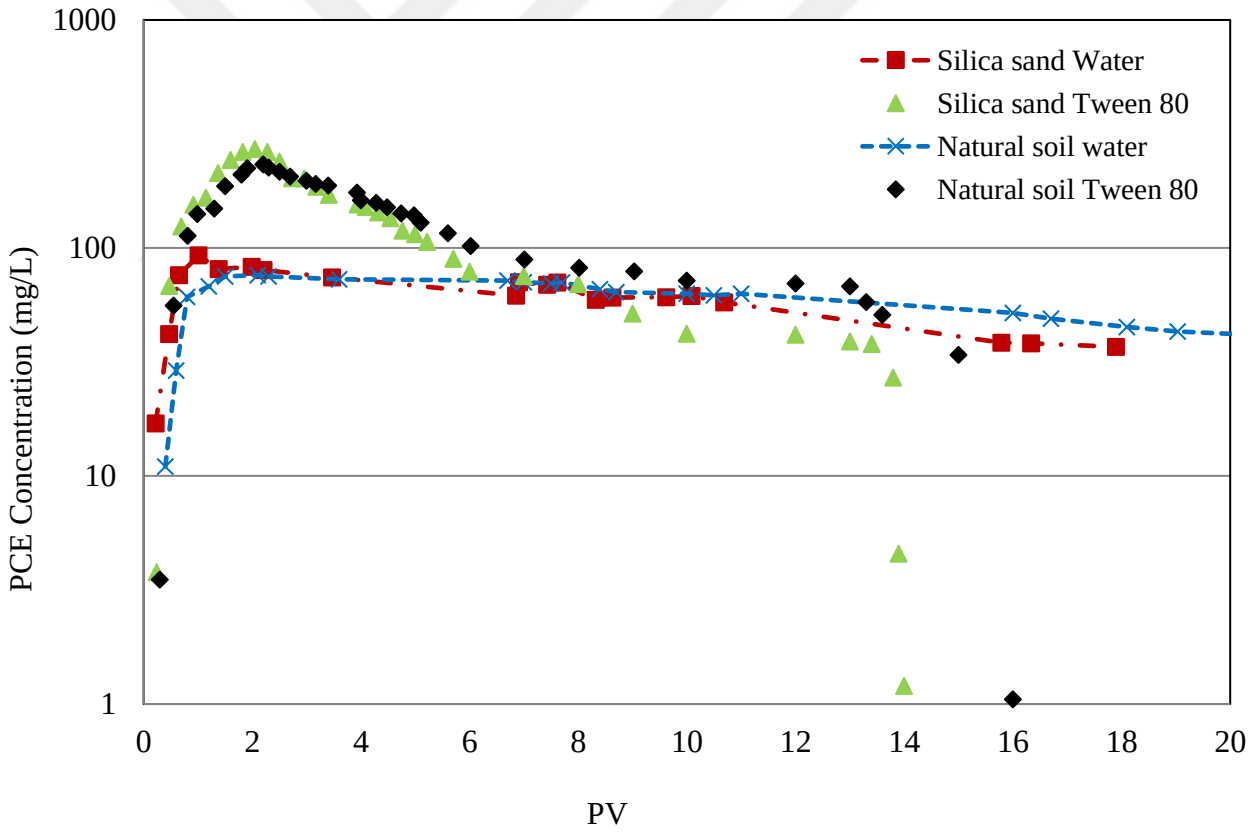

Figure 4.39. Effluent PCE concentration as a function of PV with water flood and with Tween 80 solution in silica sand, with water flood and with Tween 80 solution in natural soil (log scale).

In permanganate flushing experiments, the PCE source was flushed by a 45 mM MnO_4^- solution for 1.25 PV (3 hours). The flow was subsequently halted for a period of 4 days to allow for sufficient

reaction time, followed by water flushing. During water flushing, the elution PCE concentration was initially about 80 mg/L and remained steady for about 4 PV of flushing. The PCE concentration dropped below 1 mg/L after 9.2 and 10.5 PV of water flushing for both the silica sand (Figure 4.40) and natural soil configurations (Figure 4.41). Effluent chloride concentrations, which are indicative of the progression of the oxidation reaction, reached a maximum of 55 mg/L for the sand experiment before dropping to below its detection limit (DL) after about 9.5 PV of total flushing (Figure 4.40). The peak effluent chloride concentration for the natural soil was slightly lower at 49 mg/L before dropping to below DL after about 10.5 PV of total flushing (Figure 4.41). Additionally, the eluted pH dropped from 7.5 to 6.8 in silica sand and 6.1 in natural soil, while permanganate was not detected in the effluent. Overall little difference was observed between both porous media configurations probably due to the halting of the flow which allowed for the reaction to proceed for both configurations. Moreover, comparison of the results of permanganate flushing to Tween 80 enhanced dissolution indicates that the remediation of the PCE source zone by permanganate oxidation took almost 5 PV less than the Tween 80 flushing alone (9-10 PV for the permanganate experiments compared to 14-16 PV for Tween 80).

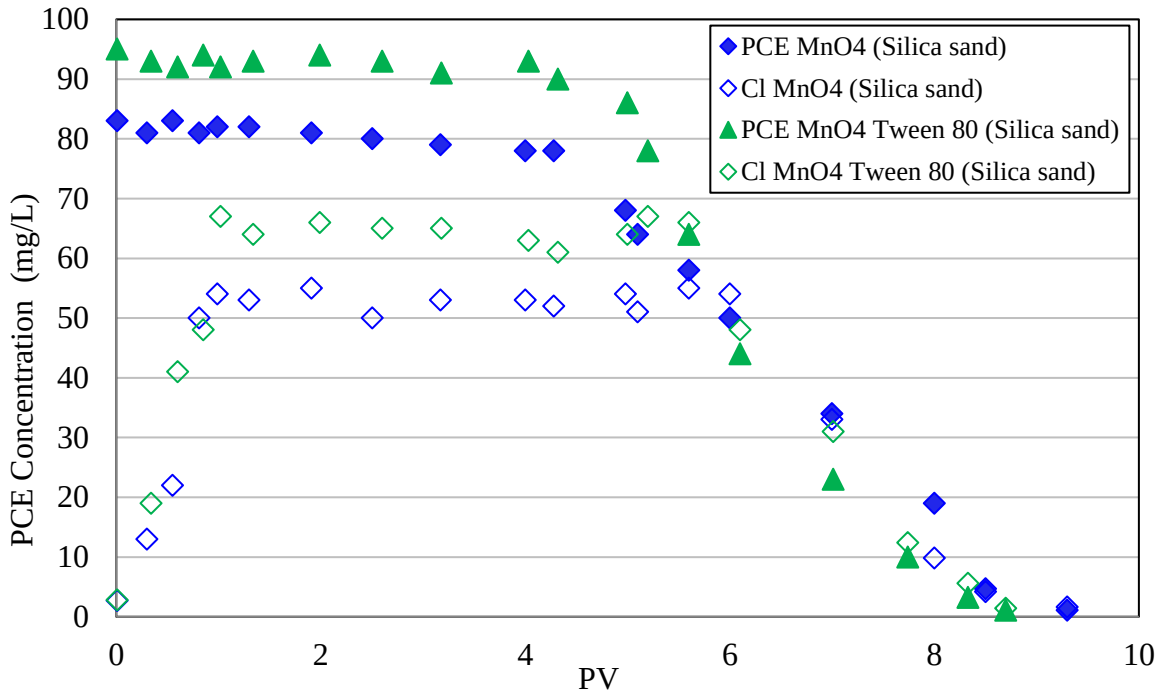

Figure 4.40. Effluent PCE and Chloride ion (Cl^-) concentrations as a function PV for permanganate and Tween 80 enhanced permanganate flushing experiments in silica sand (1PV = 2.38 hours).

In Tween 80 enhanced permanganate flushing experiments, the pooled PCE source zone was flushed with a Tween 80/MnO_4^- mixture (2.5 % Tween 80 in 45 mM MnO_4^-) for 1.25 PV (3 hours).

As in previous experiments, flow was interrupted for 4 days, followed by water flushing. The peak PCE concentration was approximately 95 and 85 mg/L for the sand and natural soil configurations, respectively. The concentrations remained steady for 5 PV, dropping to below 1 mg/L after about 9 PV of total water flushing (Figure 4.40 and 4.41). In parallel, the peak chloride concentrations were about 60-65 mg/L dropping about the same time as the PCE concentrations. The pH of the eluted solution dropped from 7.5 to 6.1-6.9, with no permanganate detected in the effluent. Comparison of the results of Tween 80 enhanced permanganate flushing and permanganate only flushing experiments indicates that when MnO_4^- and Tween 80/MnO_4^- were pulse injected into the PCE source zones to increase the contact time, the presence of Tween 80 enhanced the solubilization of PCE aqueous concentrations leading to enhanced oxidation of PCE by permanganate. The results also showed that the time of remediation for Tween 80/MnO_4^- experiments was faster than oxidation alone by about 1 PV, demonstrating the improved performance of Tween 80/MnO_4^- flooding scenario. However, chloride concentrations, which are a measure of the oxidation reaction, showed a moderate increase compared to the enhanced dissolution of PCE suggesting that the Tween 80 may be interfering with PCE oxidation. This is examined further in the modeling section (Section 4.3.2). Results of these experiments also reveal the complexities of flushing-based technologies, highlighting the importance of preliminary testing to evaluate the efficacy of DNAPL remediation prior to actual implementation of any remedial activity in the field.

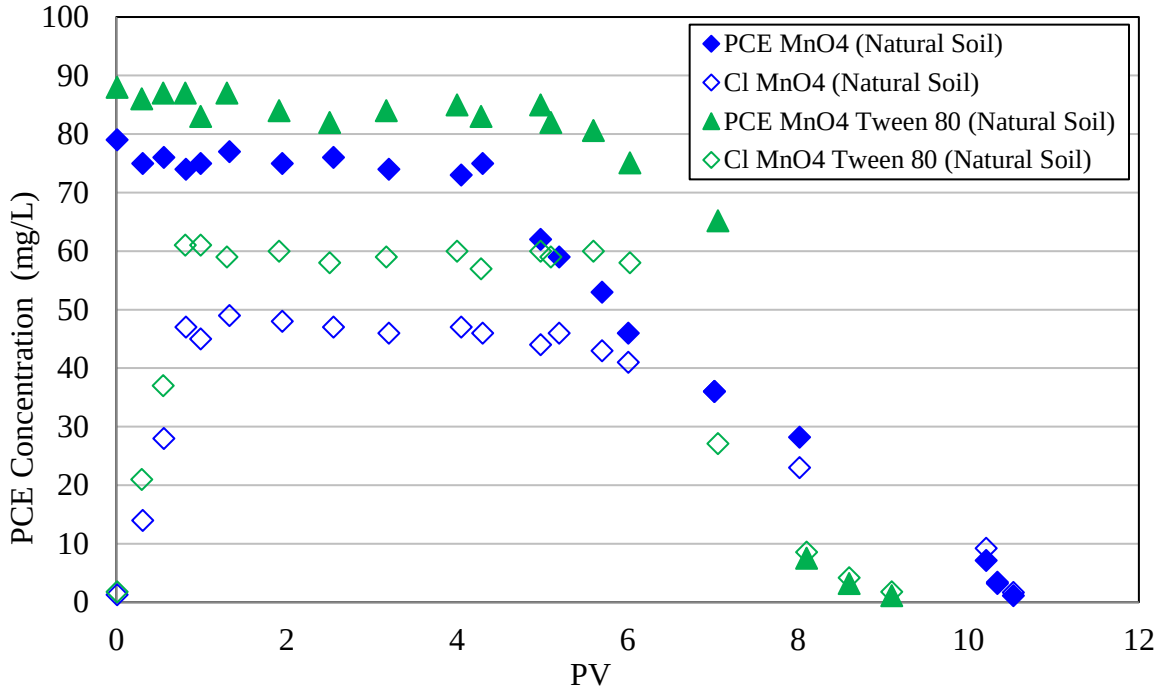

Figure 4.41. Effluent PCE and Chloride ion (Cl^-) concentrations as a function PV for permanganate and Tween 80 enhanced permanganate flushing experiments in calcareous soil (1 PV = 2.44 hours).

4.3.1.1. Mass Flux Reduction-Mass Removal

Figure 4.42 presents the MR-MFR relationships for permanganate and Tween 80-enhanced permanganate oxidation experiments. These two experiments were performed with the silica sand and natural soil configurations and pulse injection to increase the contact time between the oxidant and DNAPL. The two experiments that were obtained in the previous section, the water and Tween 80 enhanced solubilization results are also included in Figure 4.42.

As noted in Equation (3.7), in the calculation of the remaining DNAPL mass fraction was used the effluent chloride concentration to estimate the oxidized DNAPL mass. Overall, the MR-MFR curve for these two experiments shows a clear increase in the efficiency relative to the water and Tween 80 flushing experiments. When water flooding was applied after the pulse permanganate injections in both the silica sand and calcareous soil experiments, the resulting effluent concentrations exhibited steady-state behavior (Figure 4.40, 4.41) in contrast to the water and Tween 80 only flushing experiments. This causes the MR-MFR curves to remain close to the x-axis until the end of experiments, indicating more efficient remediation. A slightly more ideal behavior is observed for the less heterogeneous silica sand. The small difference between these two sets of curves is attributed to the moderate heterogeneity of the natural soil and the relatively long contact time between the oxidant and the DNAPL due to the halting of the flow leading to greater oxidation of the DNAPL.

The highest efficiencies were obtained for both porous media configurations when surfactant-enhanced dissolution was combined with in-situ oxidation (experiments with Tween 80 enhanced permanganate flushing in both configurations). These experiments yielded higher dissolution rates that allowed for the reactions to proceed more rapidly as seen from the higher chloride levels in the effluent and higher effluent PCE concentrations in the aqueous phase, with both of these processes contributing to the enhanced DNAPL mass removal efficiency from the porous media. The MR-MFR behavior for Tween 80-enhanced permanganate oxidation experiments would be expected to depend on the distribution of PCE source zones and physical heterogeneity. This however can be somewhat compensated by allowing longer contact time between the DNAPL on one hand and the dissolution and oxidation reagents on the other hand which tends to enhance both dissolution and DNAPL oxidation. The results of these experiments highlight the higher efficacy of ISCO pulsed injections as compared to continuous injection scenarios.

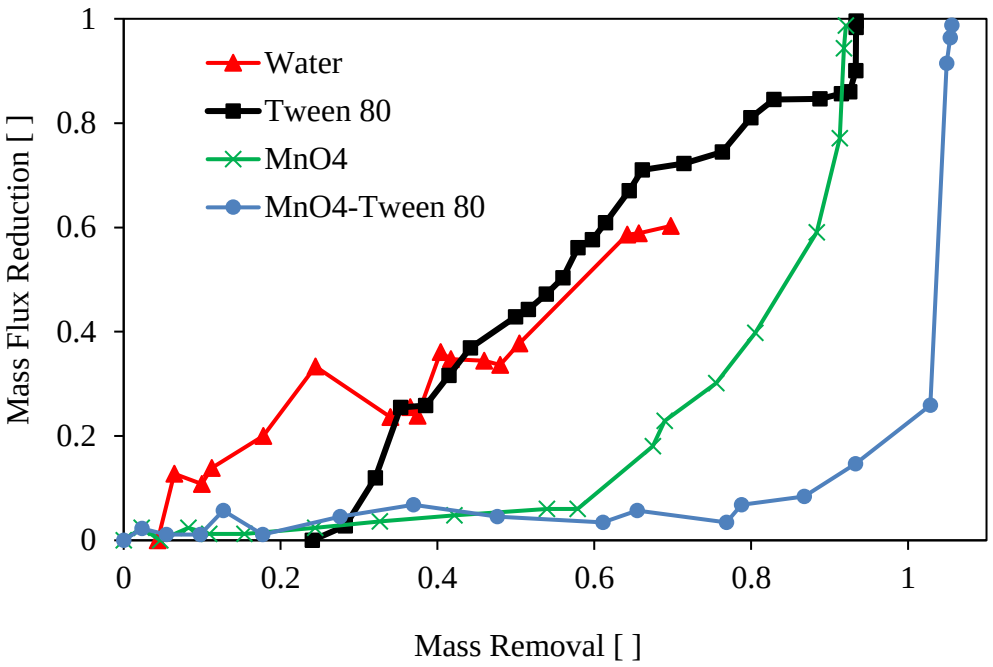

(a)

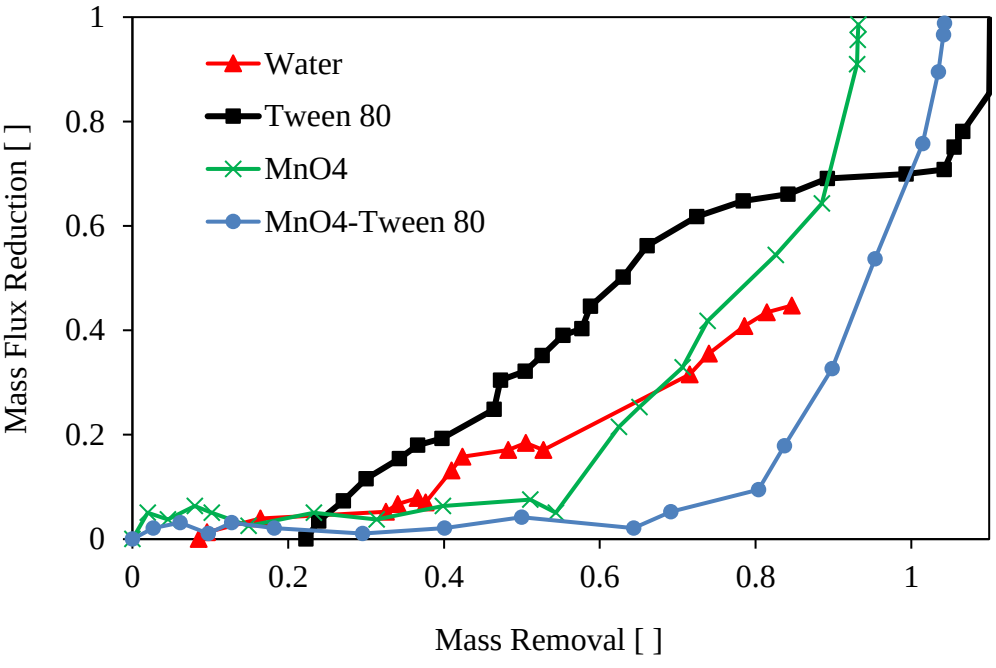

(b)

Figure 4.42. PCE mass-flux reduction versus mass removal behavior for the (i) water, (ii) Tween 80-enhanced solubilization, (iii) MnO_4^- oxidation and (iv) Tween 80-enhanced MnO_4^- oxidation flushing experiments for a) silica sand and b) natural soil.

4.3.2. Oxidation Model Calibration

The permanganate oxidation experiments described in the previous section were simulated with the UTCHEM multiphase model. A total of four DNAPL PCE oxidation experiments were simulated: permanganate with/without Tween 80 in both porous media. The model simulations included the 3 stages of the ISCO experiments: the first stage comprised of injecting the flow-cell 45 mM $KMnO_4$ solution for 3 hours; the second stage corresponded to flow interruption for four days to allow more time for the reaction to proceed; the third stage consisted of flushing the flow-cell with water until the end of the experiment. The parameters used in the oxidation model are listed in Table 4.20.

Table 4.20. List of key parameters used in the model simulations.

Porosity	
Silica sand	Flow zone: 0.36 (d_{50} = 359 μm) Impermeable zone: 0.38 (d_{50} = 172 μm)
Natural soil	Flow zone: 0.58 (d_{50} = 150 μm) Impermeable zone: 0.38 (< 76 μm)
Bulk density (ρ_b)	
Silica sand	1.74 g/cm^3
Natural soil	1.35 g/cm^3
Intrinsic permeability	
Silica sand	Flow zone: 20 darcy Impermeable zone: 2 darcy
Natural soil	Flow zone: 20 darcy Impermeable zone: 0.02 darcy
Longitudinal dispersivity	
Silica sand	0.02 m[a]
Natural soil	0.04 m[a]
DNAPL PCE solubility	
in water	0.206[b] g/L
in Tween 80 (2.5%)	10.5[c] g/L
DNAPL PCE aqueous phase interfacial tension	45 mN/m
Critical Micelle Concentration (CMC)	0.035[e] g/L
Capillary pressure parameters	λ=2[g], P_{bl} = 5.032 kPa
Residual Saturation	
low capillary number	S_r = 0.13[h] for all phases
high capillary number	S_r = 0.05[h] for all phases
Relative permeability (Brooks-Corey)	
Endpoint relative permeability ( )	
NAPL phase	$k^o_{r,l}$ = 0.46[I]
Flushing solution	$k^o_{r,l}$ = 0.46[I]
exponent (e_l)	
NAPL phase	e_l = 4 [I]
Flushing solution	e_l = 4 [I]

[a] Longitudinal dispersivity determined from tracer test; [b]Horvath et al (1999); [c] Enhanced solubility values determined from batch experiments; [d] Li and Fu (1992); [e] Zhong et al (2003); [f] Boving and Brusseau (2000); [g] Brooks and Corey (1966); [h]Shah et al (1995); [I] Corey (1994)

Appendix B provides a sample input file of the model. Examination of the spatial and temporal distributions of the simulated PCE concentrations showed that the injection of the permanganate or Tween 80/permanganate solutions into the flow-cell during the first stage initiated the PCE dissolution and oxidation processes. During the second stage when the flow was halted, dissolved DNAPL moved away from the DNAPL source zone due to lateral diffusion, allowing it to react further with permanganate. The presence of Tween 80 accelerated the dissolution process of DNAPL and led to a greater reaction between DNAPL and permanganate. During the final stage which comprises of flushing with water, the PCE effluent concentrations, due to the presence of Tween 80, reached higher values than flushing with only the permanganate solution.

The simulated and experimental effluent PCE concentrations as a function of time are shown in Figure 4.43(a-d) for the 4 experiments. All stages (there was no effluent PCE in stages 1 and 2, only stage 3) are depicted in Figure 4.43. The agreement between the simulated and observed concentrations are generally good. Table 4.21 presents the values of the best-fit reaction rate constant along with the NRMSE and the coefficient of determination R^2 for the different experiments. The NRMSE values are low, ranging between 0.083 and 0.182 while R^2 values were found to vary between 0.914 and 0.938. The reaction rate constants (K_o, Equation 3.16) are reported in Table 4.21 in units of L/g/day and 1/M-s. It is observed that the reaction rate constants are lower for experiments conducted in natural soil compared to that in silica sand. This is attributed to the heterogeneity of the calcareous soil compared to silica sand that reduces the contact between the remedial solutions and the DNAPL and the potential oxidation of the natural matter in the soil by the permanganate (e.g., Akyol and Yolcubal, 2013). The reaction rate constants obtained in the current study are consistent with values reported in literature. For example, Zhai et al (2006) reported reaction rate constants ranging between 0.031-0.043 1/M-s. These rates were determined from batch tests- which would be expected to yield larger rates than tank flushing experiments- conducted with PCE, permanganate, in the presence of acetone and TBA co-solvents.

Finally, an important finding of this analysis is that the reaction rate constants with permanganate only are about an order of magnitude lower than the corresponding reaction rates determined from the experiments with Tween 80 and permanganate for both silica sand and natural soil. The observed reduced oxidation reaction rates in the presence of Tween 80 is an indication of the interference of the Tween 80 in the reaction rate. Other studies have reported similar interferences, albeit using other reagent combinations. For example, Tsai et al (2009b) and Xu et al (2022) both reported reduced reactivity for PCE and TCE oxidation with persulfate in the presence of surfactants SDS and Tween 80. DNAPL oxidation by persulfate was inhibited in the presence of high surfactant concentrations.

Nonetheless, the much higher aqueous phase concentration in the presence of Tween 80 more than compensates for the reduced concentration.

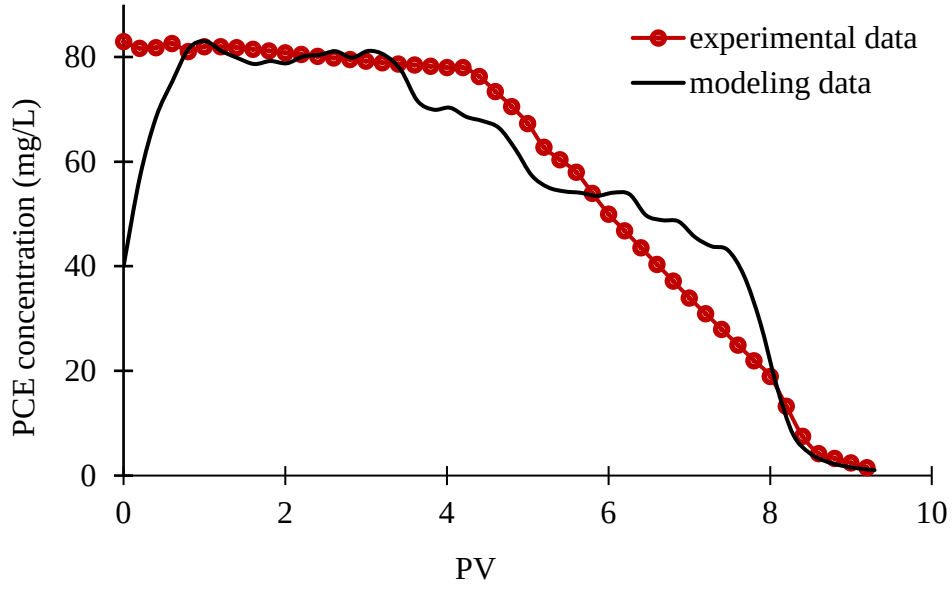

(a)

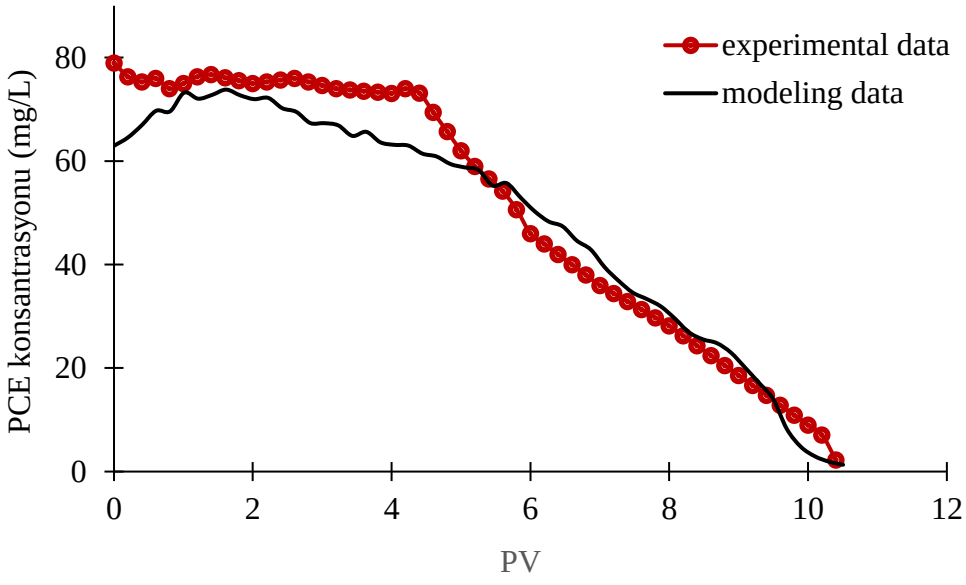

(b)

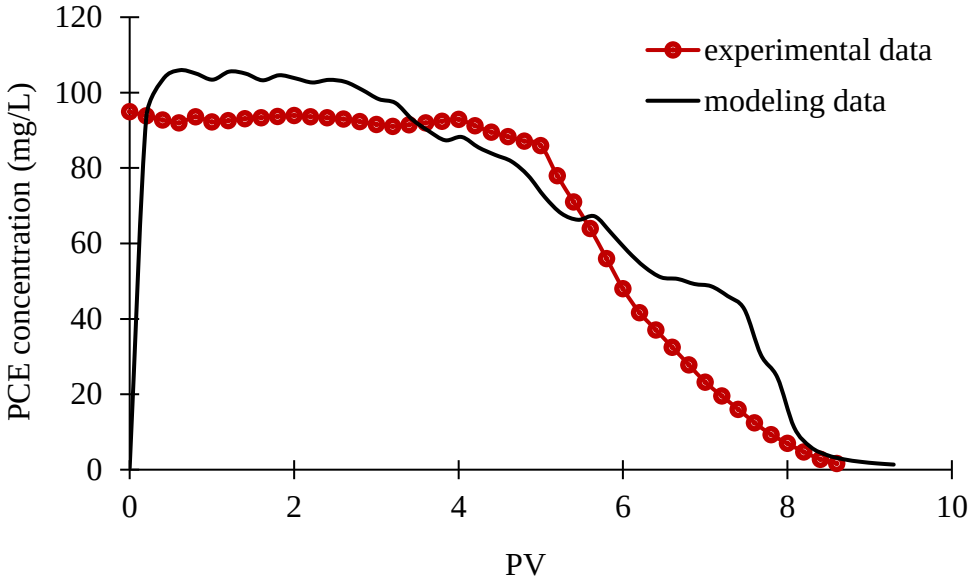

(c)

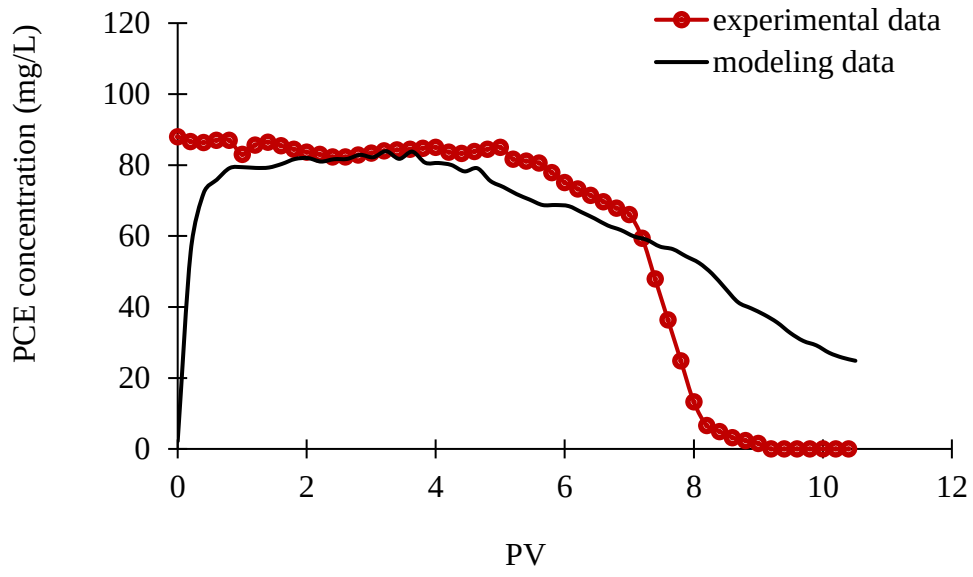

(d)

Figure 4.43. Comparison of experimental and simulated effluent PCE concentrations including stage 1; chemical flushing, stage 2; interruption, stage 3; water flushing for (a) permanganate flushing in silica sand, (b) permanganate flushing in natural soil, (c) Tween 80 enhanced permanganate flushing in silica sand, (d) Tween 80 enhanced permanganate flushing in natural soil.

Table 4.21. Best-fit oxidation reaction rate constant (K_o) and corresponding fitting statistics. The percentages of recovered and oxidized DNAPL mass are also given.

Experiment	Reaction Rate Constant		Recovered DNAPL mass	Oxidized DNAPL mass	NRMSE	R^2
	L/g/day	M^{-1} s^{-1}	%	%		
Silica sand $KMnO_4$	6.8	0.013	37.1	62.9	0.083	0.929
Natural Soil $KMnO_4$	1.5	0.0028	37.1	62.9	0.091	0.938
Silica Sand $KMnO_4$ + Tween 80	0.76	0.0015	42.8	57.2	0.111	0.914
Natural Soil $KMnO_4$ + Tween 80	0.12	0.0002	47.07	52.93	0.182	0.928

4.4. Sodium Persulfate Oxidation Coupled with Enhanced Solubilization of DNAPL PCE

In this section, the performance of sodium persulfate ($Na_2S_2O_8$) for the in-situ oxidation of DNAPLs entrapped in porous media is evaluated. The study covers batch reactivity and flow-cell experiments conducted at the Institute of Environmental Science laboratory of Bogazici University and at the Contaminant Transport Laboratory at the University of Alabama. As persulfate must be activated before it becomes an effective oxidant, different persulfate activation methods were first investigated for PCE removal. Batch experiments were divided into two classes, iron-activated persulfate and heat-activated persulfate in the presence of PCE. In addition to heat activated persulfate experiments, the effect of simultaneous usage of surfactant with persulfate on PCE removal was also investigated. In addition, batch experiments were conducted on the persulfate consumption of natural soil with control experiments.

In addition to the batch tests, flow-cell flushing experiments were performed using heat activated persulfate. All flow experiments were carried out in silica sand medium.

The batch test and flow-cell experimental results are presented in following sections.

4.4.1. Batch Experiments

4.4.1.1. PCE Degradation with ZVI-Activated Persulfate

The procedure followed for the iron activated persulfate is described in section 3.3.1. Oxidation experiments were performed with aqueous PCE (0.3 mM or 50 mg/L) oxidation in the presence of sodium persulfate (3 mM or 714 mg/L) and 20 mesh ZVI rods (Ward's Science) with 1/10 (solid/liquid) ratio (w/w). Before examining the DNAPL degradation performance, the consumption and product formation potential of the chemicals alone and in combination were examined with control experiments. Reactors were left stable in the absence of horizontal shaker and concentration values were monitored. Results indicated that raw ZVI rods were ineffective in activating persulfate to any noticeable degree. Since working with volatile contaminants requires minimum headspace in reactors, horizontal agitation in normal batch procedures is ineffective. Therefore, a set of reactors was shaken by hand for 1 minute and left stable was made for comparison purposes. Figure 4.44.a shows the consumption of persulfate for different procedures with the ZVI rods. The consumption of persulfate is the same for treated (wet) and untreated (dry) iron, with persulfate consumption of 34 % at the end of 6 hours. In the shaken sample, the consumption reached 87 % at the end of 6 hours. Total production of sulfate and iron as reaction product is also higher in this example than in the other two examples as seen in Figures 4.44.b and 4.44.c.

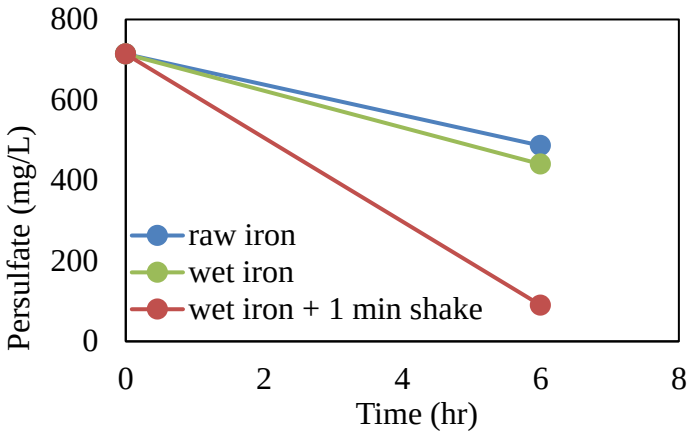

(a)

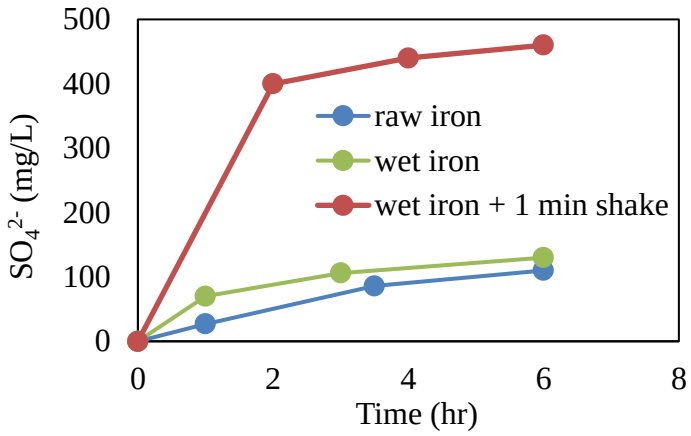

(b)

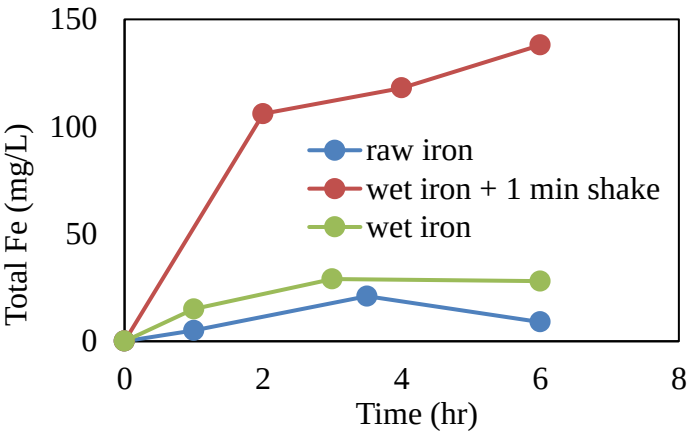

(c)

Figure 4.44. Time-dependent persulfate degradation and product release.

It is observed in control experiments that samples which contain unactivated persulfate only and DI water loaded with ZVI rods reactors were able to degrade PCE at almost the same degree, about 45 % after 6 hours (Figure 4.45.a). PCE control reactor was monitored due to the loss of PCE by volatilization, photochemical decomposition, or other potential mass-loss processes during batch experiments. After 6 hours, the remaining PCE concentration with ZVI activated persulfate was 21.8 mg/L (Figure 4.45.b). This value is close to the PCE oxidation by unactivated persulfate alone (23.15 mg/L after 6 hours). In addition, the persulfate activation with pretreated iron is almost the same in both cases; wet and dry. Removal of iron filings in the middle of the experiments resulted in an immediate start of steady concentration trend (Figure 4.45.b).

The current data were compared with the results obtained by Zhong et al (2015) where the same brand of raw ZVI material was used but with 1,4-Dioxane. Zhong et al (2015) reported rapid reduction of 1,4-Dioxane in the first hours. It is concluded that the degradation rate of DNAPL with persulfate activated by ZVI rods is most likely to depend on the type of organic compound (the contaminant) and that persulfate activated with ZVI rods may not be very effective in oxidizing tetrachloroethene (PCE) (Figure 4.45).

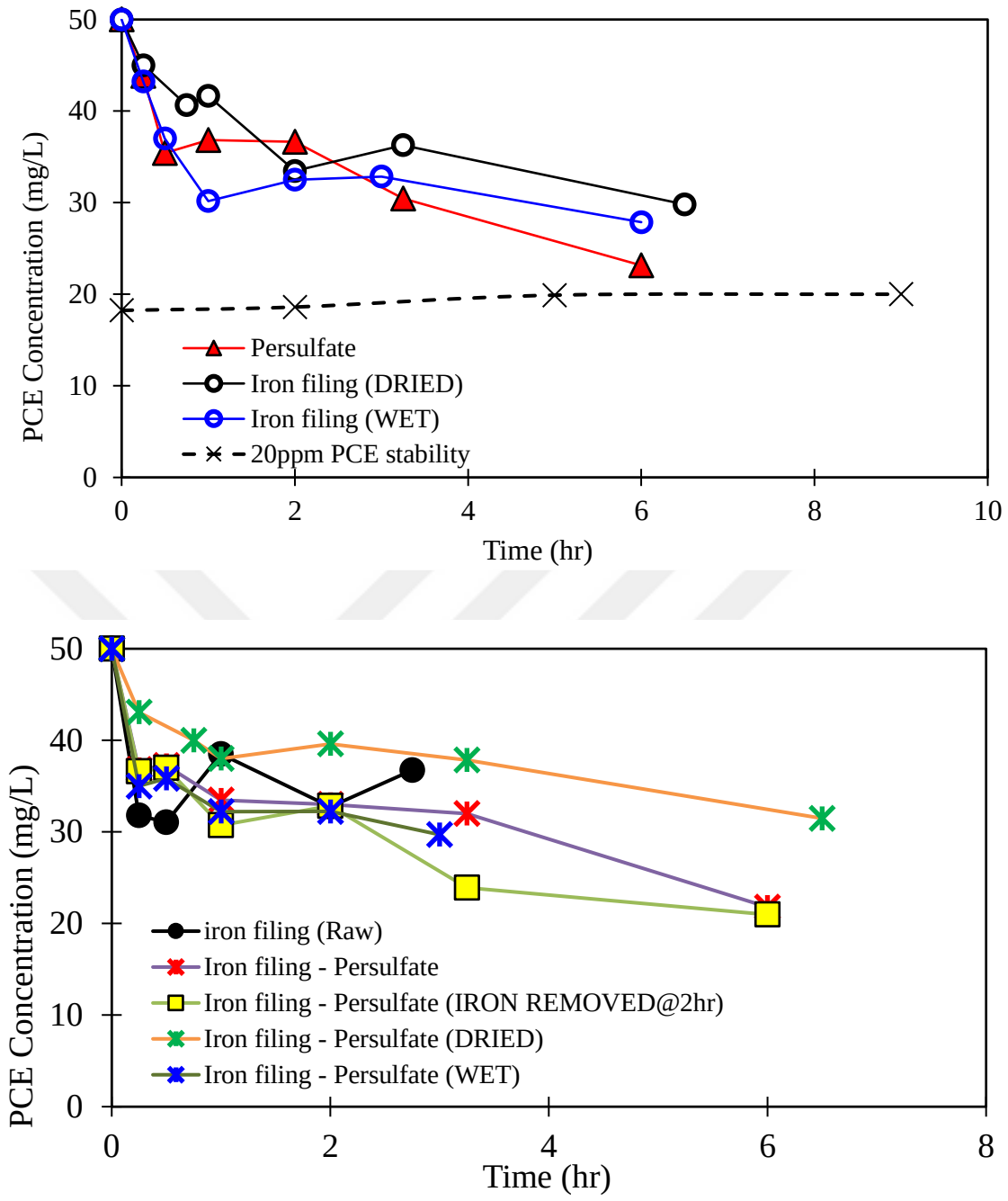

Figure 4.45. PCE degradation in the presence of iron filings .

4.4.1.2. PCE Degradation with Thermally-Activated Persulfate

A range of batch experiments were conducted on the removal of PCE with thermally-activated persulfate. These were performed in both pure and aqueous PCE phases. A summary of batch experimental conditions is shown in Table 4.22. These experiments considered different concentrations of persulfate, a range of molar ratios of DNAPL and persulfate and with/without solubilizing agents. All experiments were performed at 50 ^{o}C.

Table 4.22. Batch experimental conditions for PCE degradation at 50 ºC.

phase	DNAPL amount	Persulfate	DNAPL/Oxidant molar ratio	Solubilizing agent
DNAPL	Excess (1 mL in 40 mL solution)	-	-	-
	Excess (1 mL in 40 mL solution)	-	-	3 CMC Tween80
	Excess (1mL in 40mL solution)	20 mM	-	-
	0.3 mM (50 mg/L)	3 mM (714 mg/L)	1/10	30 % EtOH
	0.3 mM	3 mM	1/10	1 CMC Tween 80
	0.3 mM	3 mM	1/10	3 CMC Tween 80
	0.3 mM	3 mM	1/10	5 CMC Tween 80
	0.3 mM	3 mM	1/10	2.5 % Tween 80
	0.3 mM	3 mM	1/10	-
	0.3 mM (Liquid/Soil, 1/5=w/w)	3 mM	1/10	-
	0.3 mM	3 mM Unactivated	1/10	-
	0.3 mM	6 mM	1/20	-
Aqueous	0.3 mM	6 mM	1/20	-
	0.54 mM (90 mg/L)	20 mM	1/40	-
	0.54 mM	90 mM	1/170	-
	0.54 mM	20 mM	1/40	3 CMC Tween 80
	0.54 mM	20 mM	1/40	10 CMC Tween 80

4.4.1.2.1. Degradation of PCE in the Pure DNAPL Phase

In the first step, it was investigated whether the reaction continues if the heat source is not maintained after the persulfate reaches the target temperature and whether the reactions proceed if the system is allowed to cool back to room temperature. Figure 4.46 shows the PCE aqueous and chloride concentration before and after the removal of the heat source. It was observed that with the decrease in temperature, PCE degradation and Cl^- production slowed down and eventually stopped. This is likely due to the cessation of the formation of sulfate radicals from persulfate activation when the heat source is removed.

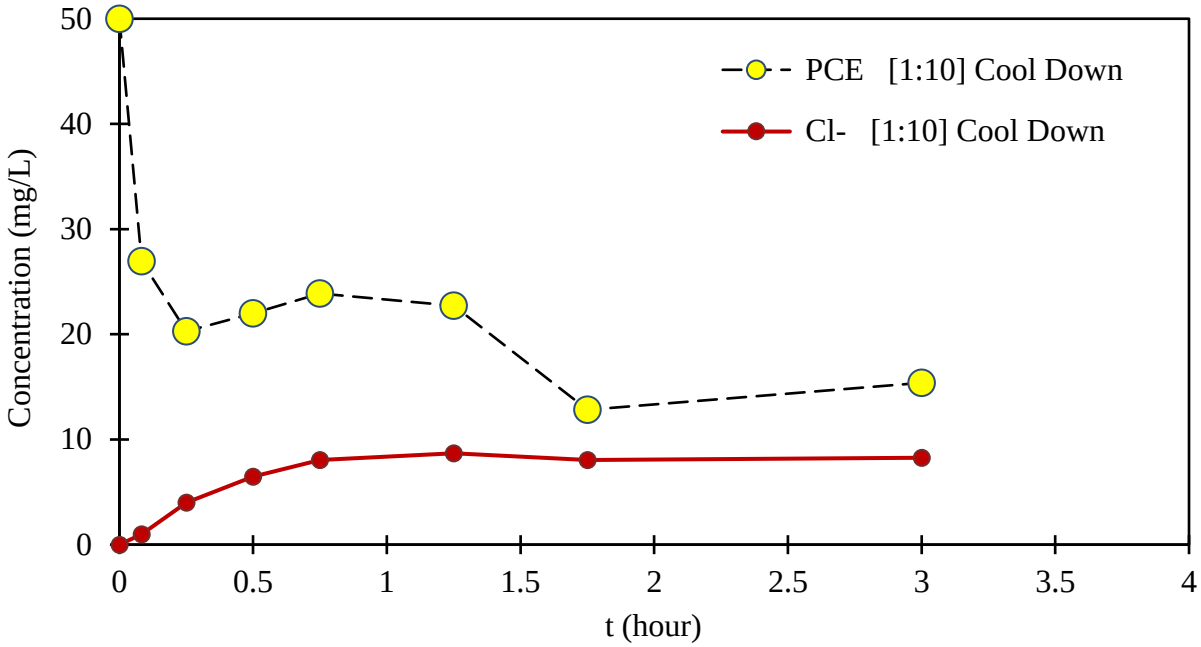

Figure 4.46. Quenching of the reaction in case of the removal of activator (pH: 3.47 - 3.72; ORP: 444 - 489 mV).

Subsequent sets of experiments were carried out to reveal how PCE oxidation kinetics was affected by various persulfate concentrations. The DNAPL PCE/persulfate molar ratio considered was 1/10 and 1/20 based on stochiometry. PCE concentration as a function of time for different persulfate experiments are given in Figure 4.47. Chloride concentration which is an indicator of the progress of the reaction is shown in Figure 4.48. As the initial persulfate concentrations increased from 3 mM to 6 mM, the oxidation rates of PCE also increased with PCE concentration decreasing to zero in almost half the time with no activation, the concentration of PCE remains high. The total amount of chloride ion produced at the end of 3 hours is approximately 35 mg/L for both activated persulfate concentrations (Figure 4.48). Chloride ion was not produced in batch experiments with unactivated persulfate.

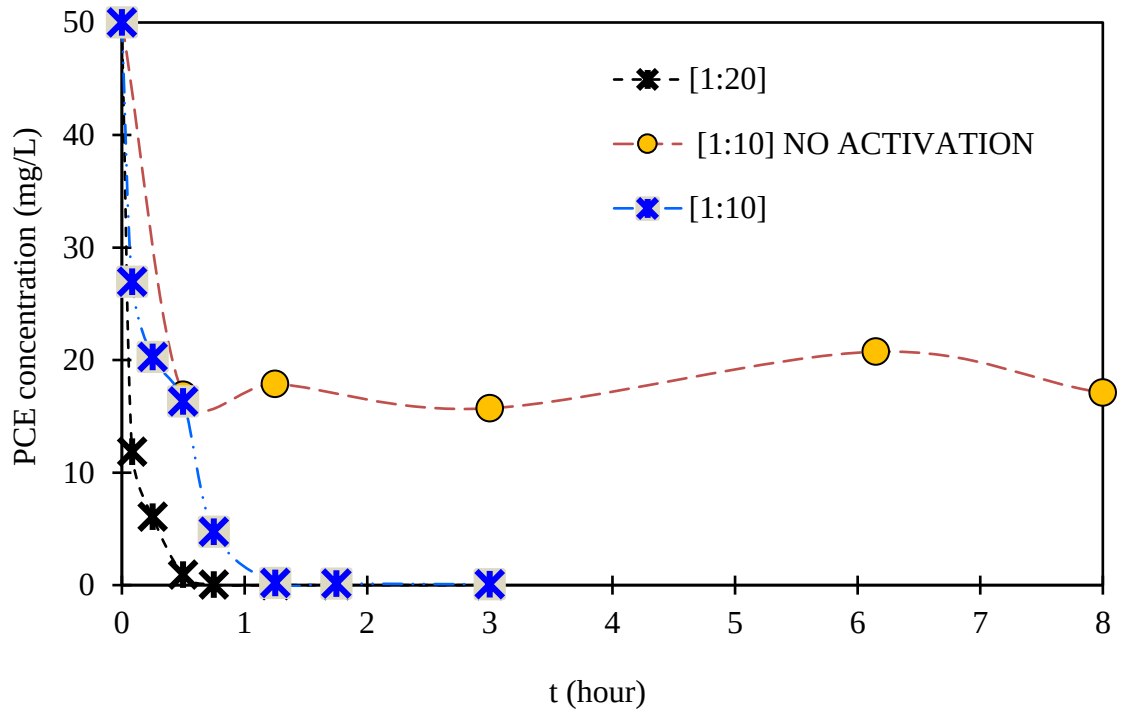

Figure 4.47. Unactivated persulfate DNAPL phase PCE oxidation capability and PCE oxidation in various activated persulfate concentrations.

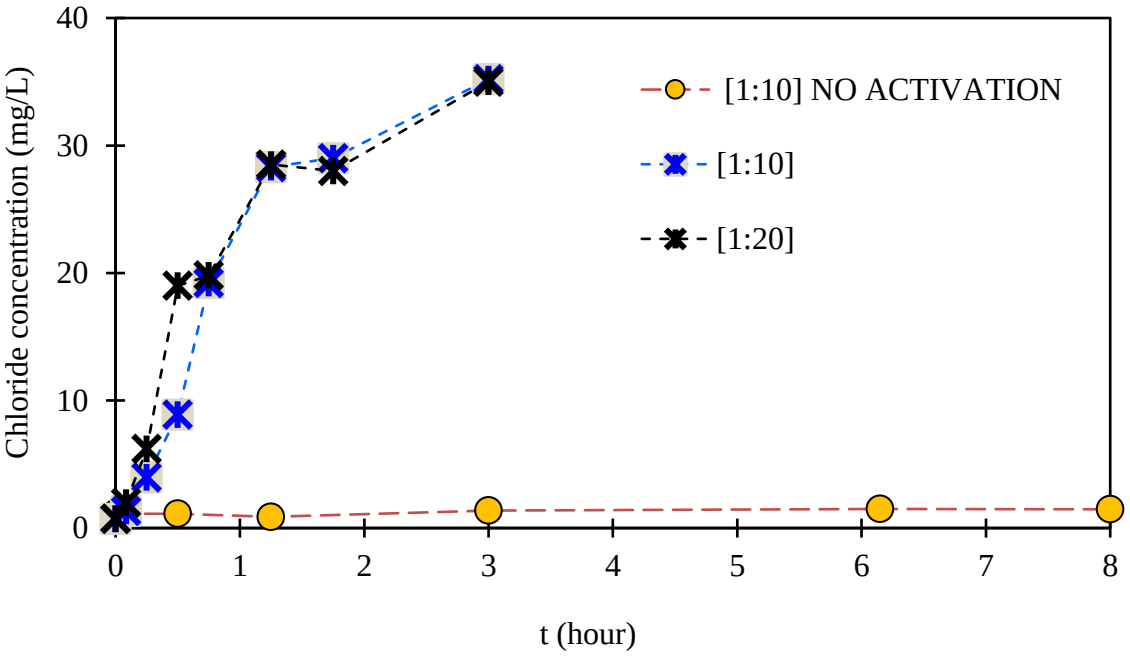

Figure 4.48. Chloride release of DNAPL phase PCE in various persulfate concentration.

Tween 80 enhanced persulfate batch experiments were also conducted to reveal the role of the surfactant in the reaction. At 2.5 % Tween 80, the PCE concentration (Figure 4.49) remains high at

about 17 mg/L. The maximum chloride concentration was 1.75 mg/L throughout the experiment (Figure 4.50). This value is about 10 % of the chloride concentration observed in the absence of Tween 80.

The surfactant effect on oxidation was further investigated by reducing the concentration of Tween 80 in the solution. Specifically, the batch experiment was repeated with CMC, 3 fold of CMC and 5 fold of CMC value. pH, ORP, PCE, and chloride concentrations measured for 8 hours showed that oxidation had taken place, albeit to a small extent. Figure 4.49 shows the aqueous PCE concentration. The corresponding chloride concentrations are shown in Figure 4.50. It is seen that with a decrease in Tween 80 concentration, the oxidation reaction was improved. The pH value decreased from 6.5 to 3 as the experiment progressed, and the ORP value increased from 330 mV to 480 mV. In the oxidation test carried out in natural soil, a decrease in pH values was not observed because the carbonate in the soil acted as a natural buffer and, therefore, the pH value remained in the range of 7.39-8.1 throughout the experiment. As no change was observed in ORP, PCE remained at very low concentrations and no significant chloride production was observed.

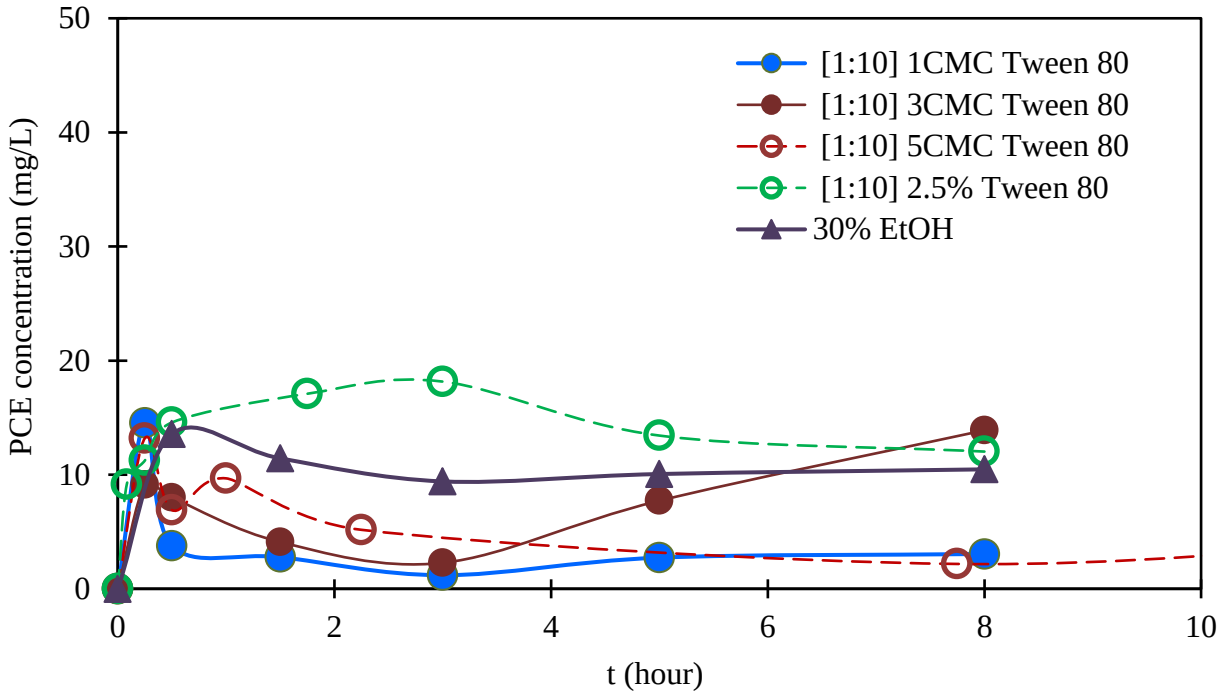

Figure 4.49. DNAPL phase PCE degradation with various concentrations of Tween 80 enhanced persulfate.

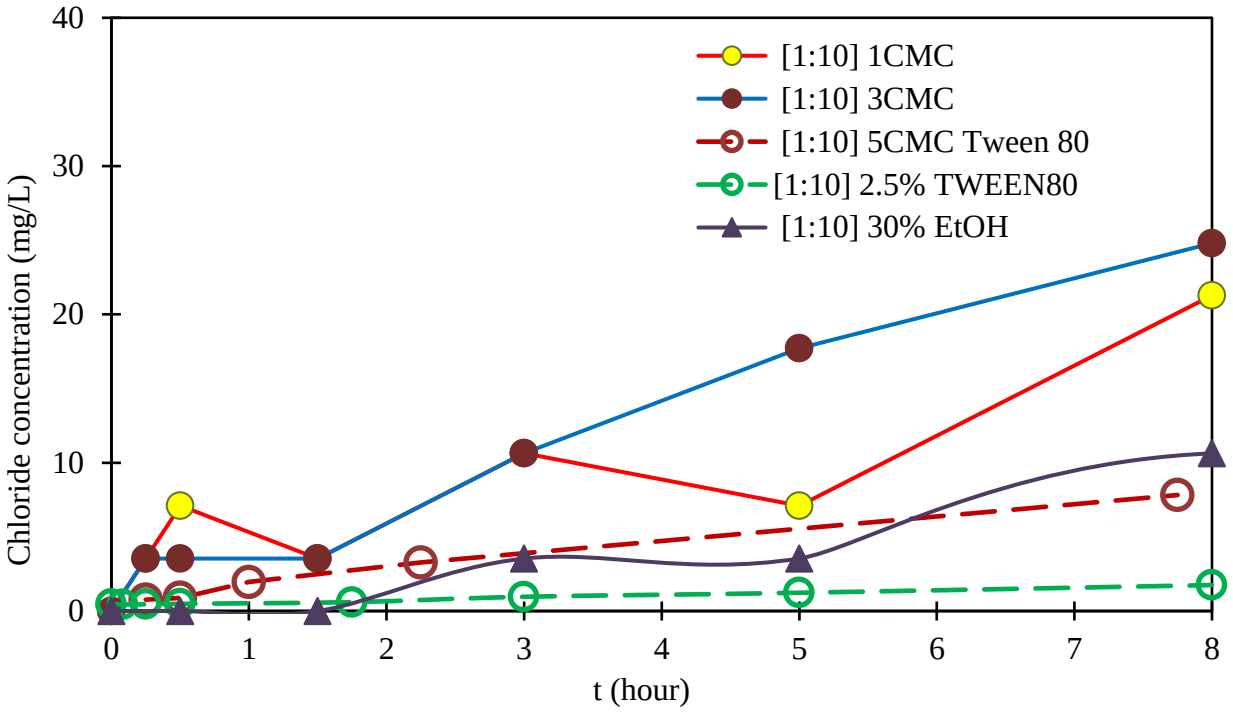

Figure 4.50. Chloride release from DNAPL phase PCE in various Tween 80 enhanced persulfate concentration.

It is reported in the literature that micelles consisting of high-concentration surfactants may interfere in oxidation experiments. Shan et al (2020), drew attention to the importance of surfactant concentration in the dechlorination of chlorinated organics and stated that surfactant concentration below the CMC value increased dechlorination, while concentrations above this value harm oxidation. The batch test results presented here support this statement.

Best-fit first-order reaction rate curves are presented in Figure 4.51 for 1/10 and 1/20 surfactant-free reactors in the DNAPL phase studies. This is because the solubility of DNAPL affects the oxidation rate, especially in the presence of surfactant during the time corresponding to the first samples of batch experiments. Corresponding reaction rate constants are presented in Table 4.23.

Table 4.23. Best fit DNAPL phase PCE degradation and dechlorination rates for heat-activated persulfate batch kinetic experiments (PCE_0 = 0.3 mM (50 mg/L)).

	PCE			Cl^-			
Molar ratio	Best-fit			Best-fit			Stoich. ratio
PCE:PS	k_{PCE} (h^{-1})	RMSE	NRMSE	k_{Cl^-} (h^{-1})	RMSE	NRMSE	$k_{stoich.}$
1:10	3.49	4.58	0.092	1.00	2.63	0.076	0.704
1:20	16.3	1.9	0.038	1.2	1.99	0.058	0.7

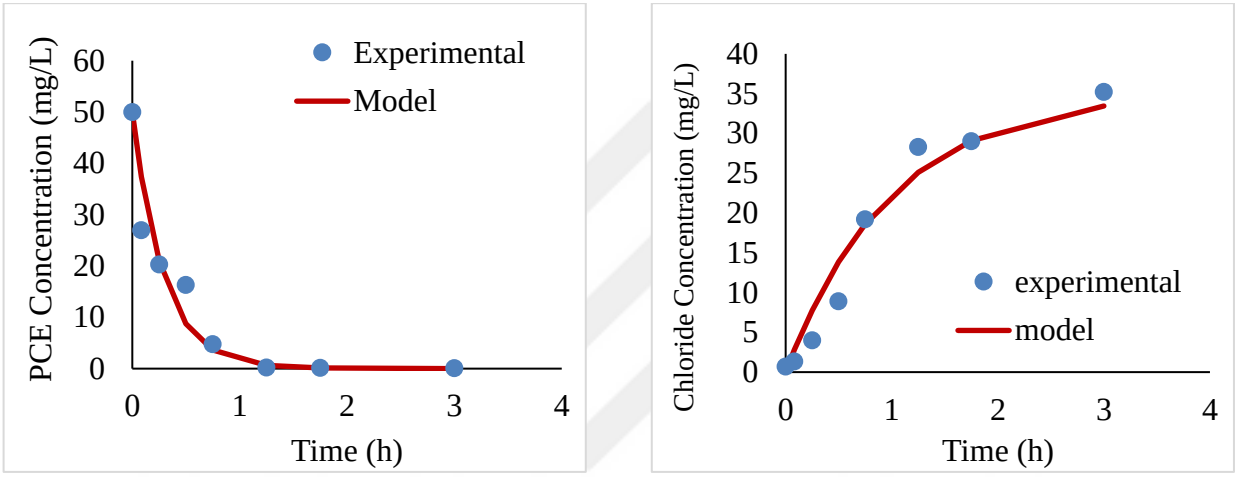

(a)

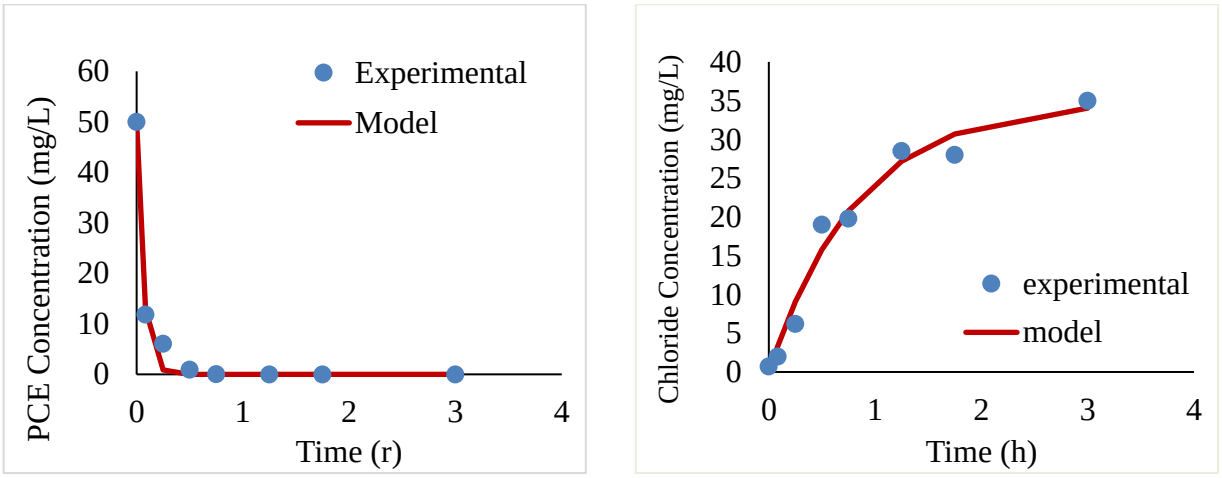

(b)

Figure 4.51. Best-fit DNAPL phase PCE degradation and Chloride production concentration curves of (a) [PCE]/[PS] = 1/10, (b) [PCE]/[PS] = 1/20.

4.4.1.2.2. Degradation of PCE in the Aqueous Phase

The experiments described in the previous section started with PCE in liquid phase. Under such conditions the DNAPL must first dissolve before it can be oxidized by persulfate. In this section, the PCE used in the reactivity tests was in the aqueous phase, subjected to various concentrations of persulfate and surfactant. Figure 4.52 presents the PCE aqueous phase concentration as a function of time. The corresponding chloride concentration is shown in Figure 4.53. The highest rate of reaction was observed with 90 mM persulfate. The chloride concentration for this case was highest. Decreasing the persulfate concentration ot 20 mM yielded lower reaction rate and lower chlroide concentration. When Tween 80 was added (at concentrations equal to 3 and 10 CMC), it was observed that the reaciton rate decreased (Figure 4.53) with lower chloride concentration suggesting again interference of Tween 80 with persulfate oxidation.

Best-fit first order reaction rates were fitted to the various aqueous PCE reactivity experiments (Figure 4.54). The corresponding best fit reaction rate constants are given in Table 4.24. It is seen that the highest reaction rate constant is obtained with persulfate at 90 mM sulfate followed by 20 mM persulfate while the lowest concentraitons are when Tween 80 is present, providing further evidence to the interference of Tween 80 with the PCE oxidation.

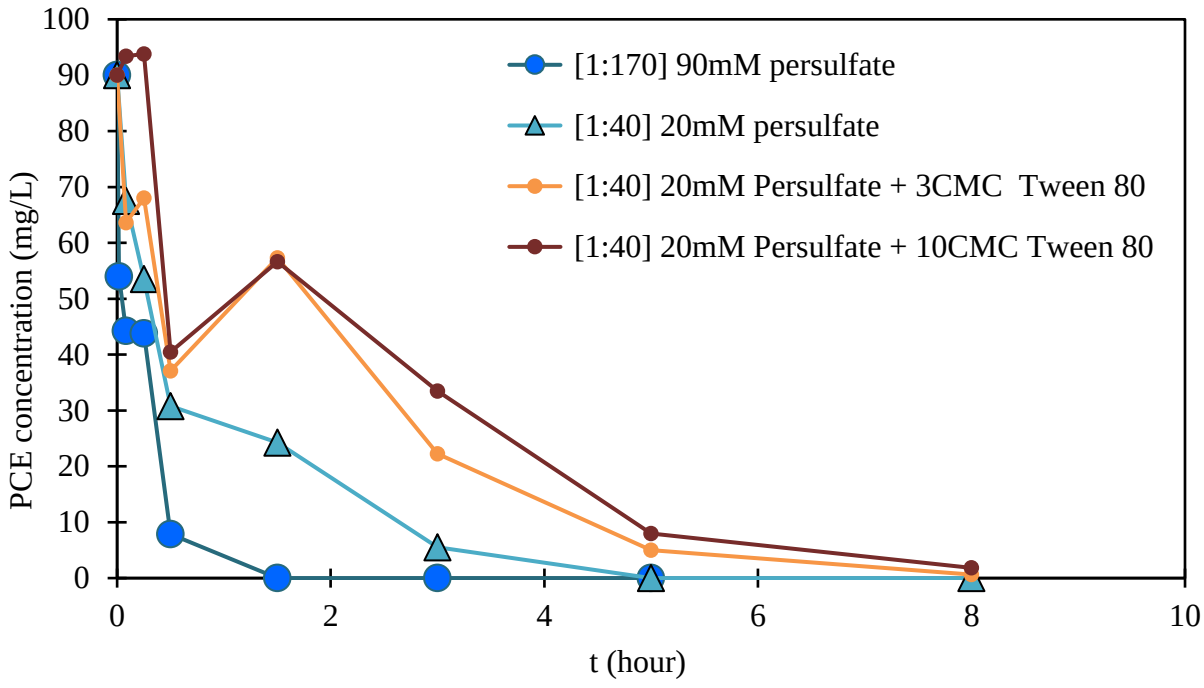

Figure 4.52. Aqueous phase PCE degradation with various concentrations of Tween 80 enhanced persulfate.

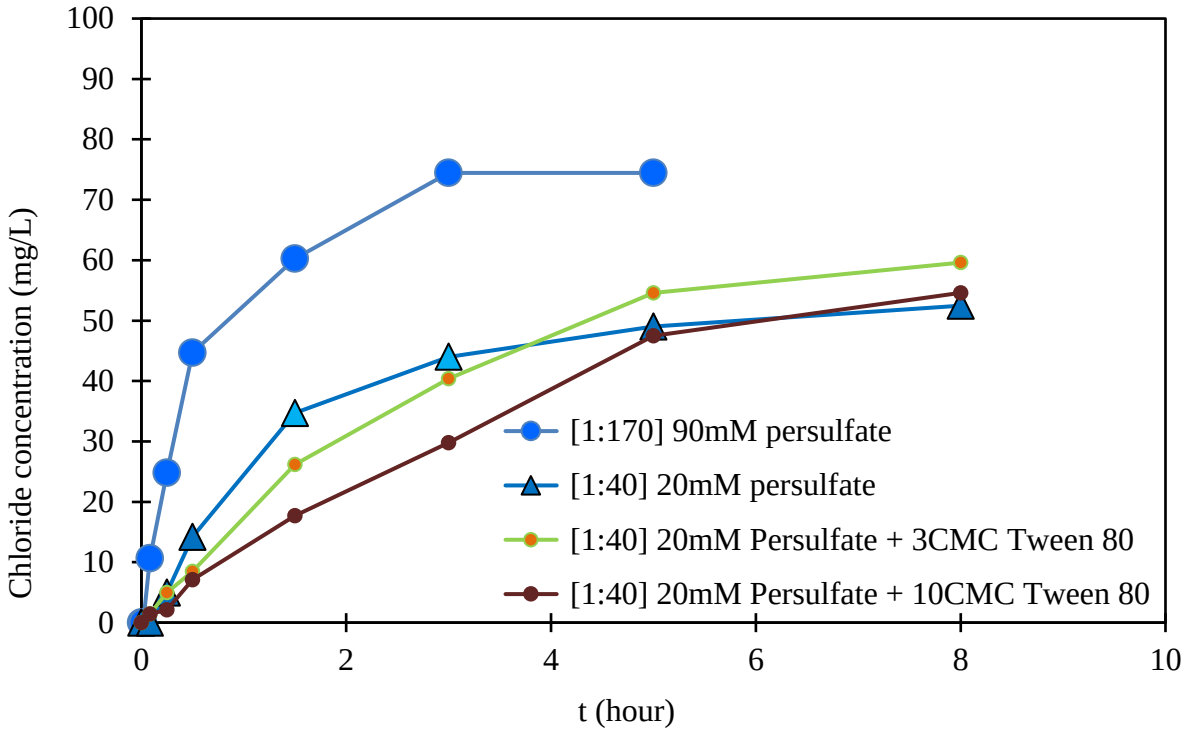

Figure 4.53. Chloride release of aqueous phase PCE in various persulfate concentration.

Table 4.24. Best fit aqueous phase PCE degradation and dechlorination rates for heat-activated persulfate batch kinetic experiments (PCE_0 = 0.54 mM (90 mg/L)).

	PCE			Cl^-			
Molar ratio	Best-fit			Best-fit			Stoich. ratio
PCE:PS	k_{PCE} (h^{-1})	RMSE	NRMSE	k_{Cl^-} (h^{-1})	RMSE	NRMSE	$k_{stoich.}$
1:170	4.941	13.14	0.146	1.600	3.06	0.041	0.827
1:40	1.925	7.90	0.087	0.637	1.69	0.032	0.583
1:40 3CMC	0.572	15.52	0.173	0.395	1.61	0.027	0.666
1:40 10CMC	0.410	13.26	0.144	0.3	2.60	0.047	0.619

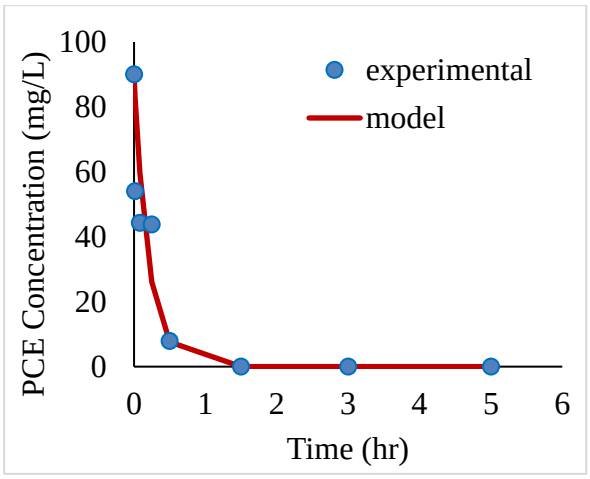
PCE Concentration (mg/L)
100
80
60
40
20
0
0 1 2 3 4 5 6
Time (hr)
experimental
model

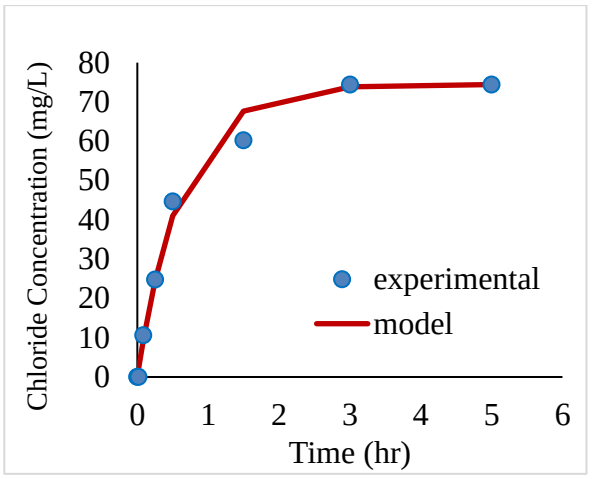
Chloride Concentration (mg/L)
80
70
60
50
40
30
20
10
0
0 1 2 3 4 5 6
Time (hr)
experimental
model

(a)

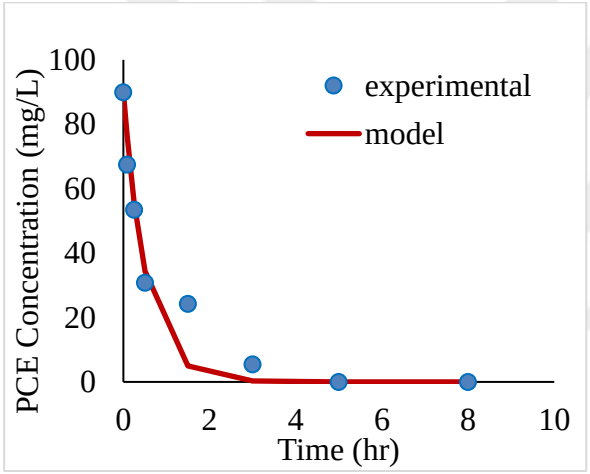
PCE Concentration (mg/L)
100
80
60
40
20
0
0 2 4 6 8 10
Time (hr)
experimental
model

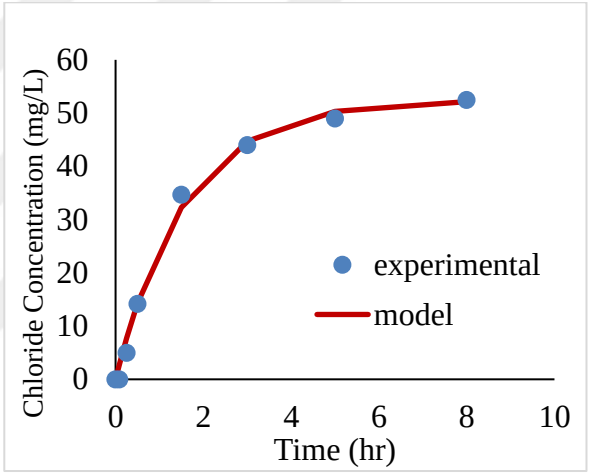
Chloride Concentration (mg/L)
60
50
40
30
20
10
0
0 2 4 6 8 10
Time (hr)
experimental
model

(b)

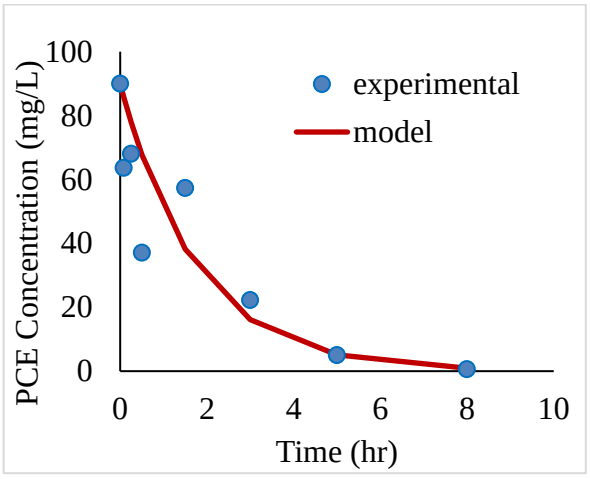
PCE Concentration (mg/L)
100
80
60
40
20
0
0 2 4 6 8 10
Time (hr)
experimental
model

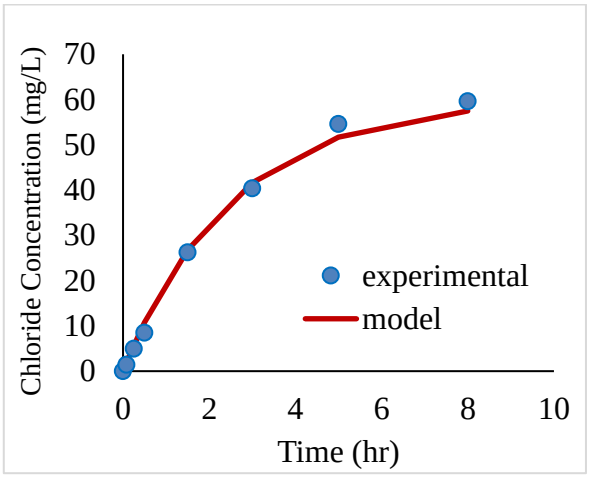
Chloride Concentration (mg/L)
70
60
50
40
30
20
10
0
0 2 4 6 8 10
Time (hr)
experimental
model

(c)

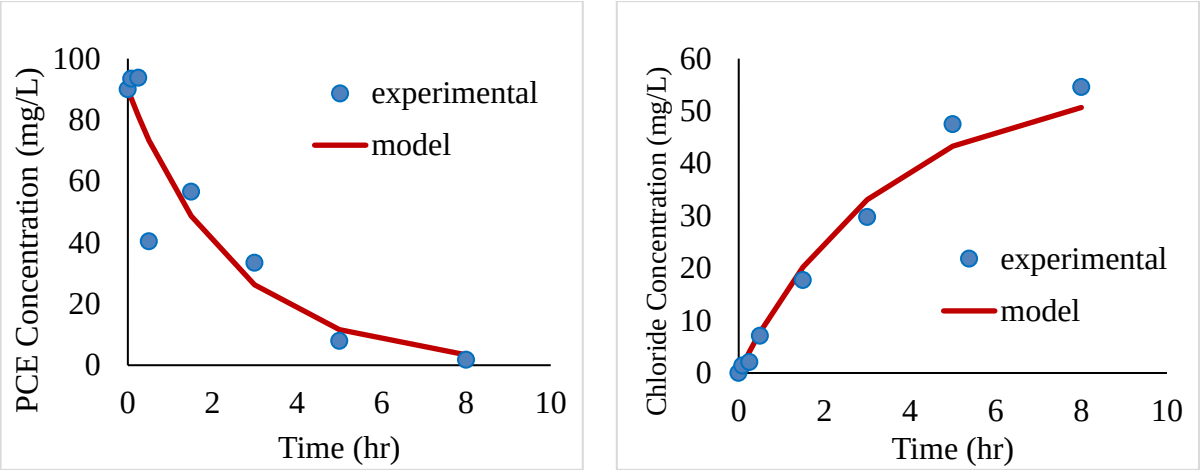

(d)

Figure 4.54. Best-fit aqueous phase PCE degradation and Chloride production concentration curves of (a) [PCE]/[PS] = 1/170, (b) [PCE]/[PS] = 1/40, (c) [PCE]/[PS] = 1/40 3CMC, (d) [PCE]/[PS] = 1/40 10CMC.

4.4.1.3. Stability and Surfactant (Tween 80) Degradation Capacity of Persulfate at Elevated Temperature

Sodium persulfate solutions were prepared at 3, 6, 30, 75, and 150 mM concentrations diluted from 150 mM stock to observe oxidant consumption in the presence/absence of natural soil and under activated (50 °C)/unactivated persulfate conditions. Experiments were performed without pH adjustment and without buffering. Samples were manually shaken gently for 1 minute every 3 hours. Persulfate concentrations were measured after 48 hours.

It was observed that the stability of unactivated sodium persulfate in the presence of natural soil was close to that of the aqueous phase without soil. The highest oxidant consumption in soil-containing samples was observed for the initial persulfate concentration of 3 mM, with an oxidant consumption of about 7 %. Persulfate consumption decreased as the initial persulfate concentration increased. The 50 °C activated persulfate consumption was 37-43 % in the presence of natural soil and 20-24 % for the aqueous solution in the absence of soil. However, it should be noted that for the soil-free aqueous solution persulfate concentrations were about 20-25 %. In the presence of soil, persulfate concentrations were about 40 % (Figure 4.55). Appendix A provides a wide source of soil oxidant demand data documented in the literature.

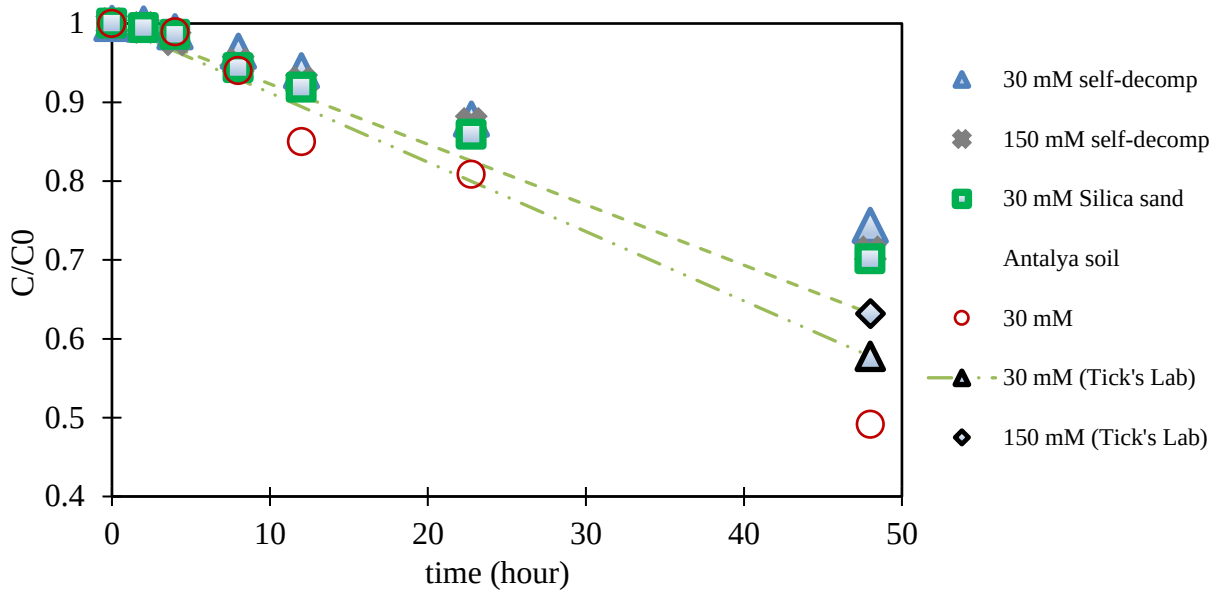

(a)

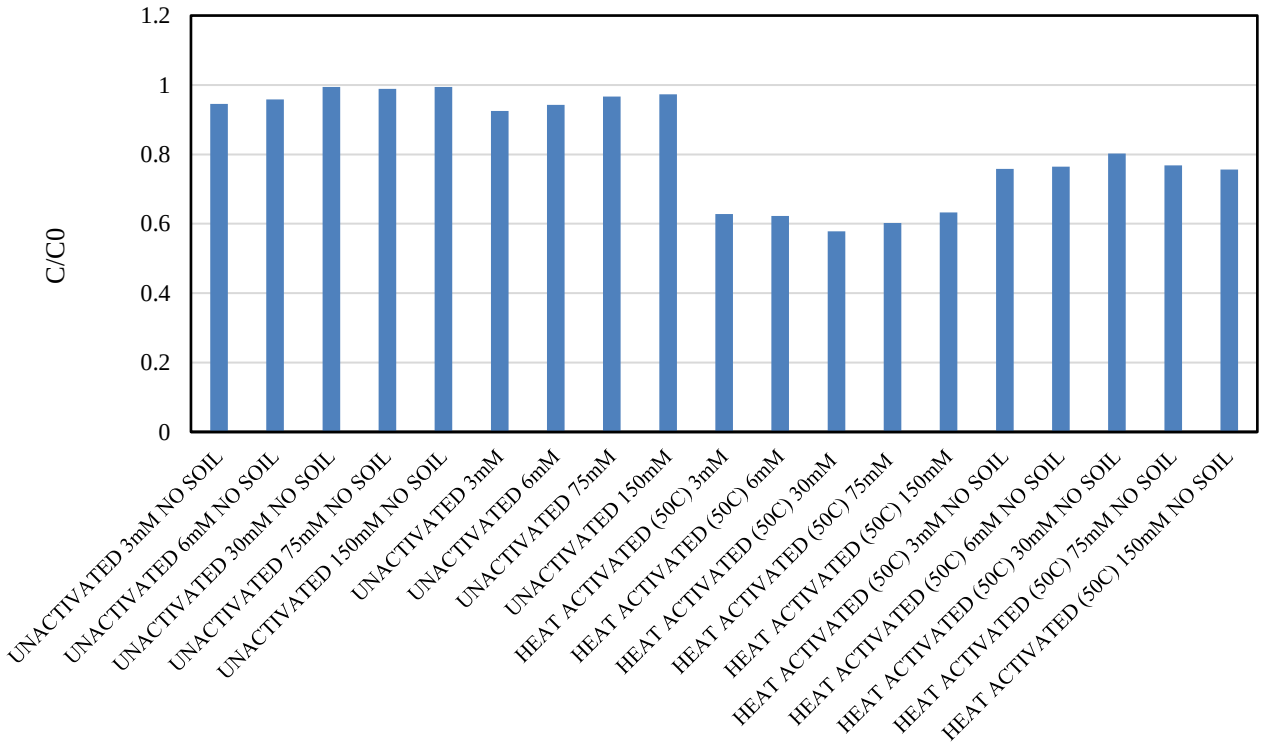

(b)

Figure 4.55. (a) Time-dependent relative persulfate concentration, (b) Relative persulfate concentrations after 48 hours.

In addition, the potential of Tween 80 to be oxidized by persulfate was investigated. To do this, a mixture solution of 0.15 % Tween 80 and 30 mM sodium persulfate was kept in a water bath at 50 °C for 12 hours. It was observed that the Tween 80 solution with the initial concentration of 0.15 % was measured as 0.026 % at the end of 12 hours, which equates to about 80 % consumption over the duration of the experiment, indicating that the Tween 80 reacted with persulfate.

4.4.2. Surfactant Enhanced Thermally-Activated Persulfate Remediation of DNAPL PCE Source Zones

The results of persulfate flushing experiments with DNAPL PCE performed in Flow-cell #1 are presented in this section. The flow-cell is rectangular with 24 cm long by 15 cm high by 3 cm wide constructed of stainless steel frame (Figure 4.56), other properties of the flow-cell were explained in Section 3.4.1. The flow-cell was packed with silica sand. The flow zone had a total volume of 690 cm^3 comprised of 40-50 mesh size sand. The tank was wrapped with aluminum to reduce heat loss from the saturated flow-cell. A total of 0.25 mL of PCE was injected into the flow zone from the middle top port of the flow-cell for each set of experiment with an injection rate of 4 µL/min. A constant temperature of 50 ℃ was applied to each set of flushing experiments.

Prior to oxidant flushing experiments, tracer tests were conducted to investigate the transport characteristics of the flow-cell system. After the tracer test, four flushing experiments were conducted as indicated in Table 4.25. In the following sections the results of the tracer tests and flushing heat activated oxidation experiments are presented.

The results of some persulfate flushing experiments with DNAPL PCE performed in Flow-cell #2 are presented also in this section. The flow-cell is rectangular with 20 cm long by 9 cm high by 5 cm wide constructed of plexiglass frame (Figure 4.60), other properties of the flow-cell are explained in section 3.4.2. The flow-cell was packed with silica sand with a flow zone volume of 612 cm^3 comprised of 40-50 mesh size sand located between two impermeable zones. The tank was wrapped with heat isolation to reduce heat loss. 0.25 mL of PCE was injected into the flow zone from the middle top port of the flow-cell for each set of experiment with an injection rate of 1 µL/min. A constant temperature of 50 ℃ is applied to each set of flushing experiments. Temperature measurement was made continuously from the effluent port of the flow-cell. It was observed that the effluent temperature reached 42 ℃ in approximately 2 hours (~1PV), indicating that the temperature inside the tank was on average about 46 ℃. Additionally, pH and ORP were measured in the experiments performed with this flow-cell. A total of four flushing experiments were conducted as

indicated in Table 4.25. Experiment 3 is repeated with the Flow-cell #1. A tracer test was also performed. The results of all these tests are presented in the following sections.

Table 4.25. List of persulfate experiments performed at 50 ℃.

		DNAPL	Media	Injection type	v (cm/h)	Chemical agent
1	Flow-cell #1	0.25 mL PCE	Silica sand	Continuous	11.9	water control
2		0.25 mL PCE	Silica sand	Continuous	11.9	0.00981 % Tween 80*
3		0.25 mL PCE	Silica sand	Continuous	11.9	20 mM Persulfate
4		0.25 mL PCE	Silica sand	Continuous	11.9	20 mM Persulfate + 0.00981 % Tween 80
1	Flow-cell #2	0.25 mL PCE	Silica sand	Continuous	19.6	water control
2		0.25 mL PCE	Silica sand	Continuous	19.6	90 mM Persulfate
3		0.25 mL PCE	Silica sand	Continuous	19.6	20 mM Persulfate
4		0.25 mL PCE	Silica sand	Continuous	19.6	20 mM Persulfate + 2.5 % Tween 80

* 0.00981 % Tween 80 corresponds to 3 folds of Tween 80 critical micelle concentration value

4.4.2.1. Tracer Test in Flow-Cell #1

The breakthrough curve and best fit analytical solution for tracer test and specific constant velocity (2.85 m/day) are presented in Figure 4.57. The tracer test was performed at 50 ℃ for consistency with the oxidation flow-cell experiments. The tracer used was pentafluorobenzoic acid (PFBA), a conservative chemical. The shape of the experimental breakthrough curve shown in Figure 4.57 is very close to the curve obtained by analytical calculation using equation (3.3), suggesting that the compaction of the tank was uniform with no preferential flow paths. The best fit dispersion coefficient values were determined by minimizing the root mean squared error (RMSE) of the experimental and calculated data.

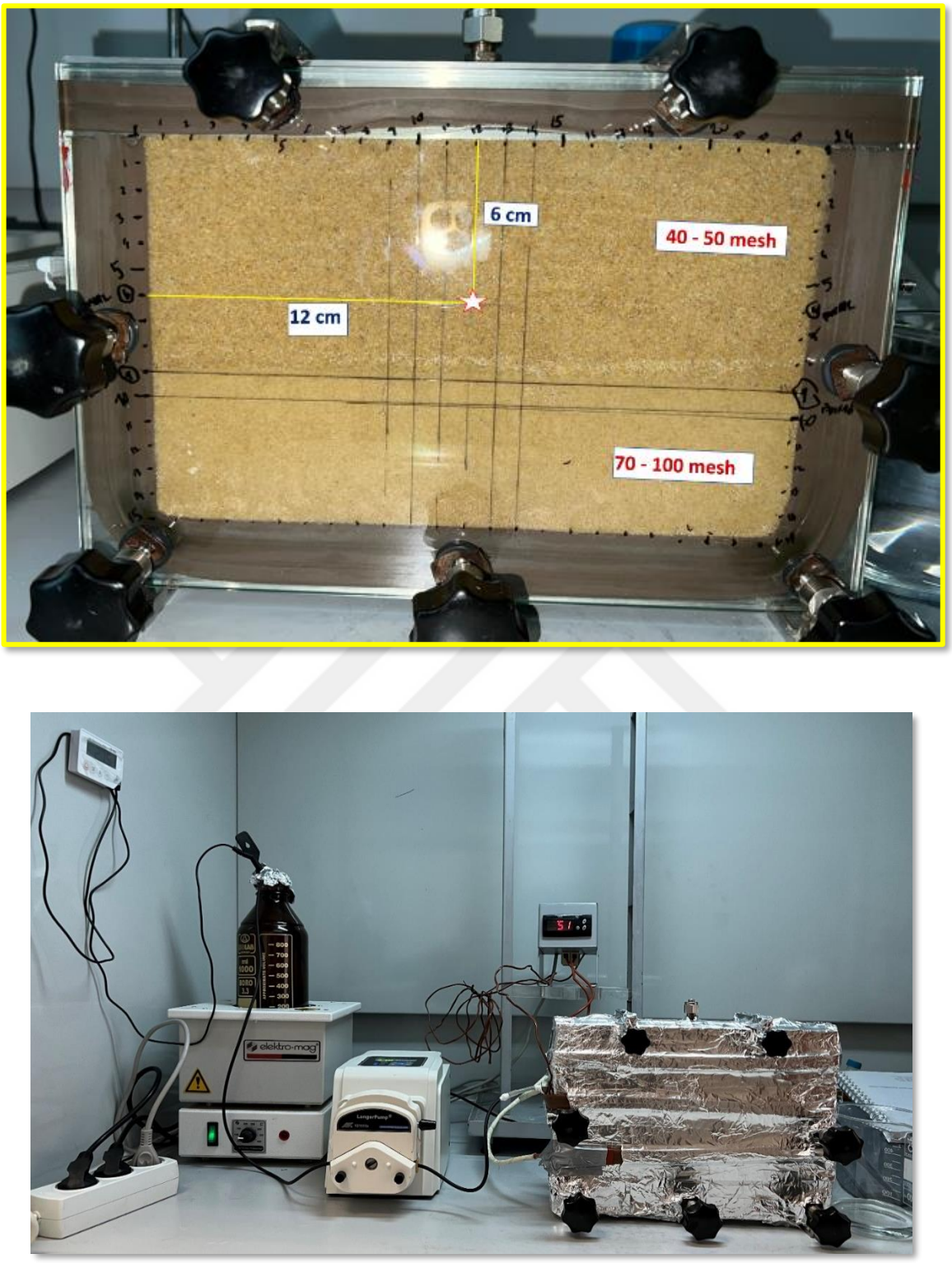

Figure 4.56. Flow-cell #1 configuration for the thermally enhanced persulfate experiments.

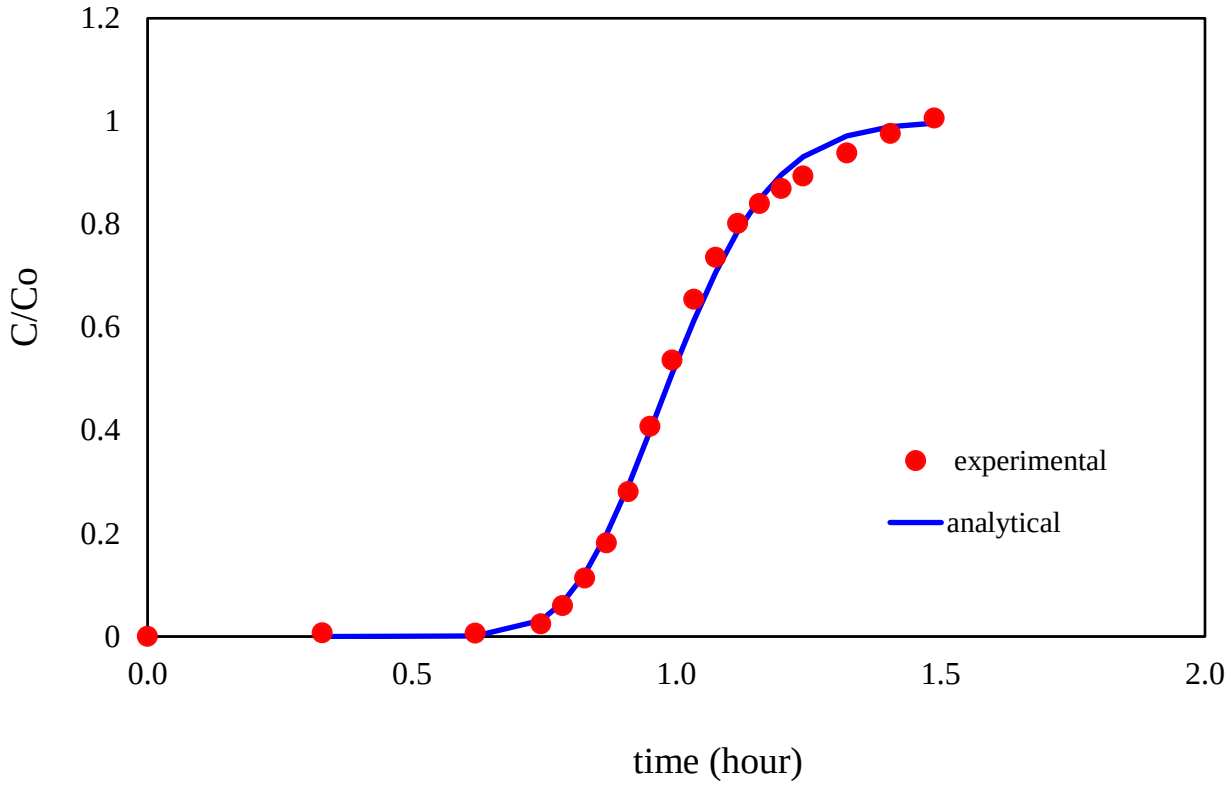

Figure 4.57. Tracer test experimental data and best-fit solution.

The porosity of the silica sand determined from the tracer test was 0.35. The molecular diffusion coefficient, needed to calculate the dispersivity, was assumed to be $Dm=1x10^{-9}$ m^2/s (Gabler et al, 1996). The best-fit longitudinal dispersion coefficient and the corresponding dispersivity values are given in Table 4.26. The corresponding dispersivity value of 0.002 m was used in the multiphase flow model described in previous sections for the estimation of the interphase mass transfer coefficient. The dispersivity is consistent with values reported in the literature that are typically about 1 % of travel distance (24 cm) (Gelhar, 1993)

Table 4.26. Dispersion coefficient and dispersivity values determined from tracer test.

Flow rate (mL/min)	2
Velocity (m/s)	3.3×10^{-5}
Dispersion coefficient (D_X) (m^2/s)	9.36×10^{-8}
Longitudinal dispersivity (α_X) (m)	0.002
Peclet number ($Pe = vL/D_X$)	84.8

4.4.2.2. Contaminant Elution Behavior in Flow-cell #1

Figure 4.58 shows the PCE effluent concentrations for the water and 0.00981 % Tween 80 (which corresponds to 3 folds of its critical micelle concentration (CMC)) at 50 ℃. The graph also includes the 5 % Tween 80 enhanced dissolution experiment from the previous section for comparison purpose. It was observed that the flushing performed with 3 fold of CMC value of Tween 80 is not much different from flushing with water. While the total removal with water flushing is 51.74 %, the PCE removal obtained with 3 fold of CMC Tween 80 is 59.17 %. This suggests that the concentration of surfactant is insufficient to efficiently dissolve PCE from the DNAPL phase to the Tween 80 aqueous phase. Moreover, the high temperature in the environment does not cause a noticeable increase. On the other hand, flushing with only high concentration Tween 80 without the effect of high temperature gives the most effective result. In washing with 5 % Tween 80, the removal of PCE took 14 PV, while the others were able to reduce the PCE value to 1 mg/L in about 4 times of this value.

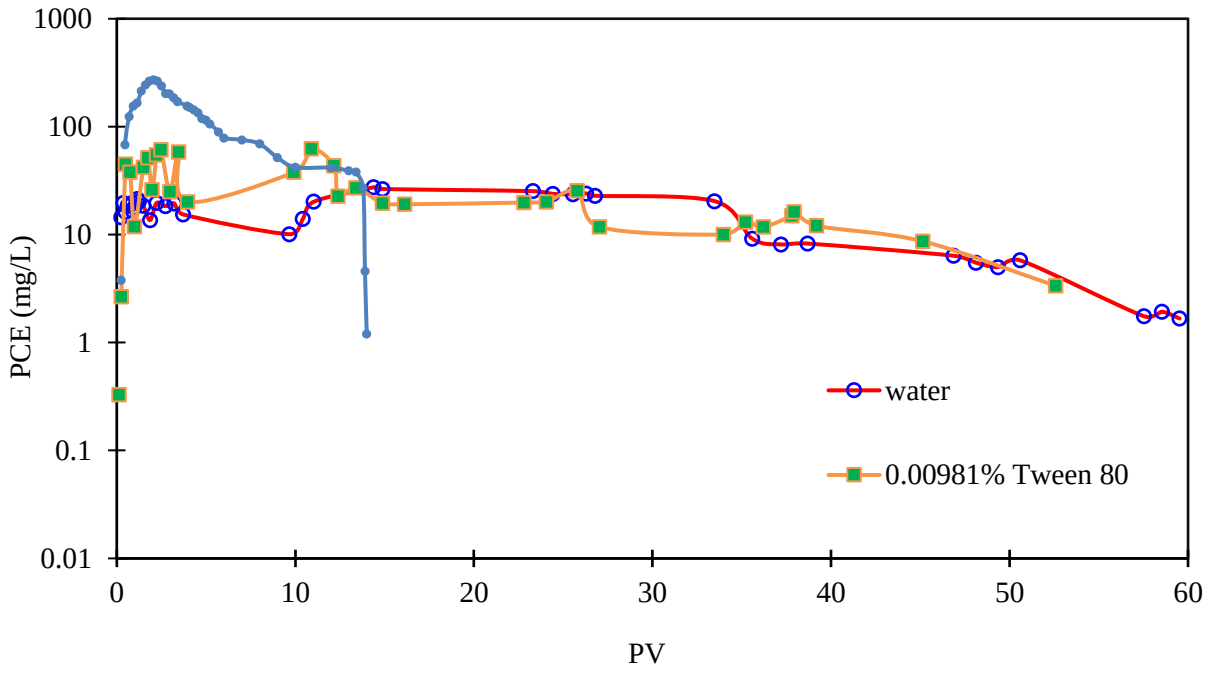

Figure 4.58. PCE elution behavior under 50 ℃ enhanced flushing.

Figure 4.59 shows the PCE elution behavior of persulfate flow experiments with Tween 80. Accordingly, the highest PCE concentration of 68 mg/L, measured in flushing with 20mM persulfate, was reached at the end of 3.5 PV. PCE concentration remained constant during the next 20 PV. After 25 PVs, the concentration tended to decrease reaching a low value of 3 mg/L after a total of 36 PVs.

Chloride also increased and reached the highest concentration of 18.8 mg/L at about 2.2 - 2.4 PV. The chloride level measured at the end of the experiment was about 15.24 mg/L.

The second set of experiments was carried out by adding 3 fold of CMC (0.00981 %) Tween 80 to 20 mM persulfate. Figures 4.58 and 4.59 show the effluent PCE and chloride concentrations, respectively. (In this case 3 fold of CMC Tween 80 did not yield significant increase in effluent concentration; even lower concentrations were observed in the first 15 PVs compared to the use of persulfate alone. This formed a tail after 25 PV as a result of the rate-limited flow. After a total of 57 PV Tween 80 persulfate injections, the PCE value decreased to only 5 mg/L. The increase in chloride started after about 1 PV and reached the highest value of 12.76 mg/L at after 4 PV. Chloride concentration graph showed reduced chloride production, with chloride decreasing below 1 mg/L after 11.5 PV.

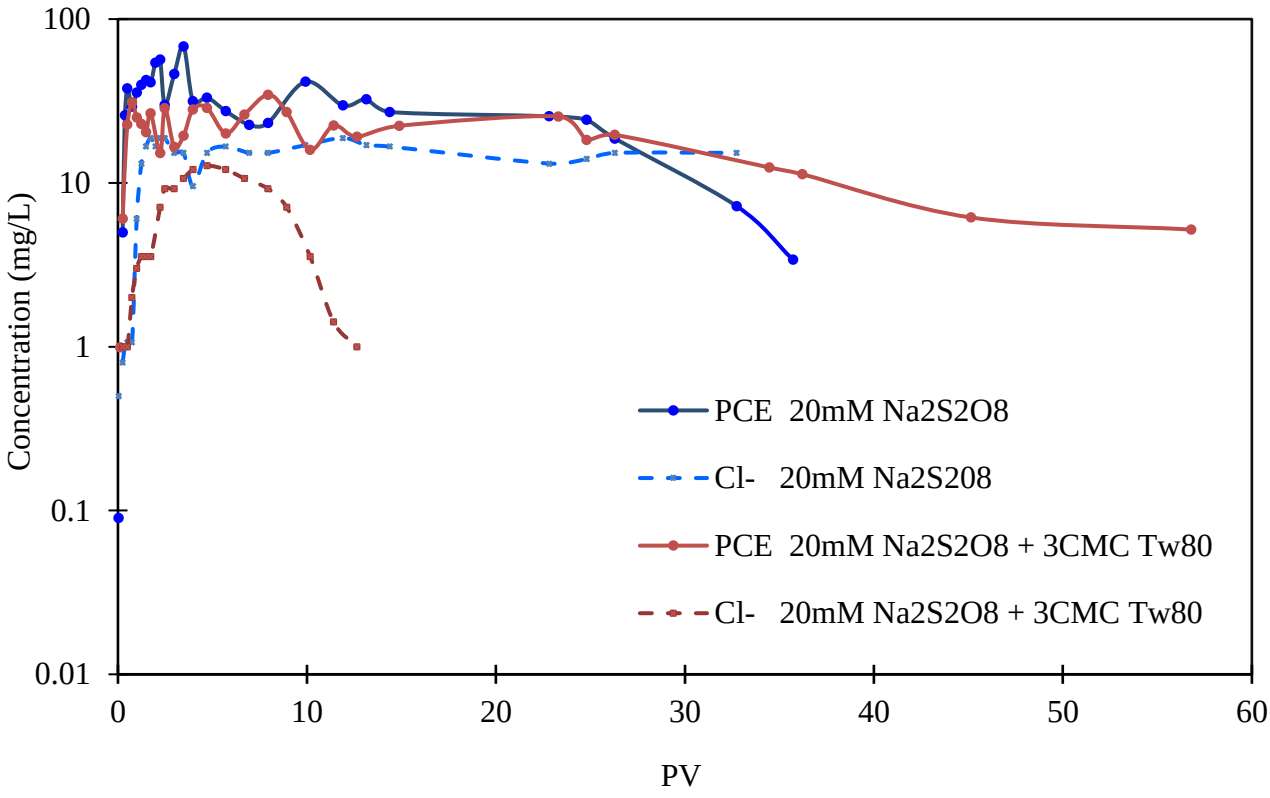

Figure 4.59. PCE elution with Tween 80 enhanced thermally activated persulfate flushing.

Considering the total percent removal of PCE, as expected, the lowest value was obtained water flooding (51.74 %) (Table 4.27). This is followed by 3 fold of CMC Tween 80 with 59.17 %. The highest removal 88.58 % was obtained with the injection of 20 mM persulfate alone. About 36 % of PCE is removed by oxidation. The remaining 52.6 % was dissolved and left the system. The use of

20 mM persulfate with Tween 80 was insufficient to oxidize PCE (6.13 %). The PCE leaving the system by dissolution is 53.7 %, which is very close to the value when persulfate is applied alone. As a result, thermally-activated persulfate, which has been shown to be a very effective oxidant when used alone in PCE removal, shows a great decrease in PCE oxidation performance when mixed with Tween 80, a nonionic surfactant. On the other hand, the presence of Tween 80 increases PCE dissolution and ensures its removal from the system. However, this may not seem very effective at low concentrations of Tween 80.

Table 4.27. Mass recovery values from the experiments in Flow-cell #1.

	PCE % recovered	PCE % oxidized	PCE % residual	% Total removal = $PCE_{recovered}$ + $PCE_{oxidized}$
Water	51.74	-	48.26	51.74
0.00981 % Tween 80	59.17	-	40.83	59.17
20 mM $Na_2S_2O_8$	52.64	35.94	11.42	88.58
20 mM $Na_2S_2O_8$ + 0.00981 % Tween 80	53.7	6.13	40.18	59.82

4.4.2.3. Tracer Test in Flow-cell #2

The tracer breakthrough curve and best fit analytical solution for specific constant velocity (4.7 m/day) are presented in Figure 4.61. As in the previous tracer test, the conservative chemical PFBA was used as the tracer. The hydrodynamic characteristics of the two flow-cells differed greatly. In one of the flow-cells (#2). This resulted in the flow zone not being fully saturated. Experiments were carried out by injecting DNAPL into this saturated portion (Figure 4.60).

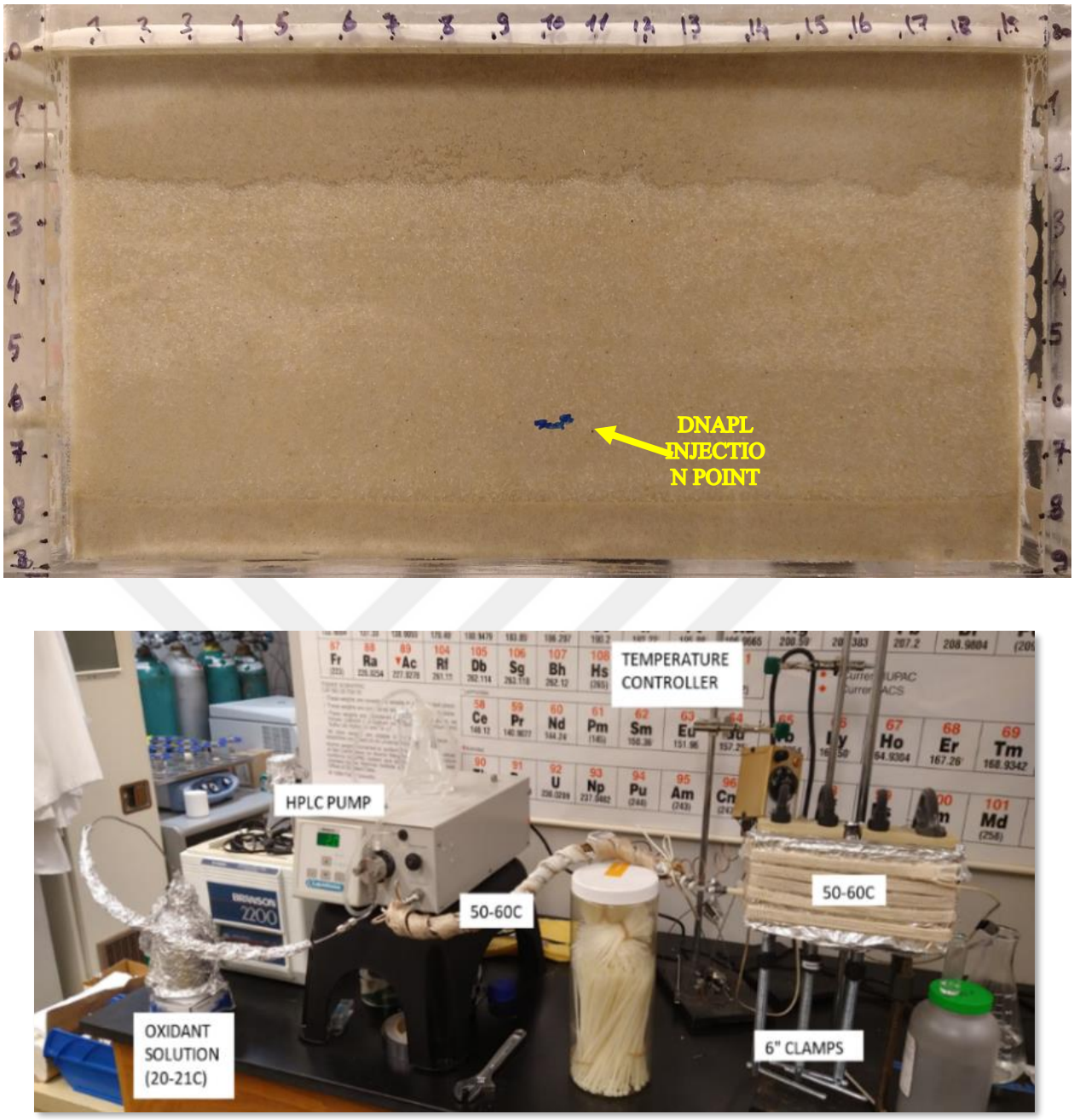

Figure 4.60. Flow-cell #2 configuration for the thermally enhanced persulfate experiments.

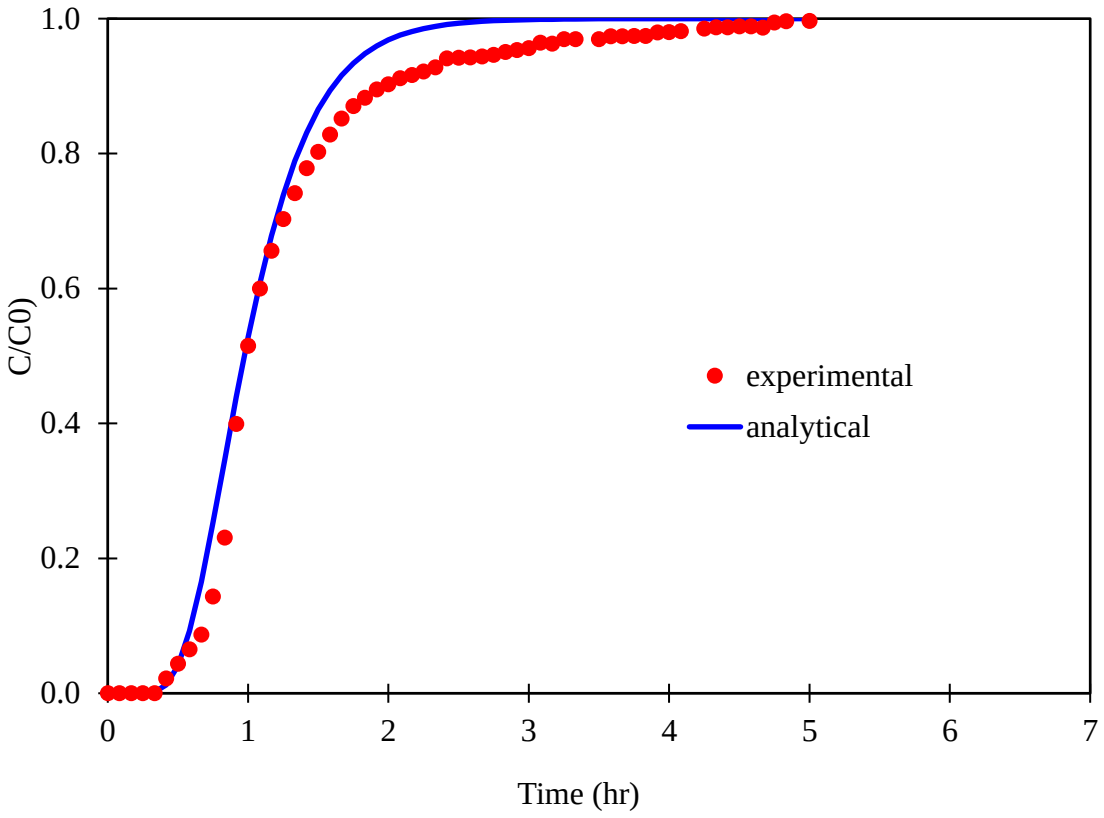

Figure 4.61. Tracer test experimental data and best-fit solution.

The porosity of the silica sand determined from the tracer test was 0.35. The molecular diffusion coefficient, needed to calculate the dispersivity, was assumed to be $Dm=1x10^{-9}$ m^2/s (Gabler et al, 1996). The best-fit longitudinal dispersion coefficient and the corresponding dispersivity values are given in Table 4.28. The dispersivity value of 0.002 m was used in the multiphase flow model described in previous sections for the estimation of the interphase mass transfer coefficient.

Table 4.28. Dispersion coefficient and dispersivity values determined from tracer test

Flow rate (mL/min)	2
Velocity (m/s)	5.4×10^{-5}
Dispersion coefficient (D_X) (m^2/s)	8.47×10^{-7}
Longitudinal dispersivity (α_X) (m)	0.016
Peclet number ($Pe = vL/D_X$)	12.48

4.4.2.4. Contaminant Elution Behavior in Flow-cell #2

In the first flow-cell experiment, water flooding was used to flush the pure-phase PCE emplaced within the 40-50 mesh sand. This experiment showed that effluent PCE concentrations reached a maximum of 45 mg/L, followed by an extensive phase at steady-state concentration for about 20 PV. It was observed that initial effluent PCE concentrations were lower than the solubility (~ 205 mg/L). Due to significant dilution effects only a fraction of the injected water comes in contact with the DNAPL (Figure 4.62).

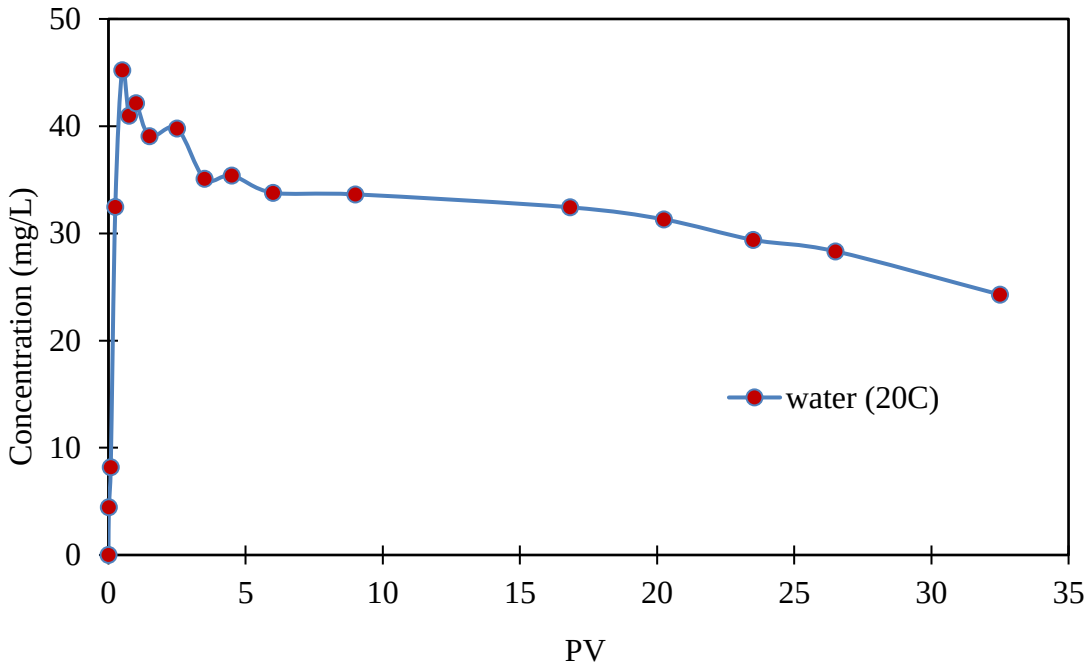

Figure 4.62. PCE elution behavior of water flooding in Flow-cell #2

In the second flow-cell experiment, the system was continuously flushed with 20 mM persulfate (Figure 4.63). Persulfate solution was delivered into the system at the target temperature of 50 °C, however continuous temperature measurements from the outlet port show that the system reached the target temperature after 3 hours. During the flushing, the PCE concentration increased rapidly, reaching the highest value of 42 mg/L in 0.5 PV. At the end of 1.5 PV, this value decreased to around 10 mg/L with fluctuations over range of 20-4 mg/L for the next 17 PVs. PCE measurements could not be continued after 18 PVs of flushing due to a problem in the GC/MS analytical instrumentation (Figure 4.63.a). The production of chloride ions started to be observed after 1.5 PV of flushing and reached the highest value of 41 mg/L after about 14.5 PV, and then began to decrease (Figure 4.63.b). The pH remained in the range of 5.4-6.4 during the first 2 PV, and it decreased to 2.9 as oxidation

continued. The ORP value, on the other hand, was 330-345 mV during the first 2 PV. With the progression of oxidation, the ORP increased to the highest value of 617 mV after 6.5 PV of flushing.

In the third flow-cell experiment, the oxidation of PCE was examined with the continuous injection of a higher persulfate concentration. The highest PCE concentration in the 90 mM persulfate injection is reached at 133 mg/L after 0.8 PV, higher than the value observed with 20 mM persulfate. After 3.5 PV, the PCE concentration dropped below 1 mg/L, and no further PCE increase was observed during the injection (Figure 4.63.a). As in the previous experiment, chloride production started to increase after 1.5 PV, with a peak value of 70 mg/L after 13 PVs of flushing (Figure 4.63.b). In addition, pH values decreased to 2.5 as observed PCE concentration declined to below 1 mg/L. ORP gradually increased, reaching the highest value of 570 mV after all PCE was consumed. To purify the system from chloride, the oxidant injection was stopped and the flow-cell was continuously flushed with 50-60 °C DI water.

In the fourth flow-cell experiment, a 20 mM persulfate solution containing 2.5 % Tween 80 was injected continuously over the entire duration of flushing. PCE concentrations increased rapidly, reaching the highest value of 710 mg/L at the end of 1.67 PV, followed by a decreasing trend in concentration until concentrations decreased below 1 mg/L after 11 PVs of flushing (Figure 4.63.a). No significant chloride ion production was observed throughout the flushing, but it was observed that the pH decreased to 2.7 after 8 PVs of flushing towards the latter stages of the experiment (Figure 4.63.b). Under this condition, the ORP values reached 500-550 mV after considerable time (after 5.5 PVs) compared to the flushing with 20 mM persulfate.

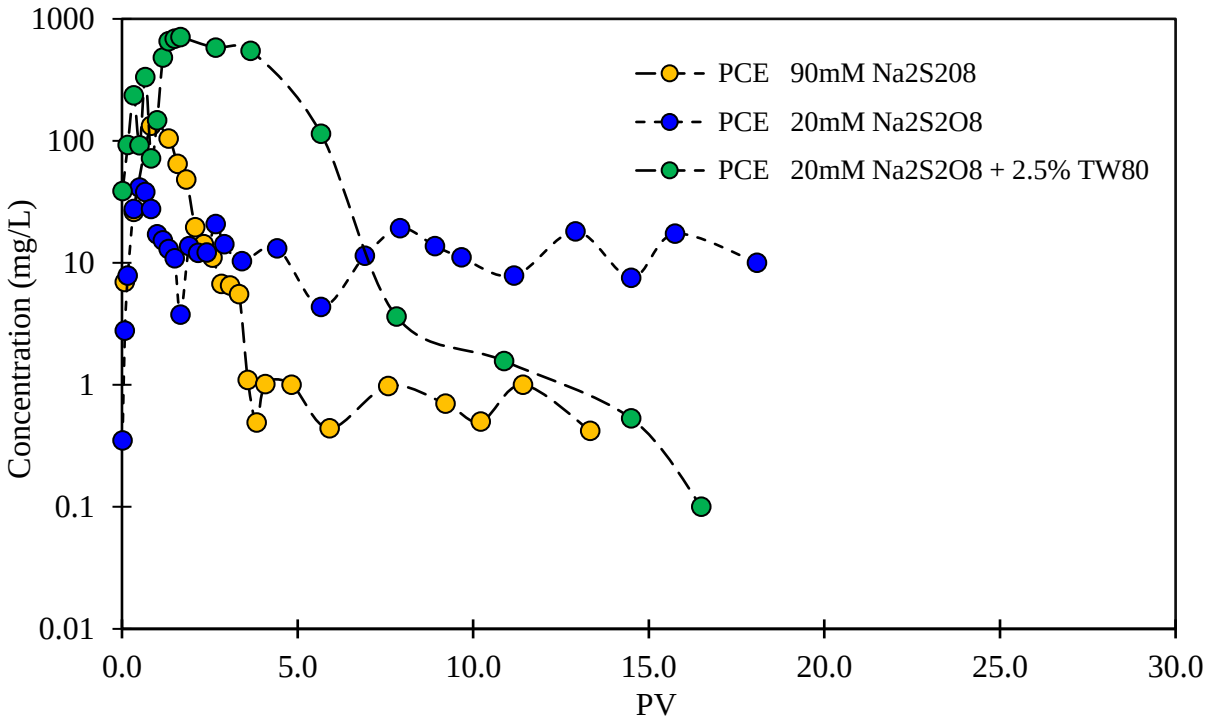

(a)

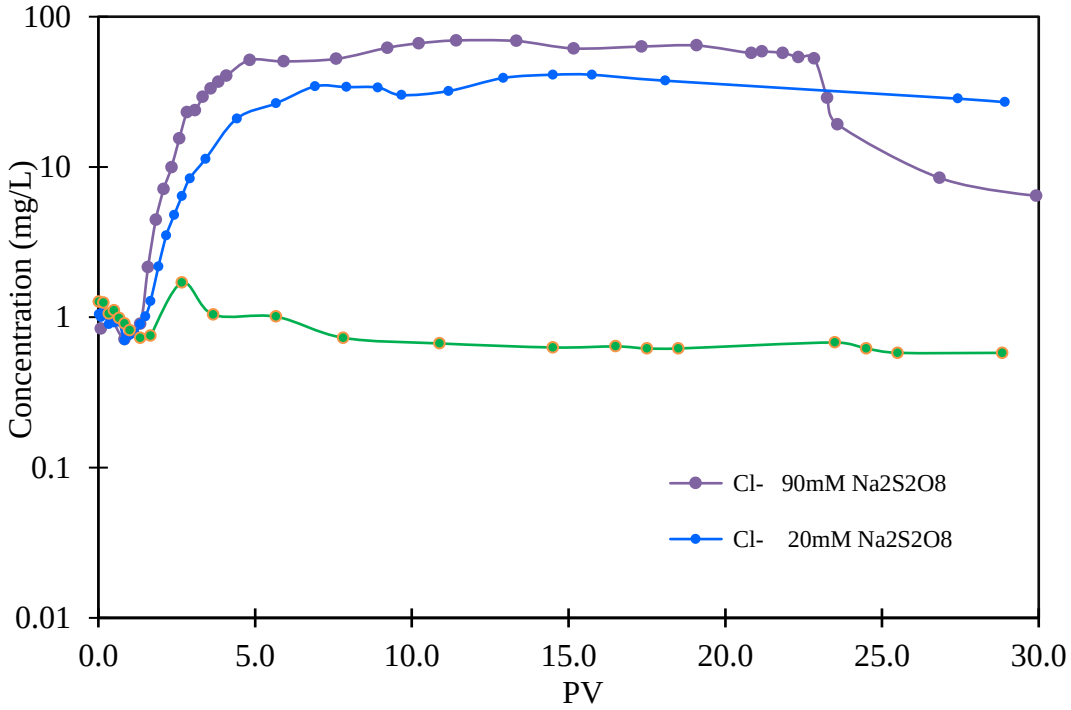

(b)

Figure 4.63. Time-dependent change of (a) PCE, (b) Chloride in silica sand (continuous injection).

Table 4.29 shows the percent mass removal. It also shows the dominant removal mechanism of DNAPL removal. The highest mass removal is observed with 2.5 % Tween 80 enhanced 20 mM persulfate with 75 % of the injected mass collected due to enhanced dissolution while only 1 % of the mass was oxidized. For 20 mM persulfate, about 30 % of the DNAPL mass was oxidized. Only 8 % of DNAPL was collected as dissolved effluent. Recovery is the lowest (5%) in the flushing with 90mM persulfate with almost 50% of the contaminant oxidized.

Table 4.29. Mass recovery values from the experiments in Flow-cell #2.

	PCE % recovered	PCE % oxidized	PCE % residual	% Total removal = $PCE_{recovered} + PCE_{oxidized}$
20mM $Na_2S_2O_8$	8.34	29.54	62.12	37.87
20mM $Na_2S_2O_8$ + 2.5% Tween 80	75.14	0.73	24.11	75.88
90mM $Na_2S_2O_8$	5.0	48.29	46.72	53.28

4.5. In-situ Sodium Persulfate Oxidation and Enhanced Solubilization in Pure Phase TCE

4.5.1. Batch TCE Degradation Experiments with Thermally-Activated Persulfate

Experiments were carried out with TCE much earlier than the persulfate experiments with PCE during the thesis project period and the results are given in this section. Several control experiments were performed before the testing of the TCE - heat-activated persulfate (PS) - Tween 80 system. Accordingly, in a system with Tween 80 and persulfate without TCE, no significant reduction in persulfate was observed after 7 hours. It was also observed that unactivated persulfate did not affect TCE in the DNAPL phase even after 7 hours. In addition, the increase in chloride ion stopped with the decline in DNAPL degradation when the system at 50 °C was left to cool after 1.5 hours. The PS/TCE molar ratio was chosen as 10/1 in the initial set of experiments. The progression of the aqueous TCE oxidation was observed indirectly through chloride ion production. The measured chloride ion concentrations were very close to the theoretical calculation (Figure 4.64.a).

A concentration of 0.38 mM TCE introduced both as aqueous and as DNAPL phases were almost completely oxidized after 5 hours and 9 hours, respectively (Figure 4.64.b). The oxidation capability of pure phase DNAPL TCE and accordingly, the chloride ion production were also measured (Figure 4.64.c). Tween 80, which is expected to have a positive effect on oxidation by increasing the solubility of TCE in water, was introduced into the system in the presence of pure-phase DNAPL TCE.

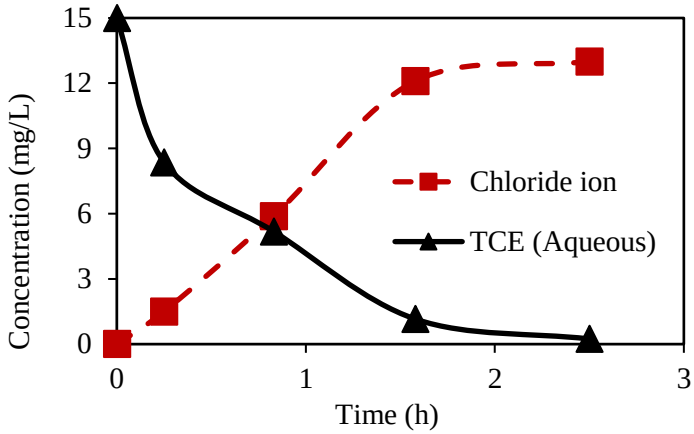

(a)

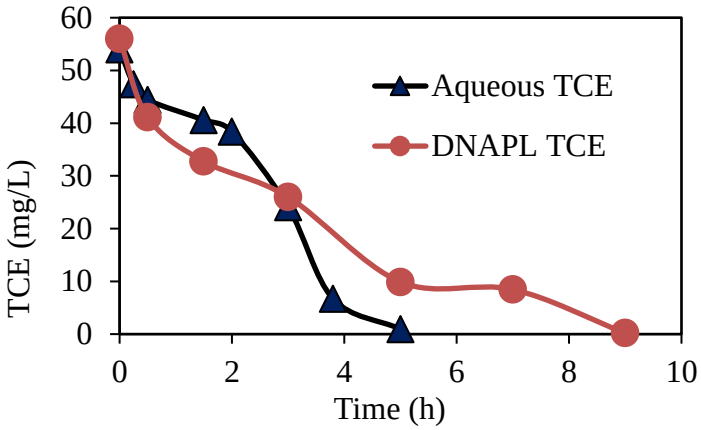

(b)

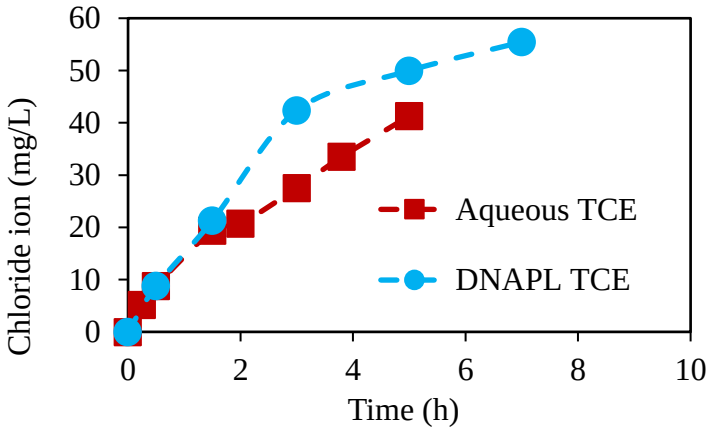

(c)

Figure 4.64. a) Aqueous TCE degradation curve. Molar ratio PS/TCE: [10/1]; C_{PS}: 1.14 mM, C_{TCE}: 0.114 mM, b) Aqueous and DNAPL TCE degradation curve. Molar ratios PS/TCE: [10/1]; C_{PS}: 3.8 mM, C_{TCE}: 0.38 mM, c) Chloride ion concentration released from aqueous and DNAPL TCE.

The oxidation of TCE dissolved in water was investigated in the presence of Tween 80, and it was observed that the consumption of TCE (Figure 4.65.a) and the production of chloride ions were noticeably reduced with an increase in Tween 80 (Figure 4.65.b).

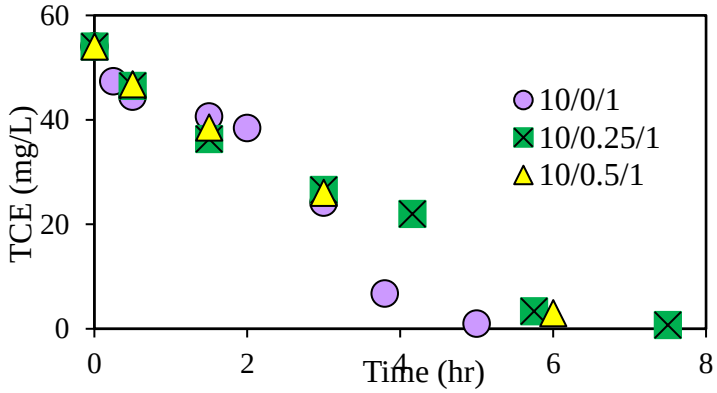

(a)

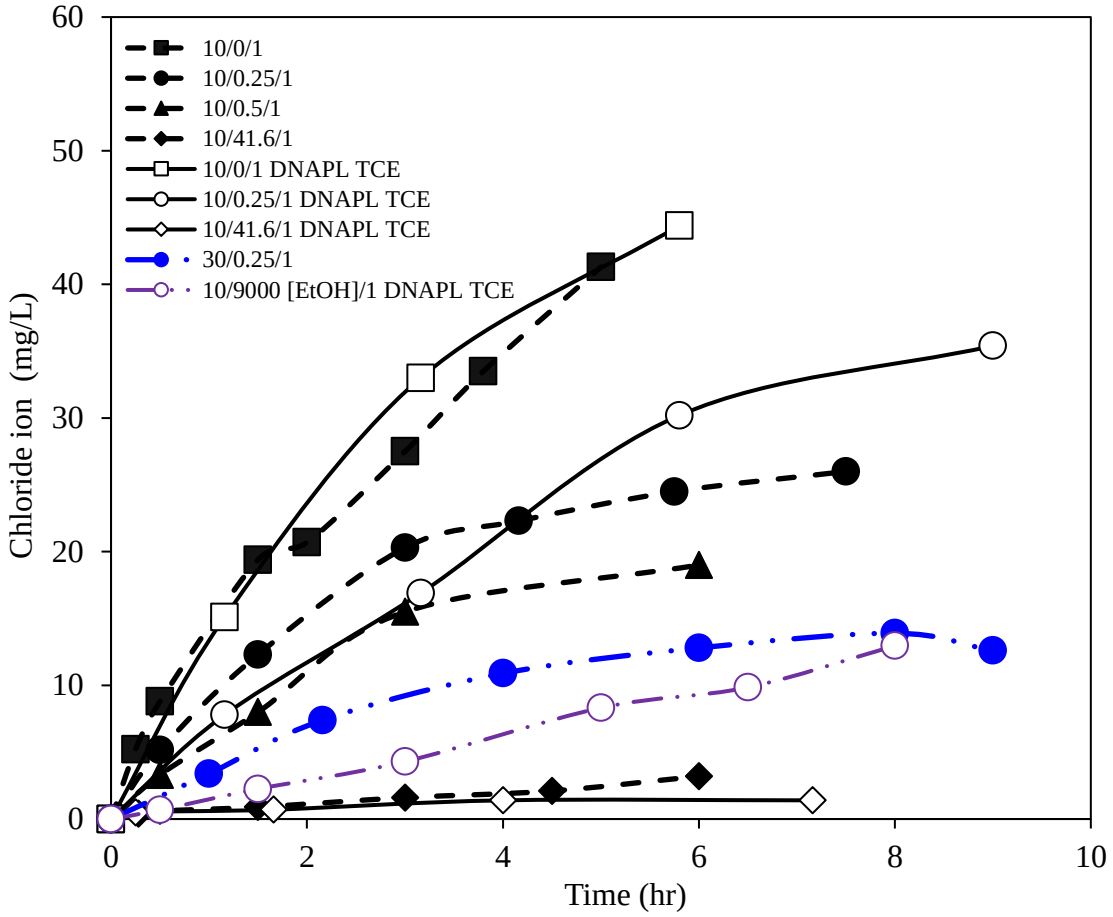

(b)

Figure 4.65. a) Aqueous TCE degradation in the presence of Tween 80. Molar ratios PS/Tween80/TCE: [10/0/1] C_{PS}: 3.8mM, $C_{Tween80}$: 0 mM, C_{TCE}: 0.38mM; [10/0.25/1] C_{PS}: 3.8mM, $C_{Tween80}$: 0.095 mM, C_{TCE}: 0.38mM; [10/0.5/1] C_{PS}: 3.8mM, $C_{Tween80}$: 0.2 mM, C_{TCE}: 0.38mM, b) Chloride ion concentration released from aqueous and DNAPL TCE in the presence of Tween 80.

4.5.2. Tween 80 Enhanced Thermally-Activated Persulfate Oxidation of DNAPL TCE Source Zones

In the first flow-cell experiment, 1 mL DNAPL TCE was injected through the middle upper port of the tank. The DNAPL mass was allowed to equilibrate for almost 48 hours. After 12 PVs of continuous flushing with heat-activated $Na_2S_2O_8$ solution, the system was stopped for 3 days (Figure 4.67). At the end of this period, the system was flushed with electrolyte solution, and TCE, pH, and chloride ion were measured. The TCE concentration increased rapidly and reached the highest value of 447 mg/L and decreased to 120 mg/L in the first PV (Figure 4.66.a). The chloride reached the highest value of 132.8 mg/L with the sharp peak of TCE in the first PV. The system shutdown also led to a similar increase in TCE and chloride ions. Above all, significant chloride production was not observed during the experiment. The initial pH of the system remained for 2 PV at 5.5, then decreased to 2.5 as continued throughout the flushing. After a total of 35 PVs of flushing time, the TCE concentration was decreased to 1.2 mg/L where the flushing was ended.

In the second flow-cell experiment; 0.35 mL DNAPL TCE was injected into the tank. The DNAPL mass was allowed to equilibrate for 26 hours (Figure 4.66.b). The heat-activated $Na_2S_2O_8$ solution was injected for 1PV (2.4 hours) and the system was stopped for 24 hours. This allowed an increased contact between the flushing solution and the DNAPL mass without the need for excessive flushing solution. After 24 hours of waiting, the tank was flushed with DI water. Similar to the previous experiment, TCE concentration increased rapidly in the first PV and reached the highest value of 308 mg/L (Figure 4.66.b). The chloride ion, which is an oxidation by-product, was not observed throughout the flushing experiment, reaching the highest value of 6.5 mg/L in the first PV. At the end of 46 PV, the TCE concentration decreased below 1 mg/L. During the first 6 PV, the pH ranged around 2-3.5 and increased gradually to 6 until the end of the flushing experiment.

In the third flow-cell experiment 0.35 mL DNAPL TCE was injected into the tank. The DNAPL mass was allowed to equilibrate for 20 hours (Figure 4.66.c). The heat-activated $Na_2S_2O_8$ solution containing 1 % Tween 80 was continuously flushed throughout the experiment. The TCE concentration increased after a lag of 0.3 PV and reached the enhanced dissolution value of 1536 mg/L at 1.25 PV (Figure 4.66.c). The chloride ion was measured between 0.95-5 mg/L throughout the experiment. Similar to the first experiment, the pH of the system remained around 6.5 for 0.65 PV, then gradually decreased to 1.5 and remained at this level for the rest for the flushing experiment.

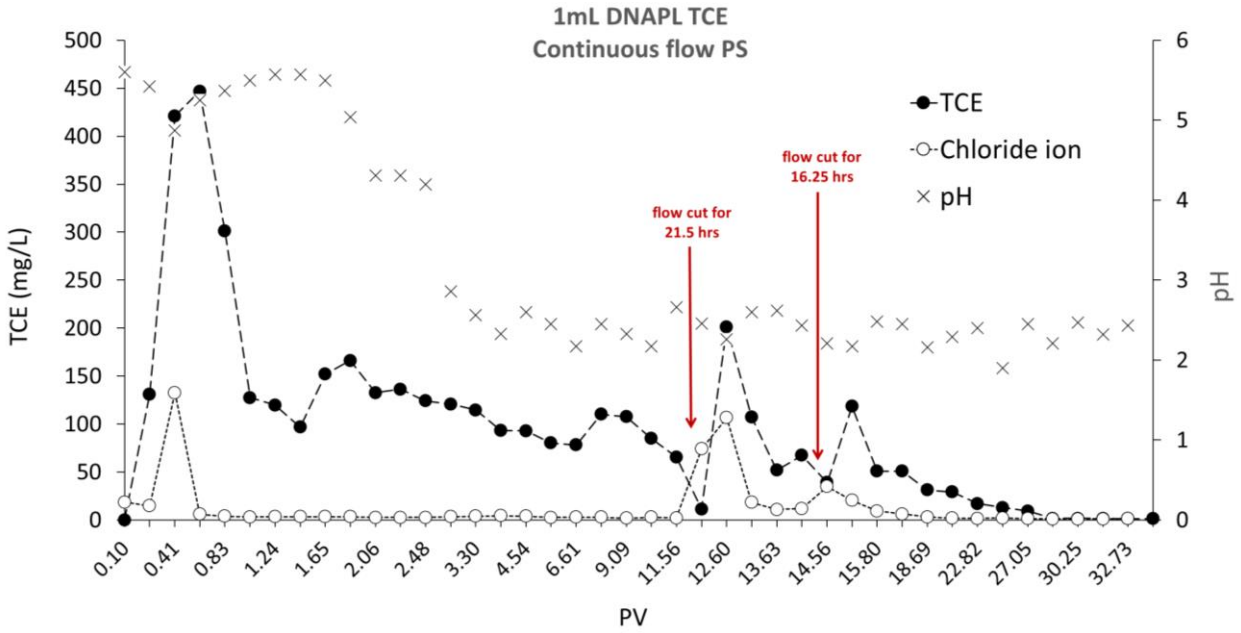
1mL DNAPL TCE
Continuous flow PS
TCE
Chloride ion
pH
flow cut for 21.5 hrs
flow cut for 16.25 hrs
TCE (mg/L)
pH
PV
0.10
0.41
0.83
1.24
1.65
2.06
2.48
3.30
4.54
6.61
9.09
11.56
12.60
13.63
14.56
15.80
18.69
22.82
27.05
30.25
32.73

(a)

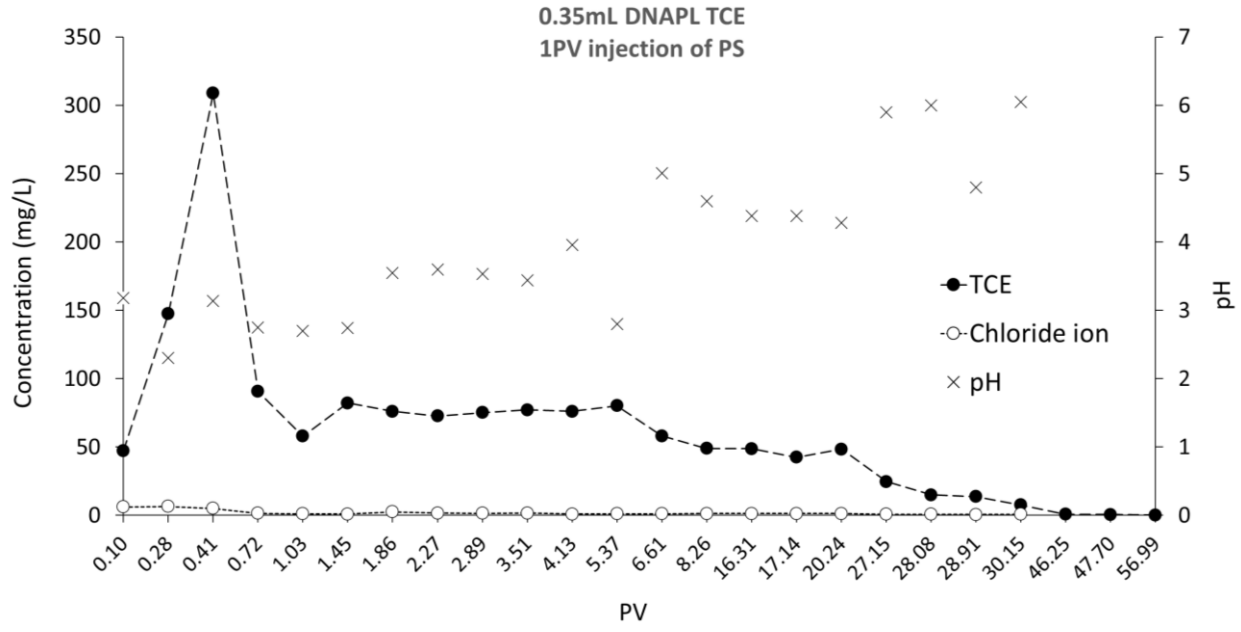
0.35mL DNAPL TCE
1PV injection of PS
TCE
Chloride ion
pH
Concentration (mg/L)
pH
PV
0.10
0.28
0.41
0.72
1.03
1.45
1.86
2.27
2.89
3.51
4.13
5.37
6.61
8.26
16.31
17.14
20.24
27.15
28.08
28.91
30.15
46.25
47.70
56.99

(b)

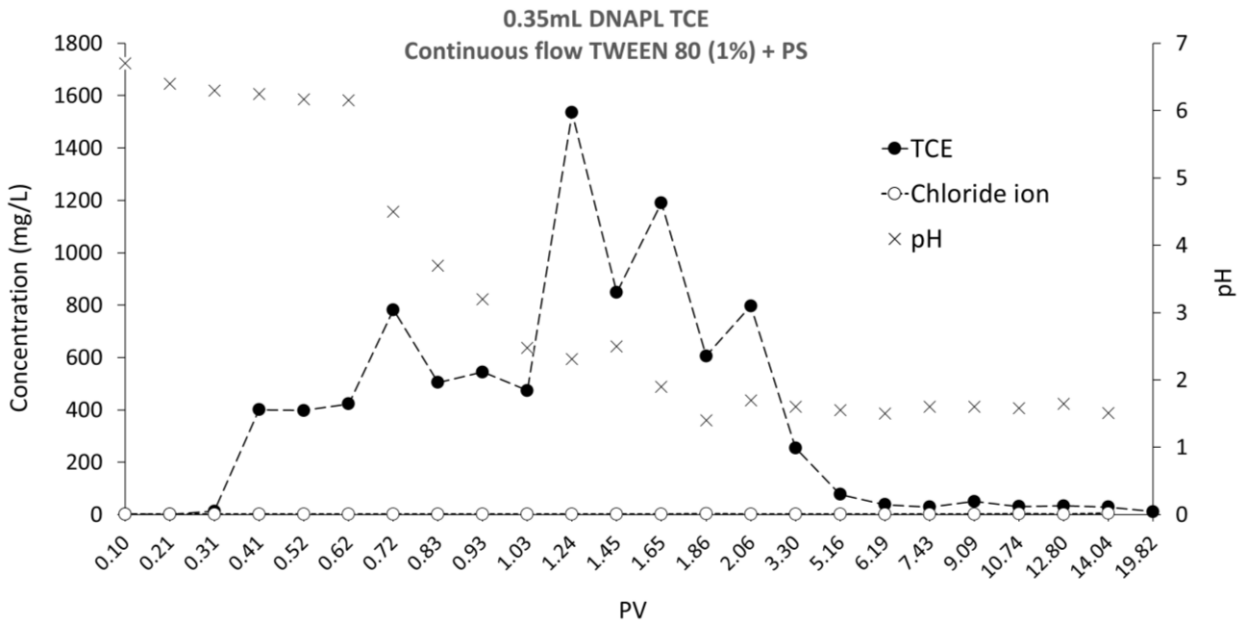

(c)

Figure 4.66. Time-dependent change of TCE, chloride ion, and pH in silica sand (1 PV = 2.4 hours) a) Continuous persulfate solution through the flow-cell, b) 1PV injection of persulfate solution and flushing with DI water through the flow-cell, c) Continuous persulfate and Tween 80 (1 %) mixture solution through the flow-cell.

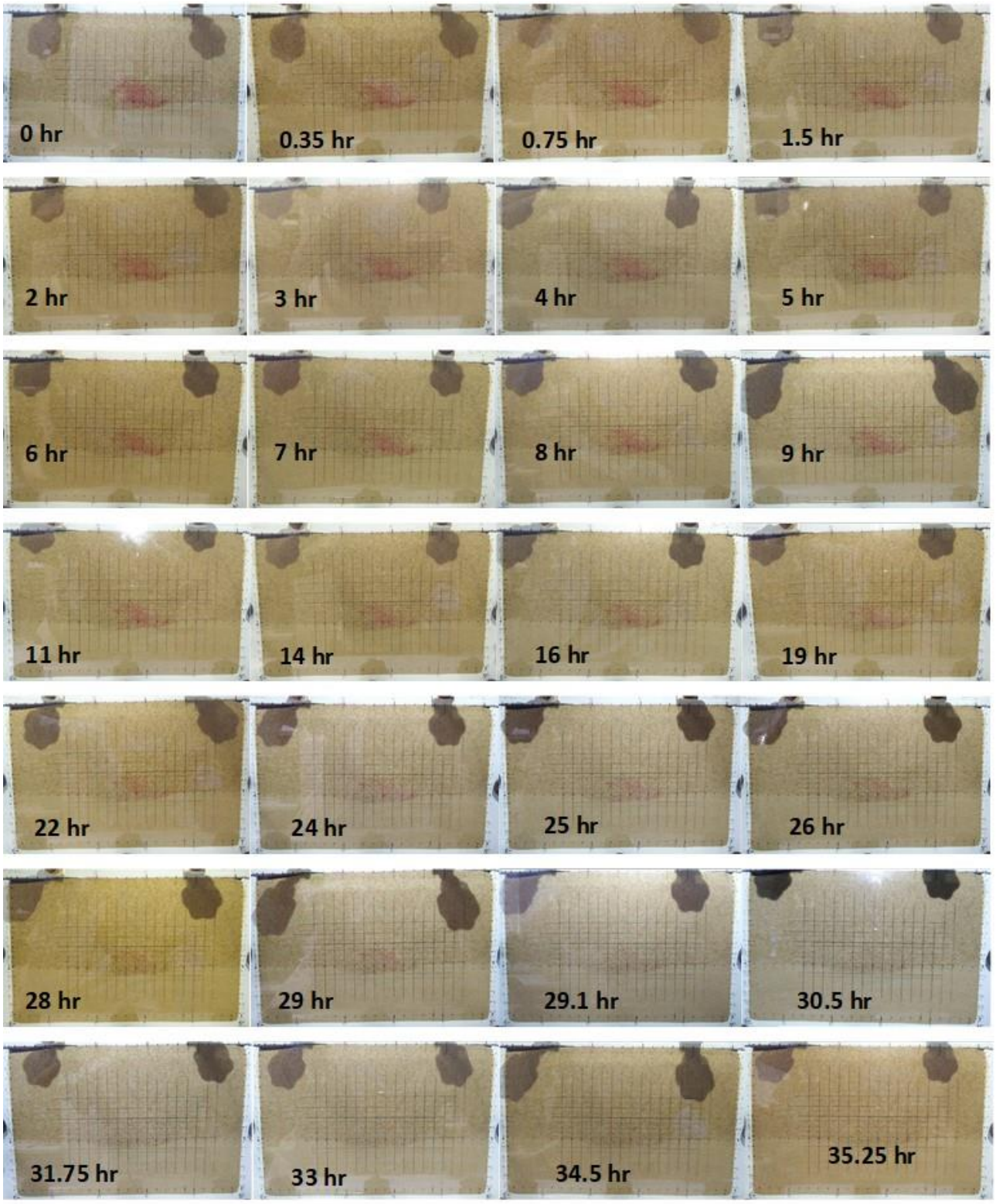

Figure 4.67. Images showed dyed 1 mL of DNAPL mass as a function of time for flushing with 111 mM (26.5 g/L) persulfate.

Overall, the batch and flushing experiments revealed that Tween 80 can enhance the dissolution of both PCE and TCE mass in the presence of persulfate. However, Tween 80 also interferes with persulfate. In particular, high Tween 80 concentration, suppress completely DNAPL oxidation. Low Tween 80 concentrations such as CMC level is not sufficient to effectively dissolve the PCE and TCE. Optimal Tween 80 concentration can be in the range of about 3 fold of CMC. The experiments performed as part of this study point to the need to conduct batch and flushing experiments prior to real field applications to identify the optimal concentrations.

The results of this study with persulfate also show the self-reactivity of persulfate and its reactability with soil. For optimal performance, the reactivity of persulfate with the soil/water system needs to be accounted for.

5. CONCLUSIONS AND FUTURE RECOMMENDATIONS

The contamination of groundwater with hydrophobic organic compounds in the form of non-aqueous phase liquids (DNAPLs) is a widespread and challenging problem. Despite the significant efforts directed to this problem, there is currently no broadly accepted technology that can fully remediate the soil and groundwater once the DNAPL infiltrates subsurface. The performance of remediation technology depends on site characteristics which play a critical role in selecting the optimal DNAPL remediation strategies for contaminated sites. Soil heterogeneity also has an important effect on DNAPL distribution once released into subsurface environment. Low permeability zones in particular can lead to the entrapment of DNAPLs and reduced dissolution rates. Another important factor is soil composition, particularly soil natural content which can sorb DNAPLs as well as react with oxidants used as part of in-situ oxidation technologies.

In-situ methods are long-standing procedure for subsurface remediation activities. In-situ enhanced solubilization (ISES) is a widely used remediation technique which facilitates the use of chemical agents in flushing to enhance the solubility of contaminants in groundwater. In-situ chemical oxidation (ISCO) involves injecting an oxidizing agent into groundwater. It enables direct contact between the oxidant and the organic contaminant source zone/plume leading to DNAPL chemical degradation in place. While both remediation methods, ISES and ISCO, have been studied extensively on their own, studies that combine these two techniques are relatively few. In this study, a series of flow-cell flushing experiments were conducted to investigate the solubilizing and oxidizing agents capability. The potential synergy was also investigated when surfactant enhanced dissolution is combined with chemical oxidation of a DNAPL entrapped in saturated porous media. Enhanced solubilization experiments focused on the use of surfactants and complex sugars as the enhanced dissolution agents. The results of in-situ enhanced solubilization flow-cell experiment formed the basis of experiments combining both technologies. On the other hand, for in-situ oxidation, potassium permanganate and activated sodium persulfate solutions were considered. Potassium permanganate, which has been used for many years in water treatment and soil remediation, has been considered for DNAPL removal. Activated sodium persulfate, on the other hand is a relatively newer oxidant that has been investigated in the last few years for groundwater remediation. The DNAPLs selected in this study are the chlorinated solvents, PCE, TCE, and 1,1-DCE which are highly toxic and have been found at numerous sites worldwide.

Modeling is an important tool that can aid in assessing the risks of groundwater contamination and in the design of remedial activities. For groundwater contaminated with DNAPL, multiphase system is present consisting of a DNAPL phase, the aqueous phase and flushing solution phase. In this thesis, the conducted laboratory experiments were simulated using different approaches to gain further insight into the remediation activities.

The laboratory experiments and/or modeling studies conducted in this thesis are described below.

Comparison of the performance of different enhanced solubilizing agents (Tween 80, MCD, and SDS) with PCE

Batch and flow-cell experiments were conducted to evaluate the performance of three solubilizing agents (Tween 80, MCD, and SDS) with PCE. It was found that all three agents significantly speed up the recovery of the entrapped DNAPL compared to that of water flooding only. Tween 80 enhancing the dissolution of PCE was found to be the most effective agent, followed by SDS and finally MCD. Enhanced solubilization flow-cell flushing results indicated a non-ideal multistep behavior and tailings at the later stages for DNAPL elution which is attributed to complex poorly-accessible DNAPL source zones.

Two modeling approaches were considered to simulate the enhanced solubility of PCE. The multiphase flow program UTCHEM was used to numerically simulate dissolution experiments performed both in silica sand and natural soil porous media configuration. The main calibration parameters were the interphase mass transfer coefficient, the transversal dispersivity and DNAPL distribution (location and initial DNAPL saturation). The calibration of multiphase model shows NRMSE (normalized root mean square of the error) ranging from 0.08 and 0.1 with R^2 (coefficient of correlation) values ranging from 0.81 to 0.93 for silica sand while the NRMSE ranged from 0.12 and 0.19 with R^2 values from 0.66 to 0.91 for natural soil. The best-fit mass transfer coefficients ranged between 3.2 and 1000 day^{-1}. Sensitivity analysis conducted with the UTCHEM model showed that solubility, flushing velocity and mass transfer coefficient were the most critical parameters.

A second simplified empirically-based modeling approach was also used to simulate the flushing experiments. The approach focuses on empirically defining the DNAPL mass-concentration relations. It was found that this model is capable of capturing the main DNAPL dissolution dynamics. In particular it allowed for the quantification of a multi-step dissolution behavior, a phenomena widely

reported in the literature. The lower discharge concentrations as the flood progresses in time is indicative of the dissolution of less accessible DNAPL mass. Further experimentation is needed to validate the application of such models to field conditions.

Comparison of the performance of different enhanced solubilizing agents (Tween 80, MCD, and SDS) with multicomponent DNAPL

Field data often show that DNAPL encountered in the subsurface are more often found in the form of multicomponent mixtures rather than single components. In this section of the thesis, the use of three enhanced solubilizing agents (Tween 80, MCD, and SDS) was investigated with multicomponent DNAPL consisting of PCE, TCE and 1,1-DCE. Based on batch tests, the selected flushing agent solutions caused the solubilities of DNAPL mixtures to increase by a factor of 10 to 300 for the surfactant agents and 3 to 20 for MCD. Moreover, the solubilization agents initiated a relatively greater solubility enhancement for PCE, which is the least soluble component of the DNAPL mixture. However, experiments showed that the IFT was not significantly lowered to cause DNAPL mobility, indicating that enhanced solubilization would be the dominant recovery mechanism for these systems. This was also confirmed by the flushing experiments which did not show any DNAPL mobility. The ternary phase diagrams (TPD) also showed that, at the selected solubilization contents, a multiple phase system will be present. Moreover, the titration method used in the construction of the TPD curves revealed that the Tween 80 solution, in particular, had a much higher viscosity than the other two flushing agent solutions.

The results of the batch tests underline the importance of understanding well the multiphase behavior of the selected agent DNAPL system prior to any field application. Specifically, it is important to identify and select the solubility enhancing agents and contents that yield high solubility enhancement and are easy to work with in the field.

Modeling of the multicomponent DNAPL flushing experiments was also done with the UTCHEM computer code. Although modeling results were consistent with experimental data, this exercise underlined the challenges of simulating the remediation of DNAPL mixtures are present. Such models require significantly more data to characterize the multiphase system. Moreover, the experimental data needed to calibrate the model are more difficult to find.

Surfactant enhanced permanganate oxidation of PCE

The enhanced flushing experiments (Section 4.1) showed that Tween 80 with PCE had the highest performance compared to other solubilizing agents. In this section of the study, the synergy of Tween 80-enhanced permanganate oxidation of PCE was investigated. The experimental results showed that combining the two technologies yields enhanced performance compared to each technology taken alone. The enhanced dissolution using Tween 80 increased the dissolved concentration which further enhanced the oxidation with permanganate. Moreover, Tween 80/MnO_4^- pulse injection allowed for a longer contact between the DNAPL and the oxidation agent leading to overall enhanced aqueous phase oxidation by permanganate. Thus, the application of Tween 80/MnO_4^- pulse injection demonstrated improved remediation and more efficient DNAPL mass removal, exhibiting more ideal behavior for source zones remediation compared to permanganate, surfactant or water flushing. The organic matter content in the soil can lead to reduced DNAPL oxidation efficiency as the oxidant can react with both the target compounds as well as non-target compounds. Depending on the oxidant type, it is important to keep the amount of oxidant high in order to meet the oxidant demand of the soil as well as to meet the pollutant requirement. Results of this study showed that for natural soils remediation times were longer than those in sand. , solubilizing agents need more time than in silica sand to remove entrapped PCE. This is attributed to the heterogeneity of the soil as well as the organic content of the soil, about 1 %, which interfere with the remedial activity. Moreover, the heterogeneity of the natural soil reduces the contact between the remedial solution and entrapped DNAPL reducing the aqueous phase PCE concentration.

To estimate the PCE-permanganate oxidation rate constants, the permanganate flushing experiments were also simulated using the UTCHEM multiphase flow model. The experimental and simulated concentrations correlated well with NRMSE varying between 0.083 and 0.182, while R^2 values exceeded 0.9. Lower oxidation rate was obtained when Tween 80 is present, indicating that Tween 80 may interfere with the oxidation reaction. However, the increase in the solubility of PCE in the presence of Tween 80 more than compensated for the decrease in reaction rate constant. The net effect is accelerated and more efficient remediation is observed when both enhanced dissolution and oxidation technologies are combined. Moreover, this study demonstrates that the UTCHEM program is a useful tool that can help in evaluating the synergistic benefits when enhanced dissolution and in-situ oxidation technologies are jointly considered.

Surfactant enhanced persulfate oxidation of PCE and TCE

In this set of experiments, the oxidation of PCE and TCE by activated sodium persulfate with and without Tween 80 was investigated using reactivity batch and flow-cell experiments. A critical step for the use of persulfate is its activation to form radicals. In the literature, a number of activation methods have been proposed. In this study, activation by iron as well as thermal activation were investigated. Results of batch tests showed limited activation with granular iron possibly due to iron corrosion. With regard to thermal activation, batch experiments demonstrated that persulfate stops activating as soon as temperature drops. The batch experiments also revealed that activated sodium persulfate plays a more active role in the removal of tetrachloroethene PCE, which consists of a single carbon and 4 chlorine atoms and has a higher density than many other chlorinated solvents. In addition, it has been observed that during the continuous injection of thermally activated persulfate, there was almost no chloride release from DNAPL in the presence of non-ionic surfactant (Tween 80) that was used at concentrations above CMC level resulting an inhibition in oxidation process. This surfactant is known to enhance the dissolution of DNAPL PCE into the aqueous phase. As a result, it was concluded that high surfactant concentrations tend to interfere with the reaction between DNAPL and the oxidant, and therefore, the flow behavior and overall PCE removal will be similar to the surfactant flushing dissolution mechanism under high surfactant conditions.

Overall, experimental studies show that flow field heterogeneity, type of contaminant, phase of the contaminant in the subsurface, type of flushing agent, flushing injection type, type of solubilizing and/or oxidizing agent, porous media properties and contact time between the contaminant and flushing agent are all key parameters in subsurface DNAPL remediation studies. Laboratory scale experiments such as those conducted in this study can provide important information about the different remedial agents and their optimum concentrations. However, for successful real life applications additional parameters need to be considered beyond those considered in a controlled laboratory setting such as effective delivery of flushing agent.

In this study, enhanced solubilization and in-situ oxidation are shown to be effective DNAPL remediation technologies. Future research is needed to further enhance our knowledge of the individual or synergetic usage of both technologies. Specifically, in relation to persulfate activation, additional work may be directed to the following issues:

- The inhibitory effect of the surfactant on persulfate oxidation is not accurately determined. Research can focus on suppressing the side inhibitory role of specific agents from the system with less side effects.
- Future research can focus on the development of surfactants that can take over the role of both solubilization enhancer and activator for oxidant.
- More work is needed to reveal the specific free radical scavenging mechanism that effect the life of radicals released from persulfate activation during the remediation process
- Focus on newly potential activation methods for persulfate such as natural minerals. Main issue that could be considered here is a sustainable source of mechanism throughout the process, an effectiveness on both remediation performance and processing cost.

Based on experimental and the numerical work conducted in this study, future recommendations on solubilizing agent enhanced oxidation of NAPL may focus on the issues below:

- Innovative imaging techniques could be used to estimate more accurately the DNAPL spatial distribution. This plays a critical role in determining the efficiency of any remedial activity.
- Heat transport models can be integrated to the heat activated persulfate reaction models
- Develop existing multiphase flow codes considering multicomponent DNAPLs allowing for the definition of all DNAPL properties when multicomponent DNAPLs are present n the system.
- Novel ideas in field design and operational strategy for the aim of developing an efficient and cost-effective way of heat activation in the field. Sodium persulfate technology is relatively new, is still in early stages of testing, and is thought to have the potential of becoming one of the most effective methods for DNAPL removal
- Innovations on energy saving via reducing activation energy cost at high temperatures for thermally activated persulfate due to augmentation of generated radicals. In contaminated areas where geothermal heating potential (renewable energy) sources can be used coupled with industrial processes
- Extend the subsurface remediation to combine the benefits of different technologies including bioremediation, thermal methods and free-radical release from chemicals
- Bench-scale batch and flushing studies in conjunction with empirical or numerical model validation can aid in the implementation of persulfate oxidation with enhanced solubilization at the field-scale

REFERENCES

Abriola, L.M., Drummond, C.D., Hahn, E.J., Hayes, K.F., Kibbey, T.C.G., Lemke, L.D., Pennell, K.D., Petrovskis, E.A., Ramsburg, C.A., & Rathfelder, K.M. (2005). Pilot-Scale Demonstration of Surfactant Enhanced PCE Solubilization at the Bachman Site. 1. Site Characterization and Test Design. Environmental Science and Technology, 39, 6, 1778-1790.

Agaoglu, B., Scheytt, T., & Copty, N.K. (2012). Laboratory-scale experiments and numerical modeling of cosolvent flushing of multi-component NAPLs in saturated porous media. Journal of Contaminant Hydrology, 140-141. http://dx.doi.org/10.1016/j.jconhyd.2012.07.005

Agaoglu, B., Copty, N.K., Scheytt, T., & Hinkelmann, R. (2015). Interphase mass transfer between fluids in subsurface formations: a review. Advances in Water Resources, 79, 162-194. http://dx.doi.org/10.1016/j.advwatres.2015.02.009

Agency for Toxic Substances and Disease Registry (ATSDR). (2022). CERCLA List of Hazardous Substances. Retrieved from https://www.atsdr.cdc.gov/spl/index.html#2022spl

Akgoze Aydin, G., Agaoglu, B., Kocasoy, G., & Copty, N.K. (2011). Effect of temperature on cosolvent flooding for the enhanced solubilization and mobilization of NAPLs in porous media. Journal of Hazardous Materials, 186, 636–644. DOI:10.1016/j.jhazmat.2010.11.046

Akyol, N.H., Yolcubal, I., & Imer, D. (2011). Sorption and transport of trichloroethylene in caliche soil. Chemosphere, 82, 809–816. DOI:10.1016/j.chemosphere.2010.11.029

Akyol N.H., Russo Lee A., & Brusseau M.L. (2013). Impact of enhanced-flushing reagents and organic liquid distribution on mass removal and mass discharge reduction. Water, Air, and Soil Pollution, 224:1731. DOI: 10.1007/s11270-013-1731-x

Akyol, N.H., & Yolcubal I. (2013). Oxidation of Nonaqueous Phase Trichloroethylene with Permanganate in Epi-karst. Water, Air, and Soil Pollution, 224:1573, 1-19. DOI: 10.1007/s11270-013-1573-6

Akyol, N. H., Ozbay, I., & Ozbay, B. (2015). Effect of organic carbon fraction on long-term atrazine elution tailing for two heterogeneous porous media: Experimental and modeling approach. Water, Air, and Soil Pollution, 226:368. DOI 10.1007/s11270-015-2639-4

Akyol, N.H., & Turkkan, S. (2018). Effect of cyclodextrine-enhanced dissolution on mass removal and mass discharge reduction for TCE source zones in heterogeneous porous media. Water, Air, and Soil Pollution, 229:30. https://doi.org/10.1007/s11270-017-3673-1

Akyol, N.H. (2018). Surfactant-enhanced permanganate oxidation on mass-flux reduction and mass removal (MFR-MR) relationships for pool-dominated TCE source zones in heterogeneous porous media. Water, Air, and Soil Pollution, 229:285. https://doi.org/10.1007/s11270-018-3946-3

Akyol, N.H., Demiray, Z., Copty, N.K., Acılıoğlu, T. & Akyol, G. (2023). Mass-flux reduction and mass removal relationships (MFR-MR) of pool-dominated multicomponent DNAPLs in a heterogeneous geological system. Global NEST Journal, 25(4), 43-55.

Allen-King, R.M., Halket, R.M., & Burris, D.R. (1997). Reductive transformation and sorption of cis- and trans-1,2- dichloroethene in a metallic iron-water system. Environmental Toxicology and Chemistry, 16:424-429.

Al-Shamsi, M. A., & Thomson, N. R. (2013a). Treatment of organic compounds by activated persulfate using nanoscale zero valent iron. Industrial Engineering Chemistry Research, 52, 13564–13571.

Ambas, V.T., & Baltas, E. (2012). Sensitivity analysis of different evapotranspiration methods using a new sensitivity coefficient. Global NEST Journal, 14 (3), 335–343.

Arvind, K., & Pradeep, K. (2008). Occurence of anionic surfactants in treated sewage: Risk assessment to aquatic environment. Journal of Hazardous Materials, 160, 362-370.

ASTM International. (2004). Standard guide for application of a ground-water flow model to a site-specific problem. D5447-04.

ASTM International. (2007). Standard Test Method for Estimating the Permanganate Natural Oxidant Demand of Soil and Aquifer Solids. D 7262-07.

Aydin-Sarikurt, D., Dokou, Z., Copty, N. K., & Karatzas, G. P. (2016). Experimental Investigation and Numerical Modeling of Enhanced DNAPL Solubilization in Saturated Porous Media. Water, Air, and Soil Pollution, 227: 441. DOI 10.1007/s11270-016-3136-0

Ayorinde, F.O., Gelain, S.V., Johnson, J.H., Jr. & Wan, L.W. (2000). Analysis of some commercial polysorbate formulations using matrix-assisted laser desorption/ionization time-of-flight mass spectrometry. Rapid Communications in Mass Spectrometry, 14: 2116-2124. https://doi.org/10.1002/1097-0231(20001130)14:22<2116::AID-RCM142>3.0.CO;2-1

Badr, T., Hanna, K., & de Brauer, C. (2004). Enhanced solubilization and removal of naphthalene and phenanthrene by cyclodextrins from two contaminated soils. Journal of Hazardous Materials, 112, 215–223. https:// doi. org/ 10.1016/j. jhazm at. 2004. 04. 017

Bąk, A., & Podgorska, W. (2016). Interfacial and surface tensions of toluene/water and air/ water systems with nonionic surfactants Tween 20 and Tween 80. Colloids and Surfaces A: Physicochemical and Engineering Aspects, 504, 414–425. https://doi.org/10.1016/j. colsurfa.2016.05.091

Baker, R.S., Nielsen, S.G., Heron, G., & Ploug, N. (2016). How effective is thermal remediation of DNAPL source zones in reducing groundwater concentrations?. Ground Water Monitoring and Remediation, 36, 1, 38-53.

Bautitz, I.R., Velosa, A.C., & Nogueira, R.F.P. (2012). Zero valent iron mediated degradation of the pharmaceutical diazepam. Chemosphere, 88, 688–692.

Behrman, E. J., & Dean, D. H. (1999). Sodium peroxydisulfate is a stable and cheap substitute for ammonium peroxydisulfate (persulfate) in polyacrylamide gel electrophoresis. Journal of Chromatography B: Biomedical Sciences and Applications, 723(1-2), 325–326. https://doi.org/10.1016/s0378-4347(98)00525-8

Bender, M.L., & Komiyama, M. (1978). Cyclodextrin Chemistry, Springer Verlag, New York, NY.

Benson, B., World Health Organization & International Programme on Chemical Safety.(2003). 1,1-Dichloroethene (vinylidene chloride). World Health Organization.

Boutonnet, M., Kizling, J., & Stenius, P. (1982). The preparation of monodisperse colloidal metal particles from micro emulsions. Colloids and Surfaces, 5, 209-225.

Boving, T.B., & Brusseau, M.L. (2000). Solubilization and removal of residual Trichloroethene from porous media: Comparison of several solubilization agents. Journal of Contaminant Hydrology, 42, 51-67.

Brooks, R.H., & Corey, A.T. (1966). Properties of porous media affecting fluid flow. Journal of the Irrigation and Drainage Division, 92(2): 61-90.

Brown, R.A., Skladany, G., Robinson, D., Fiacco, J., & McTigue, J.W. (2001). Comparing permanganate and persulfate treatment effectiveness for various organic contaminants. Proceeding of the First International Conference on Oxidation and Reduction Technologies for In-Situ Treatment of Soil and Groundwater, Niagara Falls, Ontario, Canada, June 2001; pp 25-29.

Brusseau, M. L., Zhang, Z., Nelson, N. T., Cain, R. B., Tick, G. R., & Oostrom, M. (2002). Dissolution of nonuniformly distributed immiscible liquid: Intermediate-scale experiments and mathematical modeling. Environmental Science & Technology, 36, 1033–1041. https:// doi. org/10. 1021/ es010 609f

Brusseau, M.L., Nelson, N.T., Zhang, Z., Blue, J.E., Rohrer, J., & Allen, T. (2007). Source-zone characterization of a chlorinated-solvent contaminated superfund site in Tucson AZ. Journal of Contaminant Hydrology, 90, 21–40.

Brusseau, M. L., DiFilippo, E. L., Marble, J. C., & Oostrom, M. (2008). Mass-removal and mass-flux-reduction behavior for idealized source zones with hydraulically poorlyaccessible organic liquid. Chemosphere, 71, 1511–1521. https:// doi. org/ 10. 1016/j. chemo sphere. 2007. 11. 064

Brusseau, M.L., Matthieu, D. E., Carroll, K.C., Mainhagu, J., Morrison, C., McMillan, A., Russo, A., & Plaschke, M. (2013). Characterizing long-term contaminant mass discharge and the relationship between reductions in discharge and reductions in mass for DNAPL source areas. Journal of Contaminant Hydrology, 149, 1-12.

Burden, R & Faires, J.D. (1997). Sixth Edition, Numerical Analysis, Brooks/Coles Publishing

Burris, R., Campbell, J., & Manoranjan, S. (1995). Sorption of trichloroethylene and tetrachloroethylene in a batch reactive metallic iron water system. Environmental Science and Technology, 29, 2850-2855.

Buxton, G.V., Greenstock, C.L., Helman, W.P. & Ross, A.B. (1988). Critical-Review of Rate Constants for Reactions of Hydrated Electrons, Hydrogen-Atoms and Hydroxyl Radicals(•OH/•O–) in Aqueous-Solution. Journal of Physical and Chemical Reference Data, 17, 513-886. http://dx.doi.org/10.1063/1.555805

Cai, Z.T, & Mohanty, K.K. (1997). Interfacial Tension Measurement in DNAPL/Aqueous Surfactant Systems. Journal of Colloid and Interface Science, 195, no. 2 : 408–410.

Cao, J., Zhang, W., Brown, D.G., & Sethi, D. (2008). Oxidation of Lindane with Fe(II)-Activated Sodium Persulfate. Environmental Engineering Science, 25, 221-228.

Carroll, K.C., & Brusseau, M.L. (2009). Dissolution, cyclodextrin enhanced solubilization and mass removal of an ideal multicomponent organic liquid. Journal of Contaminant Hydrology, 106, 62-72. doi:10.1016/j.jconhyd.2009.01002

Carsel, R. F., & Parrish, R. S. (1988). Developing Joint Probability Distributions of Soil Water Retention Characteristics. Water Resource Research, 24, 755-769.

Chang, Y.C., Chen, T.Y., Tsai, Y.P., & Chen, K.F. (2018). Remediation of trichloroethene (TCE)-contaminated groundwater by persulfate oxidation: a field-scale study. RSC Advances, 8, 2433-2440. https://doi.org/10.1039/C7RA10860E

Chen, X.Y., Xue, Z.Y., Wu, D., Wang, W.P., Zhu, F.X., & Wu, C.Z. (2009). Advanced oxidation technology based on sulfate radical and application in water treatment. Water Treatment, 35(5): 16–20.

Chen, X., Oh, W.D., & Lim, T.T. (2018). Graphene- and CNTs-based carbocatalysts in persulfates activation: material design and catalytic mechanisms. Chemical Engineering Journal, 354, 941-976. https://doi.org/10.1016/j.cej.2018.08.049

Cheng, Z., Gao, B., Xu, H., Sun, Y., Shi, X. & Wu, J. (2016). Effects of surface active agents on DNAPL migration and distribution in saturated porous media. The Science of the Total Environment, 571, 1147–1154. https://doi.org/10.1016/j.scitotenv.2016.07.109

Cheng, Y., & Zhu, J. (2021). Significance of mass–concentration relation on the contaminant source depletion in the nonaqueous phase liquid (NAPL) contaminated zone. Transport in Porous Media, 137, 399–416. https:// doi. org/10. 1007/ s11242- 021- 01567-5

Cho, Y., & Choi, S. (2010). Degradation of PCE, TCE and 1,1,1-TCA by nanosized Fe Pd bimetallic particles under various experimental conditions. Chemosphere, 81, 940-945.

Chowdhury, A.I.A., Gerhard, J.I., Reynolds, D., & O'Carroll, D.M. (2017). Low permeability zone remediation via oxidant delivered by electrokinetics and activated by electrical resistance heating: proof of concept. Environmental Science and Technology, 51 (22), 13295-13303.

Clark, C.J. II, Rao, P.S.C., & Annable, M.D. (2003). Degradation of perchloroethylene in cosolvent solutions by zerovalent iron. Journal of Hazardous Materials, 96: 65–78. https://doi.org/10.1016/s0304-3894(02)00162-0

Conrad, S.H., Glass, R.J., & Peplinski, W.J. (2002). Bench-scale visualization of DNAPL remediation processes in analog heterogeneous aquifers: surfactant floods and in situ oxidation using permanganate. Journal of Contaminant Hydrology, 58, 1-2, 13-49.

Corey, A.T. (1994). Mechanics of immiscible fluids in porous media. Water Resources Publications, CO.

Costanza, J., Otaño, G., Callaghan, J., & Pennell, K. D. (2010). PCE oxidation by sodium persulfate in the presence of solids. Environmental Science and Technology, 44, 9445−9450.

Cussler, E.L. (1997). Diffusion: Mass Transfer in Fluid Systems, Cambridge University Press, 580 p.

Dai, Q., & Reitsma, S. (2002). Kinetic Study of Permanganate Oxidation of Tetrachloroethylene at pH 10.60±0.1, in Remediation of Chlorinated and Recalcitrant Compounds-2002, Paper 2C-09. Proceedings of the Third International Conference on Remediation of Chlorinated and Recalcitrant

Compounds, Monterey, CA, May 20-23, 2002, eds. A. R. Gavaskar and A. S. C. Chen, ISBN 1-57477-132-9, Battelle Press, Columbus, OH.

Dangi, M.B., Urynowicz, M.A., Schultz, C.L., & Budhathoki, S. (2022). A comparison of the soil natural oxidant demand exerted by permanganate, hydrogen peroxide, sodium persulfate, and sodium percarbonate. Environmental Challenges, 7, 100456.

Delshad, M., Pope, G.A., Sepehrnoori, K. (1996). A compositional simulator for modeling surfactant enhanced aquifer remediation. Journal of Contaminant Hydrology, 23, 4, 303-327.

Demiray, Z., Akyol, N.H., & Copty, N.K. (2021). Experimental Assessment and Modeling of Enhanced Solubilization of Pool-dominated Tetrachloroethene Source Zone in Heterogeneous Porous Media. Water, Air, and Soil Pollution, 232:516. https://doi.org/10.1007/s11270-021-05454-z

Desalegn, B., Megharaj, M., Chen, Z., & Naidu, R. (2018). Green mango peel-nanozerovalent iron activated persulfate oxidation of petroleum hydrocarbons in oil sludge contaminated soil. Environmental Technology & Innovation, 11 (2018) 142–152.

DiFilippo, E.L., & Brusseau, M.L. (2008). Relationship between mass flux reduction and source-zone mass removal: analysis of field data. Journal of Contaminant Hydrology, 98, 22–35.

Difilippo, E.L., Carroll, K.C., & Brusseau, M.L. (2010). Impact of organic-liquid distribution and flow-field heterogeneity on reductions in mass flux. Journal of Contaminant Hydrology, 115, 14-25.

Dill, D.C., McCarty, W.M., Alexander, H.C. & Bartlett, E.A. (1980). Toxicity of 11-dichloroethylene (vinylidene chloride) to aquatic organisms. Midland MI Dow Chemical Company (PB 81-111098) [cited in US EPA 1980].

Distefano, T., Gossett, J., & Zinder, S. (1992). Hydrogen as an electron donor for dechlorination of tetrachloroethene by an anaerobic mixed culture. Applied and Environmental Microbiology, 58, 3622-3629.

Domenico, P.A., Schwartz, F.W. 1998. Physical and Chemical Hydrogeology. John Wiley and Sons, Inc.

Dominguez, C.M., Rodriguez, V., Montero, E., Romero, A., & Santos, A. (2020). Abatement of dichloromethane using persulfate activated by alkali: a kinetic study. Separation and Purification Technology, 241, 116679.

Doty, C.B., & Travis, C.C. (1991). The effectiveness of groundwater pumping as a restoration technology. ORNL/TM-11866, Oak Ridge National Laboratory, Oak Ridge, TN.

Eberson, L. (1987). Electron Transfer Reactions in Organic Chemistry, Spring-Verlag, Berlin.

Eichel, H., Helmig, R., Neuweiler, I., & Cirpka, O.A. (2005). Upscaling of two-phase flow processes in porous media. In: Upscaling Multiphase Flow in Porous Media. Springer, pp. 237–257.

Elloy, F.C., Teel, A.L., & Watts, R.J. (2014). Activation of persulfate by surfactants under acidic and basic conditions. Groundwater Monitoring & Remediation, 34, 51–59.

Falta, R.W., Pruess, K., Finsterle, S., & Battitelli, A.(1995). T2VOC User's Guide.

Falta, R.W., Lee, C.M., Brame, S.E., Roeder, E., Coates, J.T., Wright, C., Wood, A.L., & Enfield, C.G. (1999). Field Test of High Molecular Weight Alcohol Flushing for Subsurface Nonaqueous Phase Liquid Remediation. Water Resources Research, 35, 7, 2095-2108.

Felix-Navarro, R.M., Shui, W.L., Barrera-Diaz, N., & Perez-Sicairos, S. (2007). Kinetics of the degradation of 1,4-dioxane using persulfate. Journal of the Mexican Chemical Society, 51 (2), 67-71.

Fetter, C. W. (1999). Contaminant Hydrogeology, Prentice Hall, New Jersey, NJ.

Fordham, J.W.L., & Williams, H.L. (1951). The persulfate-iron(II) initiator system for free radical polymerizations. Journal of the American Chemical Society, 73:4855–4859.

Forsey, S.P. (2004). In Situ Chemical Oxidation of Creosote/Coal Tar Residuals: Experimental and Numerical Investigation. University of Waterloo: Waterloo, 2004.

Fountain, J.C. (1992). Field Tests of Surfactant Flooding: Mobility Control of Dense Nonaqueous Phase Liquids. In: Transport and Remediation of Subsurface Contaminants, Sabatini D.A., Knox R.C. (Eds.), American Chemical Society, 182-191, Washington, D.C., U.S.A.

Freeze, R.A. and Cherry, J.A. (1979). Groundwater. Prentice-Hall Inc., Englewood Cliffs, Vol. 7632, 604.

Fu, F.L., Dionysiou, D.D., & Liu, H. (2014). The use of zero-valent iron for groundwater remediation and wastewater treatment: a review. Journal of Hazardous Materials, 267, 194-205.

Gabler, T., Paschke, A., & Schüürmann, G. (1996). Diffusion coefficients of substituted benzenes at high dilution in water. Journal of Chemical and Engineering Data, 41, 33-36.

Gates-Anderson, D.D., Siegrist, R.L., & Cline, S.R. (2001). Comparison of Potassium Permanganate and Hydrogen Peroxide as Chemical Oxidants for Organically Contaminated Soils. Journal of Environmental Engineering, 127, 4, 337-347.

Gelhar, L.W. (1993), Stochastic subsurface hydrology: Prentice Hall, Englewood Cliffs, New Jersey, 346 p.

Geza, M., Murray, K.E., & McCray, J.E. (2010). Watershed-scale impacts of nitrogen from onsite wastewater systems: parameter sensitivity and model calibration. ASCE Journal of Environmental Engineering, 136 (9), 926‑938.

Gillham, K., & O'Hannesin, S.F. (1994). Enhanced degradation of halogenated aliphatics by zero-valent iron. Groundwater, 32, 958-967.

Goswami, L., Kim, K.H., Deep, A., Das, P., Bhattacharya, S.S., Kumar, S., & Adelodun, A.A. (2017). Engineered nano particles: nature, behavior, and effect on the environment. Journal of Environmental Management, 196, 297-315.

Hand, D.B. (1930). Dineric distribution. The Journal of Physical Chemistry, 34(9): 1961-2000.

Harendra, S., & Vipulanandan, C. (2011). Solubilization and degradation of perchloroethylene (PCE) in cationic and nonionic surfactant solutions. Journal of Environmental Sciences, 23, 8, 1240-1248.

Harvell, J.R. (2012). Solubilization of Multi-Component Immiscible Liquids in Homogeneous Systems: A Comparison of Different Flushing Agents Using a 2-D Flow Cell. M.S. Thesis, University of Alabama, U.S.A.

Haselow, J. S., Siegrist, R. L., Crimi, M. & Jarosch, T. (2003). Estimating the total oxidant demand for in situ chemical oxidation design. Remediation, 13 (4), 5–16.

Hassanizadeh (Eds.), Upscaling Multiphase Flow in Porous Media, Springer Verlag, Berlin, pp. 237-257

He, Y.T., Wilson, J.T., Su, C., & Wilkin, R.T. (2015). Review of abiotic degradation of chlorinated solvents by reactive iron minerals in aquifers. Groundwater Monitoring and Remediation, 35, 3, 57-75.

Head, N.A., Gerhard, J.I., Inglis, A.M., Nunez Garcia, A., Chowdhury, A.I.A., Reynolds, D. A., de Boer, C.V., Sidebottom, A., Austrins, L.M., Eimers, J., & O'Carroll, D.M. (2020). Field test of electrokinetically-delivered thermally activated persulfate for remediation of chlorinated solvents in clay. Water Research, 183, 116061. https://doi.org/ 10.1016/j.watres.2020.116061.

Helmke, M.F., Simpkins, W.W., & Horton, R. (2004). Experimen-tal determination of effective diffusion parameters in the matrix of fractured till. Vadose Zone Journal, 3, 1050–1056.

Hinkelmann, R. (2005). Efficient numerical methods and information-processing techniques for modeling hydro- and environmental systems. Springer Verlag, Berlin Heidelberg, Germany.

Honning, J. (2007). Use of in situ chemical oxidation with permanganate in PCE-contaminated clayey till with sand lenses. PhD Thesis, Technical University of Denmark.

Hood, E.D., Thomson, N.R., Grossi, D., & Farquhar, G.J. (2000). Experimental determination of the kinetic rate law for the oxidation of perchloroethylene by potassium permanganate. Chemosphere, 40, 1383-1388.

Horvath, A.L. (1982). Halogenated hydrocarbons: solubility-miscibility with water. Marcel Dekker, Inc, pp. 889, New York, NY.

Horvath, A.L., Getzen, F.W., & Maczynska, Z. (1999). IUPAC-NIST solubility data series 67. Halogenated ethanes and ethenes with water. Journal of Physical and Chemical Reference Data, 28, 395–627.

Hosseininoosheri, P., Lashgari, H.R., & Sepehrnoori, K. (2016). A novel method to model and characterize in-situ bio-surfactant production in microbial enhanced oil recovery. Fuel, 183, 501–511. https://doi.org/10.1016/j.fuel.2016.06.035

Huang, K., Hoag, G.E., Chheda, P., Woody, B.A., & Dobbs, G.M. (1999). Kinetic study of oxidation of trichloroethylene by potassium permanganate. Environmental Engineering Science, 16, 4, 265-274.

Huang, K.C., Hoag, G.E., Chheda, P., Woody, B.A., & Dobbs, G.M. (2002). Kinetics and mechanism of oxidation of tetrachloroethylene with permanganate. Chemosphere, 46, 815-825.
Huang, K., Zhao, Z., Hoag, G., Dahmani, A., & Block, P. (2005). Degradation of volatile organic compounds with thermally activated persulfate oxidation. Chemosphere, 61, 551-560.

Huh, C. (1979). Interfacial-tensions and solubilizing ability of a microemulsion phase that coexists with oil and brine. Journal of Colloid and Interface Science, 71 (2), 408–426.

Huling, S.C., & Weaver, J.W. (1991). Dense Nonaqueous Phase Liquids. Ground Water Issue. EPA/540/4-91/002. R.S., 21 pp, Kerr Environmental Research Laboratory, Ada, OK.

Hwang, I., & Batchelor, B. (2002). Reductive dechlorination of Tetrachloroethylene by Fe(II) in cement slurries. Environmental Science and Technology, 34, 5017-5022.

Iglesias, O., Sanroman, M.A., & Pazos, M. (2014). Surfactant-enhanced solubilization and simultaneous degradation of phenanthrene in marine sediment by electro-Fenton treatment. Industrial & Engineering Chemistry Research, 53 (8), 2917–2923. https://doi.org/10.1021/ ie4041115

Interstate Technology and Regulatory Cooperation Work Group (ITRC). (2002). Regulatory Overview DNAPL Source Reduction: Facing the Challenge., Dense Non aqueous Phase Liquids Team, 42 pp, April 2002, Washington D.C., U.S.A. http://www.itrcweb.org/user/DNAPL-2.pdf

Interstate Technology and Regulatory Council (ITRC). (2005) Technical and Regulatory Guideline for in Situ Chemical Oxidation of Contaminated Soil and Groundwater. 2nd Edition, Interstate Technology & Regulatory Council in Situ Chemical Oxidation Team, Washington DC.

Javanbakht G., & Goual L. (2016). Impact of Surfactant Structure on NAPL Mobilization and Solubilization in Porous Media. Industrial and Engineering Chemistry Research, 55, 11736-11746.

Jawitz, J.W., Sillian, R.K., Annable, M.D., Rao, P.S.C., & Warner, K. (2000). In-Situ Alcohol Flushing of a DNAPL Source Zone at a Dry Cleaner Site. Environmental Science and Technology, 32, 4, 523-530.

Jawitz, J.W., Annable, M.D., Demmy, G.G., & Rao, P.S.C. (2003). Estimating Nonaqueous Phase Liquid Spatial Variability Using Partitioning Tracer Higher Temporal Moments. Water Resources Research, 39, 7, 1-19.

Jeong, H.Y., Kim, H., & Hayes, K.F. (2007). Reductive Dechlorination Pathways of Tetrachloroethylene and Trichloroethylene and Subsequent Transformation of Their Dechlorination Products by Mackinawite (FeS) in the Presence of Metals. Environmental Science and Technology, 41, 7736-7743.

Jin, M.Q., Delshad, M., Dwarakanath, V., Mckinney, D.C., Pope, G.A., Sepehrnoori, K., Tilburg, C.E., & Jackson, R.E. (1995). Partitioning tracer test for detection, estimation, and remediation performance assessment of subsurface nonaqueous phase liquids. Water Resources Research, 31, 5, 1201-1211.

Johnson, R.L., & Pankow, J.F. (1992). Dissolution of dense chlorinated solvents into groundwater 2. Source functions for pools of solvent. Environmental Science and Technology, 26, 5, 896-901.

Johnson, R.L., Tratnyek, P.G., & Johnson, R.O. (2008). Persulfate persistence under thermal activation conditions. Environmental Science and Technology, 42, 9350-9356.

Karaoglu, A. G., Copty, N.K., Akyol, N.H., Kilavuz, S.A., & Babaei, M. (2019). Experiments and sensitivity coefficients analysis for multiphase flow model calibration of enhanced DNAPL dissolution. Journal of Contaminant Hydrology, 225, 103515.

Kaye, A.J., Cho, J., Basu, N.B., Chen, X., Annable, M.D., & Jawitz, J.W. (2008). Laboratory investigation of flux reduction from dense non-aqueous phase liquid (DNAPL) partial source zone remediation by enhanced dissolution. Journal of Contaminant Hydrology, 102, 17-28.

Kennedy, C. A., & Lennox, W. C. (1997). A pore-scale investigation of mass transport from dissolving DNAPL droplets. Journal of Contaminant Hydrology, 24, 221–246.

Kılavuz, S. A., & Akyol, N. H. (2018). TCE kaynak zonlarının yerinde kimyasal yıkama ile ıslahı: Tween 80 ve SDS ile yıkama performansı. Dokuz Eylül Üniversitesi Mühendislik Fakültesi Fen ve Mühendislik Dergisi, 20 (58) , 197-208 .

Killian, P.F., Bruell, C.J., Liang, C., & Marley, M.C. (2007). Iron (II) activated persulfate oxidation of MGP contaminated soil. Soil and Sediment Contamination, 16 (6), 523-537.

Kim, H.H., Kim, M.S., Kim, H.E., Lee, H.J., Jang, M.H., Choi, J., Hwang, Y., & Lee, C. (2017). Nanoparticulate zero-valent iron coupled with polyphosphate: the sequential redox treatment of organic compounds and its stability and bacterial toxicity. Environmental Science: Nano, 4, 2, 396-405.

Kokkinaki, A., O'Carroll, D. M., Werth, C. J., & Sleep, B. E. (2013). An evaluation of Sherwood-Gilland models for NAPL dissolution and their relationship to soil properties. Journal of Contaminant Hydrology, 155, 87–98.

Korrani, A. K. N., Sepehrnoori, K., & Delshad, M. (2015). Coupling IPhreeqc with UTCHEM to model reactive flow and transport. Computers & Geosciences, 82, 152–169.

Latimer, W.M. (1952). Oxidation potentials. 2nd Edition, Prentice-Hall, New York, NY.

Li, B., & Fu, J. (1992). Interfacial tensions of two-liquid-phase ternary systems. Journal of Chemical and Engineering Data, 37(2): 172-174.

Li, X. D., & Schwartz, F. W. (2004a). DNAPL remediation with in-situ chemical oxidation using potassium permanganate, I. Mineralogy of Mn Oxide and its dissolution in organic acids. Journal of Contaminant Hydrology, 68, 39-53.

Li, X.D., & Schwartz, F.W. (2004b). DNAPL mass transfer and permeability reduction during in-situ chemical oxidation with permanganate. Geophysical Research Letter, 31, L06504. DOI:10.1029/2003GL019218

Li, Z., & Hanlie, H. (2008). Combination of surfactant solubilization with permanganate oxidation for DNAPL remediation. Water Resources, 42, 605-614.

Li, J., Wang, L., Peng, L., Deng, Y., & Deng, D. (2020). A combo system consisting of simultaneous persulfate recirculation and alternating current electrical resistance heating for the implementation of heat activated persulfate ISCO. Chemical Engineering Journal, 385, 123803.

Liang, C.J., Bruell, C.J., Marley, M.C., & Sperry, K.L. (2003). Thermally activated persulfate oxidation of trichloroethylene (TCE) and 1,1,1-Trichloroethane (TCA) in aqueous systems and soil slurries. Soil and Sediment Contamination, 12, 207-228.

Liang, C.J., Bruell, C.J., Marley, M.C., & Sperry, K.L. (2004). Persulfate oxidation for in situ remediation of TCE. II. Activated by chelated ferrous ion. Chemosphere, 55, 1225-1233.

Liang, C., Wang, Z.S., & Bruell, C.J. (2007). Influence of pH on persulfate oxidation of TCE at ambient temperatures. Chemosphere, 66, 106-113.

Liang, C., Huang, C. F., Mohanty, N., & Kurakalva, R. M. (2008). A rapid spectrophotometric determination of persulfate anion in ISCO. Chemosphere, 73(9), 1540–1543. https://doi.org/10.1016/j.chemosphere.2008.08.043

Liang, H., & Falta, R.W. (2008). Modeling field-scale cosolvent flooding for DNAPL source zone remediation. Journal of Contaminant Hydrology, 96, 1, 1-16.

Liang, C., Chien, Y.C., & Lin, Y.L. (2012). Impacts of ISCO persulfate, peroxide and permanganate oxidants on soils: soil oxidant demand and soil properties. Soil and Sediment Contamination, 21, 701–719. https://doi.org/10.1080/15320383.2012.691129

Liang, C. J., & Bruell, C. J. (2008). Thermally activated persulfate oxidation of Trichloroethylene: experimental investigation of reaction orders. Industrial & Engineering Chemistry Research, 47(9): 2912–2918.

Liang, C.J., Liang, C.P., & Chen, C.C. (2009). pH dependence of persulfate activation by EDTA/Fe(III) for degradation of trichloroethylene. Journal of Contaminant Hydrology, 106, 173−182.

Liang, C.J., & Guo, Y.Y. (2012). Remediation of diesel-contaminated soils using persulfate under alkaline condition. Water, Air, and Soil Pollution, 223:4605–4614.

Lide, D.R. (2007). CRC Handbook of Chemistry and Physics 88th Edition 2007-2008. CRC Press, Taylor & Francis, p. 3-470, Boca Raton, FL.

Lien, H.L., & Zhang, W.X. (2001). Nanoscale iron particles for complete reduction of chlorinated ethenes. Colloids and Surfaces: A Physicochemical Engineering Aspects, 191, 1, 97-105.

Lin, K., Mdlovu, N.V., Chen, C., Chiang, C., & Dehvari, K. (2018). Degradation of TCE, PCE, and 1,2-DCE DNAPLs in contaminated groundwater using polyethylenimine-modified zero-valent iron nanoparticles. Journal of Cleaner Production, 175, 456-466.

Lominchar, M.A., Lorenzo, D., Romero, A., & Santos, A. (2018). Remediation of soil contaminated by PAHs and TPH using alkaline activated persulfate enhanced by surfactant addition at flow conditions. Journal of Chemical Technology & Biotechnology, 93 (5), 1270–1278. https://doi.org/10.1002/jctb.5485

Luo, H.S., Delshad, M., Li, Z.T., & Shahmoradi, A. (2016). Numerical simulation of the impact of polymer rheology on polymer injectivity using a multilevel local grid refinement method. Petroleum Science, 13:110–125.

Ma, J., Yang, Y., Jiang, X., Xie, Z., Li, X., Chen, C., & Chen, H. (2018). Impacts of inorganic anions and natural organic matter on thermally activated persulfate oxidation of BTEX in water. Chemosphere, 190, 296–306. https://doi.org/10.1016/j. chemosphere.2017.09.148

Mahal, M. K., Murao, A., Johnson, G. R., Russo, A., & Brusseau, M. L. (2010). Non-ideal behavior during complete dissolution of organic immiscible liquid: 2. ideal porous media. Water, Air, and Soil Pollution, 213, 191–197.

Marble, J.C. (2005). The influence of physical heterogeneity on immiscible liquid dissolution and permeaibility-based in-situ remediation, PhD. Dissertation, The University of Arizona, Tucson, U.S.A.

Marble, J. C., Carroll, K. C., Januosek, H., & Brusseau, M. L. (2010). In-situ oxidation and associated mass-flux-reduction/mass-removal behavior for systems with organic liquid located in lower-permeability sediments. Journal of Contaminant Hydrology, 117, 82-93.

Martel, R., Gélinas, P.J., & Desnoyers, J.E. (1998). Aquifer washing by micellar solutions: 1: optimization of alcohol– surfactant–solvent solutions. Journal of Contaminant Hydrology, 29, 4, 319-346.

Matzek, L.W., & Carter, K.E. (2017). Sustained persulfate activation using solid iron: kinetics and application to ciprofloxacin degradation. Chemical Engineering Journal, 307, 650–660.

Mayer, A.S., Zhong, L., & Pope, G.A. (1999). Measurement of Mass-Transfer Rates and Surfactant-Enhanced Solubilization of Non-Aqueous Phase Liquids. Environmental Science and Technology, 33, 17, 2965-2972.

McCray, J.E, & Brusseau, M.L. (1998). Cyclodextrin-enhanced in situ flushing of multiple-component immiscible organic liquid contamination at the field scale: mass removal effectiveness. Environmental Science and Technology, 32, 1285-1293.

McCray, J.E., & Brusseau, M.L. (1999a). Cyclodextrin-enhanced in situ flushing of multiple-component immiscible organic liquid contamination at the field scale: mass removal effectiveness. Environmental Science and Technology, 32, 1285–1293.

McCray, J.E., & Brusseau, M.L. (1999b). Cyclodextrin-enhanced in situ flushing of multiple-component immiscible organic liquid contamination at the field scale: analysis of dissolution behavior. Environmental Science and Technology, 33, 89–95.

McCray, J. E., Boving, T. B., & Brusseau, M. L. (2000). Cyclodextrin-enhanced solubilization of organic contaminants with implications for aquifer remediation. Ground Water Monitoring and Remediation, 20(1), 94–103.

Mohammed, M., Ozbay, I., Akyol, G., Akyol, N.H., Sahin, Y., Ozbay, B., Turkkan, S., & Karatas, T. (2019). Optimizing Process Parameters on the Remediation Efforts for the Mass Removal of DNAPL Entrapped in a Porous Media. Water, Air, and Soil Pollution, 230:161.

Mukherjee, R., Kumar, R., Sinha, A., Lama, Y., & Saha, A.K. (2016). A review on synthesis, characterization, and applications of nano zero-valent iron (nZVI) for environmental remediation. Critical Reviews in Environmental Science and Technology, 46, 5, 443-466.

Myers, D. (2005). Surfactant Science and Technology, 3rd ed.; John Wiley & Sons: New York, NY 2005.

Nambi, I.M., & Powers, S.E. (2000). NAPL dissolution in heterogeneous systems: an experimental investigation in a simple heterogeneous system. Journal of Contaminant Hydrology, 44, 161–184. https://doi.org/10.1016/S0169-7722(00)00095-4

Nambi, I. M., & Powers, S. E. (2003). Mass transfer correlations for nonaqueous phase liquid dissolution from regions with high initial saturations. Water Resources Research, 39, 1030. https://doi.org/10.1029/2001wr000667

Ni, Z., Smit, M., Grotenhuis, T., Van Gaans, P., & Rijnaarts, H. (2014). Effectiveness of stimulating PCE reductive dechlorination: A step-wise approach. Journal of Contaminant Hydrology, 164, 209-218.

Ogata, A., & Banks, R. (1961). A solution of the differential equation of longitudinal dispersion in porous media: fluid movement in earth materials. 411-A. US Government Printing Office.

Oh, S.Y., Kang S.G., & Chiu P.C. (2010). Degradation of 2,4-dinitrotoluene by persulfate activated with zero-valent iron. Science of the Total Environment, 408:34464–43468.

O'Hara, S., Krug, T., Quinn, J., Clausen, C., & Geiger, C. (2006). Field and Laboratory Evaluation of the Treatment of DNAPL Source Zones Using Emulsified Zero-Valent Iron. Remediation, Spring 2006. DOI: 10.1002.rem

Oprckal, P., Mladenovic, A., Vidmar, J., Pranjic, A.M., Milacic, R., & Scancar, J. (2017). Critical evaluation of the use of different nanoscale zero-valent iron particles for the treatment of effluent water from a small biological wastewater treatment plant. Chemical Engineering Journal, 321, 20-30.

Orth, W.S., & Gillham, R.W. (1996). Dechlorination of trichloroethylene in aqueous solution using Fe(0). Environmental Science and Technology, 30, 66-71.

Pan, L.W., Siegrist, R.L., & Crimi, M. (2012). Effects of in situ remediation using oxidants or surfactants on subsurface organic matter and sorption of trichloroethene. Groundwater Monitoring and Remediation, 32 (2), 96−105.

Pankow, J. F., & Cherry, J. A. (1996). Dense chlorinated solvents and other DNAPLS in groundwater. History, Behavior, and Remediation, Waterloo Press, Portland, Oregon.

Pardo, F., Santos, A., & Romero, A. (2016). Fate of iron and polycyclic aromatic hydrocarbons during the remediation of a contaminated soil using iron-activated persulfate: a column study. Science of Total Environment, 566–567:480–488.

Peng, L., Wang, L., Hu, X., Wu, P., Wang, X., Huang, C., Wang, X., & Deng, D. (2016). Ultrasound assisted, thermally activated persulfate oxidation of coal tar DNAPLs. Journal of Hazardous Materials, 318, 497-506.

Pennell, K.D., Jin, M., Abriola, L.M., & Pope, G.A. (1994). Surfactant enhanced remediation of soil columns contaminated by residual tetrachloroethylene. Journal of Contaminant Hydrology, 16, 35–53.

Perini, J.A.D., Silva, B.F., & Nogueira, R.F.P. (2014). Zero-valent iron mediated degradation of ciprofloxacin – assessment of adsorption, operational parameters and degradation products. Chemosphere, 117, 345–352.

Petri, B.G., Siegrist, R.L., & Crimi, M.L. (2008). Effects of groundwater velocity and permanganate concentration on DNAPL mass depletion rates during in situ oxidation. Journal of Environmental Engineering, 134, 1, 1-13.

Pope, G.A., & Nelson, R.C. (1978). A chemical flooding compositional simulator. Society of Petroleum Engineers Journal, 18, 5, 339-354.

Poteshnova, M. V, & Zadymova, N. M. (2006). Normal Micelles and Oil-in-Water Microemulsions in a Water – Toluene – Tween 80 Ternary System. Colloid Journal, 68, 201–210, DOI: 10.1134/S1061933X06020128

Powers, S.E., Abriola, L.M. & Weber Jr, W.J. (1994). An experimental investigation of nonaqueous phase liquid dissolution in saturated subsurface systems: transient mass transfer rates. Water Resources Research, 30(2): 321-332.

Rao, P.S.C., Annable, M.D., Sillan, R.K., Dai, D., Hatfield, D., Graham, W.D., Wood, A.L., & Enfield, C.G. (1997). Field-Scale Evaluation of In Situ Cosolvent Flushing for Enhanced Aquifer Remediation. Water Resources Research, 33, 12, 2674-2686.

Rebello, S., Asok, A.K., Mundayoor, S., & Jisha, M.S. (2014). Surfactants: toxicity, remediation and green surfactants. Environmental Chemistry Letters, 12 (2), 275−287.

Reitsma, S., & Kueper, B.H. (1998a). Non-equilibrium alcohol flooding model for immiscible phase remediation: 1. Equation development. Advances in Water Resources, 21, 649-663.

Reitsma, S., & Kueper, B.H. (1998b). Non-equilibrium alcohol flooding model for immiscible phase remediation: 2. Model development and application. Advances in Water Resources, 21, 663-678.

Roeder, E., & Falta, R.W. (2001). Modeling unstable flooding of DNAPL-contaminated columns. Advances in Water Resources, 24, 803-819.

Russo, A., Mahal, M.K., & Brusseau, M. L. (2009). Nonideal behavior during complete dissolution of organic immiscible liquid: 1. Natural porous media. Journal of Hazardous Materials, 172, 208–213.

Saba, T., & Illangasekare, T.H. (2000). Effect of groundwater flow dimensionality on mass transfer from entrapped nonaqueous phase liquid contaminants. Water Resources Research, 36(4): 971-979.

Saltelli, A., Tarantola, S., Campolongo, F. & Ratto, M. (2004). Sensitivity analysis in practice: a guide to assessing scientific models. John Wiley & Sons.

Schlumberger, A. (2005). ECLIPSE Technical Description.

Schnarr, M., Truax, C., Farquhar, G. Hood, E., Gonullu, T., & Stickney, B. (1998). Laboratory and Controlled Field Experiments Using Potassium Permanganate to Remediate Trichloroethylene and Perchloroethylene DNAPLs in Porous Media. Journal of Contaminant Hydrology, 29, 205-224.

Schwille, F. (1988). Dense Chlorinated Solvents in Porous and Fractured Media. Lewis, Chelsea, MI, 146 pp.

Shah, F., Hadim, H., & Korfiatis, G. (1995). Laboratory studies of air stripping of VOC-contaminated soils. Soil and Sediment Contamination, 4(1): 93-109.

Shan, A., Farooq, U., Lyu, S., Zaman, W., Abbas, Z., Ali, M., Idrees, A., Tang, P., Li, M., Sun, Y., & Sui, Q. (2020). Efficient removal of trichloroethylene in surfactant amended solution by nano Fe0-Nickel bimetallic composite activated sodium persulfate process. Chemical Engineering Journal, 386:123995. https://doi.org/10.1016/j.cej.2019.123995

Sherwood, T.K., Pigford, R.L., & Wilke, C.R. (1975). Mass Transfer. McGraw-Hill, 677 pp, New York, NY, U.S.A.

Shiau, B.J. (2003). In-Situ Surfactant and Chemical Oxidant Flushing for Complete Remediation of Contaminants and Methods of Using Same. U.S. Patent Application Publication No. 2003/0175081.

Siegrist, R.L., Lowe, K.S., Murdoch, L.C., Case, T.L., & Pickering, D.A. (1999). In Situ Oxidation by Fracture Emplaced Reactive Solids. Journal of Environmental Engineering, 125, 5, 429-440.

Siegrist, R.L., Urynowicz, M.A., West, O.R., Crimi, M.L., & Lowe, K.S. (2001). Principles and Practices of In Situ Chemical Oxidation Using Permanganate. Columbus. Ohio, OH, Battelle Press, U.S.A.

Siegrist, R. L., Crimi, M.L., Munakata-Marr, J., Illangasekare, T., Lowe, K.S., Van Cuyk, S., Dugan, P., Heiderscheidt, J., Jackson, S., Petri, B., Sahl, J., & Seitz, S. (2006). Reaction and Transport Processes Controlling In Situ Chemical Oxidation of DNAPLs. ER-1290 Final Report, Prepared for the DoD Strategic Environmental Research and Development Program (SERDP), 235p.

Sihyun, D., Yongjae, K., & Kong, S.H. (2010). Effect of metal oxides on the reactivity of persulfate/Fe(II) in the remediation of diesel-contaminated soil and sand, Journal of Hazardous Materials, 182, 933–936.

Sillan, R.K., Rao, P.S.C., Annable, M.D., Dai, D., Hatfield, K.G., Wood, A.L., & Enfield, C.G. (1998). Evaluation of In-Situ Cosolvent Flushing Dynamics Using a Network of Spatially Distributed Multilevel Samplers. Water Resources Research, 34, 9, 2191-2202.

Slavic, D.R. (2014). M.S. Thesis, The University of Alabama, Tuscaloosa.

Soga, K., Page, J.W.E., & Illangasekare, T.H. (2004). A review of NAPL source zone remediation efficiency and the mass flux approach. Journal of Hazardous Materials, 110, 13–27. https://doi.org/10.1016/j.jhazmat.2004.02.034

St-Pierre, C., Martel, R., Gabriel, U., Lefebvre, R., Robert, T., Hawari, J. (2004). TCE recovery mechanisms using micellar and alcohol solutions: phase diagrams and sand column experiments. Journal of Contaminant Hydrology, 71, 1, 155-192.

Stroo, H.F., Leeson, A., Marqusee, J.A., Johnson, P.C., Ward, C.H., Kavanaugh, M.C., Sale, T.C., Newell, C.J., Pennell, K.D., Lebrón, C.A., & Unger, M. (2012). Chlorinated ethene source remediation: lessons learned. Environmental Science and Technology, 46, 6438–6447.

Suchomel, E. J., Ramsburg, C. A., & Pennell, K. D. (2007). Evaluation of trichloroethene recovery processes in heterogeneous aquifer cells flushed with biodegradable surfactants. Journal of Contaminant Hydrology, 94, 195-214.

Tan, L., Lu, S., Fang, Z., Cheng, W., & Tsang, E.P. (2017). Enhanced reductive debromination and subsequent oxidative ring-opening of decabromodiphenyl ether by integrated catalyst of nZVI supported on magnetic Fe3O4 nanoparticles. Applied Catalysis B: Environment, 200, pp. 200-210.

Tang, X., Hashmi, M.Z., Zeng, B., Yang, J., & Shen, C. (2015). Application of iron-activated persulfate oxidation for the degradation of PCBs in soil. Chemical Engineering Journal, 279, 673–680.

Taylor, T.P., Rathfelder, K.M., Pennell, K.D., & Abriola, L.M. (2004). Effects of ethanol addition on micellar solubilization and plume migration during surfactant enhanced recovery of tetrachloroethene. Journal of Contaminant Hydrology, 69 (1–2), 73–99.

Teel, A.L., Elloy, F.C., & Watts, R.J. (2016). Persulfate activation during exertion of total oxidant demand. Chemosphere, 158, 184–192.

Thompson, S., Riggenbach, J., Brown, R.A., Hines, J., & Haselow, J. (2006). Catalyzed persulfate remediation of chlorinated and recalcitrant compounds in soil. In: Proceedings of the Fifth International Conference on Remediation of Chlorinated and Recalcitrant Compounds, Monterey, CA, USA, Paper D-76, May 2006.

Tick, G.R. (2003). Dissolution and enhanced solubilization of immiscible phase organic liquids in porous media: Theoretical, laboratory, and field investigations. PhD Thesis, The University of Arizona, U.S.A.

Tick, G. R., Lourenso, F., Wood, A. L., & Brusseau, M. L. (2003). Pilot-scale demonstration of cyclodextrin as a solubility-enhancement agent for the remediation of a tetrachloroethene-contaminated aquifer. Environmental Science and Technology, 37, 5829-5834.

Tick, G.R., & Rincon, E.A. (2009). Effect of enhanced solubilization agents on dissolution and mass flux from uniformly distributed immiscible liquid trichloroethene (TCE) in homogeneous porous media. Water, Air, and Soil Pollution, 204, 1-4, 315-332.

Tick, G.R., Harvell, J.R., & Murgulet, D. (2015). Intermediate scale investigation of enhanced solubilization agents on the dissolution and removal of a multicomponent dense nonaqueous phase liquid (DNAPL) source. Water, Air, and Soil Pollution, 226, 11, 1-21.

Tsai, T.T., Kao, C.M., Yeh, T.Y., Liang, S.H., & Chien, H.Y. (2009). Application of surfactant enhanced permanganate oxidation and biodegradation of trichloroethylene in groundwater. Journal of Hazardous Materials, 161, 1, 111-119.

Tsitonaki, A., Petri, B., Crimi, M., Mosbæk, H., Siegrist, R.L., & Bjerg, P.L. (2010). In situ chemical oxidation of contaminated soil and groundwater using persulfate: a review. Crit. Rev. Environmental Science and Technology, 40 (1), 55:91.

Urynowicz, M.A. (2000). Dense Nonaqueous Phase Trichloroethene Degradation with Permanganate Ion. PhD Dissertation, 149 pp, Colorado School of Mines, Golden, CO, U.S.A.

Usman, M., Tascone, O., Faure P., & Hanna, K. (2014). Chemical oxidation of hexachlorocyclohexanes (HCHs) in contaminated soils. Science of Total Environment, 476–477:434–439.

US Environmental Protection Agency. (2006). In-situ Chemical Oxidation. EPA/600/R-06/072. Cincinnati, Ohio: Office of Research and Development, National Risk Management Research Laboratory.

US Environmental Protection Agency. (2008). National primary drinking water regulations: list of drinking water contaminants and their MCLs. Washington, DC: US Environmental Protection Agency. Retrieved from: http://www.epa.gov/safewater/contaminants/index.ht ml#listmcl

US Environmental Protection Agency. (2016). Chemical Data Reporting Summary: 1,1,2,2-Tetrachloroethene. U.S. Environmental Protection Agency. https://chemview.epa.gov/chemview and search on CAS number or substance name and select Manufacturing, Processing, Use, and Release Data Maintained by EPA and select Chemical Data Reporting Details.

Valletti, N., Budroni, M.A., Lagzi, I., Marchettini, N., Sanchez-Dominguez, M., & Rossi, F. (2021). Interfacial Mass Transfer in Trichloroethylene/Surfactants/ Water Systems: Implications for Remediation Strategies. Reactions, 2, 312-322. https://doi.org/10.3390/reactions2030020

Volpe, A., DelMoro,G., Rossetti, S., Tandoi, V., & Lopez, A. (2007). Remediation of PCE-contaminated groundwater from an industrial site in southern Italy:a laboratory-scale study. Process Biochemistry, 42, 1498–1505. DOI: 10.1016/j.procbio.2007.07.017

Waldemer, R.H., Tratnyek, P.G., Johnson, R.L., & Nurmi, J.T. (2007). Oxidation of chlorinated ethenes by heat-activated persulfate: kinetics and products. Environmental Science and Technology, 2007, 41, 1010–1015.

Wang, X., & Brusseau, M.L. (1993). Solubilization of some low polarity organic compounds by hydroxypropyl-beta-cyclodextrin. Environmental Science and Technology, 27, 13, 2821-2825.

Wang, L., Peng, L.B., Xie, L.L., Deng, P.Y., & Deng, D.Y. (2017). Compatibility of surfactants and thermally activated persulfate for enhanced subsurface remediation. Environmental Science and Technology, 2017, 51, 7055−7064.

Wang, J., & Wang, S. (2018). Activation of persulfate (PS) and peroxymonosulfate (PMS) and application for the degradation of emerging contaminants. Chemical Engineering Journal, 334; 1502–1517. https://doi.org/10.1016/j.cej.2017.11.059

Wilkin, R. T., Acree, S. D., Ross, R. R., Beak, D. G., & Lee, T. R. (2012). Project Update: ZVI Used for Arsenic from Lead Smelting Facility. In: Technology News & Trends, U.S. EPA Office of Superfund Remediation and Technology Innovation, Washington, DC, (60):10-12.

Wu, B., Li, H., Du, X., Zhong, L., Yang, B., Du, P., Gu, Q., & Li, F. (2016). Correlation between DNAPL distribution area and dissolved concentration in surfactant enhanced aquifer remediation effluent: A two-dimensional flow cell study. Chemosphere, 144, 2142-2149.

Xu, Z., Cai, L., Liang, X., & Lyu, S. (2022). Insight into trichloroethene removal in alkaline condition with the presence of surfactant based on persulfate system. Journal of Environmental Chemical Engineering, 10, 108492.

Yaksi, K., Demiray, Z., & Copty, N. K. (2021). Impact of cosolvents on the interphase mass transfer of NAPLs in porous media. Water Resources Research, 57, e2020WR029326. https:// doi. org/ 10. 1029/ 2020W R0293 26

Yalkowsky, S., He, Y. & Jain, P. (2016). Handbook of aqueous solubility data. CRC Press: Boca Raton, FL.

Yan, Y.E., & Schwartz, F.W. (1999). Oxidative Degradation and Kinetics of Chlorinated Ethylenes by Potassium Permanganate. Journal of Contaminant Hydrology, 37, 343-365.

Yan, E.Y., & Schwartz, F.W. (2000). Kinetics and Mechanisms for TCE Oxidation by Permanganate. Environmental Science and Technology, 34, 12, 2535-2541.

Yang, J. S., Baek, K., Kwon, T. S., & Yang, J. W. (2006). Competitive immobilization of multiple component chlorinated solvents by cyclodextrin derivatives. Journal of Hazardous Materials, 137, 1866–1869. https:// doi. org/ 10.1016/j. jhazm at. 2006. 04. 020

Yang, J.S., & Yang, J.W. (2018). Partitioning effects of nonionic surfactants on the solubilization of single or binary chlorinated solvents: Batch and column experiments. Journal of Industrial and Engineering Chemistry, 58, 140-147.

Yen, C., Chen, K., Kao, C., Liang, S., & Chen, T. (2011). Application of persulfate to remediate petroleum hydrocarbon-contaminated soil: Feasibility and comparison with common oxidants, Journal of Hazardous Materials, 186, 2097–2102.

Zhai, X., Hua, L., & Rao, P. (2006). Cosolvent enhanced chemical oxidation of perchloroethylene by potassium permanganate. Journal of Contaminant Hydrology, 82, 61-74.

Zhang, M., Li, J., & Wang, Y. (2019). Impact of biochar-supported zerovalent iron nanocomposite on the anaerobic digestion of sewage sludge. Environmental Science and Pollution Research, 26, 10292–10305.

Zheng, F., Gao, B., Sun, Y., Shi, X., Xu, H., Wu, J., & Gao, Y. (2016). Removal of tetrachloroethylene from homogeneous and heterogeneous porous media: Combined effects of surfactant solubilization and oxidant degradation. Chemical Engineering Journal, 283, 595-603.

Zhong, L.R., Mayer, A.S., & Pope, G.A. (2003). The effects of surfactant formulation on nonequilibrium NAPL solubilization. Journal of Contaminant Hydrology, 60 (1–2), 55–75.

Zhong, H., Brusseau, M.L.,Wang, Y., Yan, N., Quig, L., & Johnson, G.R. (2015). Insitu activation of persulfate by iron filings and degradation of 1,4-dioxane. Water Research, 83:104–111.

Zhou, Z., Liu, X., Sun, K., Lin, C., Ma, J., He, M., & Ouyanga, W. (2019). Persulfate-based advanced oxidation processes (AOPs) for organic contaminated soil remediation: A review. Chemical Engineering Journal, 372:836–851.

Zhu, Y., Yue, M., Natarajan, V., Kong, L., Ma, L., Zhang, Y., Zhao, Q. & Zhan, J. (2018). Efficient activation of persulfate by Fe3O4 @ β-cyclodextrin nanocomposite for removal of bisphenol A. RSC Advances, 8 (27), 14879–14887. https://doi.org/10.1039/C8RA01696H

APPENDIX A: SOIL OXIDANT DEMAND, COMPARISON WITH LITERATURE STUDIES

Table A. Selected batch procedures for the soil oxidant demand (SOD) in the literature

Oxidant	Soil properties	Procedure/Process	Duration	Soil/water (w/w)	SOD (g oxidant/ kg of soil)	Initial conditions	Reference
$50°C/S_2O_8^{2-}$	Antalya calcareous (carbonate-rich) soil (sandy loam) Bulk density (ρ), g/cm^3: 1.34 pH: 8.4 Total organic carbon (TOC),% ; 0.97 Total inorganic carbon (as $CaCO_3$) (TIC), % ; 73 Total Organic Matter (TOM),% ; 1.67 Specific surface area, m^2/g; 0.383	- 4 g of calcareous soil adding solution in 20mL glass vial (no headspace) - no shaken -unbuffered	24 hrs	1/5.25	0.89 g $50°C/S_2O_8^{2-}$	3 mM $S_2O_8^{2-}$	This study
				1/5	1.58 g $50°C/S_2O_8^{2-}$	6 Mm $S_2O_8^{2-}$	
				1/5	9.2 g $50°C/S_2O_8^{2-}$	30 mM $S_2O_8^{2-}$	
				1/5.25	19.9 g $50°C/S_2O_8^{2-}$	75 mM $S_2O_8^{2-}$	
				1/5.25	40.67 g $50°C/S_2O_8^{2-}$	150 mM $S_2O_8^{2-}$	
$S_2O_8^{2-}$		- 3 g of calcareous soil adding 20mL solution in 20mL glass vial (no headspace) - during the experiment vials manually shaken every 3 hr for 1 min using constant force -unbuffered	48 hrs	1/6.6	1.77 g $50°C/S_2O_8^{2-}$	3 mM $S_2O_8^{2-}$	
					3.6 g $50°C/S_2O_8^{2-}$	6 Mm $S_2O_8^{2-}$	
					20.1 g $50°C/S_2O_8^{2-}$	30 mM $S_2O_8^{2-}$	
					47.3 g $50°C/S_2O_8^{2-}$	75 mM $S_2O_8^{2-}$	
					87.5 g $50°C/S_2O_8^{2-}$	150 mM $S_2O_8^{2-}$	
					0.35 g $S_2O_8^{2-}$	3 mM $S_2O_8^{2-}$	
					0.55 g $S_2O_8^{2-}$	6 Mm $S_2O_8^{2-}$	
					-	30 mM $S_2O_8^{2-}$	
					4 g $S_2O_8^{2-}$	75 mM $S_2O_8^{2-}$	
					6.45 g $S_2O_8^{2-}$	150 mM $S_2O_8^{2-}$	
MnO_4^-	-	Place 50g of soil then add 100mL of 20g/L of KMnO4 - 2mm-sieved soil - Ovendried @105°C for 24hrs - Use 250mL glass vial - Zero headspace is not required - Triplicate	48 hrs	1/2	-	20g/L of KMnO4	ASTM D7262
$S_2O_8^{2-}$	Based on numerous TOD tests, the TOD can be as little as 0.05 grams of oxidant per kilogram of saturated soil (for carbonate aquifers, for example) or as high as 15 grams of oxidant per kilogram of saturated soil (for organic-rich sediments under sulfate-reducing conditions, for example).	- A starch-iodide indicator is used to visually determine the ORP change. The colorimetric technique uses a selected maximum ratio of oxidant mass to soil mass (10 g/kg)	48 hrs	-	-	10g $S_2O_8^{2-}$/kg	Haselow et al., 2003

Total oxidant demand (TOD) = Soil Oxidant Demand (SOD) + loss of persulfate due to decomposition.

Table A. *continued*

Oxidant	Soil properties	Procedure/Process	Duration	Soil/water (w/w)	SOD (g oxidant/ kg of soil)	Initial conditions	Reference
$S_2O_8^{2-}$	Great Lakes (silty clay loam, fine, illitic, stick and plastic, strongly effervescent upon addition of mild acid) Natural organic matter (NOM), g/mol; 5000	-200 g of each soil into separate glass jars, adding 100mL of the oxidant solution - unbuffered soil slurry - no activator - Given that the TOD as exceeded the measured TOC content for Fort Lewis and Appling soils, these TOD results were not thought to represent the true oxidant demand of these solids but reflect the unstable nature of unbuffered sodium persulfate in soil slurries	12 hrs	2/1	28.9 g $S_2O_8^{2-}$ (soil slurry method) After 11.5 g $S_2O_8^{2-}$/kg dosage, no PCE oxidation (sequential treatment)	7.65 g/L $S_2O_8^{2-}$	Costanza et al., 2010
	Fort Lewis (glacial till) Total organic carbon (TOC),%; 0.069 (or 0.69 g TOC/kg soil) Specific surface area, m^2/g; 8.8 Natural organic matter (NOM), g/mol; 5000				9.65 g $S_2O_8^{2-}$ (soil slurry method) 0.63 g $S_2O_8^{2-}$/kg was required to degrade 92% of PCE in 80min (sequential treatment) 0.08 g $S_2O_8^{2-}$/kg demand based on SO_4^{2-} formed		
	Appling soils (loamy coarse sand, clayey, kaolinitic) Organic carbon (OC),%; 0.77 (or 7.7 g OC/kg soil) Natural organic matter (NOM), g/mol; 5000				19.6 g $S_2O_8^{2-}$ (soil slurry method) After 1.9 g $S_2O_8^{2-}$/kg dosage, no PCE oxidation (sequential treatment)		

Table A. *continued*

Oxidant	Soil properties	Procedure/Process	Duration	Soil/water (w/w)	SOD (g oxidant/ kg of soil)	Initial conditions	Reference
$S_2O_8^{2-}$ $Fe^{2+}/S_2O_8^{2-}$	<u>SANDY soil</u> Bulk density (ρ), g/cm³: 2.56 pH: 5.6 Soil Oxidizable Matter (OM),%; 0.53 Total carbon (TC),%; 0.09 Total organic carbon (TOC),%; 0.06 Cation Exchange Capacity (CEC), meq/100g; 7.5	1/6 - Place 5g of soil then add 30mL solution 1/4 - Place 10g of soil then add 40mL solution 1/2 - Place 15g of soil then add 30mL solution For 1/4 Persulfate tests; (34mL Fe^{2+} activator + 5mL of Persulfate + few drops of 1N NaOH or H_2SO_4) - Ovendried @50°C for 48 hrs - 40mL amber glass bottles - Fe^{2+} activator; pH 3 initially adjusted using H_2SO_4 - NaOH or H_2SO_4 added to adjust the pH to 3 or 7 before adding 5 ml of Persulfate - shaken at 160 rpm for 1 hr - bottles were placed @20°C - hand-shaken once every day - duplicate	4 weeks	1/6	15 g $S_2O_8^{2-}$	pH: 3; 168 mM $S_2O_8^{2-}$	Liang et al., 2012
				1/4	17 g $S_2O_8^{2-}$	pH: 3; 168 mM $S_2O_8^{2-}$	
				1/2	6 g $S_2O_8^{2-}$	pH: 3; 168 mM $S_2O_8^{2-}$	
			1 week	1/6	2 g $S_2O_8^{2-}$	pH: 3; 16,8 mM $S_2O_8^{2-}$	
				1/4	1.5 g $S_2O_8^{2-}$	pH: 3; 16,8 mM $S_2O_8^{2-}$	
				1/2	1.2 g $S_2O_8^{2-}$	pH: 3; 16,8 mM $S_2O_8^{2-}$	
			1 week	1/6	18 g $Fe^{2+}/S_2O_8^{2-}$	pH: 7; 168 mM $S_2O_8^{2-}$; 10 mM Fe^{2+}	
				1/4	22 g $Fe^{2+}/S_2O_8^{2-}$	pH: 7; 168 mM $S_2O_8^{2-}$; 10 mM Fe^{2+}	
				1/2	7.5 g $Fe^{2+}/S_2O_8^{2-}$	pH: 7; 168 mM $S_2O_8^{2-}$; 10 mM Fe^{2+}	
			1 week	1/6	<2,5 g $Fe^{2+}/S_2O_8^{2-}$	pH: 7; 16,8 mM $S_2O_8^{2-}$; 1 mM Fe^{2+}	
				1/4		pH: 7; 16,8 mM $S_2O_8^{2-}$; 1 mM Fe^{2+}	
				1/2		pH: 7; 16,8 mM $S_2O_8^{2-}$; 1 mM Fe^{2+}	
	<u>SILTY soil</u> Bulk density (ρ), g/cm³: 2.56 pH: 7.1 Soil Oxidizable Matter (OM),% ; 1.64 Total carbon (TC),% ; 1.57 Total organic carbon (TOC),% ; 1.51 Cation Exchange Capacity (CEC), meq/100g; 18.8		4 weeks	1/6	48 g $S_2O_8^{2-}$	pH: 3; 168 mM $S_2O_8^{2-}$	
				1/4	33 g $S_2O_8^{2-}$	pH: 3; 168 mM $S_2O_8^{2-}$	
				1/2	25 g $S_2O_8^{2-}$	pH: 3; 168 mM $S_2O_8^{2-}$	
			1 week	1/6	<5 g $S_2O_8^{2-}$	pH: 7; 16,8 mM $S_2O_8^{2-}$	
				1/4		pH: 7; 16,8 mM $S_2O_8^{2-}$	
				1/2		pH: 7; 16,8 mM $S_2O_8^{2-}$	
			4 weeks	1/6	43 g $Fe^{2+}/S_2O_8^{2-}$	pH: 3; 168 mM $S_2O_8^{2-}$; 1 mM Fe^{2+}	
				1/4	38 g $Fe^{2+}/S_2O_8^{2-}$	pH: 3; 168 mM $S_2O_8^{2-}$; 1 mM Fe^{2+}	
				1/2	23 g $Fe^{2+}/S_2O_8^{2-}$	pH: 3; 168 mM $S_2O_8^{2-}$; 1 mM Fe^{2+}	
			1 week	1/6	<5 g $S_2O_8^{2-}$	pH: 7; 16,8 mM $S_2O_8^{2-}$; 1 mM Fe^{2+}	
				1/4		pH: 7; 16,8 mM $S_2O_8^{2-}$; 1 mM Fe^{2+}	
				1/2		pH: 7; 16,8 mM $S_2O_8^{2-}$; 1 mM Fe^{2+}	

Table A. *continued*

Oxidant	Soil properties	Procedure/Process	Duration	Soil/water (w/w)	SOD (g oxidant/ kg of soil)	Initial conditions	Reference
$S_2O_8^{2-}$ $NaOH/S_2O_8^{2-}$	Low SOC (silt loam) Organic carbon,% ; 0.3 Cation Exchange Capacity (CEC), cmol(+)/kg; 20 Medium SOC (silt loam) Organic carbon,% ; 0.75 Cation Exchange Capacity (CEC), cmol(+)/kg; 24 High SOC (silt loam) Organic carbon,% ; 1.4 Cation Exchange Capacity (CEC), cmol(+)/kg; 27	- soil was air-dried and 0.5mm sieved - triplicate at 20 ± 2°C in 20 mL borosilicate VOA vials with PTFE-lined caps, with a set of vials established for each time point - Each vial contained 10 g of soil and 10 mL of reactant solution. - vials were placed on a shaker table at 100 rpm for the duration of the reactions.	5 days	1/1 Low SOC	<1 g $S_2O_8^{2-}$ (pH_f=5.1)	pH: 5.7-5.9 42 mM $S_2O_8^{2-}$ (10 g $S_2O_8^{2-}$/kg)	Teel et al., 2016
				1/1 Medium SOC	2.5 g $S_2O_8^{2-}$ (pH_f=4.5)		
				1/1 High SOC	4 g $S_2O_8^{2-}$ (pH_f=4.2)		
				1/1 Low SOC	1 g $S_2O_8^{2-}$ (pH_f=6.8-8.4)	pH= 10 42 mM $S_2O_8^{2-}$ (10 g $S_2O_8^{2-}$/kg) 84 mM NaOH	
				1/1 Medium SOC	5 g $S_2O_8^{2-}$ (pH_f=6.8-8.4)		
				1/1 High SOC	7 g $S_2O_8^{2-}$ (pH_f=6.8-8.4)		
MnO_4^-	Total organic carbon (TOC), mg/g ; 3.03 A NEW CALCULATION METHOD: PCOD removal by different oxidants at different doses (low, medium, and high) equivalent to KMnO4 (g/L) Persulfate has the highest oxidation potential using the lowest mass of oxidant, yet it showed the lowest PCOD removal of all the oxidants. Persulfate also had the widest range of PCOD removal between the high and low concentrations, indicating that NOD removal from persulfate is highly dependent upon oxidant concentration.	- 2 g of soil + 10mL of DI water + 14.4mL of oxidant solution	1 week	1/7.2	8.5 g MnO_4^-	Low: 0.41 g/L $KMnO_4$	Dangi et al., 2022
			1 week		13 g MnO_4^-	Medium: 2.36 g/L $KMnO_4$	
			1 week		16 g MnO_4^-	High: 4.72 g/L $KMnO_4$	
			2 weeks		10 g MnO_4^-	Low: 0.41 g/L $KMnO_4$	
			2 weeks		15 g MnO_4^-	Medium: 2.36 g/L $KMnO_4$	
			2 weeks		20 g MnO_4^-	High: 4.72 g/L $KMnO_4$	
$S_2O_8^{2-}$		- 3 g of soil were added to 45 ml vials, then added 30 ml of each different oxidant - ovendried @ 105 °C for 24 hours - shaken vigorously for 5-10s and then placed in a rotating tumbler	2 weeks	1/10	Low: <0.5 g $S_2O_8^{2-}$ (0.5 eq. to KMnO4 g/L)	Low: 0.41 g/L $S_2O_8^{2-}$	
					Medium: <1 g $S_2O_8^{2-}$ (1 eq. to KMnO4 g/L)	Medium: 0.83 g/L $S_2O_8^{2-}$	
					High: 6 g $S_2O_8^{2-}$ (2 eq. to KMnO4 g/L)	High: 1.66 g/L $S_2O_8^{2-}$	

APPENDIX B: MULTIPHASE FLOW UTCHEM INPUT FILE FOR TWEEN 80 ENHANCED PERMANGANATE FLUSHING IN SILICA SAND

```
CC*****************************************************************
CC                                      *
CC    BRIEF DESCRIPTION OF DATA SET : UTCHEM (VERSION 9.3 )      *
CC                                      *
CC*****************************************************************
CC                                      *
CC  COSOLVENT FLUSHİNG,                          *
CC                                      *
CC  LENGTH (M) : 0.24            PROCESS : COSOLVENT FLUSHING   *
CC  THICKNESS (M) : 0.03                         *
CC  HEIGHT (M): 0.15             COORDINATES : CARTESIAN       *
CC                                      *
CC  GRID BLOCKS : 48 X 1 X 30                    *
CC  DATE : 08/02/2019    ZEYNEP                  *
CC                                      *
CC*****************************************************************
CC
CC*****************************************************************
CC                                      *
CC   RESERVOIR DESCRIPTION                       *
CC                                      *
CC*****************************************************************
CC
CC12:27 08.02.2019
*----RUNNO
2DTWEEN
CC
CC
*----TITLE
2DTWEEN
PCE flushing with 2.5% TWEEN80 enhanced KMnO4
Experiment
CC
CC SIMULATION FLAGS
*---- IMODE IMES IDISPC ICWM ICAP IREACT IBIO ICOORD ITREAC ITC IGAS IENG
      1   3   3     0   0    0     1   1    0     0   0  0
CC
CC NO. OF GRIDBLOCKS,FLAG SPECIFIES CONSTANT OR VARIABLE GRID SIZE, UNIT
*----NX   NY  NZ  IDXYZ   IUNIT
   48    1   30   0       1
CC
CC  CONSTANT GRID BLOCK SIZE IN X, Y, AND Z
*----DX1       DY1      DZ1
   0.005     0.03    0.005
CC
CC TOTAL NO. OF COMPONENTS, NO. OF TRACERS, NO. OF GEL COMPONENTS
```

```
*----N   NO  NTW NTA  NGC NG  NOTH
   10   0   0   0   0   0   2
CC
CC  NAME OF SPECIES
*---- SPNAME(I) FOR I=1,N
WATER
PCE
TWEEN80
POLYMER (NO)
ANION
CATION
ALCOHOL (NO)
GAS (NO)
MNO4
BIO
CC
CC FLAG INDICATING IF THE COMPONENT IS INCLUDED IN CALCULATIONS OR NOT
*----ICF(KC) FOR KC=1,N
   1  1  1  0  0  0  0 0  1  1
CC
CC*********************************************************************
CC                                        *
CC    OUTPUT OPTIONS                                  *
CC                                        *
CC*********************************************************************
CC
CC
CC FLAG FOR PV OR DAYS TO PRINT OR TO STOP THE RUN
*----ICUMTM  ISTOP  IOUTGMS
     0      0    0
CC
CC FLAG INDICATING IF THE PROFILE OF KCTH COMPONENT SHOULD BE WRITTEN
*----IPRFLG(KC),KC=1,N
   1  1  1  0  0 0 0 0  1  1
CC
CC FLAG FOR individual map files
*----IPPRES IPSAT IPCTOT IPBIO IPCAP IPGEL IPALK IPTEMP IPOBS
    0     1     1     1     0    0   0    0      0
CC
CC FLAG for individual output map files
*----ICKL IVIS IPER ICNM ICSE ihystp  ifoamp  inoneq
    1    0    1    1    0    0       0       0
CC
CC FLAG  for variables to PROF output file
*----IADS IVEL IRKF IPHSE
    0    1    0    0
CC
CC*********************************************************************
CC                                        *
CC    RESERVOIR PROPERTIES                              *
CC                                        *
CC*********************************************************************
```

```
CC
CC
CC MAX. SIMULATION TIME ( DAYS)
*---- TMAX
    4.126
CC
CC ROCK COMPRESSIBILITY (1/PSI), STAND. PRESSURE(PSIA)
*----COMPR   PSTAND
    0.    101.0
CC
CC FLAGS INDICATING CONSTANT OR VARIABLE POROSITY, X,Y,AND Z
PERMEABILITY
*----IPOR1 IPERMX IPERMY IPERMZ  IMOD
     2     2     0     3     0
CC
CC VARIABLE POROSITY OVER RESERVOIR, 48x1x30
*---- POR(I),FOR I=1 TO NX x NY x NZ
0.36          0.36          0.36          0.36          0.36          0.36          0.36
              0.36          0.36          0.36          0.36          0.36          0.36 0.36
0.36 0.36 0.36 0.36 0.36 0.36 0.36 0.36 0.36 0.36 0.36 0.36 0.36 0.36 0.36 0.36 0.36 0.36 0.36
0.36 0.36 0.36 0.36 0.36 0.36 0.36 0.36 0.36 0.36 0.36 0.36 0.36 0.36
0.36 0.36 0.36 0.36 0.36 0.36 0.36 0.36 0.36 0.36 0.36 0.36 0.36 0.36 0.36 0.36 0.36 0.36 0.36
0.36 0.36 0.36 0.36 0.36 0.36 0.36 0.36 0.36 0.36 0.36 0.36 0.36 0.36 0.36 0.36 0.36 0.36 0.36
0.36 0.36 0.36 0.36 0.36 0.36 0.36 0.36
0.36 0.36 0.36 0.36 0.36 0.36 0.36 0.36 0.36 0.36 0.36 0.36 0.36 0.36 0.36 0.36 0.36 0.36 0.36
0.36 0.36 0.36 0.36 0.36 0.36 0.36 0.36 0.36 0.36 0.36 0.36 0.36 0.36 0.36 0.36 0.36 0.36 0.36
0.36 0.36 0.36 0.36 0.36 0.36 0.36 0.36
0.36 0.36 0.36 0.36 0.36 0.36 0.36 0.36 0.36 0.36 0.36 0.36 0.36 0.36 0.36 0.36 0.36 0.36 0.36
0.36 0.36 0.36 0.36 0.36 0.36 0.36 0.36 0.36 0.36 0.36 0.36 0.36 0.36 0.36 0.36 0.36 0.36 0.36
0.36 0.36 0.36 0.36 0.36 0.36 0.36 0.36
0.36 0.36 0.36 0.36 0.36 0.36 0.36 0.36 0.36 0.36 0.36 0.36 0.36 0.36 0.36 0.36 0.36 0.36 0.36
0.36 0.36 0.36 0.36 0.36 0.36 0.36 0.36 0.36 0.36 0.36 0.36 0.36 0.36 0.36 0.36 0.36 0.36 0.36
0.36 0.36 0.36 0.36 0.36 0.36 0.36 0.36
0.36 0.36 0.36 0.36 0.36 0.36 0.36 0.36 0.36 0.36 0.36 0.36 0.36 0.36 0.36 0.36 0.36 0.36 0.36
0.36 0.36 0.36 0.36 0.36 0.36 0.36 0.36 0.36 0.36 0.36 0.36 0.36 0.36 0.36 0.36 0.36 0.36 0.36
0.36 0.36 0.36 0.36 0.36 0.36 0.36 0.36
0.36 0.36 0.36 0.36 0.36 0.36 0.36 0.36 0.36 0.36 0.36 0.36 0.36 0.36 0.36 0.36 0.36 0.36 0.36
0.36 0.36 0.36 0.36 0.36 0.36 0.36 0.36 0.36 0.36 0.36 0.36 0.36 0.36 0.36 0.36 0.36 0.36 0.36
0.36 0.36 0.36 0.36 0.36 0.36 0.36 0.36
0.36 0.36 0.36 0.36 0.36 0.36 0.36 0.36 0.36 0.36 0.36 0.36 0.36 0.36 0.36 0.36 0.36 0.36 0.36
0.36 0.36 0.36 0.36 0.36 0.36 0.36 0.36 0.36 0.36 0.36 0.36 0.36 0.36 0.36 0.36 0.36 0.36 0.36
0.36 0.36 0.36 0.36 0.36 0.36 0.36 0.36
0.36 0.36 0.36 0.36 0.36 0.36 0.36 0.36 0.36 0.36 0.36 0.36 0.36 0.36 0.36 0.36 0.36 0.36 0.36
0.36 0.36 0.36 0.36 0.36 0.36 0.36 0.36 0.36 0.36 0.36 0.36 0.36 0.36 0.36 0.36 0.36 0.36 0.36
0.36 0.36 0.36 0.36 0.36 0.36 0.36 0.36
0.36 0.36 0.36 0.36 0.36 0.36 0.36 0.36 0.36 0.36 0.36 0.36 0.36 0.36 0.36 0.36 0.36 0.36 0.36
0.36 0.36 0.36 0.36 0.36 0.36 0.36 0.36 0.36 0.36 0.36 0.36 0.36 0.36 0.36 0.36 0.36 0.36 0.36
0.36 0.36 0.36 0.36 0.36 0.36 0.36 0.36
0.36 0.36 0.36 0.36 0.36 0.36 0.36 0.36 0.36 0.36 0.36 0.36 0.36 0.36 0.36 0.36 0.36 0.36 0.36
0.36 0.36 0.36  0.36 0.36 0.36 0.36 0.36 0.36 0.36 0.36 0.36 0.36 0.36 0.36 0.36 0.36 0.36 0.36
0.36 0.36 0.36 0.36 0.36 0.36 0.36 0.36
0.36 0.36 0.36 0.36 0.36 0.36 0.36 0.36 0.36 0.36 0.36 0.36 0.36 0.36 0.36 0.36 0.36 0.36 0.36
0.36 0.36 0.36 0.36 0.36 0.36 0.36 0.36 0.36 0.36 0.36 0.36 0.36 0.36 0.36 0.36 0.36 0.36 0.36
0.36 0.36 0.36 0.36 0.36 0.36 0.36 0.36
```

0.36 0.36 0.36 0.36 0.36 0.36 0.36 0.36 0.36 0.36 0.36 0.36 0.36 0.36 0.36 0.36 0.36 0.36 0.36 0.36
0.36 0.36 0.36 0.36 0.36 0.36 0.36 0.36 0.36 0.36 0.36 0.36 0.36 0.36 0.36 0.36 0.36 0.36 0.36 0.36
0.36 0.36 0.36 0.36 0.36 0.36 0.36 0.36
0.36 0.36 0.36 0.36 0.36 0.36 0.36 0.36 0.36 0.36 0.36 0.36 0.36 0.36 0.36 0.36 0.36 0.36 0.36 0.36
0.36 0.36 0.36 0.36 0.36 0.36 0.36 0.36 0.36 0.36 0.36 0.36 0.36 0.36 0.36 0.36 0.36 0.36 0.36 0.36
0.36 0.36 0.36 0.36 0.36 0.36 0.36 0.36
0.36 0.36 0.36 0.36 0.36 0.36 0.36 0.36 0.36 0.36 0.36 0.36 0.36 0.36 0.36 0.36 0.36 0.36 0.36 0.36
0.36 0.36 0.36 0.36 0.36 0.36 0.36 0.36 0.36 0.36 0.36 0.36 0.36 0.36 0.36 0.36 0.36 0.36 0.36 0.36
0.36 0.36 0.36 0.36 0.36 0.36 0.36 0.36
0.36 0.36 0.36 0.36 0.36 0.36 0.36 0.36 0.36 0.36 0.36 0.36 0.36 0.36 0.36 0.36 0.36 0.36 0.36 0.36
0.36 0.36 0.36 0.36 0.36 0.36 0.36 0.36 0.36 0.36 0.36 0.36 0.36 0.36 0.36 0.36 0.36 0.36 0.36 0.36
0.36 0.36 0.36 0.36 0.36 0.36 0.36 0.36
0.36 0.36 0.36 0.36 0.36 0.36 0.36 0.36 0.36 0.36 0.36 0.36 0.36 0.36 0.36 0.36 0.36 0.36 0.36 0.36
0.36 0.36 0.36 0.36 0.36 0.36 0.36 0.36 0.36 0.36 0.36 0.36 0.36 0.36 0.36 0.36 0.36 0.36 0.36 0.36
0.36 0.36 0.36 0.36 0.36 0.36 0.36 0.36
0.36 0.36 0.36 0.36 0.36 0.36 0.36 0.36 0.36 0.36 0.36 0.36 0.36 0.36 0.36 0.36 0.36 0.36 0.36 0.36
0.36 0.36 0.36 0.36 0.36 0.36 0.36 0.36 0.36 0.36 0.36 0.36 0.36 0.36 0.36 0.36 0.36 0.36 0.36 0.36
0.36 0.36 0.36 0.36 0.36 0.36 0.36 0.36
0.38 0.38 0.38 0.38 0.38 0.38 0.38 0.38 0.38 0.38 0.38 0.36 0.36 0.36 0.36 0.36 0.36 0.36 0.36 0.36
0.36 0.36 0.36 0.36 0.36 0.36 0.36 0.36 0.36 0.36 0.36 0.36 0.36 0.36 0.36 0.36 0.36 0.36 0.38 0.38
0.38 0.38 0.38 0.38 0.38 0.38 0.38 0.38
0.38 0.38 0.38 0.38 0.38 0.38 0.38 0.38 0.38 0.38 0.38 0.38 0.38 0.38 0.38 0.38 0.38 0.38 0.38 0.38
0.38 0.38 0.38 0.38 0.38 0.38 0.38 0.38 0.38 0.38 0.38 0.38 0.38 0.38 0.38 0.38 0.38 0.38 0.38 0.38
0.38 0.38 0.38 0.38 0.38 0.38 0.38 0.38
0.38 0.38 0.38 0.38 0.38 0.38 0.38 0.38 0.38 0.38 0.38 0.38 0.38 0.38 0.38 0.38 0.38 0.38 0.38 0.38
0.38 0.38 0.38 0.38 0.38 0.38 0.38 0.38 0.38 0.38 0.38 0.38 0.38 0.38 0.38 0.38 0.38 0.38 0.38 0.38
0.38 0.38 0.38 0.38 0.38 0.38 0.38 0.38
0.38 0.38 0.38 0.38 0.38 0.38 0.38 0.38 0.38 0.38 0.38 0.38 0.38 0.38 0.38 0.38 0.38 0.38 0.38 0.38
0.38 0.38 0.38 0.38 0.38 0.38 0.38 0.38 0.38 0.38 0.38 0.38 0.38 0.38 0.38 0.38 0.38 0.38 0.38 0.38
0.38 0.38 0.38 0.38 0.38 0.38 0.38 0.38
0.38 0.38 0.38 0.38 0.38 0.38 0.38 0.38 0.38 0.38 0.38 0.38 0.38 0.38 0.38 0.38 0.38 0.38 0.38 0.38
0.38 0.38 0.38 0.38 0.38 0.38 0.38 0.38 0.38 0.38 0.38 0.38 0.38 0.38 0.38 0.38 0.38 0.38 0.38 0.38
0.38 0.38 0.38 0.38 0.38 0.38 0.38 0.38
0.38 0.38 0.38 0.38 0.38 0.38 0.38 0.38 0.38 0.38 0.38 0.38 0.38 0.38 0.38 0.38 0.38 0.38 0.38 0.38
0.38 0.38 0.38 0.38 0.38 0.38 0.38 0.38 0.38 0.38 0.38 0.38 0.38 0.38 0.38 0.38 0.38 0.38 0.38 0.38
0.38 0.38 0.38 0.38 0.38 0.38 0.38 0.38
0.38 0.38 0.38 0.38 0.38 0.38 0.38 0.38 0.38 0.38 0.38 0.38 0.38 0.38 0.38 0.38 0.38 0.38 0.38 0.38
0.38 0.38 0.38 0.38 0.38 0.38 0.38 0.38 0.38 0.38 0.38 0.38 0.38 0.38 0.38 0.38 0.38 0.38 0.38 0.38
0.38 0.38 0.38 0.38 0.38 0.38 0.38 0.38
0.38 0.38 0.38 0.38 0.38 0.38 0.38 0.38 0.38 0.38 0.38 0.38 0.38 0.38 0.38 0.38 0.38 0.38 0.38 0.38
0.38 0.38 0.38 0.38 0.38 0.38 0.38 0.38 0.38 0.38 0.38 0.38 0.38 0.38 0.38 0.38 0.38 0.38 0.38 0.38
0.38 0.38 0.38 0.38 0.38 0.38 0.38 0.38
0.38 0.38 0.38 0.38 0.38 0.38 0.38 0.38 0.38 0.38 0.38 0.38 0.38 0.38 0.38 0.38 0.38 0.38 0.38 0.38
0.38 0.38 0.38 0.38 0.38 0.38 0.38 0.38 0.38 0.38 0.38 0.38 0.38 0.38 0.38 0.38 0.38 0.38 0.38 0.38
0.38 0.38 0.38 0.38 0.38 0.38 0.38 0.38

0.38 0.38 0.38 0.38 0.38 0.38 0.38 0.38 0.38 0.38 0.38 0.38 0.38 0.38 0.38 0.38 0.38 0.38 0.38 0.38
0.38 0.38 0.38 0.38 0.38 0.38 0.38 0.38 0.38 0.38 0.38 0.38 0.38 0.38 0.38 0.38 0.38 0.38 0.38 0.38
0.38 0.38 0.38 0.38 0.38 0.38 0.38 0.38
0.38 0.38 0.38 0.38 0.38 0.38 0.38 0.38 0.38 0.38 0.38 0.38 0.38 0.38 0.38 0.38 0.38 0.38 0.38 0.38
0.38 0.38 0.38 0.38 0.38 0.38 0.38 0.38 0.38 0.38 0.38 0.38 0.38 0.38 0.38 0.38 0.38 0.38 0.38 0.38
0.38 0.38 0.38 0.38 0.38 0.38 0.38 0.38
CC
CC VARIABLE X-PERMEABILITY (MILIDARCY) FOR I=1, NX x NY x NZ
*----PERMX(I) (MILIDARCY)
20000. 20000. 20000. 20000. 20000. 20000. 20000. 20000. 20000. 20000. 20000. 20000.
20000. 20000. 20000. 20000. 20000. 20000. 20000. 20000. 20000. 20000. 20000. 20000.
20000. 20000. 20000. 20000. 20000. 20000. 20000. 20000. 20000. 20000. 20000. 20000.
20000. 20000. 20000. 20000. 20000. 20000. 20000. 20000.

20000. 20000. 20000.

```
2000.  2000.  2000.  2000.  2000.  2000.  2000.  2000.  2000.  2000.  2000.  2000.  2000.  2000.
2000.  2000.  2000.  2000.  2000.  2000.
 2000.  2000.  2000.  2000.  2000.  2000.  2000.  2000.  2000.  2000.  2000.  2000.  2000.  2000.
2000.  2000.  2000.  2000.  2000.  2000.  2000.  2000.  2000.  2000.  2000.  2000.  2000.  2000.
2000.  2000.  2000.  2000.  2000.  2000.  2000.  2000.  2000.  2000.  2000.  2000.  2000.  2000.
2000.  2000.  2000.  2000.  2000.  2000.
 2000.  2000.  2000.  2000.  2000.  2000.  2000.  2000.  2000.  2000.  2000.  2000.  2000.  2000.
2000.  2000.  2000.  2000.  2000.  2000.  2000.  2000.  2000.  2000.  2000.  2000.  2000.  2000.
2000.  2000.  2000.  2000.  2000.  2000.  2000.  2000.  2000.  2000.  2000.  2000.  2000.  2000.
2000.  2000.  2000.  2000.  2000.  2000.
 2000.  2000.  2000.  2000.  2000.  2000.  2000.  2000.  2000.  2000.  2000.  2000.  2000.  2000.
2000.  2000.  2000.  2000.  2000.  2000.  2000.  2000.  2000.  2000.  2000.  2000.  2000.  2000.
2000.  2000.  2000.  2000.  2000.  2000.  2000.  2000.  2000.  2000.  2000.  2000.  2000.  2000.
2000.  2000.  2000.  2000.  2000.  2000.
 2000.  2000.  2000.  2000.  2000.  2000.  2000.  2000.  2000.  2000.  2000.  2000.  2000.  2000.
2000.  2000.  2000.  2000.  2000.  2000.  2000.  2000.  2000.  2000.  2000.  2000.  2000.  2000.
2000.  2000.  2000.  2000.  2000.  2000.  2000.  2000.  2000.  2000.  2000.  2000.  2000.  2000.
2000.  2000.  2000.  2000.  2000.  2000.
 2000.  2000.  2000.  2000.  2000.  2000.  2000.  2000.  2000.  2000.  2000.  2000.  2000.  2000.
2000.  2000.  2000.  2000.  2000.  2000.  2000.  2000.  2000.  2000.  2000.  2000.  2000.  2000.
2000.  2000.  2000.  2000.  2000.  2000.  2000.  2000.  2000.  2000.  2000.  2000.  2000.  2000.
2000.  2000.  2000.  2000.  2000.  2000.
 2000.  2000.  2000.  2000.  2000.  2000.  2000.  2000.  2000.  2000.  2000.  2000.  2000.  2000.
2000.  2000.  2000.  2000.  2000.  2000.  2000.  2000.  2000.  2000.  2000.  2000.  2000.  2000.
2000.  2000.  2000.  2000.  2000.  2000.  2000.  2000.  2000.  2000.  2000.  2000.  2000.  2000.
2000.  2000.  2000.  2000.  2000.  2000.
CC
CC CONSTANT Y-PERMEABILITY (MILIDARCY) FOR LAYER K=1, NZ
*----PERMY(1) (MILIDARCY)
   1.
CC
CC VARIABLE Z-PERMEABILITY DEPENDENT ON X DIRECTION PERMEABILITY FOR
LAYER K=1, NZ
*----FACTZ
   0.1
CC
CC FLAG FOR CONSTANT OR VARIABLE DEPTH, PRESSURE, WATER SATURATION
*----IDEPTH  IPRESS  ISWI  ICWI
    0       1       2   2
CC
CC CONSTANT DEPTH (FT)
*----D111
    0.0
CC
CC CONSTANT PRESSURE (PSIA)
*----PINIT   HINIT
   101.0    0.0
CC
CC INITIAL WATER SATURATION FOR EACH GRIDBLOCK IS SPECIFIED
*----S(I),I=1 TO NX*NY*NZ
1.0 1.0 1.0 1.0 1.0 1.0 1.0 1.0 1.0 1.0 1.0 1.0 1.0 1.0 1.0 1.0 1.0 1.0 1.0 1.0 1.0 1.0 1.0 1.0
1.0 1.0 1.0 1.0 1.0 1.0 1.0 1.0 1.0 1.0 1.0 1.0 1.0 1.0 1.0 1.0 1.0 1.0 1.0 1.0 1.0 1.0 1.0 1.0
```

1.0 1.0 1.0 1.0 1.0 1.0 1.0 1.0 1.0 1.0 1.0 1.0 1.0 1.0 1.0 1.0 1.0 1.0 1.0 1.0 1.0 1.0 1.0 1.0
1.0 1.0 1.0 1.0 1.0 1.0 1.0 1.0 1.0 1.0 1.0 1.0 1.0 1.0 1.0 1.0 1.0 1.0 1.0 1.0 1.0 1.0

```
1.0 1.0 1.0 1.0 1.0 1.0 1.0 1.0 1.0 1.0 1.0 1.0 1.0 1.0 1.0 1.0 1.0 1.0 1.0 1.0 1.0 1.0 1.0
1.0 1.0 1.0 1.0 1.0 1.0 1.0 1.0 1.0 1.0 1.0 1.0 1.0 1.0 1.0 1.0 1.0 1.0 1.0 1.0 1.0 1.0 1.0
1.0 1.0 1.0 1.0 1.0 1.0 1.0 1.0 1.0 1.0 1.0 1.0 1.0 1.0 1.0 1.0 1.0 1.0 1.0 1.0 1.0 1.0 1.0
1.0 1.0 1.0 1.0 1.0 1.0 1.0 1.0 1.0 1.0 1.0 1.0 1.0 1.0 1.0 1.0 1.0 1.0 1.0 1.0 1.0 1.0 1.0
1.0 1.0 1.0 1.0 1.0 1.0 1.0 1.0 1.0 1.0 1.0 1.0 1.0 1.0 1.0 1.0 1.0 1.0 1.0 1.0 1.0 1.0 1.0
1.0 1.0 1.0 1.0 1.0 1.0 1.0 1.0 1.0 1.0 1.0 1.0 1.0 1.0 1.0 1.0 1.0 1.0 1.0 1.0 1.0 1.0 1.0
1.0 1.0 1.0 1.0 1.0 1.0 1.0 1.0 1.0 1.0 1.0 1.0 1.0 1.0 1.0 1.0 1.0 1.0 1.0 1.0 1.0 1.0 1.0
1.0 1.0 1.0 1.0 1.0 1.0 1.0 1.0 1.0 1.0 1.0 1.0 1.0 1.0 1.0 1.0 1.0 1.0 1.0 1.0 1.0 1.0 1.0
CC
CC
*----INITIAL WATER CONC. IN AQ IN EACH GRIDBLOCK
    1440*1.0
CC
CC
*----INITIAL OIL CONC. IN AQ IN EACH GRIDBLOCK
    1440*0.0
CC
CC
*----INITIAL SURF. CONC. IN AQ IN EACH GRIDBLOCK
    1440*0.0
CC
CC*****************************************************************
CC                                    *
CC    PHYSICAL PROPERTY DATA                    *
CC                                    *
CC*****************************************************************
CC
CC
CC OIL CONC. AT PLAIT POINT FOR TYPE II(+)AND TYPE II(-), CMC
*---- C2PLC   C2PRC  EPSME  IHAND
      0.0   1.0    0.000032    0
CC
CC FLAG INDICATING TYPE OF PHASE BEHAVIOR PARAMETERS
*---- IFGHBN
       0
CC SLOPE AND INTERCEPT OF BINODAL CURVE AT ZERO, OPT., AND 2XOPT
SALINITY
CC FOR ALCOHOL 1
*----HBNS70 HBNC70 HBNS71 HBNC71 HBNS72 HBNC72
    0.000  0.1736  0.000  0.1736  0.000  0.1736
CC SLOPE AND INTERCEPT OF BINODAL CURVE AT ZERO, OPT., AND 2XOPT
SALINITY
CC FOR ALCOHOL 2
*----HBNS80 HBNC80 HBNS81 HBNC81 HBNS82 HBNC82
    0.000  0.1736  0.000  0.1736  0.000  0.1736
CC
CC LOWER AND UPPER EFFECTIVE SALINITY FOR ALCOHOL 1 AND ALCOHOL 2
*----CSEL7  CSEU7  CSEL8  CSEU8
   0.0527  0.055  0.0527 0.055
CC
CC THE CSE SLOPE PARAMETER FOR CALCIUM AND ALCOHOL 1 AND ALCOHOL 2
*----BETA6  BETA7  BETA8
```

```
   0.0     0    0.
CC
CC FLAG FOR ALCOHOL PART. MODEL AND PARTITION COEFFICIENTS
*----IALC  OPSK7O  OPSK7S  OPSK8O  OPSK8S
   0     0.000001 0.000001 0.     0.0
CC
CC NO. OF ITERATIONS, AND TOLERANCE
*----NALMAX   EPSALC
   20       .0001
CC
CC ALCOHOL 1 PARTITIONING PARAMETERS IF IALC=1
*----AKWC7   AKWS7  AKM7  AK7     PT7
   4.671   1.79   48.   35.31   .222
CC
CC ALCOHOL 2 PARTITIONING PARAMETERS IF IALC=1
*----AKWC8   AKWS8  AKM8  AK8     PT8
   0.      0.     0.    0.      0.
CC
CC IFT MODEL FLAG
*---- IFT
     1
CC
CC INTERFACIAL TENSION PARAMETERS
*----CHUH  AHUH
   0.30   10
CC
CC LOG10 OF OIL/WATER INTERFACIAL TENSION
*----XIFTW
   1.65
CC
CC MASS TRANSFER FLAG
*----IMASS  icor
   2      0
CC
CC OIL SOLUBILITY
*----WSOL
     0.014237
CC
CC ISOL, CNEM
*----ISOL  CNEM
     1    0.2
CC
CC CAPILLARY DESATURATION PARAMETERS FOR PHASE 1, 2, AND 3
*----ITRAP   T11       T22       T33
   2       6000.      6000.     6000.
CC
CC RELATIVE PERM. FLAG (0:IMBIBITION COREY,1:FIRST DRAINAGE COREY)
*----IPERM
   0
CC
CC FLAG FOR CONSTANT OR VARIABLE REL. PERM. PARAMETERS
*----ISRW  IPRW  IEW
```

```
   0    0    0
CC
CC CONSTANT RES. SATURATION OF PHASES 1,2,AND 3 AT LOW CAPILLARY NO.
*----S1RWC  S2RWC  S3RWC
   0.15   0.13   0.10
CC
CC CONSTANT ENDPOINT REL. PERM. OF PHASES 1,2,AND 3 AT LOW CAPILLARY NO.
*----P1RW  P2RW  P3RW
  0.46  0.46  0.46
CC
CC CONSTANT REL. PERM. EXPONENT OF PHASES 1,2,AND 3 AT LOW CAPILLARY NO.
*----E1W  E2W  E3W
   4.  4.  4.
CC
CC CONSTANT RES. SATURATION OF PHASES 1,2,AND 3 AT HIGH CAPILLARY NO.
*----S1RC  S2RC  S3RC
   0.  0.05  0.
CC
CC CONSTANT ENDPOINT REL. PERM. OF PHASES 1,2,AND 3 AT HIGH CAPILLARY NO.
*----P1RC  P2RC  P3RC
   0.46  0.46  0.46
CC
CC CONSTANT REL. PERM. EXPONENT OF PHASES 1,2,AND 3 AT HIGH CAPILLARY
NO.
*----E13C  E23C  E31C
   4.    4.    4.
CC
CC WATER AND OIL VISCOSITY , RESERVOIR TEMPERATURE
*----VIS1   VIS2  TEMPV
  0.890   0.839   25
CC
CC VISCOSITY PARAMETERS
*----ALPHAV1 ALPHAV2  ALPHAV3  ALPHAV4  ALPHAV5
   7.14     2.86    2.16     0.0001  0.0001
CC
CC PARAMETERS TO CALCULATE POLYMER VISCOSITY AT ZERO SHEAR RATE
*----AP1     AP2     AP3
   52.     2340.   40000.
CC
CC PARAMETER TO COMPUTE CSEP,MIN. CSEP, AND SLOPE OF LOG VIS. VS. LOG
CSEP
*----BETAP CSE1  SSLOPE
   2.    .01   .175
CC
CC PARAMETER FOR SHEAR RATE DEPENDENCE OF POLYMER VISCOSITY
*----GAMMAC  GAMHF  POWN
   4.      20.    1.1
CC
CC FLAG FOR POLYMER PARTITIONING, PERM. REDUCTION PARAMETERS
*----IPOLYM EPHI3 EPHI4 BRK    CRK
   1      1.    1.0   1000.  0.0186
CC
```

```
CC SPECIFIC WEIGHT FOR COMPONENTS 1,2,3,7,AND 8 , AND GRAVITY FLAG
*----DEN1  DEN2  DEN23  DEN3  DEN7  DEN8 IDEN
   0.998  1.62  1.62  1.09  0.0    0.   2
CC
CC  FLAG FOR CHOICE OF UNITS ( 0:BOTTOMHOLE CONDITION , 1: STOCK TANK)
*-----ISTB
    0
CC
CC COMPRESSIBILITY FOR VOL. OCCUPYING COMPONENTS 1,2,3,7,AND 8
*----COMPC(1)  COMPC(2)  COMPC(3)  COMPC(7)  COMPC(8)
   0.       0.       0.       0.       0.
CC
CC CONSTANT OR VARIABLE PC PARAM., WATER-WET OR OIL-WET PC CURVE FLAG
*----ICPC   IEPC  IOW
   0      0     0
CC
CC CAPILLARY PRESSURE PARAMETER, CPC0
*----CPC0
   10.
CC
CC CAPILLARY PRESSURE PARAMETER, EPC0
*----EPC0
   4.35
CC
CC MOLECULAR DIFFUSION COEF. KCTH COMPONENT IN PHASE 1 (D(KC),KC=1,N)
*----D(1) D(2) D(3) D(4) D(5) D(6) D(7) D(8) D(9)
   0.0001  0.0001  0.0001  0.0001  0.0001  0.0001  0.0001  0.0001  0.0001  0.0001
CC
CC MOLECULAR DIFFUSION COEF. OF KCTH COMPONENT IN PHASE 2 (D(KC),KC=1,N)
*----D(1) D(2) D(3) D(4) D(5) D(6) D(7) D(8) D(9)
   0.   0.   0.   0.   0.   0.   0.   0. 0.   0.
CC
CC MOLECULAR DIFFUSION COEF. OF KCTH COMPONENT IN PHASE 3 (D(KC),KC=1,N)
*----D(1) D(2) D(3) D(4) D(5) D(6) D(7) D(8) D(9)
   0.   0.   0.   0.   0.   0.   0.   0. 0.   0.
CC
CC LONGITUDINAL AND TRANSVERSE DISPERSIVITY OF PHASE 1
*----ALPHAL(1)    ALPHAT(1)
     .02         .002
CC
CC LONGITUDINAL AND TRANSVERSE DISPERSIVITY OF PHASE 2
*----ALPHAL(2)    ALPHAT(2)
     .02         .002
CC
CC LONGITUDINAL AND TRANSVERSE DISPERSIVITY OF PHASE 3
*----ALPHAL(3)    ALPHAT(3)
     .02         .002
CC
CC FLAG TO SPECIFY ORGANIC ADSORPTION CALCULATION
*----IADSO
    0
CC
```

```
CC SURFACTANT AND POLYMER ADSORPTION PARAMETERS
*----AD31  AD32  B3D    AD41   AD42  B4D   IADK  IADS1  FADS REFK
    0.0    0.0  1000.  0.7    0.    100.  0      0     0    500
CC
CC PARAMETERS FOR CATION EXCHANGE OF CLAY AND SURFACTANT
*----QV     XKC   XKS  EQW
    0.0    .0    .0   419.
CC
CC*****************************************************************
CC                                                                *
CC    BIOLOGICAL DATA                                             *
CC                                                                *
CC*****************************************************************
CC
CC
CC  BULK DENSITY
*----  DENBLK
      1.74
cc
cc  min. conc.,  tolerance, time step control flag
*--- cmin, epsbio, ibtim
    1.0d-1 1.0d-4  2
cc
cc  maximum acceptable error, maximum biodegradation timestep
*--- biorme, btmax
    0.1    0.0001
CC
CC METABOLIC COMBINATIONS, FLAGS FOR INHIBITION, COMPETITION, KINETICS
*----NBC   NMET    IBKIN  IBPP
     3      1       2     0
CC
CC INITIAL AQEUOUS PHASE CONCENTRATIONS
*----KC   ITYPE   CINIT   RABIO  NPABIO
     2     1      0.0      0.     0
     9     1      7110.       0.     0
    10     2      0.       0.     0
CC
CC BIOLOGICAL SPECIES PARAMETERS
*----IBS DEN   RCOL    TCOL   COLNUM  ENDOG  ENDOGB  CBI   CBIOMN adsbio
    10  0.1   0.01    0.001     100.  0.0    0.0   1.0D+6  0.0D+6   1.0E+7
CC
CC METABOLIC COMBINATION INFORMATION
*----ISUB IEA  IBS  BRMAX  BRMAXB  YXS     AKS   AKA    FEA
     2    9   10    0.0   5.0   1.0e-5 1.0E+6 1.0E+6  1.267
CC
CC  FLAGS FOR COMPETITION, INHIBITION, PRODUCT GEN., NUTRIENT LIM.,
COMETABOLISM
*----ISUB IEA  IBS  COMPBIO  NIHB  NPROD  NNUT  ICOMET
     2     9   10     0        0     0     0      0
CC
CC*****************************************************************
CC                                                                *
```

```
CC    WELL DATA                                    *
CC                                          *
CC*****************************************************************
CC
CC
CC FLAG FOR RIGHT AND LEFT BOUNDARY
*---- IBOUND izone
     0      0
CC
CC TOTAL NUMBER OF WELLS, WELL RADIUS FLAG, FLAG FOR TIME OR COURANT
NO.
*----NWELL   IRO   ITSTEP  NWREL
     2      2      0      2
CC
CC WELL ID, LOCATIONS, SPECIFYING WELL TYPE, WELL RADIUS, SKIN
*----IDW IW JW IFLAG RW SWELL IDIR IFIRST ILAST IPRF
     1  48  1  4   0.00080  0.  3    16      16   0
CC
CC WELL NAME
*----WELNAME
PRODUCER
CC
CC ICHECK, MAX. AND MIN. ALOWABLE BOTTOMHOLE PRESSURE AND RATE
*----ICHECK PWFMIN PWFMAX QTMIN QTMAX
    0      0.0    50000.  0.0  6000.
cc
CC WELL ID, LOCATIONS, SPECIFYING WELL TYPE, WELL RADIUS, SKIN
*----IDW IW JW IFLAG RW SWELL IDIR IFIRST ILAST IPRF
    2   1  1  1  0.0008  0.  3      16     16    0
CC
CC WELL NAME
*----WELNAME
INJECTOR
CC
CC ICHECK, MAX. AND MIN. ALOWABLE BOTTOMHOLE PRESSURE AND RATE
*----ICHECK PWFMIN PWFMAX QTMIN QTMAX
    0      0.0    50000.  0.0  6000.
CC
CC ID,INJ. RATE AND INJ. COMP. FOR RATE CONS. WELLS FOR EACH PHASE (L=1,3)
*----ID QI
    1  -2.88E-03
CC
CC ID,INJ. RATE AND INJ. COMP. FOR RATE CONS. WELLS FOR EACH PHASE (L=1,3)
*----ID,QI(M,L)  C(M,KC,L)
    2   2.88E-03     1.0     0.0   0.0   0.0  0.0  0.0  0.0 0.0  7110.0   0.0
    2   0.0           0.000    1.0   0.0   7*0.0
    2   0.00          0.0      0.0   0.0   7*0.0
CC
CC CUM. INJ. TIME , AND INTERVALS (PV OR DAY) FOR WRITING TO OUTPUT FILES
*----TINJ      CUMPR1    CUMHI1   WRHPV     WRPRF     RSTC
    0.126      0.1       1.0      0.02       0.02      3000
CC
```

```
CC FOR IMES=3,THE INI. TIME STEP,CONC. TOLERANCE,MIN. AND MAX. TIME STEP
*----DT      DCLIM      DTMAX     DTMIN
   1E-5    10*0.00001    0.001    0.00001
CC
CC FLAG FOR INDICATING BOUNDARY CHANGE
*---- IBMOD
      0
CC
CC IRO, ITIME, NEW FLAGS FOR ALL THE WELLS
*----  IRO    ITIME     IFLAG
      2       0        4      1
CC
CC NUMBER OF WELLS CHANGES IN LOCATION OR SKIN OR PWF
*----  NWEL1
       0
CC
CC NUMBER OF WELLS WITH RATE CHANGES, ID
*---- NWEL2     ID
      2        1     2
CC
CC ID,INJ. RATE AND INJ. COMP. FOR RATE CONS. WELLS FOR EACH PHASE (L=1,3)
*----  ID      QI(M,L)      C(M,KC,L)
   1  -8.88E-06
CC
CC ID,INJ. RATE AND INJ. COMP. FOR RATE CONS. WELLS FOR EACH PHASE (L=1,3)
*----  ID      QI(M,L)      C(M,KC,L)
   2   8.88E-06     1.0     0.0   0.0   0.0  0.0  0.0  0.0 0.0  0.0   0.0
   2   0.0          0.000    1.0   0.0   7*0.0
   2   0.00         0.0      0.0   0.0   7*0.0
CC
CC CUM. INJ. TIME , AND INTERVALS (PV OR DAY) FOR WRITING TO OUTPUT FILES
*----TINJ      CUMPR1    CUMHI1   WRHPV     WRPRF     RSTC
   4.125      0.1       1.0      0.02        0.02      3000
CC
CC FOR IMES=3,THE INI. TIME STEP,CONC. TOLERANCE,MIN. AND MAX. TIME STEP
*----DT      DCLIM      DTMAX     DTMIN
   1E-4    10*0.00001    0.01    0.0001
CC
CC FLAG FOR INDICATING BOUNDARY CHANGE
*---- IBMOD
      0
CC
CC IRO, ITIME, NEW FLAGS FOR ALL THE WELLS
*----  IRO    ITIME     IFLAG
      2       0        4      1
CC
CC NUMBER OF WELLS CHANGES IN LOCATION OR SKIN OR PWF
*----  NWEL1
       0
CC
CC NUMBER OF WELLS WITH RATE CHANGES, ID
*---- NWEL2     ID
```

```
      2       1      2
CC
CC ID,INJ. RATE AND INJ. COMP. FOR RATE CONS. WELLS FOR EACH PHASE (L=1,3)
*----  ID      QI(M,L)      C(M,KC,L)
    1  -2.88E-03
CC
CC ID,INJ. RATE AND INJ. COMP. FOR RATE CONS. WELLS FOR EACH PHASE (L=1,3)
*----  ID      QI(M,L)      C(M,KC,L)
    2   2.88E-03     1.0     0.0   0.0   0.0  0.0  0.0  0.0 0.0  0.0   0.0
    2   0.0          0.000    1.0   0.0   7*0.0
    2   0.00         0.0      0.0   0.0   7*0.0
CC
CC CUM. INJ. TIME , AND INTERVALS (PV OR DAY) FOR WRITING TO OUTPUT FILES
*----TINJ      CUMPR1    CUMHI1   WRHPV     WRPRF     RSTC
    4.126      0.1       1.0      0.02        0.02      3000
CC
CC FOR IMES=3,THE INI. TIME STEP,CONC. TOLERANCE,MIN. AND MAX. TIME STEP
*----DT      DCLIM      DTMAX     DTMIN
    1E-5    10*0.00001    0.001    0.00001
```

APPENDIX C: MAIN DATA REQUIREMENT OF THE MODEL

(silica sand flow zone, PCE enhanced solubilization with 5%Tween 80)

Input data name		Value	Source	Range	Source
Porosity		0.36	Estimated from tracer test	0.31-0.46	Domenico and Schwartz (1998)
Intrinsic permeability		20 darcy	Field test (Akyol and Yolcubal, 2013)	1-1000	Freeze and Cherry (1979)
Longitudinal dispersivity		0.02 m	Estimated from tracer test	Typically 1-10% of travel distance	Gelhar (1993)
Solubility		23 g/L	Estimated from batch test	20-33.5 g/L	Taylor et al (2004)
Interfacial Tension (IFT)		45 mN/m	Estimated from batch test	44-47.5	Mercer and Cohen (1990) Cheng et al (2016)
Critical Micelle Concentration (CMC)		35 mg/L	from Cheng et al (2016)	35 mg/L	from Cheng et al (2016)
Capillary pressure	Pore size distribution coefficient	2	Corey (1994)	Soil type dependent	Corey (1994)
	Entry pressure	5.032 kPa	Eichel et al (2005)	Soil type dependent	Eichel et al (2005)
Residual saturation		0.05-0.13 for high/lowcapillarynumber	from Shah et al (1995)	0.03-0.15 Soil type dependent	Carsel and Parrish (1988)